NTRD Program Disclaimers

1. Disclaimer of Endorsement:

The posting herein of progress reports and final reports provided to TCEQ by its NTRD Grant Agreement recipients does not necessarily constitute or imply an endorsement, recommendation, or favoring by TCEQ or the State of Texas. The views and opinions expressed in said reports do not necessarily state or reflect those of TCEQ or the State of Texas, and shall not be used for advertising or product endorsement purposes.

2. Disclaimer of Liability:

The posting herein of progress reports and final reports provided to TCEQ by its NTRD Grant Agreement recipients does not constitute by TCEQ or the State of Texas the making of any warranty, express or implied, including the warranties of merchantability and fitness for a particular purpose, and such entities do not assume any legal liability or responsibility for the accuracy, completeness, or usefulness of any information,apparatus, product, or process disclosed, or represent that its use would not infringe privately owned rights.

Final Report

Development of Emissions Factors and/or Correlation Equations for Gas Leak Detection, and the Development of an EPA Protocol for the Use of a Gas-imaging Device as an Alternative or Supplement to Current Leak Detection and Evaluation Methods

The preparation of this report was funded by a grant from the State of Texas
through the
Texas Council on Environmental Technology
and the
Texas Commission on Environmental Quality

October 29, 2004

ACKNOWLEDGMENTS

The work reported herein was performed under TCET Contract No. 02-R04-01G by the Mountain View, California office of ENVIRON International Corporation. Mr. Vince Torres at the Texas Council of Environmental Technology (TCET) was the project coordinator with Ms. Kathy Pendleton at the Texas Commission on Environmental Quality (TCEQ) providing technical support. Mr. Randy Baylor was the grant manager for the New Technology Research and Development Program (NRTD) at the TCEQ.

Michael Smylie of ENVIRON directed the overall effort. Several subcontractor companies and independent experts provided significant contributions to this effort including Don Robinson, Brian Gillis, and Vineet Aggarwal of ICF Consulting; Buzz Harris, Eric Anderson, and David Ranum of URS Corporation; Tom Kulp and Karla Armstrong of Sandia National Laboratories; Tom McRae of Laser Imaging Systems; Bob, Michele, and Brad Hinnrichs of Pacific Advance Technology; David Furry and Jason Hatchett of Leak Survey, Inc.; Jeff Panek of Innovative Environmental Solutions; and Doug Hausler.

The authors wish to thank several key people for providing data, information, and consultation without which this study could not have been completed. These include Jeffrey Siegell with ExxonMobil Corporation; Dave Fashimpaur and Jeff Richardson with BP; and David Markwordt at the U.S. Environmental Protection Agency.

TABLE OF CONTENTS

APPENDICES

EXHIBITS

TABLES

FIGURES

EXECUTIVE SUMMARY

In June 2003, a project team headed by ENVIRON International Corporation (ENVIRON) was retained by the Texas Council on Environmental Technology (TCET) to manage a project entitled "Development of Emissions Factors and/or Correlation Equations for Gas Leak Detection, and the Development of an EPA Protocol for the Use of a Gas-imaging Device as an Alternative or Supplement to Current Leak Detection and Evaluation Methods" under TCET Contract No. 02-R04-01G.[1] The four primary objectives of this project were grouped into two general tasks as follows:

Task 1: Evaluate the ability of gas-imaging devices to detect fugitive emissions under typical conditions found at petroleum and chemical plants.

- Evaluate optical gas-imaging devices to determine the detection sensitivity of these devices to detect fugitive leaks of 14 highly reactive organic compounds (HRVOCs) selected by TCEQ and to various environmental factors that would be encountered during routine use at petroleum and chemical plants.

- Develop and demonstrate the ability of gas-imaging devices to estimate fugitive mass emissions.

- Develop a protocol for the use of a gas-imaging device as an alternative work practice or a supplement to current leak detection and evaluation methods.

Task 2: Develop correlation equations for individual ethylene/propylene sources

- Collect data of sufficient quality to develop emission factors or correlation equations for individual ethylene/propylene sources.

This executive summary discusses the laboratory and field activities conducted by the project team as part of this project. In addition, technical results obtained from laboratory and field activities are summarized.

EVALUATION OF THE ABILITY OF GAS-IMAGING DEVICES TO DETECT FUGITIVE EMISSIONS

To evaluate the ability of gas-imaging devices to detect fugitive emissions typically encountered in petroleum refineries and chemical plants, laboratory and field studies were conducted on four gas-imaging cameras. These cameras were identified as follows:

[1] On June 22, 2003, Texas Governor Perry issued a "Proclamation by the Governor of the State of Texas" that eliminated the Texas Council on Environmental Technology (TCET) as a stand-alone agency. The proclamation stated in part that the TCET "serves a valuable and important purpose, but should be operated by the Texas Commission on Environmental Quality (TCEQ)". Consequently, management and technical oversight of this contract moved to the TCEQ.

- Pacific Advanced Technology's (PAT) IMSS passive IR imaging camera;
- Laser Imaging Systems' (LIS) Long-wave BAGI active IR imaging camera;
- Sandia National Laboratory's (Sandia) Mid-wave BAGI active IR imaging camera.
- Leak Survey Incorporated's passive IR camera.

Of the four optical imaging technologies evaluated in this study, only the long-wave BAGI camera developed by LIS is a commercially available instrument. Each of the other technologies is currently in some phase of development and/or enhancement. As such, the results presented for both the laboratory and field phases of the study reflect the performance of the camera at the time of the study.

Laboratory Evaluation

In August 2003 and March 2004, laboratory testing of the four gas-imaging cameras was performed at the BP Laboratory in Naperville, Illinois. The objectives of the laboratory testing were as follows:

- Demonstrate the applicability of the gas imaging technologies to detect fugitive leaks of 14 candidate chemical groups:

Propylene	all Pentenes
Formaldehyde	all Trimethylbenzenes
Acetaldehyde	all Xylenes
Isoprene	all Ethyltoluenes
all Butenes (butylenes)	all Hexenes
1,3, Butadiene	all Butanes
Toluene	all Pentanes

- Determine the minimum gas detection levels of the gas-imaging technologies in a controlled laboratory environment.
- Collect data to begin to establish the sensitivity of the gas-imaging technologies to various factors that might be encountered during routine use at a chemical plant or refinery.

In the series of laboratory tests, the gas species, wind speed, background, and distance from the camera to the leaking component was varied to determine the minimum detectable gas flow rate for each camera.[2] The tests followed a laboratory test protocol developed for this project. The

[2] The minimum mass detection level was defined as the flow rate at which a gas leaking from a component could be detected by a camera. In an attempt to ensure viewing consistency, the protocol was interpreted to require that a single test team member be responsible for identifying and contrasting a leak against the background within the

matrix of test runs for each chemical included high and low wind speeds (ranging from approximately 1.5 and 4.5 miles per hour), two reflective backgrounds (concrete and painted metal cylinders), and two distances between the camera lens and the leak component (10 and 20 feet). Selected tests were run at 30 feet. The leak component used during all test runs was a valve with the stem packing removed.

Because test time was not available for all candidate chemicals listed above, the TCET gave priority to ethylene, 1,3 butadiene, 1-butene, and propylene. Other candidate chemicals were tested with available test time, and the test protocol designated that non-tested chemicals could draw upon the results of tested chemicals with similar infrared absorption spectra; in other words, some tested chemicals acted as spectral surrogates for non-tested chemicals.

Laboratory Test Results

Exhibits ES-1 to ES-4 are a comprehensive matrix of the test results, separated by camera. This matrix provides a summary of the tests and also provides visualization of what species a given camera could detect.[3]

For simplicity, the results matrix displays minimum detection thresholds in two categories: thresholds at or below 60 grams per hour and thresholds above 60 grams per hour. This split was chosen based on a Monte Carlo analysis for the mass flow rate equivalent to a 500, 1,000 and 10,000 ppmv leak definition by Method 21 for valves.[4] The Monte Carlo analysis determined a leak definition for an Alternative Work Practice (e.g. gas imaging) that would result in equivalent environmental protection to Method 21 monitoring.[5] Based in part on the Monte Carlo analysis, the EPA has accepted the 60 grams per hour threshold for gas imaging as a level that meets the environmental equivalency requirement.

Blank cells in the results matrix indicate that a test was not attempted. Test runs were not attempted because:

---

technology vendor's display and for determining the detection limit for each of the four technologies. Vendors and other team members were able at times to identify a leak when the designated team member was not able. Viewing angles and distance from the displays affected the ability to contrast the leak against the background.

Gas detection for a camera was defined as a stream of gas seen exiting the component within a given five second interval. In identifying the stream, it was determined that a stream would not be defined as several pixels changing color around the leak component (as viewed on a computer monitor or video screen); rather, a stream, cloud, trail, or plume from the component had to be readily identifiable and larger than the noise or pixilation inherent in the display. Furthermore, the leak had to be seen originating from the leak source. Gas detected elsewhere in the field of view, but not extending back to the leak source, did not characterize a leak.

[3] For the IMSS and mid-wave BAGI cameras, propylene tests were completed on one day, and selected propylene tests were repeated again on a different day. These two sets of propylene tests are separated in the results matrix. Similarly, the long-wave BAGI has two sets of ethylene tests, which the results matrix displays separately.

[4] Epperson, David. L., Siegell, Jeffery, H., *"Equivalent Leak Levels & Monitoring Frequencies for Smart LDAR,"* Valve World 2002, November, 2002

[5] Current federal fugitive emissions regulations allow stakeholders to petition the EPA Administrator to recognize alternative work practices that provide equal or better environmental protection than that resulting from current requirements or methodologies.

- A species was not seen under less rigorous conditions, so the test team did not spend laboratory time testing at higher wind speeds or distances;

- 30 foot test runs were performed on an optional, as-time-permits basis;

- Camera operators believed that certain gas species could not be seen; because they were outside their spectral response range;

- Liquid species had insufficient vapor pressure; and/or

- Limited chemical quantities prevented the completion of the entire test parameter matrix.

Quantification of Leaks Observed with Gas Imaging Devices

While Method 21 does not require that fugitive emissions be quantified, other regulatory programs do require the development of plant-wide emission inventories that include fugitive emissions. The gas-imaging cameras used in this study have not evolved to the point where they can provide a quantitative measure of a gas leak. As a result, mass emissions were quantified during the field study by either bagging components found to be leaking or using Method 21 screening results (which measure concentration) with correlation equations.

During the course of the laboratory evaluation, an effort was made to develop a technique to quantify fugitive emissions detected by the gas-imaging cameras. The test team considered several different approaches. While no approach proved to successful, the information developed may provide a starting point for future studies of quantification.

Field Study

The purpose of the field evaluation was to gain insight into the application of the four optical gas-imaging devices for the detection of fugitive emissions of hydrocarbons from refinery and petrochemical plant process equipment and piping systems. Objectives of the evaluation were as follows:

- Determine the mass emissions rate for various gases that each device could detect under normal refinery/chemical plant operating conditions; and

- Document (as appropriate) the apparent impact of external factors such as distance, angle of view, background objects, hydrocarbon type, and meteorological conditions on the ability of the gas-imaging devices to detect fugitive emissions.

Exhibit ES-1. IMSS test results.

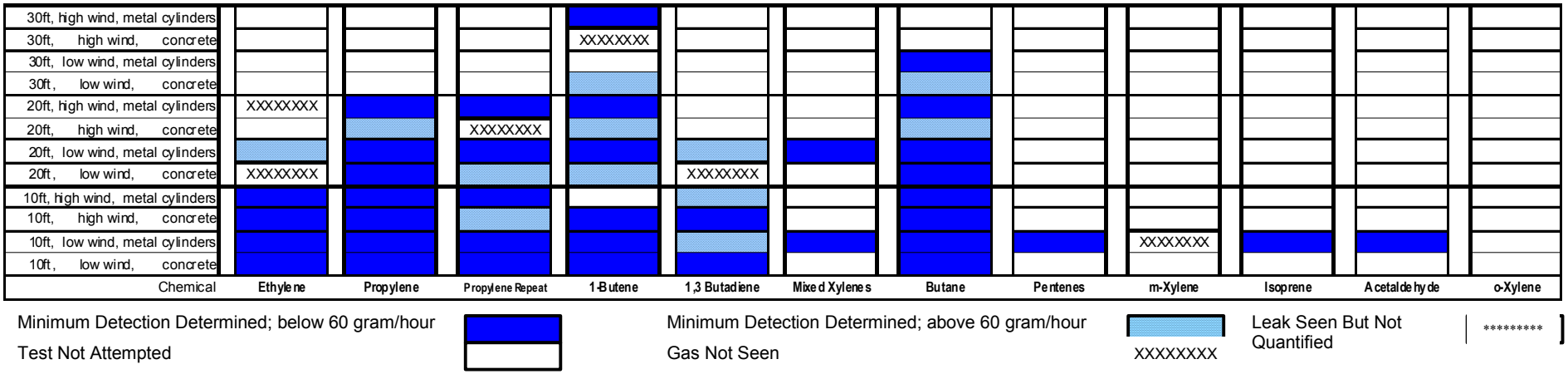

Exhibit ES-2. Long-wave BAGI test results.

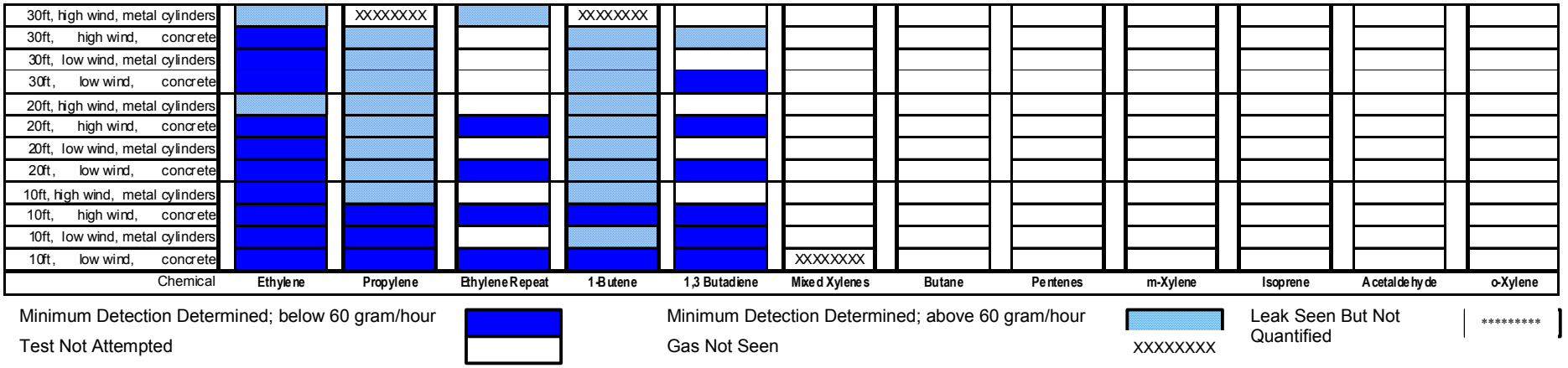

Exhibit ES-3. Mid-wave BAGI test results.

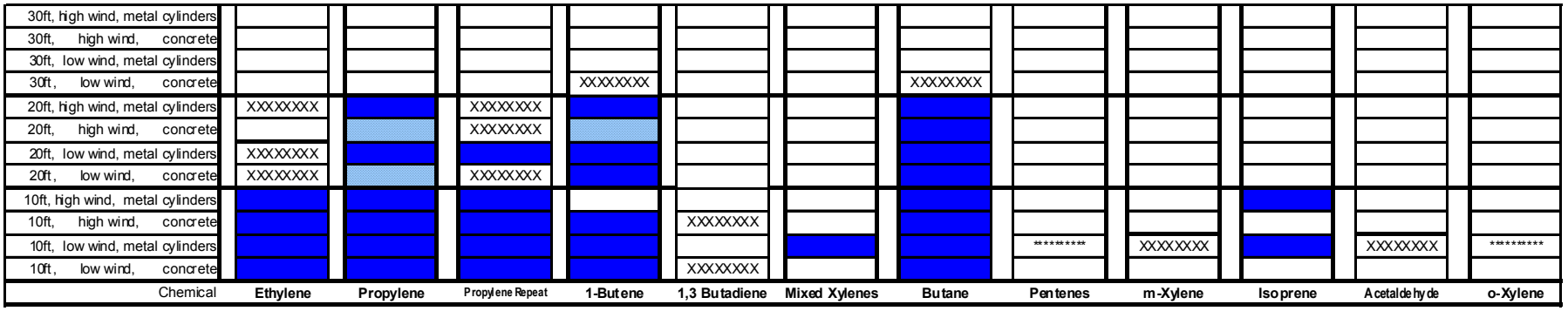

Exhibit ES-4. PIR test results.

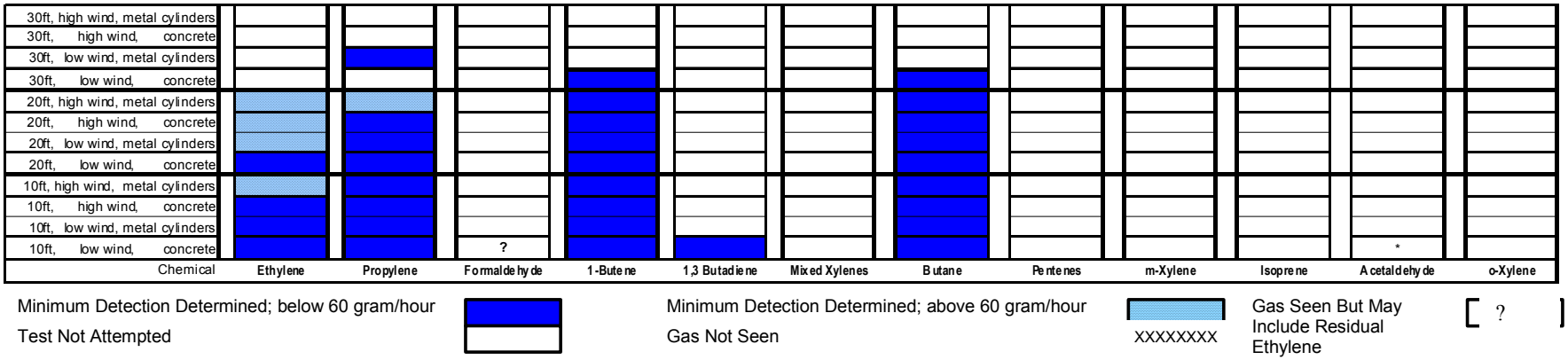

The field evaluation of the four gas-imaging cameras was carried out over three days at Sites C_{04} and D_{04}.[6] On February 2 and 3, 2004, the project team was at Site C_{04} where chemicals such as ethylene, butane/butylenes and hexene were present. On February 4, 2004, the project team was at Site D_{04} where propylene, butylene and 1,3 butadiene were present.

Field Study Results

The field study resulted in the discovery of 66 leaks at the two test sites. The four infrared cameras imaged 31 leaks, while the Method 21/Bagging team discovered 49 leaks. Exhibit ES-5 provides a summary of leaks attributable to each survey method.
As seen in Exhibit ES-5, neither the Method 21/Bagging method nor the infrared camera survey method alone discovered all fugitives at the test sites, and both methods found the same 21.2% of the total discovered leaks (14 leaks seen by both methods of a total of 66 leaks).

Exhibit ES-6 presents the 66 leaks found in the field study with respect to the infrared cameras. The leaks are tallied according to the measured leak rate, with successively larger leaks appearing near the right. The y-axis is a measure of leak count.

Exhibit ES-5. Leaks Discovered by Different Survey Methods.

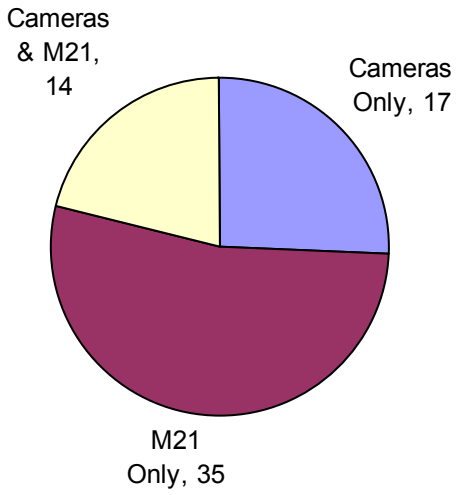

[6] In 2002, a field test to evaluate one optical imaging technology was conducted in the Houston-Galveston, Texas area (HGA) at ethylene facilities designated as Sites A and B. In addition, other field evaluations were conducted in the 2002 study to assess the accuracy of fugitive emissions component counts. These evaluations were conducted at facilities in the HGA identified as Sites C through H. A copy of the 2002 study is available at www.harc.edu/harc/Projects/AirQuality/Projects/Status/H5.aspx. To provide a degree of consistency between the 2002 study and this study, the two facilities used in this study are identified throughout this report as Sites C_{04} and D_{04}.

Exhibit ES-6. Leak Survey Summary by Leak Size.

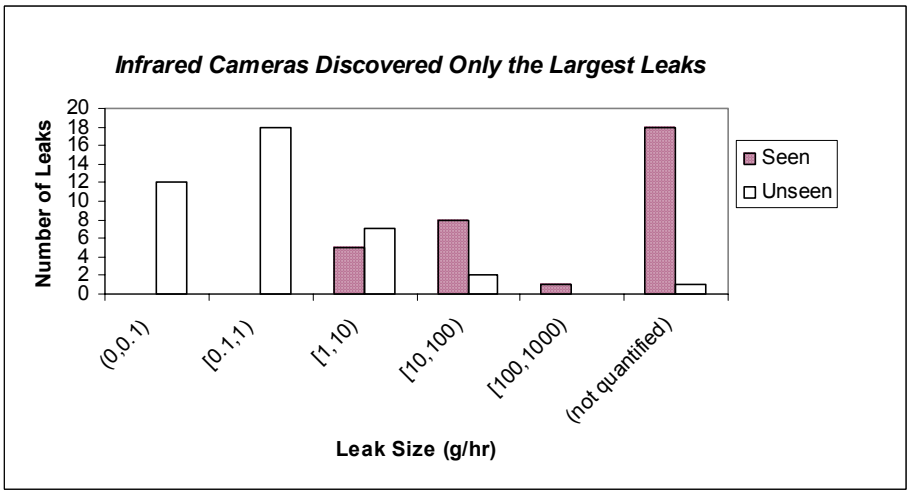

Exhibit ES-6 indicates that the infrared camera survey discovered only the larger leaks. The cameras discovered most of the fugitives emitting 1 gram per hour (g/hr) or higher, and the cameras did not discover any leaks measuring between 0 and 1 g/hr. The right-most column in Exhibit ES-6 shows leaks that were not measured during testing.

Regardless of their size, the cameras successfully imaged all but one of the leaks that are not quantified which supports the conclusion that the infrared cameras do not detect most small leaks but do detect large leaks – the fugitives that are the most prominent source of emissions and the most-effective to repair. The 30 undetected leaks between 0 and 1 g/hr were emitting only 0.6 g/hr, so locating and repairing these leaks gave diminishing benefits compared to the more than 533.9 g/hr imaged by the cameras.

Survey Results by Camera

Exhibit ES-7 is a comprehensive summary of each camera's survey results. The exhibit shows the 49 measured leaks and each camera's performance on surveying the leaks. The leaks shown in Exhibit ES-7 include sources that are predominantly ethylene, butane, hexane, propylene, or butadiene. The y-axis lists the different cameras and is unitless. The x-axis shows measured leak rates on a logarithmic scale, so leaks are progressively larger moving to the right.

The left-most region of the x-axis is reserved for components considered to be non-leaking components. A camera that indicated the presence of a leak from these components, which could not be verified with Method 21, received a "false positive" for that component, and false positives are presented in Exhibit ES-7's zero region.

Hollow data points represent a measured leak that was not detected by a camera, while filled data points represent a measured leak successfully imaged by a camera. The *X* data points represent measured leaks discovered by the Method 21/bagging team but not discovered by any camera.

Exhibit ES-7. Performance Summary of Infrared Cameras.

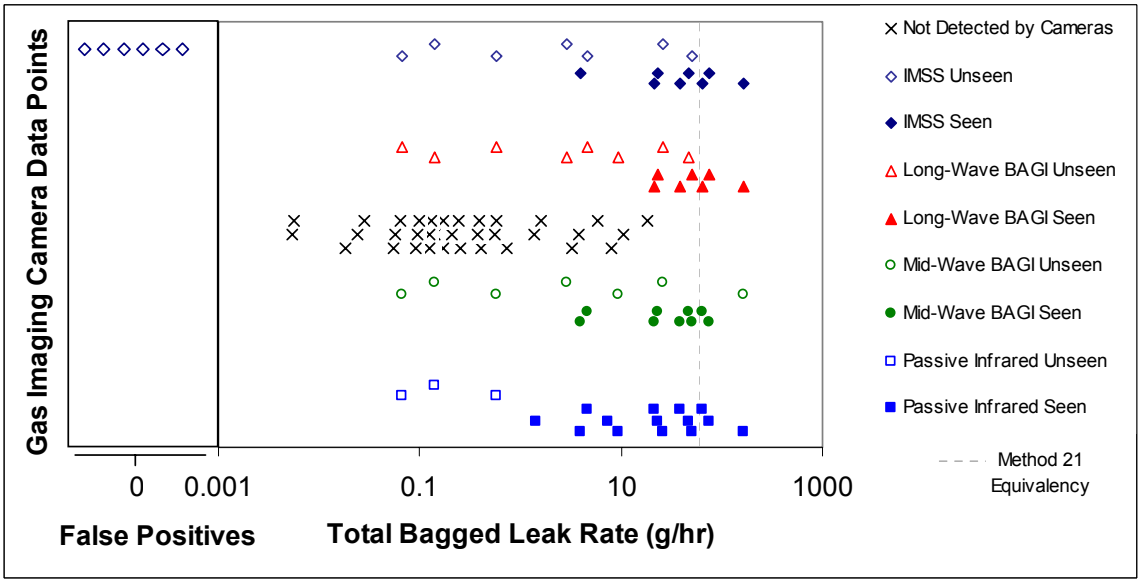

Exhibit ES-7 indicates that the gas-imaging camera survey discovered all of the large leaks, including all leaks at or above the 60 g/hr Method 21 equivalency leak rate. None of the cameras discovered any of the leaks emitting below 1.4 g/hr. Of the 42 leaks at or below 10 g/hr, the cameras detected five. In this field demonstration, the gas-imaging cameras detected 533.9 g/hr of the 595.4 g/hr of mass emissions determined by Method 21 and bagging, or approximately 90% of the bagged fugitive emissions from the demonstration sites.

Exhibit ES-7 also includes a vertical line marking the Method 21 equivalency leak rate for valves and other components. Three of the 49 leaks in Exhibit ES-7 emitted higher than the 60 g/hr Method 21 equivalency. The IMSS, PIR, and long-wave BAGI cameras detected all leaks above 60 g/hr. The mid-wave BAGI camera detected two of the three leaks above 60 g/hr. All four cameras detected numerous emissions sources below the Method 21 equivalency leak rate.

Alternative Work Practice Protocol

The EPA's Office of Air Quality Planning and Standards (OAQPS) is currently in the process of developing an alternative work practice that would allow the use of gas-imaging devices for detecting fugitive emissions. During the course of this project, discussions were held with OAQPS on the status of the EPA's efforts. In addition, the study team contributed comments to EPA on various drafts as they were circulated. The study team participated in these activities to ensure that the protocol developed as part of this study was consistent with that under development by EPA.

Based on the results of work conducted in the laboratory and field studies and discussions with EPA, an alternative work practice protocol for gas-imaging monitoring was developed. The alternative work practice protocol encompasses four distinct areas: instrument specifications, daily instrument check, leak survey procedures, and recordkeeping.

The suggested alternative work practice protocol takes advantage of the experience gained from the various field studies that have taken place over the last several years. Clearly technical and operational issues will arise as gas-imaging devices become more widely accepted by regulatory agencies and used by industry. It is proposed that regulations be adopted that provide the flexibility needed to adjust operating protocols as these issues are addressed.

DEVELOPMENT OF CORRELATION EQUATIONS FOR INDIVIDUAL ETHYLENE/PROPYLENE SOURCES

Activities were conducted as part of this project to gather mass emission rate data for use in developing emission correlation equations specific to highly reactive volatile organic compounds (HRVOC) service components. Using these data, regression equations were developed to predict Mass Emission Rates (MERs) for valves and connectors in all service categories.

Data Availability for HRVOC Correlation Equations

A previous project conducted for the Houston Advanced Research Center (HARC) performed field testing at two olefin manufacturing sites (Sites A and B) that resulted in data that could be used for the development of correlation equations specific to HRVOC service.[7] That study concluded that the data gathered at two ethylene facilities to characterize optical imaging technologies did not adequately cover lower screening value ranges. The work conducted as part of this study gathered additional mass emission data at two olefins-using facilities to complete the data needed for HRVOC correlation equations (identified in this report as Sites C_{04} and D_{04}).

Table ES-1 presents a matrix of the data available for developing correlation equations.

Table ES-1. Data available in required screening value ranges.

Method 21 Monitoring Range (ppm)	Sites A & B		Sites C_{04} & D_{04}		Total	
	Connector	Valve	Connector	Valve	Connector	Valve
1 – 100			4	6	4	6
101 – 1000		2	7	7	7	9
1,001 – 10,000	3	4	6	2	9	6
10,001 – 100,000	7	9	1	1	8	10
> 100,000	4	5	11	5	15	10
Totals	14	20	29	21	43	41

The combined data collected at Sites A through D_{04} are sufficient to develop two correlation equations: one for connectors in all service categories and one for valves in all service categories. All of the minimum values for each screening range, as defined in the EPA's 1995 *Protocol for Equipment Leak Emission Estimates*, were met with the exception of connectors screening between 1 and 100 ppm. Optical imaging did not identify any components in this low range. To

[7] Houston Advanced Research Center. *Measurement and Assessment of Equipment Leak Fugitives in Industrial Ethylene and Other Chemical Sources.* 2003.

address this, some effort was expended to try to find connectors in this range by conducting Method 21 surveys, but only four connectors could be found in this low range without expending an undue amount of time. The total data sets include more than the minimum 30 components, so this small deviation is not believed to compromise the validity of the correlation equations.

Development of Correlation Equations

Regression equations were developed to predict Mass Emission Rates (MERs) based on Screening Values (SVs, EPA Method 21 monitoring values expressed in ppmv). These regression equations had the following form:

$$Y_i = \beta_0 + \beta_1 X_i$$

where:

Y_i = Logarithm of the leak rate determined by bagging equipment piece *i*
X_i = Logarithm of the screening value for equipment piece *i*
β_0 = Intercept of the regression line; and
β_1 = Slope of the regression line.

Base 10 logarithms were used for all calculations.

In addition, a scale bias correction factor (SBCF) was computed according to the method described in the EPA protocol. The SCBF is used in the translation of the regression equation from log space to arithmetic space. The regression equation in arithmetic space has the following form:

$$Y'_i = \beta_0' * X_i^{\beta_1}$$

where:

Y'_i = Predicted leak rate for equipment piece *i* (kg/hr)
X_i = Screening value for equipment piece *i*
$\beta_0' = SBCF \times 10^{\beta_0}$ (β_0 = intercept of the log-space regression line); and
β_1 = Slope of the log-space regression line.

Regression equations were developed separately for connectors and valves. In both cases, two regression equations were developed using

- All the data collected for the subject component type, and
- Only those data pairs for which the screening value was less than 100,000 ppmv.

Table ES-2 gives the regression coefficients and SBCFs for each case and the current SOCMI coefficients for comparison.

Table ES-2. Comparison of TCEQ correlation equations to SOCMI correlation equations.

Case	β_0	β_1	SBCF	β'_0	R^2
Current Report Data					
All connectors	-5.476	0.6573	3.765	1.257E-05	0.577
Connectors for which SV < 100,000	-5.152	0.519	3.034	2.138E-05	0.414
All Valves	-5.423	0.624	2.143	8.091E-06	0.717
Valves for which SV < 100,000	-5.378	0.604	2.109	8.839E-06	0.647
SOCMI Data					
Connectors	-6.434	0.885	8.298	3.053E-06	0.525
Light Liquid Valves	-6.069	0.797	7.520	6.410E-06	0.677
Gas Valves	-6.529	0.873	6.315	1.870E-06	0.715
All Valves[8]	-6.262	0.827	7.351	4.021E-06	0.688

Assessment of Correlation Equations Specific to Ethylene/Propylene Sources

The data collected for components in HRVOC service are adequate to develop emission correlation equations specific to this service. The resulting correlation equations are very close to the SOCMI correlation equations that are already available for emission estimating. Both correlation lines fall within the confidence intervals of the other correlation. A statistical analysis of the HRVOC and SOCMI correlation equations indicates that they are not significantly different.

The HRVOC correlations are of slightly lower slope than the SOCMI correlations, which will cause lower emission estimates than SOCMI for components with higher screening values. Since the majority of mass emissions are known to result from a relatively small group of components with high emission rates, the HRVOC correlation equations should result in a lower overall emission estimate than use of the SOCMI correlation equations.

It is recommended that TCEQ continue to advise facilities to use the SOCMI correlation equations to estimate emissions from HRVOC streams. In the interest of furthering the science of emission estimation, it is also recommended TCEQ forward the HRVOC data to EPA for inclusion in some future update of the SOCMI correlation equations.

If the correlation equations based on the new HRVOC data were to be used, it is recommended that the correlations based on all connector and all valve data be used. The correlations with all data (including components over 100,000 ppm) showed better correlation coefficients and lower mean squared errors, which indicates a better fit of the regression line to the data. The pegged emission factors for connectors and valves can also be used when readings greater than 100,000 ppm are encountered.

[8] The regression for all SOCMI valves (i.e., both gas and light liquid service) was derived from the data given in Appendix B of the 1995 EPA report *Protocol for Equipment Leak Emission Estimates*, EPA-453/R-95-017).

1. INTRODUCTION

In August and September 2000, an intensive field study, called the Texas Air Quality Study (TxAQS), was conducted in the Houston-Galveston area (HGA) to study ozone and other air pollution issues in that region. As part of TxAQS, aerial surveys of chemical species in the atmosphere above the HGA showed higher ozone and ozone-precursor concentrations than would be expected from the emission inventory of volatile organic compounds (VOCs). In a Technical Support Document dated June 5, 2002, the Texas Commission on Environmental Quality[1] noted this discrepancy:

> *"Much of the early analysis focused on why the HGA is different from other areas of the nation. A survey of the area indicates the most striking difference in HGA and other areas of the nation is the extensive refining and petrochemical industry located around the Houston Ship Channel. The HGA produces over half of the chemical and refining needs of the nation. Not surprisingly, the early results have pointed to high levels of VOC emissions from industrial sources in the area; which are much higher than those reported in the annual and special emissions inventories."*[2]

One possible source of unreported emissions from industrial facilities are fugitive emissions. Fugitive emissions are relatively small and hard-to-detect emissions from valve packings, pump seals, compressor seals, and piping connections that occur as part of normal industrial plant operations. They are characterized by a diffuse release of volatile organic compounds (VOCs) or hydrocarbons into the atmosphere.

In June 2003, a project team headed by ENVIRON International Corporation (ENVIRON) was retained by the Texas Council on Environmental Technology (TCET)[3] to manage a project entitled "Development of Emissions Factors and/or Correlation Equations for Gas Leak Detection, and the Development of an EPA Protocol for the Use of a Gas-imaging Device as an Alternative or Supplement to Current Leak Detection and Evaluation Methods".[4,5] The four primary objectives of this project were as follows:

- Evaluate optical gas-imaging devices to determine the detection sensitivity of these devices to detect fugitive leaks of 14 candidate chemicals and to various factors that would be encountered during routine use at petroleum and chemical plants.

---

[1] On September 1, 2002, the Texas Natural Resource Conservation Commission (TNRCC) formally changed its name to the Texas Commission on Environmental Quality, or the TCEQ.

[2] TNRCC Technical Analysis Division, Air Modeling and Data Analysis Section. *Technical Support Document*. June 5, 2002

[3] On June 22, 2003, Texas Governor Perry issued a "Proclamation by the Governor of the State of Texas" that eliminated the Texas Council on Environmental Technology (TCET) as a stand-alone agency. The proclamation stated in part that the TCET "serves a valuable and important purpose, but should be operated by the Texas Commission on Environmental Quality (TCEQ)".

[4] The work documented in this report was performed under TCET Contract No. 02-R04-01G.

[5] In addition to ENVIRON, other project team members include ICF Consulting, URS Corporation, Sandia National Laboratories, Pacific Advanced Technology, Laser Imaging Systems, and Innovative Environmental Solutions.

- Develop and demonstrate the ability of gas-imaging devices to estimate fugitive mass emissions.

- Collect data of sufficient quality to develop emission factors or correlation equations for individual ethylene/propylene sources.

- Develop a protocol for the use of a gas-imaging device as an alternative work practice or a supplement to current leak detection and evaluation methods.

This report discusses the laboratory and field activities conducted by the project team as part of this project and the technical results obtained. The report is organized as follows:

- **Section 2: Background** – In this section of the report, a discussion on leak detection and repair regulations is provided. In addition, the four gas-imaging technologies evaluated in the laboratory and field tests are described.

- **Section 3: Laboratory Evaluation of Gas-Imaging Devices** - Section 3 provides information on the test methods and materials used in the laboratory evaluation of the four gas-imaging cameras studied in this project. Test results obtained in the laboratory evaluation are also included in this section.

- **Section 4: Field Evaluation of Gas-Imaging Devices** – In this section, the results of field studies conducted to measure and detect fugitive emissions using portable optical gas-imaging devices are presented.

- **Section 5: Alternative Monitoring Protocol** – In Section 5, information is provided on efforts conducted in this study related to the development of a protocol for the use of gas-imaging devices as an alternative work practice or a supplement to current leak detection and evaluation methods.

- **Section 6: Correlation Equations for HRVOC Service** – In Section 6, activities related to the gathering of mass emission rate data for use in developing emission correlation equations specific to highly reactive volatile organic compounds (HRVOC) service components are discussed. In addition, the development of regression equations to predict mass emission rates for valves and connectors in all service categories are discussed.

In addition to the information contained in the sections described above, other relevant information to support study results are shown in Appendices.

2. BACKGROUND

Fugitive emissions from refineries and chemical plants have historically represented a large percentage of the volatile organic compound (VOC) and hazardous air pollutant (HAP) emissions from these facilities. In its FY00-01 Memorandum of Agreement (MOA) guidance, the U. S. EPA (EPA) Office of Enforcement and Compliance Assistance (OECA) said that the EPA's Toxic Release Inventory (TRI) database shows that "over 50% of the emissions to the air from refineries come from fugitive emissions." According to the TRI database, these emissions include substances covered under the Clean Air Act's leak detection and repair (LDAR) provisions, as well as Resource Conservation and Recovery Act (RCRA) subpart AA, BB, and CC, and air rules governing emissions from benzene waste handling operations. OECA notes that the TRI data shows that in 1996, each of the 157 U.S. refineries averaged 493,162 pounds of pollution, with 75% of those pollutants coming in the form of air emissions – meaning that roughly 164,686 pounds of pollution are released annually due to LDAR and RCRA-regulated emissions.

Since the late 1970's, federal regulations have existed to control these emissions through the application of Reasonable Achievable Control Technology (RACT) and Maximum Available Control Technology (MACT). The Clean Air Act Amendments of 1990, as well as requirements in a large number of states, require all major sources of VOCs and hazardous air pollutants to reduce fugitive emissions. As a result, nearly all refineries and chemical plants in the U.S. are required to implement a leak detection and repair program (LDAR) to control fugitive emissions.

LEAK DETECTION AND REPAIR PROGRAMS

At present, federal and state fugitive emission monitoring programs are based on EPA Method 21[1], which involves the use of a portable hydrocarbon analyzer to monitor for a leak at the leak interface of equipment such as valves, pumps, compressors, and connectors. Leaks are identified by comparing the hydrocarbon analyzer reading, or screening value, with the leak definition in the applicable regulation. Data gathered from monitoring is then used to determine what actions are needed to decrease and/or eliminate the leak concentration. Generally if a component is found to be leaking, an attempt to repair the component must be completed within a specified time frame. If the component cannot be repaired within this time frame, it must be repaired at the next available plant shutdown.

Under Method 21, an operator is required to visit and screen each regulated component on a defined frequency to determine if the component is leaking. Given the variations in state fugitive emission regulations, and between the federal RACT and MACT requirements, leak definitions for different components and monitoring frequencies can vary substantially, even within the same refinery/chemical plant complex. The actual number of components to be tested in a refinery or chemical plant can be quite large, making Method 21 monitoring both time intensive and expensive – in a typical U.S. refinery with over 200,000 traditional components, the annual

[1] U.S. Environmental Protection Agency, Method 21, Code of Federal Regulations, Title 40, Part 60, Appendix A – Test Methods.

cost for an LDAR program can exceed $1,000,000. Furthermore, a study in 1994 sponsored by the American Petroleum Institute (API) found that over 90% of controllable fugitive emissions come from only about 0.13% of the piping components.[2]

In addition to being costly and labor intensive, Method 21 is limited in its ability to identify all sources of fugitive emissions in a refinery or chemical facility and therefore to provide a full accounting of all fugitive emissions in a facility emissions inventory. In a study conducted in 2003, 23% of the components found leaking during two field studies conducted at ethylene facilities in the HGA were from components not currently monitored under existing federal or state programs.[3] This equipment included manways, heat exchanger heads, insulated components, buried components, sight glasses, and some instrumentation components (such as transmitters).[4] While it is somewhat difficult to accurately estimate the impact on a facility's emissions inventory from these nontraditional components because there are no directly applicable emission factors or correlation equations available that can be applied, rough emission estimates showed that the potential to underestimate a facility's emission inventory ranged from 5% to 18% as a result of the omission of nontraditional fugitive emission components.

OPTICAL GAS-IMAGING DEVICES

As a result of concerns over the cost and effectiveness of Method 21, efforts at finding more productive ways to identify and repair fugitive emission components with high leak rates are underway in both the public and private sectors. An emerging class of technology, generally referred to as optical imagers, offers an operator the ability to monitor traditional and nontraditional components from a distance and identify – in some cases instantaneously – leaking components (of a sufficient mass flux) within the line of sight of the optical imager. The remote sensing and instantaneous detection capabilities of optical imaging technologies allow an operator to scan areas containing tens to hundreds of potential leaks, thus eliminating the need to visit and manually measure all potential leak sites.

In 1999, ICF Consulting was tasked by the Equipment Leaks Project Team of EPA's Common Sense Initiative Petroleum Refining Sub-Committee to investigate and evaluate the new and emerging sensing technologies that might form the basis for alternative work practices under LDAR regulations at U.S. refineries. Their report, published in 1999 and entitled *Compendium of Sensing Technologies to Detect and Measure VOCs and HAPs in the Air*, contained information on technologies that could be considered as candidates for an alternative work practices program in refineries and chemical facilities. The technologies examined by ICF in the report were categorized as follows:

- **Direct Component Inspection Technologies:** This includes technologies that take measurements or operate at the source of the leak. In this category are traditional

[2] American Petroleum Institute. *Analysis of Refinery Screening Data*, API Publication 310. 1997.
[3] Houston Advanced Research Center. *Measurement and Assessment of Equipment Leak Fugitives in Industrial Ethylene and Other Chemical Sources.* 2003.
[4] Components that are not required to be monitored under current federal, state, or local requirements are termed "nontraditional components" throughout this report.

organic vapor analyzers, high flow rate samplers, ring sensors, and VOC detection paints and tapes.

- **Plume Imaging Technologies:** This includes technologies that provide plume images in near real-time or real-time. Backscatter Absorption Gas Imaging and Hyperspectral Imaging systems are in this category.

- **Remote Detection Technologies:** This includes optical remote sensing instruments, such as Open-path Fourier Transform Infrared (OP-FTIR), Differential Absorption Spectroscopy (DOAS), Light Detection and Ranging (LIDAR-DIAL), and Tunable Diode Laser Absorption Spectroscopy (TDLAS).

Table 2-1 shows a number of plume imaging technologies applicable for leak detection and repair programs. These technologies are in various stages of development and commercialization.

GAS IMAGING TECHNOLOGIES INCLUDED IN THE LABORATORY AND FIELD STUDIES

In the laboratory and field studies conducted as part of this project and documented in Sections 3 and 4 of this report, four gas-imaging cameras were evaluated. These cameras were selected for evaluation based on their state of development and the fact that a prototype or commercially available camera capable of laboratory and field-testing was available at the time of this project. Two of the cameras tested are considered active gas-imagers and are based on Backscatter Absorption Gas Imaging (BAGI) technology. The other two cameras are considered passive infrared gas-imagers; one camera is based on Image Multi-Spectral Sensing (IMSS) technology with the other utilizes a cold-filtered passive infrared (PIR). In their current state of development, these technologies can display images of different species of vapor clouds that are invisible to the unaided eye. However, at present these cameras do not quantify the mass emission rate of a leak cloud.

A detailed overview of the active BAGI technologies and the IMSS technology is presented below. A brief summary of the PIR is also provided below.

Active Gas-Imaging Overview

Active gas imaging is accomplished by illuminating a viewing area with laser light tuned to a wavelength that is absorbed by the target gas to be detected. As the viewing area is illuminated, a camera sensitive to light at the laser wavelength images it. If a plume of the target gas is present in the imaged scene, it absorbs the laser illumination and the gas appears in a video picture as a dark cloud. Because it relies on the detection of backscattered radiation from surfaces in the scene, the process is referred to as Backscatter Absorption Gas Imaging (BAGI). Both BAGI instruments used in the laboratory and field studies conducted as part of this project operate in the infrared (IR) -- one in the long-wave IR (at wavelengths between 9 and 11 μm) and one in the mid-wave IR (at wavelengths between 3.1 and 3.6 μm). The terms long-wave and

Table 2-1. Summary of Available Technology Options.

	Laser Imaging System	Sandia National Laboratory	Pacific Advanced Technology	Leak Surveys Inc.	Power Diagnostics Tech. Ltd.	Gas Optics Sweden AB	Ion Optics	Argonne National Laboratory	Block Engineering
Principal of operation	IR	IR	IR	IR	IR	IR	IR	mm-wave	FT-IR
Active or Passive	active	active	passive	passive	Passive (7-11 Microns) Active/Passive combination (3-5 microns)	passive	passive (?)	active and/or passive	passive
Real-time imaging	yes	yes	yes	yes	yes	yes	possible	possible	yes
Status	Commercially available	Portable prototype tuneable laser developed for VOCs; engaged in vendor discussions	Methane leak detector currently being developed; total/specific VOC leak detector is next phase	Commercially available for leak surveys service work	Portable prototype gas-correlation camera for SF_6 developed. Methane camera under development.	Portable prototype gas-correlation using cassegrain telescope and camera for ethylene developed. Methane camera under development.	methane leak detector proposed; seeking DOE or other funding	R&D done, DOE field test performed; technology may be adaptable to smartLDAR; prototype design not started	Commercially available for SF_6; looking to expand capabilities to VOCs
Expected availability	Now	12 to 36 months	6 to 12 months	Now	12 to 24 months	Commercial version Q4 2004	12 to 24 months	12 to 36 months	6 to 12 months
Expected cost/unit	$125,000	$200,000 to $300,000	$150,000	$150,000	$60,000		$50,000 to $60,000	$50,000	?
Advantages			Reflective background not required	Reflective background not required	Cost and reduced sensitivity	Reflective background not required, water/CO_2 interference minimized, species specific detection, volumetrics		Reflective background not required; no interference from H_2O or CO_2	Reflective background not required
Disadvantages	Reflective background required; not tuneable for total VOCs	Reflective background required	Interference from H_2O or CO_2 (?)	Interference from H_2O or CO_2 (?)	Did not image leaks outdoors; Longwave (7 to 13 microns) limits HRVOC detection; No midwave		interference from H_2O or CO_2 (?)		

	Laser Imaging System	Sandia National Laboratory	Pacific Advanced Technology	Leak Surveys Inc.	Power Diagnostics Tech. Ltd.	Gas Optics Sweden AB	Ion Optics	Argonne National Laboratory	Block Engineering
					prototype available; high output infrared light source needed for midwave; overly complicated optics and soflware required to produce false colored plumes				
VOCs tested	ethylene, propylene, 1,3 butadiene, butene, mixed xylenes, SF_6 (non VOC)	aliphatic hydrocarbons 1,3 butadiene, butene, propene, propylene, mixed xylenes, pentene, isoprene, acetylehyde, formaldehyde	methane, ethane, propane, butane, acetone, 1,3 butadiene, butene, propene, propylene, mixed xylenes, pentene, isoprene, acetylehyde, formaldehyde	methane, ethane, propane, butane, Ethylene, 1,3 butadiene, butene, propene, propylene, mixed xylenes, pentene, isoprene, acetylehyde, formaldehyde	SF_6 (non VOC) Methane seen in laboratory testing under tightly controlled environmental conditions.	methane, ethylene, methanol		methylchloride, butanol	SF_6 (non VOC)
Website	www.laserimagingsystem.com		www.patinc.com	www.keaksurveysinc.com		www.gasoptics.com	www.ion-optics.com		www.blockeng.com

mid-wave refer to the two atmospheric "windows" of the infrared, which are defined as regions of the spectrum where there is minimal or no light absorption by oxygen, nitrogen, carbon dioxide, and water vapor that are normally present in air. The major atmospheric windows in the infrared region are found in the 3 to 4.2 micron and in the 8 to 13 micron wavelength regions.[5] An infrared laser beam propagating through the atmosphere at wavelengths within one of these two windows will experience minimal attenuation. Currently, the wavelength ranges of these devices are limited by the laser configuration available at the time of the test.

Figure 2-1 shows how BAGI works.[6] Laser light is transmitted to a hard target where it is backscattered toward the camera, which uses that radiation to make an image of the scene. If there is no gas plume in front of the backscattering surface, the radiation is not (or only slightly) attenuated by the atmosphere between the imager and the surface. If a gas plume is in the beam path, the radiation is attenuated. The contrast between parts of the scene where the gas absorbs backscatter and those without absorption causes the operator to see a gas image. It should be noted that dense particulates in the air, such as the water droplets in steam, could also attenuate the laser radiation and appear in a BAGI image. Since these are also visible to the naked eye (while fugitive gases are not), the BAGI operator can distinguish between the two types of cloud displays. For example, if the cloud can be seen with the unaided eye and with the BAGI camera, the cloud is likely particulates or steam. If, on the other hand, the cloud can only be seen with the BAGI camera, it is likely gas.

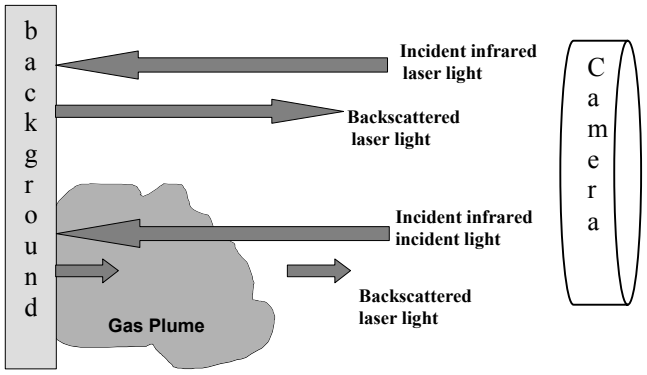

Figure 2-1. Schematic Description of BAGI Process.[7]

Both BAGI systems tested in this project consist of two units -- a shoulder-mounted camera and a power unit. An umbilical cable connects these units. The camera component contains both the laser and the video camera. The operator uses the camera in the same way an ordinary video

[5] This report refers to the 3 to 4.2 micron atmospheric window as the mid-wave region and the 8 to 13 micron atmospheric window as the long-wave region.

[6] McRae, Tom, *GasVue: A Rapid Leak Location Technology for Large VOC Fugitive Emissions*. (Presented at the CSI Petroleum Refining Sector Equipment Leaks Group, Washington, DC, September 9, 1997). For a more complete description, see US Patent # 4,555,627.

[7] Although Figure 2-1 shows the gas in contact with the background material, it is not a requirement that the gas be in contact with the background; the gas plume need only be between the background and the infrared camera.

camera is used – the operator aims the camera at the scene to be imaged and views the image through a video eyepiece. The video signal is also available for display on a separate monitor or for storage on a video tape recorder.

Active Gas-Imaging Detection Discussion

Because an active imager generates a picture by illuminating with laser radiation, its image quality is the same whether performed in daylight or at night. As discussed in more detail below, imaging requires only sufficient backscatter generated by the infrared laser light source, and not passive sources of radiation such as the sun or thermal emission. Thus, active imaging is not affected by the temperature or emissivity of the scene.

In order to produce an image, an active imager requires a solid surface to be present at a relatively close (~30 ft for the cameras evaluated in this project) distance to the camera. The image produced by backscattering from this surface must be bright enough to allow the operator to discern the darkening produced by the gas plume.

In some cases, "clutter" in an IR image (either passive or active) can hinder gas recognition. Clutter refers to the condition where the image contains bright and dark objects that can make it difficult to recognize the presence of an absorbing gas plume against one of the surfaces. Adjusting the camera gain can decrease the intensity of the brightest surfaces— but at the same time, this will cause less reflective background surfaces to appear very dark in the camera image. This creates a tradeoff for viewing a dark gas cloud: the image must be bright enough for the cloud to contrast with the less reflective objects, or the image must be dark enough for the gas cloud to register against the intensely bright part of the background. Figure 2-2 illustrates this concept as it was experienced during laboratory testing with a curved metal cylinder background.

Backscatter is so intense at the apex of the curve that the camera's detector registers at maximum scale

Decreasing the gain puts the apex back on the detector's scale, but darkens the rest of the image

Figure 2-2. Gas Detection with a Highly Reflective Background Object.

Ultimately, the operator must determine whether the image is bright enough for gas detection by viewing it and assessing whether a gas plume would be visible against that surface. If the brightness is not high enough, viewing from a different angle can increase it. In the future, a

greyscale bar could be displayed at the side of the image for comparison to indicate how bright the image must be for successful gas imaging. It should be noted that Sandia has developed an imager (different than that used in this study), which uses differential imaging to increase the visibility of gases in images that are affected by clutter. That device illuminates at two different laser wavelengths (one absorbed by the gas and one not) and ratios the resulting images. This eliminates all contrasts from the scene except that caused by the gas plume, making the gas plume detection much less ambiguous.

The active imager return signal from the backscattering surface falls off in proportion to the inverse of the square of the imaging range. Thus, the maximum imaging range of the active imager is determined by the laser power. It is also determined by the spatial dimensions of the plume relative to the field-of-view of the camera. Resolution of the plume can be assisted by a zoom function built into the camera; however, that is done at the expense of field-of-view and thus, the number of components viewed at one time.

Long-Wave BAGI Camera Description

The long-wave BAGI imager used in this study is a commercially available instrument, manufactured and marketed by Laser Imaging Systems (LIS) under the GasVue® brand. The long-wave camera is applicable for detecting hydrocarbons absorbing in the 9 to 11 micron wavelength region, which includes olefinic hydrocarbons such as ethylene and propylene, SF_6, rocket fuels, NH_3, and CFC's. It is currently used to detect SF_6 at electric power facilities.

The CO_2 wave-guide laser used in the long-wave BAGI system operates in the 9 to 11 micron spectral region at about 1.9 to 2.5 watts.[8] Use of such a relatively low laser power is possible due to the optical arrangement as shown in Figure 2-3, which permits synchronous scanning of a laser beam and the instantaneous field-of-view (IFOV) of an infrared detector across the area of interest. The IFOV produced by the small (.005 cm X .005 cm), cooled IR detector and a collimating lens is scanned in a raster-like fashion across the target area by two scan mirrors, one for horizontal motion and another for vertical motion (in the same fashion as a television picture tube). As shown in Figure 2-3, the laser beam is directed onto, and scanned across the target area by these same two scan mirrors. This ensures that the detector IFOV and the laser beam are in perfect synchronization, and that the laser only need irradiate that region of the target area viewed by the detector. In these long-range systems (>10 m), a beam expander is used to reduce the laser beam divergence so that it is less than the IFOV divergence. This keeps the laser power requirements to a minimum.

The long-wave BAGI imager weighs 23 pounds and is about the size of a TV camera. The camera unit can be connected to a mobile power pack that plugs into an external 110V AC outlet. The power pack converts AC to DC. The long-wave BAGI imager also has video outputs for viewing on a monitor or recording on videotape. Figure 2-4 shows the system during laboratory testing.[9]

[8] US Patent 4,555,627.

[9] The long-wave BAGI camera used for these tests was mounted on a tripod, as shown in Figure 2-4. The power/control unit is shown behind the laptop computer, and an external monitor is shown to the left of the laptop computer.

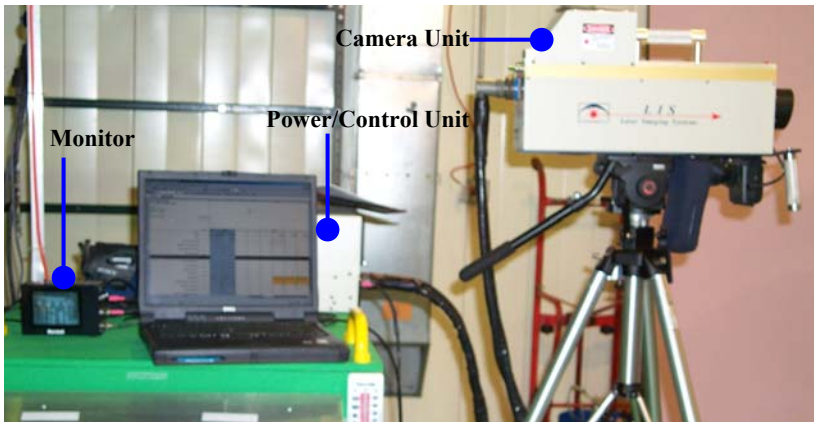

Figure 2-3. CO_2 laser synchro-scan optical configuration.

Source: BP

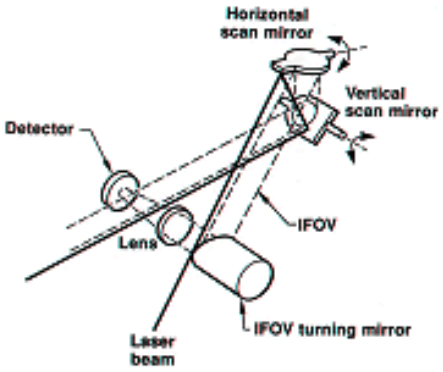

Figure 2-4. Long-Wave BAGI Camera.

The model used in both the laboratory and field tests (GasVue MG-30) is a field-tunable system. The camera calibration data for each gas is provided to the operator by an on-screen display, and the desired gas settings are adjusted by controls on the side of the camera. Field tuning of the camera requires less than two to three minutes. The imager can be operated in a shoulder-mounted position or on top of a tripod. The tripod has a swivel fitting that permits the operator to move the instrument from left to right and up and down while scanning for leaks. The tripod also has wheels that allow it to be easily moved around the process unit area. A zoom lens allows the operator to adjust the focal distance to obtain a tighter field of view.

BAGI Mid-Wave Camera Description

The mid-wave BAGI laser source is effective for VOC emissions at refineries. The laser device is an optical parametric oscillator (OPO), which uses the nonlinear optical crystal periodically poled lithium niobate (PPLN) as its active medium. An OPO is a laser-like device with an optical cavity, which contains a nonlinear crystal (i.e., the PPLN). To operate the OPO, a beam

from a separate laser (the pump laser) is focused into the PPLN crystal. Light from the pump laser is converted by the OPO into two new beams (called the signal and idler) whose frequencies add to that of the pump laser. The basic elements of the PPLN-based imager are shown in Figure 2-5. They consist of the pump laser, the OPO, and the raster scanner.

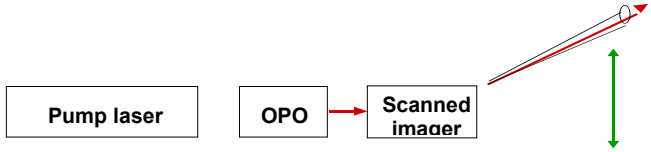

(1) The pump laser creates the initial laser radiation
(2) The OPO converts the pump light to the infrared
(3) The scanned imager creates the laser-illuminated image

Figure 2-5. PPLN Imager Elements.

The mid-wave BAGI imager used in this study emits and detects in the mid-wave atmospheric window. Sandia National Laboratories built this prototype imager using the PPLN laser and a custom-built SSM provided by LIS. The camera portion of the imager plugs into a backpack-borne power/control unit that is powered by a 28V lithium-ion battery. Battery lifetime while the mid-wave infrared laser is operational is between 1 and 1.5 hrs, and batteries recharge in twelve hours. Batteries can be changed without shutting down the device. The mid-wave infrared imager can also be operated on a 110 volt AC outlet through the power unit's 28V DC converter. Figure 2-6 shows the system during laboratory testing.

For the laboratory tests, the mid-wave BAGI camera was placed on a camera bench constructed to accommodate both the mid-wave BAGI camera and the IMSS camera simultaneously. The camera cover remained off for the duration of the tests to allow for adjustments to the crystal position. This allowed the laser wavelength to be changed as different chemicals were tested. A zoom lens on the camera also allowed the operator to adjust the focal distance to obtain a tighter view.

During laboratory testing, the mid-wave BAGI camera experienced laser power fluctuations larger than typically observed in field use of the system. These fluctuations were attributed by the camera operator to the heat produced by the overhead lighting installed to illuminate the target during the test, which were situated approximately 3.5 to 4 feet over the camera when operated at close range, and resulted in various parts of the laser system to heat to the point that they were difficult to handle. The heat caused a mirror in the OPO to misalign, thereby reducing the power of the laser.
Mid-wave BAGI setup time ranged from about 20 to 40 minutes. While the laser wavelength was adjusted between chemicals for these tests, this prototype camera operates at a chosen fixed wavelength during field use.

Passive Gas-Imaging Detection Discussion

Passive gas imaging is based on a complex relationship between emission, absorption, reflection, and scatter of electromagnetic radiation. The IMSS and PIR systems evaluated in this study use photon detection technology that is sensitive to infrared radiation and form an image of the scene such that the intensity is directly related to the number of photon striking the detector. The photons emitted, reflected, and scattered in the scene have a complex radiative transfer phenomenology. VOCs in the vapor phase have unique spectral emission and absorption properties. By measuring these properties, the gas species can be uniquely identified. Both the IMSS and PIR systems tune the instrument's spectral response to the unique spectral region of the VOC, where the IMSS camera has a much finer spectral sampling resolution than the PIR camera. Using this tuned capability, these instruments measure the spectral emission, absorption, scattering, and reflective properties of the gases as the primary means of detecting the signal.

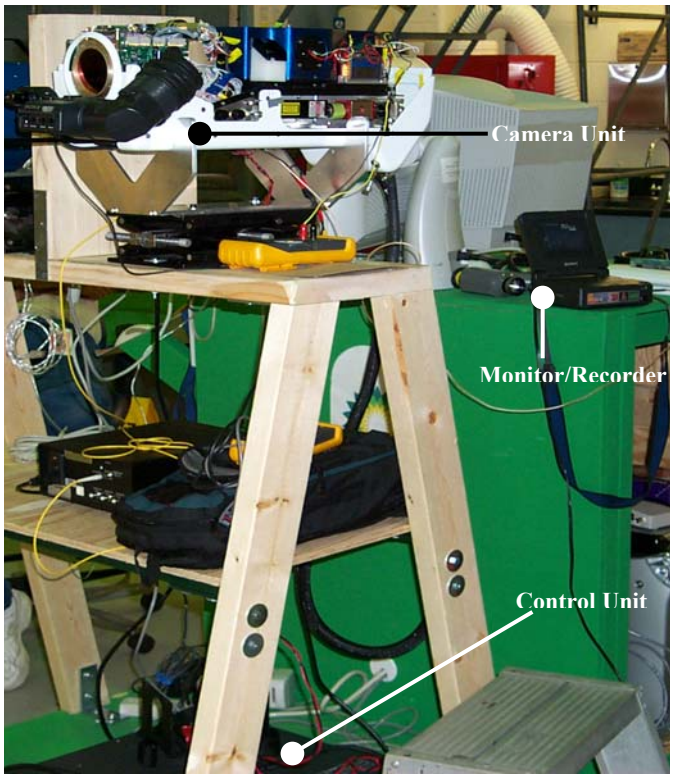

Source: BP

Figure 2-6. Mid-Wave BAGI Camera.

If the optical frequency range of the camera is properly restricted, the camera can make an image of a gas plume. The strength of the image is dependent upon several factors — the concentration-pathlength product, the temperature of the gas, the temperature of the surface behind the gas, and the emissivity of the surface behind the gas. The visibility of the gas depends on a complex phenomenology that is dependent on the spectral emission, absorption, reflection and scattering of the gas and the background, the concentration of the gas within the field of view of the spectral imager, and environmental conditions.

IMSS Technology Overview

Image Multi-Spectral Sensing (IMSS) is a passive infrared technology based on the principal of diffractive optics. As such, it is a combination of a diffractive imaging spectrometer and an adaptive tunable filter. Using a single lens, IMSS performs both imaging and dispersion, producing an imaging spectrometer. The IMSS has a high throughput with a spectral resolution on the order of 6 wave numbers. Its noise equivalent spectral response NESR has been measured at 6 x 10^{-7} w/cm^2 - µm-sr (watts/centimeter squared per micron per steradian).

The basic concept of IMSS is shown in Figure 2-7, where it is compared with a monochrometer or dispersive spectrometer. A conventional monochrometer has an entrance and exit slit and a dispersive element such as a prism or grading. Light coming through the entrance slit is dispersed onto the plane of the exit slit, and the exit slit is scanned through the dispersed light. To obtain fine spectral resolution, the dispersive spectrometer must reduce the size of the entrance and exit slits, and thus reduce the throughput of the instrument.

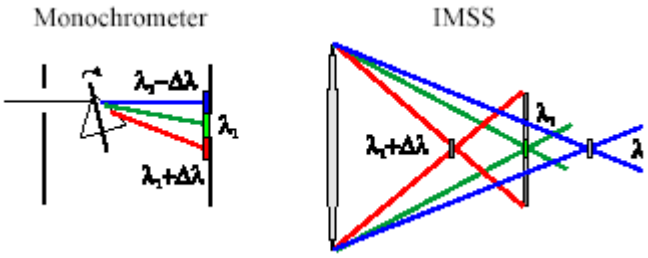

Figure 2-7. Basic Principal of IMSS.

The IMSS uses the dispersive power of a diffractive optic to disperse the light along the optical axis, and the light gathering capability of the lens provides a very high throughput instrument. IMSS uses a single optical element to perform both imaging and dispersion.

The IMSS camera collects spectral images in a band sequential mode as shown in Figure 2-8. Each frame of the camera is a spectral color, and subsequent frames can be different colors if the IMSS lens is scanned along the optical axis; alternatively, subsequent frames can be the same color as demonstrated in Figure 2-9.

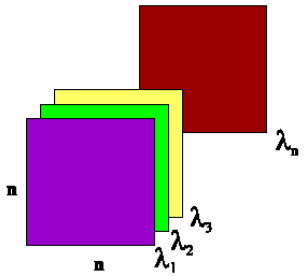

Figure 2-8. IMSS collects band sequential data.

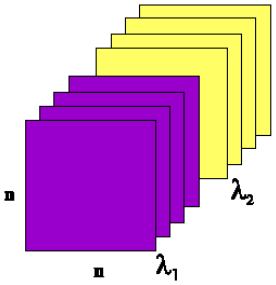

Figure 2-9. If desired, IMSS can collect only those spectral bands of interest.

In this manner, the IMSS imaging spectrometer can collect only those spectral bands of interest, and can also dwell at a single spectral band indefinitely. This adaptability of IMSS is suited for gas leak detection as compared to other spectral imaging techniques that require the collection of all spectral bands within the spectral free range of the instrument, such as conventional dispersive instruments and FTIR spectrometers. For gas leak detection, certain spectral regions are of greater interest than others, and thus there is no need to collect more than the necessary number of spectral bands. This saves time and necessary processing power. This ability also allows the IMSS to be adapted to other applications where real-time spectral processing is of interest.

IMSS Camera Description

The IMSS camera used in this study and shown in Figure 2-10 is a hand-held, battery-operated device that is based on IMSS technology developed and patented by Pacific Advanced Technology (PAT) under U.S. Patents 5,479,258 and 5,867,264. It is marketed under the Sherlock name. The camera weighs 12 pounds (including battery) and is 12(L) x 6(W) x 8(H) inches in size. It is an autonomous instrument, which includes an imbedded processor based on a Power PC, and a Linux operating system; however, the camera used during the laboratory test was controlled from an external PC system running Linux. Keyboard and mouse inputs controlled the camera for these tests instead of the camera's built-in input device.

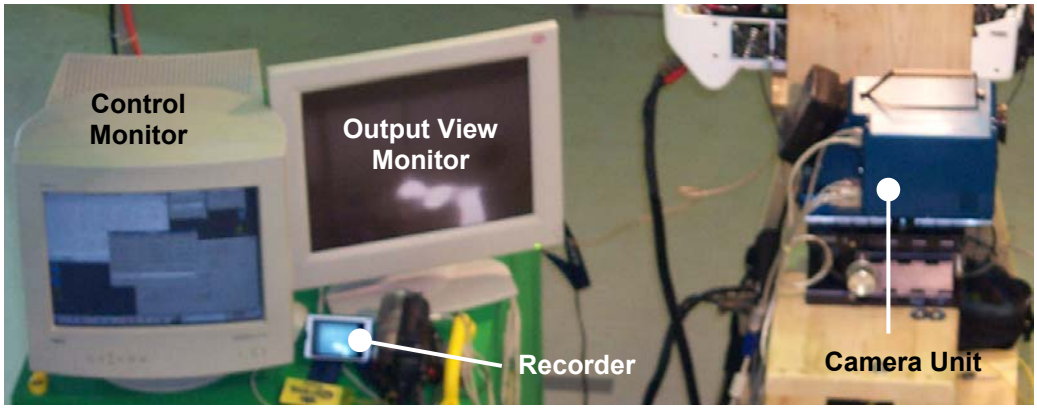

Figure 2-10. IMSS Camera.[10]

Although a small LCD screen can be attached to the camera, the camera output was viewed from an LCD computer monitor for the laboratory tests. The output was also sent to a video recorder. During field tests, the camera output was viewed on a side-mounted imager.

The camera also contains special digital processing circuits with the ability to perform real-time processing algorithms using programmable FPGA. The camera can be controlled remotely over an Ethernet port. An IEEE 1394 FireWire interface allows high-speed data transfer to remote storage media such as FireWire removable drives.

During the field study the camera's operator identified that the main detection algorithm's automatic gain control for displaying leak imagery was not working properly. This resulted in reduced performance and an inability to quickly screen leaks. PAT defaulted to a backup algorithm that generated several false positives and decreased the image quality, resulting in an inability to differentiate a leak from the motion induced (e.g., compressor deck vibration) interferences. According to PAT, it was not intended for this algorithm to be applied in a field environment where there is significant vibration or motion.

In addition, following the field study it was determined that the IMSS camera cold shield was inefficient below 3.6 microns caused by a fault in the lens design for the camera. A re-prescribed leans and a narrow band pass filter have been added to the camera to eliminate stray light and improve overall instrument sensitivity. These changes necessitated algorithm revisions including an increase in the integration time.

PIR Camera Description

Leak Survey, Inc. (LSI) provided the PIR camera used in the laboratory and field tests. LSI commercially operates the PIR camera currently under the Hawk brand name. The camera is built on a modified version of an Indigo Merlin mid-wave infrared camera with proprietary modifications to the base camera. LSI has equipped the camera with a user interface, image

[10] The IMSS camera was mounted next to the mid-wave BAGI camera on a bench during the tests. The camera was controlled through a GUI interface on the CRT monitor as shown in Figure 2-10 (Power PC-based computer not shown in Figure 2-10).

recorder, and LCD display. The display provides a greyscale infrared image of the background, the leaking source, and the gas plume.

The PIR is equipped with a cryogenically cooled infrared wavelength filter. The PIR camera images in a single, proprietary wavelength region. At present, LSI maintains trade secrecy on this technology and therefore no additional technical information was made available. The camera used in the field test was battery operated. LSI currently uses the PIR camera for imaging natural gas leaks.

PRACTICAL ISSUES ASSOCIATED WITH GAS-IMAGING AND EQUIPMENT LEAK DETECTION

One of the basic questions evaluated in this study is whether gas-imaging devices can be used to effectively detect fugitive emissions under conditions typically found in refineries and chemical plants. The results of the laboratory and field tests presented in the next two sections of this report show that the four cameras evaluated in this study were successful, to varying degrees, in positively answering this basic question. Notwithstanding this, certain variables do have the potential, at least theoretically, to affect the ability of gas-imaging devices to detect fugitive emissions. The more significant of these variables are discussed below.

BAGI Technology and Background

As mentioned earlier in this section, an active gas-imaging camera using the BAGI technology requires a solid surface to be present behind the component at a relatively close distance to the camera. When monitoring components in a refinery or chemical facility, it is generally evident whether a solid surface is present within the range of the camera. In some instances, the need for a relatively close background might require the camera operator to reposition the camera to a more appropriate view that includes a background, or position a clipboard or other flat surface behind the component. In other instances, such as elevated process vents or other emission points where the camera is pointed towards the sky and no background is available, a gas-imaging device using the BAGI technology is not suitable.

While a background is needed to image a gas, the type of background may impact the quality of the image. For this study, two types of backgrounds that simulate typical equipment environments in hydrocarbon processing plants were chosen: curved, painted metal surfaces and flat concrete surfaces. The typical “floor” of most hydrocarbon processing plants is a bare concrete surface. The support columns for many vessels and large equipment are similarly bare concrete pillars. Many support beams in pipe racks are coated with a fire protective coating similar to concrete. Virtually all metal pipes, vessels, valves, pumps and connectors in hydrocarbon processing plants are painted for corrosion protection. Two exceptions are stainless steel tubing and sheet metal cladding on insulation. These shiny metal surfaces reflect a BAGI laser light beam either obliquely away from the camera or directly toward the camera, presenting an extra bright streak of the perpendicular surface sandwiched between darker images of the sides curving away. This was graphically represented in Figure 2-2. In the laboratory testing conducted as part of this study where the cameras were set in a fixed position relative to the

curved metal surfaces, this presented some difficulty for BAGI cameras because the leak plume was passing from a dark curvature to the bright streak back to the dark curvature. In a plant environment, this is not expected to be a practical issue; as mentioned above, the camera operator can simply move to different position where the equipment presents a satisfactory image.

Passive Technology and Temperature/Emissivity

While the phenomenology behind passive gas imaging is quite complex, the simple basis of passive infrared (IR) gas imaging is the fact that matter reflects incident radiation (e.g., solar) and in addition radiates IR blackbody radiation at ambient temperatures. Thus, IR cameras can see in the dark (or light) because most surfaces will radiate sufficient IR to make a picture of them. The intensity of the radiation depends primarily on four factors:

(1) Incident radiation reflected from the background;

(2) Thermal emission from the background;

(3) Thermal emission from the gas; and

(4) Background components absorbed by the gas

The temperatures and emissivities of the background and gas relate the thermal components of IR intensity arriving at the camera. When thermal photons (factors 2 and 3) are the dominant components of intensity at the camera and the emissivity of the background is close to that of the gas, then the contrast between the gas and the background intensities will be proportional to the temperature difference between the gas and the background (delta T).

As part of this project, a literature review was conducted on both the theoretical and laboratory/field experimentation that has been reported with respect to passive infrared imaging and the temperature difference required for detection. This review is included as Appendix A. While at times the literature discusses in an offhand or glib manner the term delta T, it should be understood that the "real" criteria for detection is a difference between the radiance of the background and target object.

At the 1995 International Gas Research Conference, the results of a study on active and passive infrared imaging were presented.[11] These results graphically represented the variation of incident or received infrared energy with respect to gas concentration at various gas temperatures and a constant background temperature over a range of 292 to 300 K gas temperature (background at 300 K). The paper showed that the detection of a gas is related to the difference in background temperature and background emissivity and the gas temperature and gas emissivity. Another study indicated that in the cases of gas leaks where the cloud is small, the

[11] Kanagawa, , Toshihide, Hirofumi Ueda, Kohichi Sumida, Takeshi Nishio, "Flammable gas imaging system using infrared adsorption", Proceedings of the International Gas Research Conference, 1995, 1058-1067

temperature of the cloud is relatively homogeneous. In those cases, the primary criteria are the temperature of the target cloud and the effective radiometric temperature of the background.[12]

MEASUREMENT OF MINIMUM DELTA T FOR GAS-IMAGE DETECTION USING PASSIVE INFRARED CAMERAS

To assess the impact of temperature and emissivity on the ability of passive infrared cameras to detect fugitive emissions during routine refinery and/or chemical plant operations, an evaluation was conducted at the BP Laboratory in Naperville, Illinois on the two passive infrared cameras used in the laboratory and field tests. Admittedly, this evaluation was designed to be a relatively simple and straightforward experiment, given operational, budgetary, and time constraints. As such, it was not the intent of this evaluation to rigorously address all conditions that might be encountered in a refinery or chemical plant that might result in situation where there is no difference between the background temperature and emissivity and the gas temperature and emissivity (Δ radiance=0), but rather to address the practical implications of temperature/emissivity on the ability of passive infrared cameras to detect fugitive emissions, given the changing dynamics of a gas as it leaks from a component. The fundamental physics of hydrocarbon separation/combination requires energy input (i.e., temperature and pressure gradients). These pressure vessels provide the fluids and gases in the piping system where leak inspections are required. There is little opportunity for these fluids to equilibrate to ambient conditions.

In the evaluation, two experiments using a copper plate as a temperature adjustable background were conducted. The copper plate was either cooled below ambient temperature or heated above ambient temperature and allowed to equilibrate to ambient temperature. The temperature of the leaking gas temperature during the first experiment was not changed from ambient temperature, while during the second experiment the gas was varied from ambient to temperatures above ambient in an effort to observe a delta T transition within the gas when observed against the uniform background.

Testing was conducted on March 18, 2004 using two IR cameras: the PIR camera provided by Leak Survey, Inc. and the IMSS camera provided by Pacific Advanced Technology (PAT). Detailed information on both of these cameras was provided earlier in this section. During the testing, the PIR camera used a cold bandpass filter with either a 25 or 50 mm lens. The IMSS Sherlock camera used proprietary software for image enhancement and detection. The IMSS camera was limited in its image analysis in the 3-micron region due to a configuration issue. This limitation manifested itself as a bright image artifact that limited detectability due to automatic gain control adjustments.

Experimental Procedure

The configuration of the laboratory was generally similar to that used in the minimum detection level (MDL) evaluations that will be discussed in Section 3 of this report. The IMSS and PIR

[12] Flanigan, Dennis F. "Detection of Organic Vapors with Active and Passive Sensors: a Comparison", Applied Optices, 25(23), December 1986, 4253-4260.

cameras were positioned 10 feet from a leaking valve. A thermal imaging camera was positioned between the two gas-imaging cameras at the same distance from the leaking valve.[13] Figure 2-11 shows the arrangement of a valve with a scored valve seat that served as the leak source. A thermocouple was inserted inside the gas line and terminates near the valve body so that a record of gas temperature inside the gas line could be obtained. As seen in a schematic of the gas distribution system in Figure 2-12, the gas line could be heated to elevate the gas temperature primarily to ensure that the material remained in the gas phase. The initial plume gas temperature was determined using a thermocouple placed immediately adjacent to the leak. Ambient temperature was determined using an additional thermocouple.

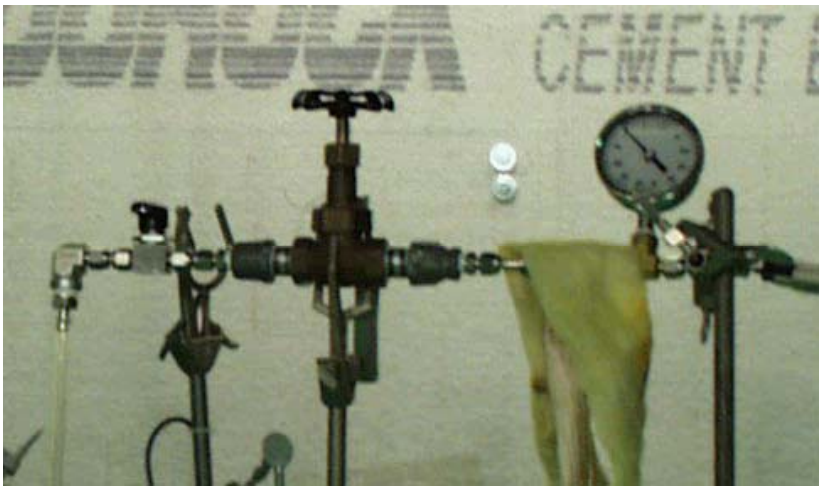

Figure 2-11. Gas distribution valve without thermal insulation.

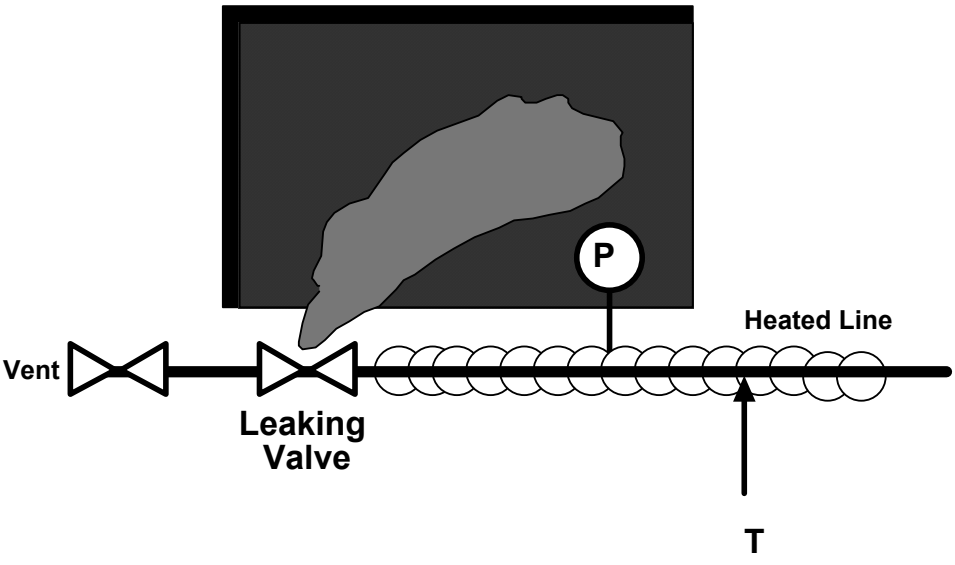

Figure 2-12. Schematic of gas distribution.

[13] The thermal imaging camera used in the laboratory analysis was Merlin by Indigo Systems. The Merlin used ThremaGRAM software. Emissivity was set at 0.95.

In separate experiments, butane and nitrous oxide were leaked from the valve. The leak rate was set at 60 grams per hour using a mass flow controlled system. Nitrous oxide was used because the IMSS camera had an optical arrangement that precluded a more sensitive experiment using butane. Experiments with the PIR camera were conducted using butane as the leaking gas.

A flat black painted copper plate (1/2 inch thick by 18 inches high by 18 inches wide) was used as the background. The emissivity of the copper plate ranged from 0.85 to 0.95. The copper plate was placed in a box insulated on five sides and open on the sixth so that the cameras could observe the leaking gas with the copper plate centered at the leak site. In one experiment the copper plate was cooled below room temperature and allowed to warm up to room temperature. The temperature of the background copper plate was recorded for temperature distribution uniformity and absolute temperature periodically during the upward temperature excursion. In the second experiment, the same copper plate was heated to a temperature above room temperature and allowed to cool to room temperature. The distance from the leaking valve to the copper plate was 49.5 inches and the cameras were placed 10 feet from the valve.

Warming Experiment

The copper plate was initially cooled to 55^{o} F, placed in an insulated box, and allowed to warm to ambient temperature. A typical thermal image, as seen in Figure 2-13, shows the recorded temperature scale on the left of picture. The image shown is taken during the warming of the cooled copper plate; in the image, the copper plate shows as a darker image (cooler than the background) located behind the leaking valve and a pressure gauge (the color scheme and temperature range are selected to highlight the anticipated temperature range of the copper plate).

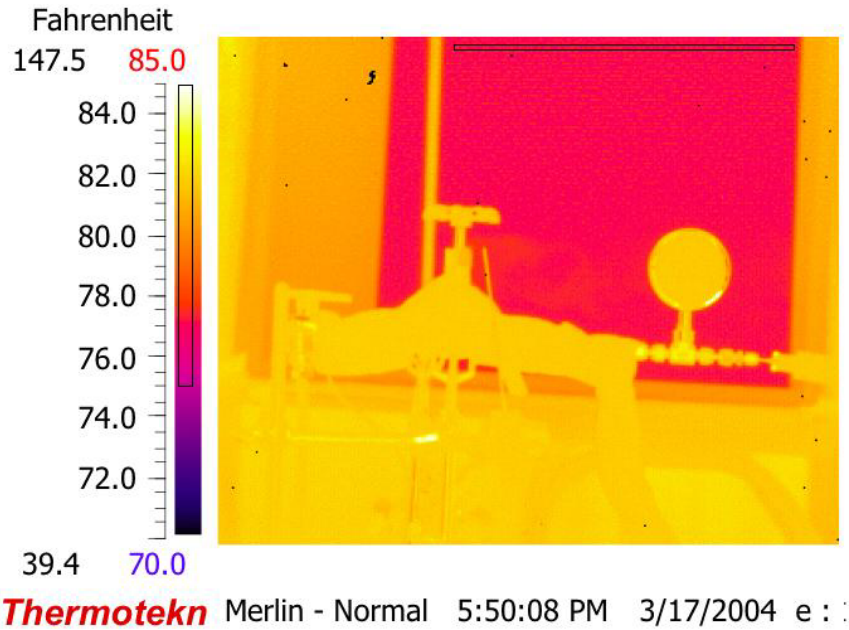

Figure 2-13. The cooler copper block can be observed as a darker image in the middle of the figure. The vertical scale on the left relates color to temperature. The outlined rectangle (75-85 F) captures the color data for calibration. The rectangle outlined at the top of the thermal image provides the data for estimation of the heat distribution across the copper plate.

During the ambient heating of the cooled copper plate (allowing the copper plate to slowly warm to ambient temperature using the heat of the room), no heat was applied to the piping that transferred the gas to the leaking valve. The temperature of the copper plate was recorded using the Merlin thermal imaging camera and an Omega infrared thermometer with emissivity correction (ε=0.95). The temperature of the gas was recorded by three sources: a thermocouple inserted in the gas line and terminating near the valve body, the use of the Merlin thermal imaging camera by placing the cursor at the estimated gas emission point, and a thermistor placed immediately adjacent to the location of the gas leak external to the valve. Table 2-2 lists the instantaneous temperatures recorded during the experiment and a plot of the warming rate is shown in Figure 2-14.

Table 2-2. Instantaneous measurements of copper block warming to room temperature.

		Blackbody Temperature		Gas	
Time*	Time Diff	Merlin	Thermocouple	Merlin	Thermistor
17:07	0:00	71.2	71	72.0	81.3
17:11	0:04	71.9	71	73.4	81.3
17:14	0:07	71.9	71	73.4	81.3
17:16	0:09	72.7	72	74.4	81.3
17:18	0:11	73.0	72	74.4	81.3
17:21	0:14	73.5	73*	75.0	81.3*
17:25	0:18	74.3	74	75.5	81.3
17:29	0:22	74.9	74	75.8	81.2
17:33	0:26	75.3	75*	76.1	80.7
17:36	0:29	75.8	76	76.7	81.0
17:40	0:33	75.9	76	76.8	81.0
17:42	0:35	76.4	77	77.2	81.1
17:47	0:40	76.8	77	77.6	81.0
18:05	0:58	78.0	78	78.4	80.8
18:15	1:08	78.7	78	80.7	78.9
18:28	1:21	79.4	80	79.5	80.8

* Estimated

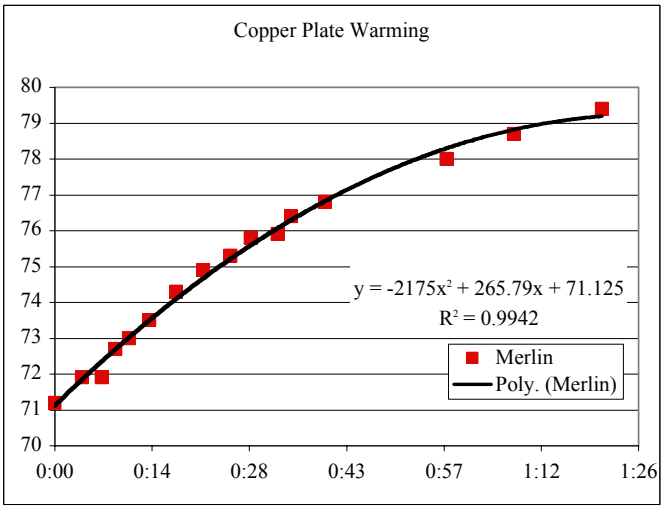

Figure 2-14. Instantaneous temperature measurements made during the warming experiment using the cursor to locate a point near the upper LH corner of the copper plate to register the temperature.

Cooling Experiment

In the cooling experiment, the copper plate was subsequently heated to approximately 110° F and allowed to cool to ambient temperature in the insulated box. A plot of the cooling rate is shown in Figure 2-15. The copper plate temperature was recorded as stated above. The gas temperature was adjusted by heating the tubing leading to the leak. A thermocouple was placed just outside of the gas leak in an effort to measure the gas temperature approximately 1/2 inch away from the valve body. Table 2-3 lists the cooling instantaneous temperatures that were recorded.

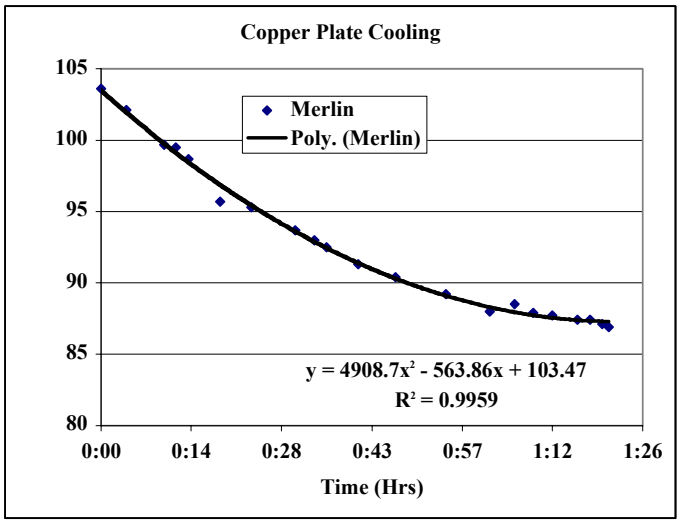

Figure 2-15. Instantaneous temperature measurements made during the cooling experiment using the cursor to locate a point near the upper LH corner of the copper plate to register the temperature.

Table 2-3. Instantaneous measurements of copper block warming to room temperature.

		Blackbody Temperature		Gas	
Time*	Time Diff	Merlin	Thermocouple	Merlin	Thermistor
12:06	0:00	103.6	100	99.5	79.2
12:10	0:04	102.1	99	85.4	79.6
12:16	0:10	99.7	97	83.2	79
12:18	0:12	99.5	96		79.2
12:20	0:14	98.7	96		79.5
12:25	0:19	95.7	94		79.6
12:30	0:24	95.3	93		80.7
12:37	0:31	93.7	93		88.8
12:40	0:34	93	91		90.6
12:42	0:36	92.5	91		85
12:47	0:41	91.3	90		83
12:53	0:47	90.4	90		82.7
13:01	0:55	89.2	89		82.6
13:08	1:02	88	88		83.3
13:12	1:06	88.5	88		84.4
13:15	1:09	87.9	87	89.2	83.4
13:18	1:12	87.7	87		86
13:22	1:16	87.4	85		85.7
13:24	1:18	87.4	85		86
13:26	1:20	87.1	86		86
13:27	1:21	86.9	86		88.1

To provide an indication of the overall uniformity of the temperature of the copper plate, temperature measurements were made using the Merlin thermal camera on the upper left, upper right, lower right, and lower left corners. Table 2-4 lists the four corner temperatures and the time when the temperatures were recorded. The standard deviation of this corner measurement during the warming experiment was 0.2^{o} F and 0.6^{o} F during the cooling experiment.

Table 2-4. Instantaneous corner temperatures as measured by Merlin camera.

	Warming (17:52)	Cooling (13:03)
LH Top Corner	76.4	89.3
RH Top Corner	76.8	88.0
LH Bot Corner	76.4	89.0
RH Bot Corner	76.4	89.1
Average	76.5	88.9
Std. Dev.	0.2	0.6

Thermal Image Analysis

The time/date stamps from the three cameras were recorded so that data could be subsequently sequenced and compared. At specified times, the thermal image of the observed scene was

recorded as a digital image using ThermaGRAM®[14] and an Indigo Merlin camera.[15] A piece of insulation was placed immediately in front of the heated gas lines to minimize the observed temperature range. Shielding the relatively high heat region allowed the use of a smaller temperature range to visualize the heat distribution of the copper plate.

The acquisition software was set so that the temperature scale was typically within 20° F of the ambient temperature. Figure 2-13 shows the typical image that was collected during the experiment involving the warming of the copper plate to ambient temperature. These figures were converted to a JPEG file format and analyzed using ImageJ, an image processing and analysis software written in JAVA.[16] The temperature distribution of the plate can be determined by extracting the color range of the temperature scale on the left (the rectangle drawn) and converting it to a grayscale scalar, and applying this transformation to the grayscale of the remaining image. The discrete data was fitted to a 2nd degree polynomial. A typical calibration is shown as Figure 2-16. The least squares fit for this calibration had an R^2 factor of 0.9956, which was typical of the fits for each of the images used in this report. Calibration of the temperature versus grayscale was determined for each of the thermal images.

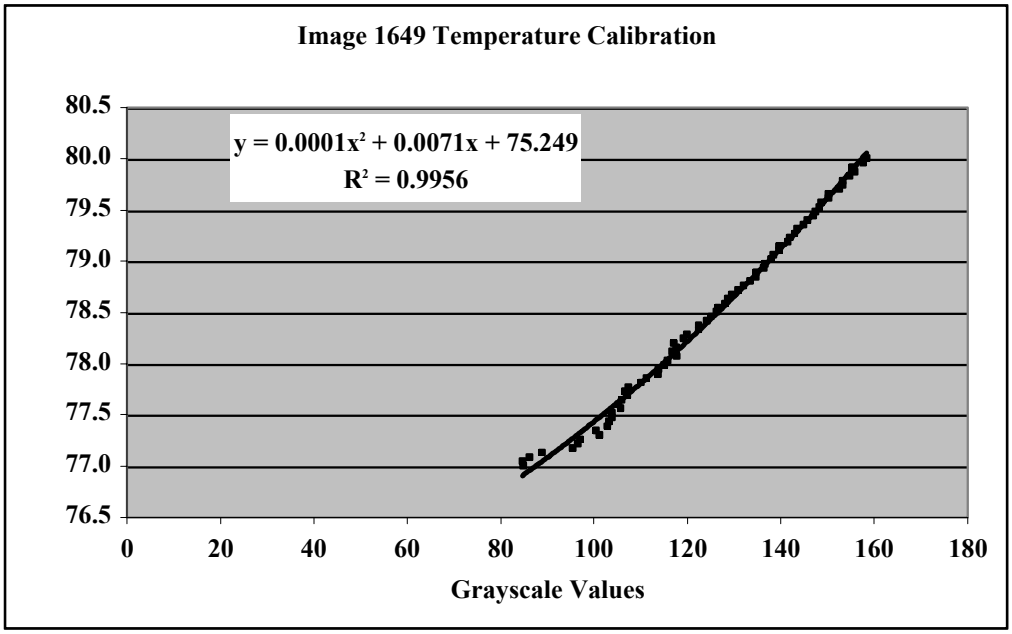

Figure 2-16. Temperature calibration of grayscale values taken from Image 1649.

The average of 140 pixels of temperature information across the top of the copper plate was 76.96° F with a standard deviation of 0.07° F. From the thermal images that were collected during the warming of the copper plate, the average temperatures and the standard deviations are

[14] Real-Time Thermographic Data Acquisition & Analysis, Indigo Systems, Santa Barbara, CA

[15] Merlin Thermographic cameras are factory-calibrated to provide temperature information for each pixel in the array with an accuracy of 2 degrees or 2%. The thermal precision (sensitivity) is typically less than 18 milli-Kelvin. http://www.indigosystems.com/product/merlin_specs.html.

[16] Download from http://rsb.info.nih.gov/ij/download.html.

presented in Table 2-5. The data are plotted in Figure 2-17 with the standard deviation plotted as the y-axis error bars. A polynomial fit of the data has correlation coefficient of 0.9974.

Table 2-5. Image analysis of top of copper plate during warming of copper plate.

Image Nr	Time	Delta Time	Average T (F)	Std. Dev. (F)
59	16:44:35	0:00:00	65.19	0.12
1633	16:45:01	0:00:26	65.11	0.22
1643	17:25:22	0:40:47	74.53	0.19
1645	17:30:09	0:45:34	75.38	0.08
1646	17:36:49	0:52:14	75.91	0.25
1648	17:40:18	0:55:43	76.15	0.05
1649	17”50:08	1:05:33	76.96	0.07
1650	18:08)22	1:23:47	78.45	0.07

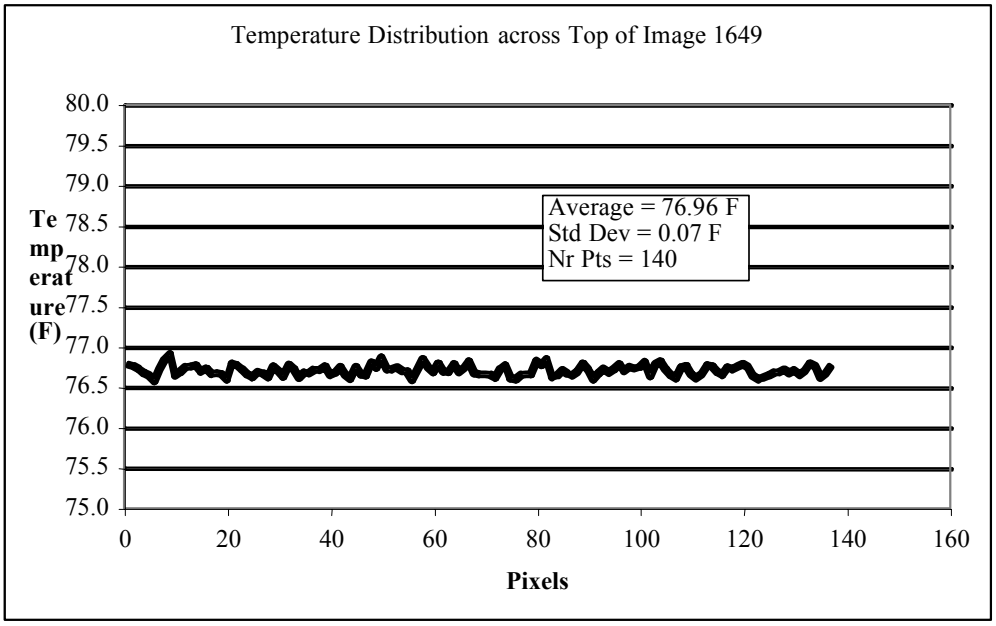

Figure 2-17. Average temperature and standard deviation of the temperature distribution across the top of Image 1649.

One should compare the data in Figure 2-18 with the instantaneous, on-screen measurements that are shown in Figure 2-14. The differences between these two plots may be attributed to the fact that when determining the temperature using image analysis, the grayscale values for which temperatures are calculated represent an average of 10 or so pixels of data while the data contained in Figure 2-14 represent explicit single pixel information.

In a similar manner, the instantaneous temperatures recorded during the cooling of the heated copper plate, which are depicted in Figure 2-15, can be compared to the plotted data of Figure 2-19 where the thermal images are analyzed during the cooling process at the top of the copper plate. Table 2-6 contains the tabulated data from the analysis of the image data.

Gas Imaging Detection

Each of the gas imaging cameras recorded the images at various times during either the cool down or heat up of the copper plate while gas was leaking. In addition, the Merlin camera used in thermographic mode was able to image the plume within a narrow delta T. The passive infrared cameras were able to contrast the plumes exhibiting emission and absorption simultaneously with no noticeable gas between the emitting and absorbing sections relative to the background. The instantaneous images were observed on the video screens. Confirmation of the detection of the gas image was obtained by agreement of at least three observers. The images were recorded on digital magnetic tape (Sony GV-D200 Digital8 video recorder) and processed by the two companies into AVI format (LSI) and WMV format (PAT). The digital movies were captured as individual frames and processed using ImageJ software. Translation from the original images caused some loss of image integrity but an approximation of the detection limits could be obtained.

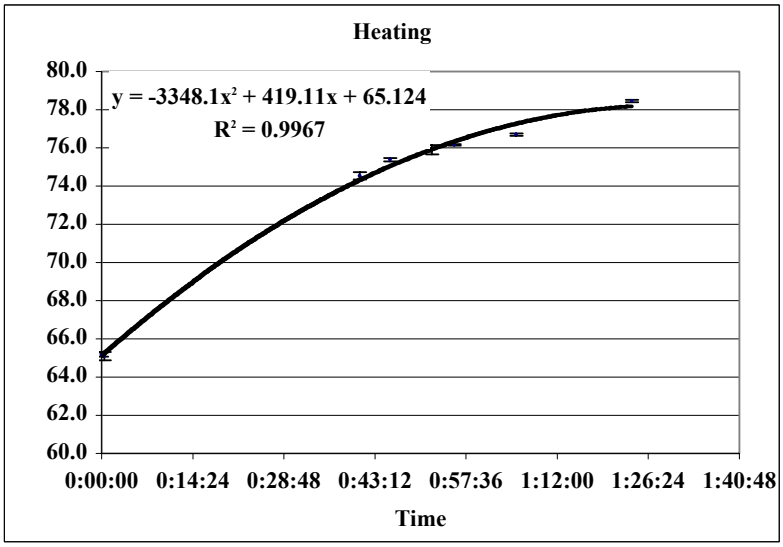

Figure 2-18. Calculated average temperature of the top of the copper plate during the warm-up from a cooled start. Temperatures were calculated from the average temperatures of the thermal images. The error bars are determined from the standard deviation.

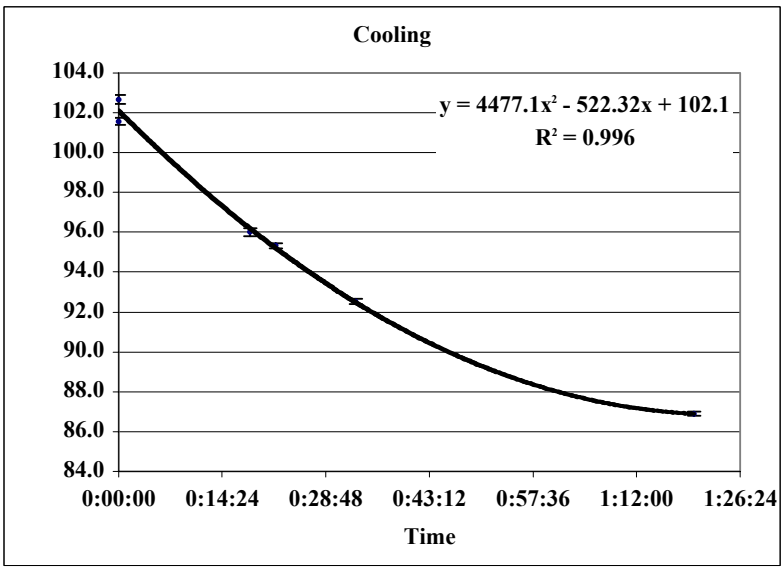

Figure 2-19. Average Temperature of the top of copper plate during cooling to ambient temperature as determined from post experiment analysis of capture images using the Merlin ThermoGRAM software.

The WMV format videos from PAT were not as high quality as the AVI format videos from LSI due to the temporary optical limitations of the PAT camera at the time of the laboratory experiments. Although the PAT images when viewed instantaneously obviously showed a gas image, the digital images used for this report are from the PIR camera. DVD frames captured as BMP pictures provided the best quality for further analysis.

Table 2-6. Image analysis of top of copper plate during cooling of copper plate.

Image Nr	Time	Delta Time	Average T (F)	Std. Dev. (F)
1634	12:08:49	0:00:00	101.56	0.17
1635	12:08:50	0:00:01	102.67	0.22
1636	12:27:05	0:18:16	96.00	0.20
1637	12:30:40	0:21:51	95.32	0.13
1638	12:41:48	0:32:59	92.53	0.13
1640	13:28:48	1:19:59	86.89	0.11

Temperatures were recorded in degrees Fahrenheit. The copper plate temperature was measured using the observed temperatures from the Merlin thermal camera as well as measurements using the Omega optical thermometer. The gas temperature was measured using the internal thermocouple in the gas supply line.

Warming Experiment

Table 2-7 shows the compiled delta temperatures observed from the warming experiment. The gas image (Figure 2-20) was taken from the March 17, 2004 run during the warming of a cooled copper plate. The valve body, thermocouple, and pressure gauge are clearly visible. The image

is from the PIR camera and shows a crosshair, which locates the gas leak at the valve stem. The image was taken 42 seconds into the run. The gas cloud shows as a light cloud (higher temperature) on a darker (colder) background. The image was enhanced following the experiment by adjusting the contrast to highlight the gas plum. Images of the gas cloud were observed as the copper plate equilibrated to room temperature.

Table 2-7. Observed delta temperature during warming experiments.[17]

Time Diff	Copper Plate Temperature	Gas Temperature	Delta T	Gas Image Observed[18]
0:00	71.2	81.3	-10.1	B
0:04	71.9	81.3	-9.4	B
0:07	71.9	81.3	-9.4	B
0:09	72.7	81.3	-8.6	B
0:11	73.0	81.3	-8.3	B
0:14	73.5	81.3	-7.8	B
0:18	74.3	81.3	-7.0	B
0:22	74.9	81.2	-6.3	B
0:26	75.3	80.7	-5.4	B
0:29	75.8	81.0	-5.2	B
0:33	75.9	81.0	-5.1	B
0:35	76.4	81.1	-4.7	B
0:40	76.8	81.0	-4.2	B
0:58	78.0	80.8	-2.8	B
1:08	78.7	78.9	-0.2	B
1:21	79.4	80.8	-1.4	B

As the background copper plate equilibrated to room temperature, the gas plume image was observed on both the LSI and PAT cameras as indicated in Table 2-7, even as the temperature differential between the copper plate and the gas temperature approached 1^{o} F. Each camera recorded the entire warming experiment on digital tape.

Cooling Experiment

Table 2-8 is a compilation of the delta temperatures observed from the cooling experiment. In this experiment, the copper plat was heated above room temperature. Additionally, the gas feed line was heated during the cooling of the copper plate but not held at a constant temperature. An external thermocouple was placed immediately in the gas path approximately 0.5 inches from the valve body to observe the exiting gas temperature. The experiment was modified slightly from the warming experiment described above by removing the valve stem from the valve body to ensure that no potential Joule-Thompson cooling took place even though the gas line pressure

[17] Temperatures were recorded in Fahrenheit. The copper plate temperature was measured using the observed temperatures from the Merlin thermal camera. The gas temperature was measure using the external thermocouple located at the gas leak. Delta T is the temperature difference between the observed copper plate temperature and the observed gas temperature as measure by the thermocouple located at the gas leak.

[18] B indicates that both passive cameras observed the gas image as determined by mutual inspection of the instantaneous images.

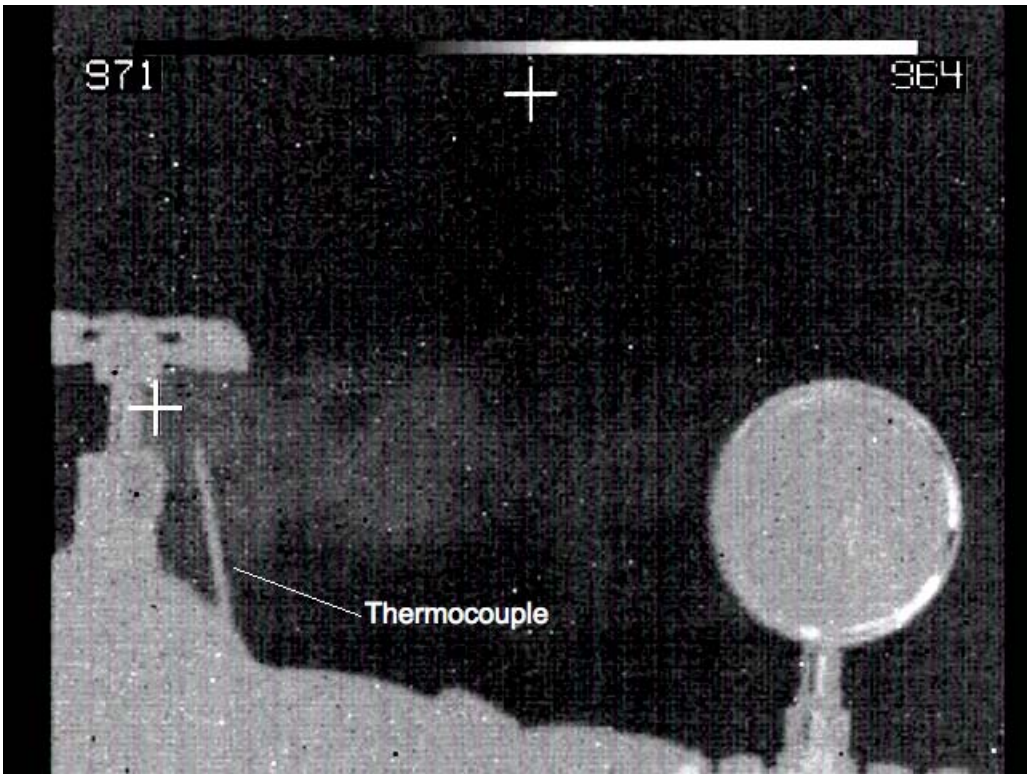

Figure 2-20. Image from LSI Camera with cold background.

never exceeded 1 psi above atmosphere. The gas was allowed to leak through the open 1/4" pipefitting. A thermocouple was positioned in the gas cloud. A piece of rigid insulation was placed between the camera and the heated gas line to minimize observation of the higher temperatures of the gas line by the camera.

Table 2-8. Observed delta temperature during cooling experiment.[19]

Time Diff	Copper Plate Temperature	Gas Temperature	Delta T[20]	Gas Image Observed[21]
0:00	103.6	79.2	24.40	B
0:04	102.1	79.6	22.50	B
0:10	99.7	79	20.70	B
0:12	99.5	79.2	20.30	B
0:14	98.7	79.5	19.20	B
0:19	95.7	79.6	16.10	B
0:24	95.3	80.7	14.60	B

[19] Temperatures were recorded in Fahrenheit. The copper plate temperature was measured using the observed temperatures from the Merlin thermal camera. The gas temperature was measured using the external thermocouple located at the gas leak.

[20] Delta T is the temperature difference between the observed copper plate temperature and the observed gas temperature as measured by the thermocouple located at the gas leak.

[21] B indicates that both passive cameras observed the gas image as determined by mutual inspection of the instantaneous images.

Time Diff	Copper Plate Temperature	Gas Temperature	Delta T[20]	Gas Image Observed[21]
0:31	93.7	88.8	4.90	B
0:34	93	90.6	2.40	B
0:36	92.5	85	7.50	B
0:41	91.3	83	8.30	B
0:47	90.4	82.7	7.70	B
0:55	89.2	82.6	6.60	B
1:02	88	83.3	4.70	B
1:06	88.5	84.4	4.10	B
1:09	87.9	83.4	4.50	B
1:12	87.7	86	1.70	B
1:16	87.4	85.7	1.70	B
1:18	87.4	86	1.40	B
1:20	87.1	86	1.10	B
1:21	86.9	88.1	-1.20	B

The components can be observed in Figure 2-21. At the times indicated in Table 2-8, the detection of the gas plume was confirmed by mutual observation. In Figure 2-21, the gas can be seen as it changes temperatures while mixing with atmosphere (the lighter image shows the gas at a higher temperature than background; the darker image shows the gas temperature to be lower temperature than background). The temperature of the background was 100^{o} F.

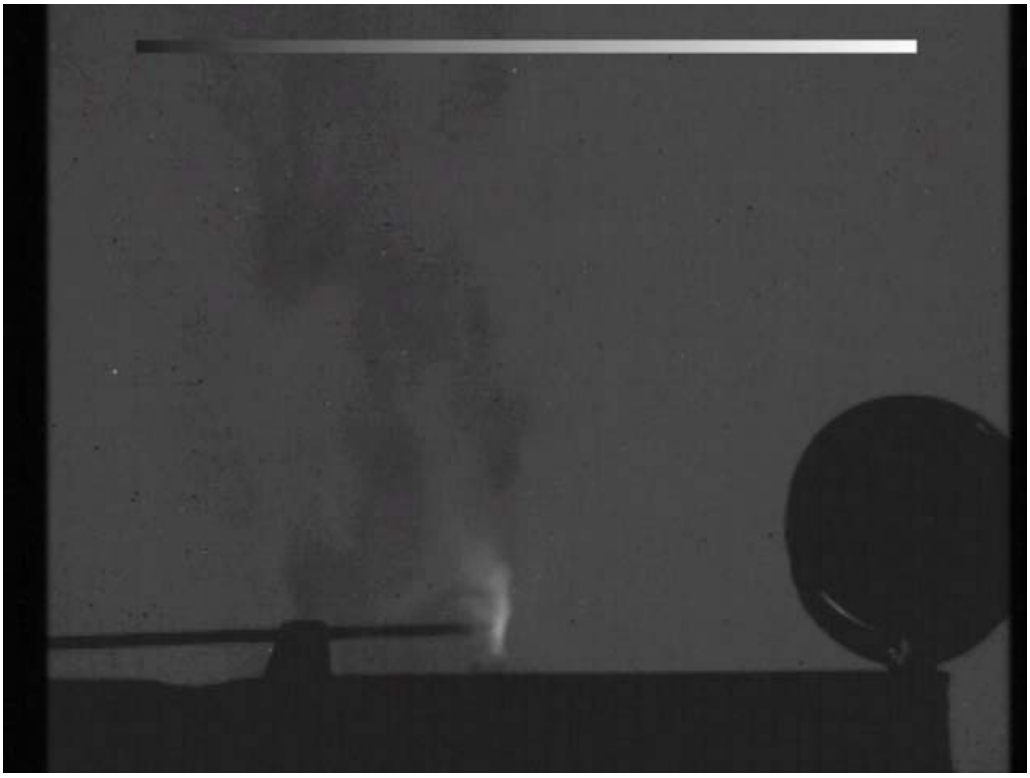

Figure 2-21. Gas image during the cooling experiment.

The image in Figure 2-21 was analyzed using the ImageJ program. The four areas selected to determine the grayscale levels are depicted in Figure 2-22 (identified as A, B, C, and background). The background was determined as having an average grayscale level of 54+/- 9 units. The image had a range of grayscale between 17 and 154 units. Area A was selected to include the light area of the gas plume (hotter than the background) and the darker area of the gas plume (cooler than the background). Subtracting the background from these measurements produced a series of plots contained in Figure 2-23. An approximate linear distance scale (x-axis) was obtained using the diameter of the pressure gauge image as a point of calibration.

For simplicity, only the differential values from the average background are plotted for the background, Area A, and Area B in Figure 2-23. Area A included both hot gas and cool gas (relative to the background). As observed in Figure 2-23, the large positive values for the initial portion of Area A indicates a temperature hotter than the background and the darker areas representing the cooler-than-background gas image observed are represented as negative (below background) numbers. Curve A demonstrates the rapid cooling of the hot gas as indicated by the short distance (approximately 1 inch) between the positive peak maxima and the negative peak minima. This indicates that the gas plume is cooling rapidly from the elevated temperature at the exit to an atmospheric thermal equilibrium in a short period of time/distance. In the plot of Area B, all of the values are below the background average but show two distinct concentrations of gas that are better illustrated in Figure 2-24 where the y-axis is expanded. The lower values in both areas A and B have approximately the same values.

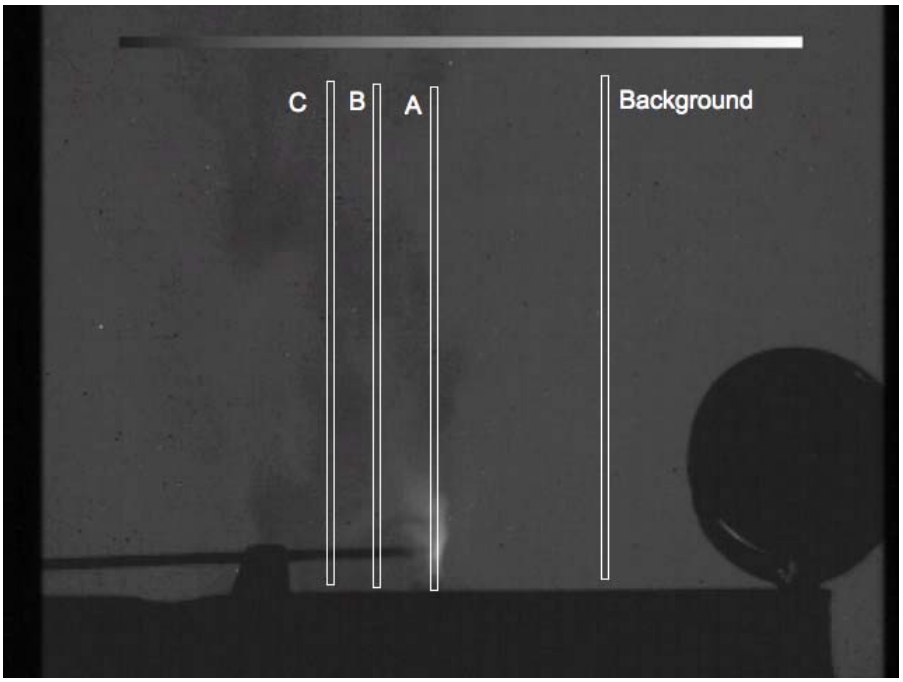

Figure 2-22. Figure 2-21 with areas selected to determine the grayscale level.

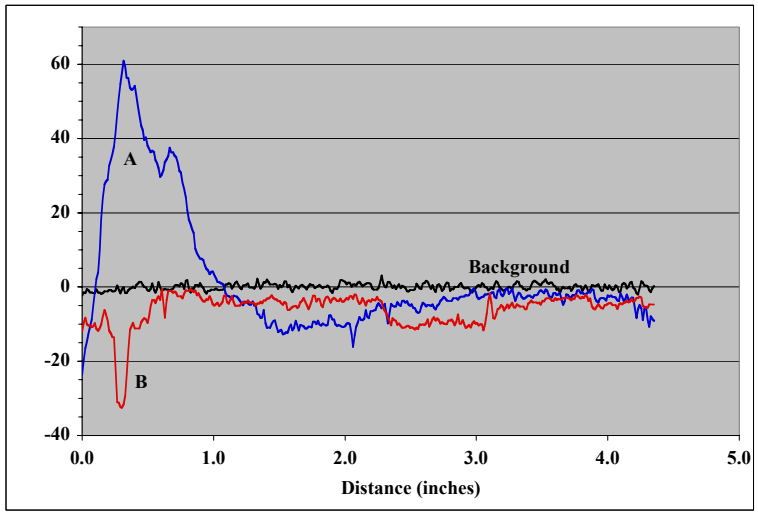

Figure 2-23. Grayscale plots.

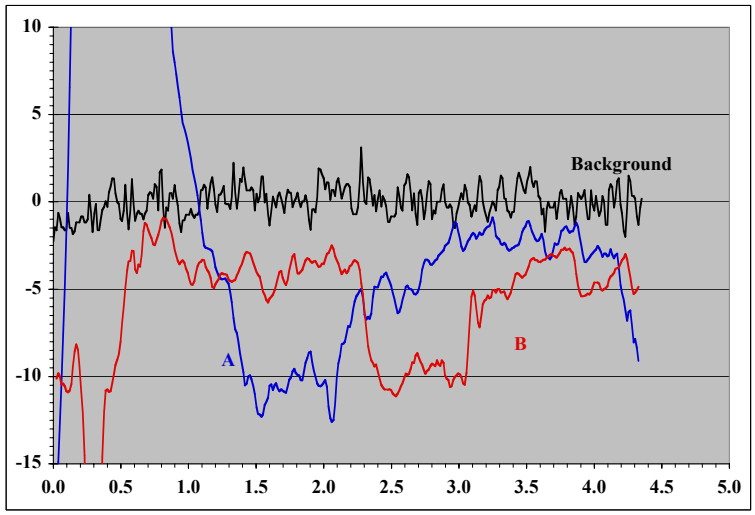

Figure 2-24. Grayscale plots with expanded y-axis.

Conclusions

During both experiments conducted to evaluate the ability of passive infrared cameras to detect fugitive emissions, the gas image was observed at all temperature differentials whether approaching the ambient temperature from below or above. When a heated copper plate was cooled, the gas temperature was adjusted by heating the delivery lines. The observed gas images showed the heated gas cooling during its transit through the atmosphere when the temperature of the gas was higher than the background copper plate temperature. When using a cooler background and a constant gas temperature, the gas could be observed by both IR technologies within a delta T of 1^{o} F. The transition of the heated gas to atmospheric temperature was shown to be rapid and observable with both cameras. The transition of $\Delta T=0$ was shown to be of very short duration and spatially limited.

3. LABORATORY EVALUATION OF GAS-IMAGING DEVICES

In August 2003 and March 2004, laboratory testing of four gas-imaging cameras were performed at the BP Laboratory in Naperville, Illinois. This testing was conducted as part of the project entitled "Development of Emissions Factors and/or Correlation Equations for Gas Leak Detection, and the Development of an EPA Protocol for the Use of a Gas-imaging Device as an Alternative or Supplement to Current Leak Detection and Evaluation Methods" funded by the Texas Council on Environmental Technology.

The objectives of the laboratory testing were as follows:

- Demonstrate the applicability of the gas imaging technologies to detect fugitive leaks of 14 candidate chemical groups:

Propylene	all Pentenes
Formaldehyde	all Trimethylbenzenes
Acetaldehyde	all Xylenes
Isoprene	all Ethyltoluenes
all Butenes (butylenes)	all Hexenes
1,3, Butadiene	all Butanes
Toluene	all Pentanes

- Determine the minimum gas detection levels of the gas-imaging technologies in a controlled laboratory environment.

- Collect data to begin to establish the sensitivity of the gas-imaging technologies to various factors that might be encountered during routine use at a chemical plant or refinery.

The test methods and materials used to conduct the laboratory evaluation on the four gas-imaging cameras are described in this section of the report. In addition, test results obtained in the laboratory evaluation are also included in this section.

GAS-IMAGING CAMERAS EVALUATED

From August 4 to August 15, 2003, three infrared cameras were evaluated. These cameras included:

- Pacific Advanced Technology's (PAT) IMSS passive IR imaging camera;

- Laser Imaging Systems' (LIS) Long-wave BAGI active IR imaging camera;

- Sandia National Laboratory's (Sandia) Mid-wave BAGI active IR imaging camera.

Subsequent to the August 2003 testing, a fourth infrared camera was added to the project. To provide consistent data and results that could be used to assess the capability of all four cameras for use in detecting fugitive gas emissions, testing on Leak Survey Incorporated's cold-filter passive infrared (PIR) imaging camera was conducted at the BP Naperville laboratory from March 15 to 18, 2004.

In Section 2 of this report, a complete description of each gas-imaging technology is provided. In addition, technical information and specifications on each camera is presented in Section 2.

TEST METHODS

In the series of laboratory tests conducted for this project, the gas species, wind speed, background, and distance from the camera to the leaking component was varied to determine the minimum detectable gas flow rate for each camera. The tests followed the laboratory test protocol developed for this project (Appendix B). The matrix of test runs for each chemical included high and low wind speeds (ranging from approximately 1.5 and 4.5 miles per hour), two reflective backgrounds (concrete and painted metal cylinders), and two distances between the camera lens and the leak component (10 and 20 feet). Selected tests were run at 30 feet.

Chemical Priority

Because test time was not available for all candidate chemicals listed above, the TCET gave priority to ethylene, 1,3 butadiene, 1-butene, and propylene.[1] Other candidate chemicals were tested with available test time, and the test protocol designated that non-tested chemicals could draw upon the results of tested chemicals with similar infrared absorption spectra; in other words, some tested chemicals acted as spectral surrogates for non-tested chemicals. The absorbance spectra data for the chemicals tested in shown in Appendix C. Appendix D provides information on spectral surrogates used to reduce the number of chemicals tested.

Test Runs

For each camera, primary data collected for each test run included:

- Gas species;
- Wind speed;
- Background type;

[1] The basis for the TCET's interest in ethylene, 1-3 butadiene, 1-butene, and propylene stems from analysis conducted as part of the Texas AQS. In Rule Log No. 2002-046b-115-AI of Chapter 115 (Control of Air Pollution from Volatile Organic Compounds), the TCEQ states "Analysis showed that plumes stemming from HGA's industrial areas produce ozone very rapidly due to the collocation of large NO_x and VOC emissions from industrial facilities. Initial efforts were focused on the most remarkable findings - that a select number of highly reactive VOCs - ethylene, propylene, and 1,3 butadiene contributed to very large portions of reactivity observed airborne samples, and were previously underreported in the emissions inventory used in the December 2000 HGA SIP".

- Camera-lens-to-leak-component distance; and
- Camera's minimum mass detection level if the gas species could be seen.

Immediately following a test run, a detection test was conducted at two-thirds the leak flow rate of the determined minimum detection level. This QA/QC measure helped to ensure the minimum detectable leak rate was determined accurately.

Minimum Mass Detection Level

The minimum mass detection level was determined for each camera and each test run by the assigned QA/QC test team member. In developing the test protocol, it was determined that although the detection level may vary based on individual perception, having one test team member determine the detection level for all runs helped to ensure consistency in the test results.

Gas detection for a camera was defined as a stream of gas seen exiting the component within a given five second interval. In identifying the stream, it was determined that a stream would not be defined as several pixels changing color around the leak component (as viewed on a computer monitor or video screen); rather, a stream, cloud, trail, or plume from the component had to be readily identifiable and larger than the noise or pixilation inherent in the display. Stray, infrequent puffs more than five seconds apart, or several flashing pixels did not constitute a leak. Furthermore, the leak had to be seen originating from the leak source. Gas detected elsewhere in the field of view, but not extending back to the leak source, did not characterize a leak.

Gas Detection

For the two BAGI cameras, detections were made by identifying a gas plume, cloud, stream, or trail to the right of the leak source (directly downwind of the leak source). For the IMSS and PIR cameras, detections were made in a similar fashion to the BAGI cameras by identifying gas directly to the right of the leak source. Additionally, all four cameras imaged gas directly at the leak source, showing a concentrated plume at the valve stem. Thus, leak detections occurred either at the source or immediately downwind of the source.

Repeatability

To determine the repeatability of the minimum detection level determination, a test under low wind speed conditions with a concrete background and a distance of 10 feet from camera lens to the component was conducted three times for each chemical. These tests were inserted at different points during each camera's test matrix rather than conducting the same test in three sequential runs.

Additional Tests

In addition to the test matrix defined in the laboratory test protocol and followed by each camera, several other tests were conducted to address various technical points of interest. These additional tests included the following:

- Field of view tests at 10, 20, and 30 feet were conducted on each camera to determine the camera's horizontal viewing capabilities at different distances.

- Tests were conducted on the long-wave BAGI camera to gather data that could be used to evaluate the capability of the camera to quantify mass emission rates as required in Task 4 of this project. Using ethylene, video recordings were taken at six different measured leak rates with the intention of comparing video footage to estimate mass emissions.

- An informal lighting test was conducted using the long-wave BAGI camera. In this test, the laboratory lighting was turned off; no minimum detection level data was recorded. Based on tests results, no effects on leak detection were observed under lights on or lights off conditions. No similar tests were conducted on the IMSS, long-wave BAGI, or PIR cameras.

Appendix E contains additional information on the test materials and methods including other secondary data collected for each test run. In addition, information on test equipment details and other quantitative test observations are included in Appendix E.

Additions and Deviations to the Test Protocol

During testing, several additions and/or deviations were made to the test protocol as a result of conditions or events that were encountered during the two-week test period. These are discussed below:

- In August 2004, testing was completed on three cameras. To accommodate the three camera teams, laboratory testing took place over a two-week period. During the first week, testing on the long-wave BAGI camera took place. The mid-wave and IMSS cameras completed the test matrix together during the second week.

- Since the PIR camera is capable of imaging gas with different types of lenses, the standard chosen for these tests was the camera's 50 mm lens. Additionally, selected tests were repeated using the higher-powered 100 mm lens to demonstrate the effect of stronger lenses on the minimum detection limit.

- As discussed in Section 2, the long-wave and mid-wave BAGI cameras both have a zoom feature. During the first week of testing, it was decided that a camera would not be allowed to use its zoom feature to determine minimum detection levels. Notwithstanding this, several test runs were conducted on the long-wave BAGI camera in the zoom mode. During the second week, the mid-wave BAGI camera was initially tested without using its zoom. In discussions between the project management team and the BAGI camera operators, it was determined that the zoom feature was used routinely in plant operations as a way to better identify components. As a result, a modification to the test plan was made allowing the zoom feature to be used in the test matrix. The implication of this change in test methodology is that minimum detection levels are not directly comparable between cameras.

- In addition to the modification allowing the use of a camera's zoom feature, several other factors prevent direct comparisons between cameras. These factors include:

    - During the August 2003 testing, test rotameters were changed resulting in one camera using one set of rotameters while the other cameras used a second set. For the March 2004 tests, the series of rotameters used to measure gas flow was replaced with an Environics model 4040 gas dilution and flow system.

    - Ambient conditions varied slightly between the first and second weeks. Information on the ambient temperatures and humidity measured in the laboratory during the August 2003 test are included in Appendix E.

    - Ethylene tests with the long-wave BAGI were run at a different set of wind conditions than tests with the other two cameras.

    - During the August testing, a leak in the gas delivery system occurred and was undetected for several test runs. This may have caused larger detection level measurements that what was actually seen.

  As a result of these factors that prevent direct comparisons between the cameras, it is noted that while this report provides performance results of individual cameras, the results are from independent camera test conditions.

- The gas delivery lines were heated throughout the testing to prevent less volatile chemicals from condensing in the delivery system. To assess the potential impact on minimum detection levels, the mid-wave BAGI and IMSS cameras completed propylene tests twice, once with heated lines and once without. Propylene was used, as it was volatile enough to remain a gas without additional heating. While not explicitly addressed in the test protocol, the use of heated delivery lines was discussed among test team participants prior to laboratory testing.

- During the first week, testing commenced using the two wind speeds specified in the protocol: 2.0 mph and 6.5 mph. After completing all ethylene runs, the test team decided that the upper wind speed was impractical and not likely to be found in field observations. As a result, wind speeds were revised to 1.5 mph and 4.5 mph. These new wind speeds were used for the remainder of the test runs.

TEST SETUP AND FACILITY

Figure 3-1 shows the orientation in the test facility of the leak component, camera cart, backgrounds, airflow system, and gas delivery system. In the figure, diamonds indicate the location of instrumentation used to collect data; red lines indicate heated/insulated gas lines.

Backgrounds – Curved Metal and Concrete

To simulate the curved metal piping found in refineries and chemical plants, four blue Helium gas cylinders from AirGas were placed side-by-side on a wooden platform twelve and three quarters (12 ¾) inches above the floor.[2] As Figure 3-2 illustrates, the cylinders were 9" in diameter, and the base was 49" high. On top of the base, the nozzle (top) part of the cylinder was 10" high. The cylinders were 48" away from the leak component.

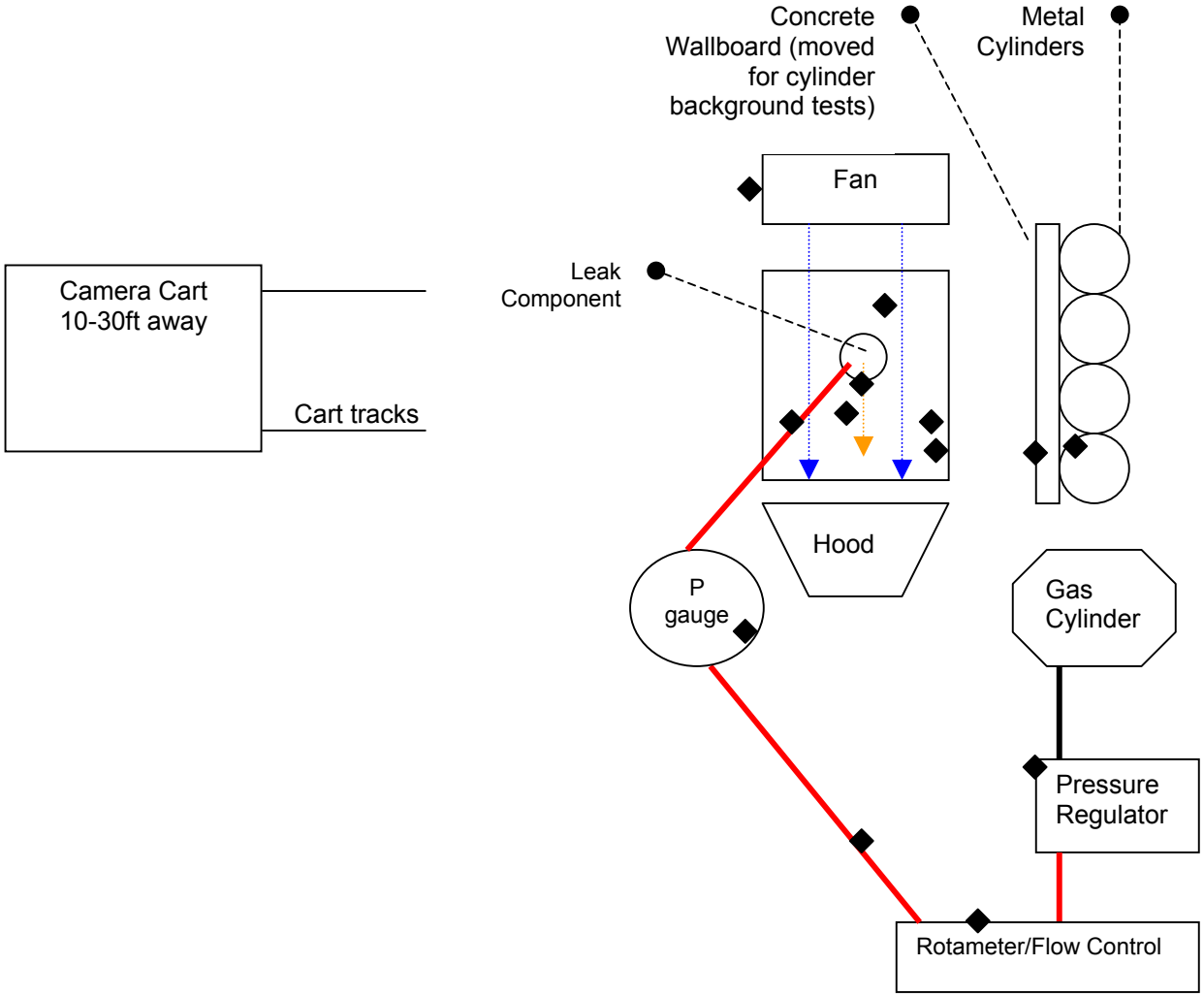

Figure 3-1. Test setup.

In addition to curved metal pipes, refinery and chemical processes also include flat surfaces. To simulate these surfaces, a 36" x 60" Durock brand cement board was hung in front of the metal cylinders for test runs using the concrete background. A 7.5" wooden block was used to keep the wallboard angle the same throughout the tests. The block was placed perpendicular against the cylinders and the wallboard until it could fit between them without dropping to the floor.

[2] During the March 2004 testing, the four metal cylinders used during the August 2003 testing were replaced with cylinders of the same dimension but with a lighter, green-blue paint.

To hang the wallboard in front of the cylinders, it was necessary to attach three bolts to the board, and three metal washers that secured the bolts were visible behind the leak component. On August 12th, the washer directly behind the leak component was removed, and the bolt directly behind the component was covered with non-reflective tape. The wallboard was 40" away from the component.

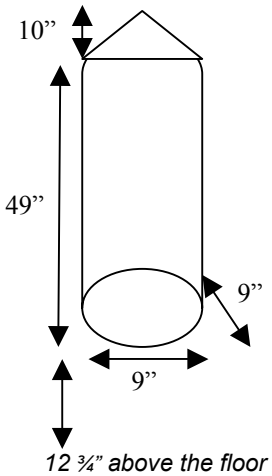

12 ¾" above the floor on a wooden stand

Figure 3-2. Metal cylinder.

Airflow

To generate constant wind speeds for the test runs, a fan with a "flow homogenizer" was used. The flow homogenizer consisted of a wooden frame placed in front of the fan and completely filled with 2-inch diameter PCV pipe approximately 7-inches in length. The purpose of the flow homogenizer was to limit rotational airflow caused by the fan.

An exhaust hood was mounted vertically, downstream of the leak component, to capture leak gas in the same direction as the fan blew the leak gas. These can be seen in Figure 3-3. With the fan turned off, the airflow at the throat of the exhaust was 3.9 to 4.0 mph. With the fan off, the airflow at the leak component was less than 0.1 mph. The exhaust remained on for the entire test period. The lab exit to the outside was closed for all test runs. It was observed that opening a door leading to a control room caused fluctuations in wind speed so entering/exiting the lab was avoided during data collection.

Leak Component

The leak component used during all test runs was a valve with the stem packing removed. The valve was taped and marked with permanent marker to assure that the leak remained constant across different runs. An external thermistor was attached to the back of the valve for the second week of tests beginning on August 11th. The valve height above the floor was measured at 62.25" to 62.75" several times during testing.

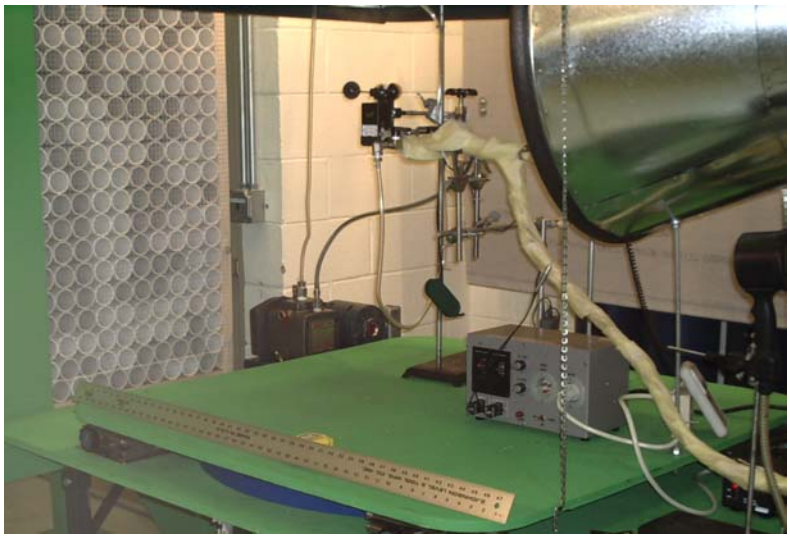

Source: BP

Figure 3-3. Airflow.[3]

Camera Positioning

The cameras were placed on a camera cart mounted on a cart track (Figure 3-4). The track was setup to run perpendicular to the leak component's wind path. The cart could be positioned between about 5' to 35' from the leak component.

A tape measure was run along the floor next to the camera cart track with the 12" tape measure mark directly under the leak component. On the cart, the external camera lens was positioned about 12" from the front of the cart; therefore, the tape measure reading at the front of the cart corresponded to the distance between the external camera lens and the leak valve.[4] A laser level was attached to the front of the cart with the laser pointing downward, and the cart was positioned by aligning the laser mark to the floor tape measure.

For the first test week, the long-wave BAGI camera was mounted on a tripod; the tripod was not adjusted for the duration of the tests. The tripod legs were placed in depressions drilled into the camera cart so that the tripod location would be constant for each test run. At the start of each test day, verification was made that the external camera lens was 12" from the front of the cart. When the camera was attached to the tripod and the tripod was placed on the cart, the center lens height from the floor equaled 63.4".

[3] The fan (not pictured in Figure 3-3) is behind the flow homogenizer. The metal straight edge between the flow homogenizer and the hood is 48" long and is included for scale.

[4] For the BAGI systems, the external lens is a cover/protector, and the optical, internal lens is about six inches behind the external lens inside the camera unit. The IMSS camera also has external and internal lenses, but the distance between the two lenses is different. This test measured from the external lenses. This document refers to the external lens unless otherwise specified.

Source: BP

Figure 3-4. Camera cart and cart track.

A bench was constructed to support the mid-wave BAGI and IMSS cameras simultaneously, where one camera received the portion of the bench to the left of the leak component, and the other camera received the portion of the bench to the right of the leak component. The mid-wave BAGI camera's position on its side of the bench was altered during testing to better view the leak against the metal cylinder background. The mid-wave BAGI camera lens was between 12 to 12.5" from the cart edge and the IMSS camera lens was between 13.5" to 15" from the cart edge as measured several times during the test week.

Lighting

Two banks of lights were used in the test setup; these lights were selected for approximation of mid-wave solar spectra. The bank of foreground lights contained two 250-watt Westinghouse Clear IR bulbs and two 300-watt Sylvania incandescent bulbs (total of 4 bulbs). The bank of background lights contained one IR bulb and two incandescent bulbs (total of 3 bulbs). All lights except the foreground IR light were mounted in a brooder enclosure. The foreground bulbs were hung from the ceiling at approximately the 11' mark on the floor tape measure. The background bulbs were hung from the ceiling behind the leak component and were about 50" to 60" away from the background.

In addition to the lights setup for the test runs, the lab also contained fluorescent lights about 40' away from the leak component, and ten mercury vapor UV overhead lights were on the ceiling for all tests.

On August 14, a light meter was used to measure incident light. The meter reading at the valve was 9.5, the reading at the background was 10.5, and readings taken outdoors were 16 and 18. Light intensity doubles with each meter increment.

TEST DATA AND MEASUREMENTS

As described in Appendix B, the test protocol developed for the laboratory evaluation was designed to provide as complete a performance evaluation of anticipated plant conditions as possible given the limitations of the laboratory. The various types of test data and measurements obtained in the laboratory testing are discussed below. In addition, several test parameters were discussed in the development of the test protocol but not included in the final test protocol. These parameters are also presented below.

Test Data and Measurements included in the Laboratory Evaluation

An itemized discussion of the test data and other measurements used in the laboratory evaluation is provided below. In addition, information on the lens position and field of view measurements for the four cameras are shown in Appendix E.

- Camera type: Information on the types of cameras used in this study is discussed in Section 2 of this report.

- Chemical: The four priority chemicals (1,3 butadiene, 1-butene, ethylene, and propylene) were found to be 99.0 to 99.9% pure. The cylinder of mixed xylenes obtained for testing was found to contain 23% ethylbenzene, 17% p-xylene, 43% m-xylene, and 17% o-xylene.

- Time (hh/mm/ss): The time corresponded to the time stamp on the long-wave BAGI camera recording. This was used to locate a test run on the video recordings of the test.

- Lens-valve Distance (ft): This was determined by moving the camera cart beside a tape measure. The lens used in the distance measurement was the outside camera lens (the cameras have internal lenses with the outside lens being simply a protective cover). The long- and mid-wave BAGI internal camera lenses were about six inches behind the external lens used for measurements.

- Wind Speed (mph): Wind speed measurements below 1.5 mph were not reliable with the digital anemometer used in the test setup. A cup anemometer was present for the first week of testing but removed for the second week at the request of a camera operator.

- Background: One of two backgrounds was used. Information on both the concrete and curved metal background is provided above.

- Leak Rate Rotameter Reading (Rotameter Set Point): The rotameter set point and rotameter model was recorded for each test run. This data was later used to determine mass flow rates from the rotameter calibration curves.

- Leak Detected (Y/N): This data point indicated if a leak was seen for a given test run.

- Determined Minimum Mass Detection Threshold? (Y/N): This data point explicitly indicated if a given run resulted in the determination of a minimum detection level for the run's test conditions. In some cases, a leak could be detected but a minimum level was not determined because the rotameter reading was above or below the scale.

- Threshold Approached by increasing/decreasing flow: This data point indicated how the minimum detection level was approached: from below the threshold, above it, or both.

- Valve Pressure (psi): A pressure gauge by the leak valve gave the pressure reading. This test aimed for zero gauge pressure in the delivery system. Higher pressures were recorded if they occurred.

Parameters Not Tested

The test matrix was designed so that collected data could be used to help determine the effects of background type, wind speed, distance, and chemical on camera performance. Other variables may affect camera detection performance but were not explored during the laboratory tests. This section provides a discussion of non-tested parameters that can possibly affect detection sensitivity.

- Field use of the cameras will likely occur under ambient light conditions, which are predominantly determined by the sun. The laboratory tests aimed to maintain a constant, artificial light source for all test runs and did not collect data under ambient light conditions. Furthermore, the infrared, fluorescent, and incandescent lights used for all test runs may not be representative of the spectrum produced by the sun – particularly the infrared spectrum of the sun.

- Test runs were conducted in an indoor facility without climate control. As a result, the tests did not control the effects of ambient temperature, humidity, and pressure.

- Cameras operating in the field will experience ever-changing conditions. In discussions held among test team members during the preparation of the laboratory study protocol, six condition parameters were identified but not fully tested:

    1. Background material, which affects background reflectivity (two types for these tests)

    2. Background shape, which affects background reflectivity (two types for these tests)

    3. Background temperature, which affects background emissivity[5]

    4. Distance between background and leak (each tested background at constant distance)

    5. Distance between camera and background (three distances for these tests)

[5] More complete information on background temperature was discussed in Section 2 of this report.

6. Angle between camera and background (perpendicular for these tests)

- Wind speed was also controlled during these tests and limited to constant, unidirectional flow. Gusts or variable wind velocity were not tested in the laboratory. Also, the eye is sensitive to movement, but tests comparing leaks in stagnant air to various airflow conditions were not performed.

- Each camera conducted tests using a pure gas stream leak at about constant temperature. Furthermore, the gas pressure was regulated to keep the leaking component at ambient pressure. Detection tests for dilutions, mixtures, and different gas temperatures were not conducted. Tests conducted under the laboratory test matrix also did not explore the Joule-Thompson effect on leaks; most leaks outside of a laboratory setting will come from pressured lines, and escaping gas will change temperature as it expands from the leak into the environment.

Tests were also conducted with a single known leaking component in a camera's field of view. This configuration made the leak source obvious; however, field use of a gas-imaging camera may occur with multiple components in a camera's field of view. These tests did not explore a camera operator's ability to identify leaking components among nearby non-leaking components.

TEST OBSERVATIONS

The information included above provides an overview of the four gas-imaging cameras used in the laboratory tests and a description of the test methods. Below, information is provided on the following:

- Qualitative evaluation of how each camera images gas;

- Test results by camera; and

- Quantitative test observations.

Data analysis of these results, including data fits and a discussion of trends, and laboratory study conclusions are found later in this section of the report.

Leak Imaging

Human perception of a camera's display of a leaking gas was the most subjective data collected during testing. At times, the QA/AC test team member was unable to identify a leak that other test participants could see. Moreover, on several occasions the leak rate was kept constant and the QA/QC test team member stated that he was able to visualize the gas plume where in the previous attempt he was not. Although the minimum detection level criteria were applied evenly, each camera imaged leaks differently. Below is a subjective discussion of leak imaging for each camera.

IMSS Leak Imaging

The IMSS display algorithm used different hues of one color to produce an image, and gas plumes were displayed as brighter than the rest of the image. Because of the camera's fixed position on the test bench, the standard viewfinder, normally attached to the camera, was not used to display the image. Camera output was sent to a large LCD computer monitor as well as a small (about 2.5") video recorder monitor. Because of the pixilation inherent in the IMSS image, using a larger monitor did not offer enhanced resolution, as the pixilation simply increased in size. The QA/QC team member preferred to view the image from the larger LCD monitor, and detections were made consistently from that monitor.

At any time during the camera's operation, the operator could adjust the display gain to tweak how well the field of view was displayed versus how well the leak appeared on the image. When the camera displayed a high-contrast leak, the objects in the field of view were not visible in the camera image. When the camera displayed the field of view, the leak did not contrast as well with the rest of the image. Different operators had different viewing preferences, though the QA/QC team member preferred to view the image with visible objects, as the leak detection criteria required some indication that the gas could be seen originating from the component. When the gain was set to show the field of view, the leaking component as well as the heated gas line that lead to the component was the most distinguishable objects. Setting the gain towards high gas contrast produced an image with no distinguishable objects except the gas plume. Operators for all cameras needed to orient the QA/QC team member by pointing out the leak component in the camera image on several occasions during testing.

Pixilation was present throughout the entire IMSS image: cubic blocks the same color as the gas flickered in the image as noise, and these blocks often recurred in the same part of the image. This required leaks to be larger than the pixilation in order to make a positive detection. Pixilation was also a function of the adjustable display sensitivity: a high-contrast leak that did not display objects in the field of view had a larger amount of pixilation than a low-contrast leak with visible objects.

The QA/QC team member's detection was more dependent on the bright gas contrasting with the rest of the image than on the motion of the gas plume from the air flow. Less airflow produced a more concentrated, brighter image of the gas, while more airflow produced a less concentrated, dimmer image of the gas.

Long-Wave and Mid-wave BAGI Leak Imaging

The long-wave and mid-wave BAGI cameras produced a black and white image, with gas appearing as dark spots. The BAGI images were viewable in each camera's eyepiece and were also sent to a small (about 2.5") monitor on a video recorder. Detections by the QA/QC team member were consistently made through the camera eyepiece. Brightness and contrast controls on the cameras similar in function to those found on a computer monitor were set by the long-wave BAGI operator and seldom changed by the QA/QC team member.

BAGI cameras display objects in the field of view along with any detectable leak gas. The leak component, gas delivery lines, pressure gauges, and anemometer were distinguishable in the camera image. The two backgrounds, which were 40.5" and 48" away from the leak component, were also distinguishable in the camera image.

Since other objects besides gas in the field of view can appear dark in the camera image, leak detections needed to occur behind objects that appeared brighter than the gas. This phenomenon became apparent during tests with the metal cylinders background. Although the metal cylinders rendered gas undetectable against certain dark areas, brighter portions of the cylinders allowed for detections. Thus, dark areas in the image did not limit the test team's ability to find minimum detection levels; however, the dark areas did limit the area in which the gas was visible.

Although contrast between the dark gas and brighter portions of the background was apparent, the QA/QC team member's detection also depended on motion of the plume from the airflow. This was particularly true for the mid-wave BAGI camera where fluctuating low laser power resulted in gas plumes that were somewhat distinguishable from the rest of the dark image. For both cameras, some plume motion helped to distinguish the gas from non-moving dark portions of the background.

PIR Leak Imaging

The PIR camera produced a grayscale image where the background, leak component, and various items in the field of view were discernable. For leaks that could be detected, gases hotter than the background appeared as a light-colored plume, while gases cooler than the background appeared as a dark-colored plume. Since other objects besides gas in the field of view appeared dark in the camera image, leak detections needed to occur behind objects that appeared brighter than the gas. This became an issue when testing with the curved metal cylinders background. Although the metal cylinders rendered the gas undetectable against certain dark areas, brighter portions of the cylinders allowed for detections. Thus, dark areas in the image did not severely limit the test team's ability to find minimum detection levels; however, the dark areas did limit the area in which the gas was visible. Leak detection depended on both the gas contrast with the rest of the image as well as on plume motion. In some cases, the only method of distinguishing the dark gas plume from the dark background was by observing motion of the gas plume. Adjusting the camera's brightness controls had a large effect on the visibility of the plume, and the brightness was adjusted for nearly every test run.

Test Results Matrix

Exhibits 3-1 to 3-4 are a comprehensive matrix of the test results, separated by camera. This matrix provides a summary of the tests and also provides visualization of what species a given camera could detect.

For simplicity, the results matrix displays minimum detection thresholds in two categories: thresholds at or below 60 grams per hour and thresholds above 60 grams per hour. This split was chosen based on an API Monte Carlo analysis for the mass flow rate equivalent to a 500, 1,000

and 10,000 ppmv leak definition by Method 21 for valves.[6] The Monte Carlo analysis determined a leak definition for an Alternative Work Practice (e.g. gas imaging) that would result in equivalent environmental protection to Method 21 monitoring. Based in part on the Monte Carlo analysis, the EPA has accepted the 60 grams per hour threshold for gas imaging as a level that meets the environmental equivalency requirement. This is discussed in more detail in Section 5 of this report.

Although the Exhibits 3-1 to 3-4 show only two minimum detection level categories for simplicity, the thresholds at or below 60 grams per hour spanned the entire spectrum from 1 gram per hour to 60 grams per hour. Thus, this category has a large variance.

For the IMSS and mid-wave BAGI cameras, the propylene tests were completed on one day, and selected propylene tests were repeated again on a different day. These two sets of propylene tests have been separated in the results matrix. Similarly, the long-wave BAGI has two sets of ethylene tests, which the results matrix displays separately.

Blank cells in the results matrix indicate that a test was not attempted. Test runs were not attempted because:

- A species was not seen under less rigorous conditions, so the test team did not spend laboratory time testing at higher wind speeds or distances;
- 30 foot test runs were performed on an optional, as-time-permits basis;
- Camera operators believed that certain gas species could not be seen; and/or
- Limited chemical quantities prevented the completion of the entire test parameter matrix.

[6] Epperson, David. L., Siegell, Jeffery, H., *"Equivalent Leak Levels & Monitoring Frequencies for Smart LDAR,"* Valve World 2002, November, 2002

Exhibit 3-1. IMSS test results.

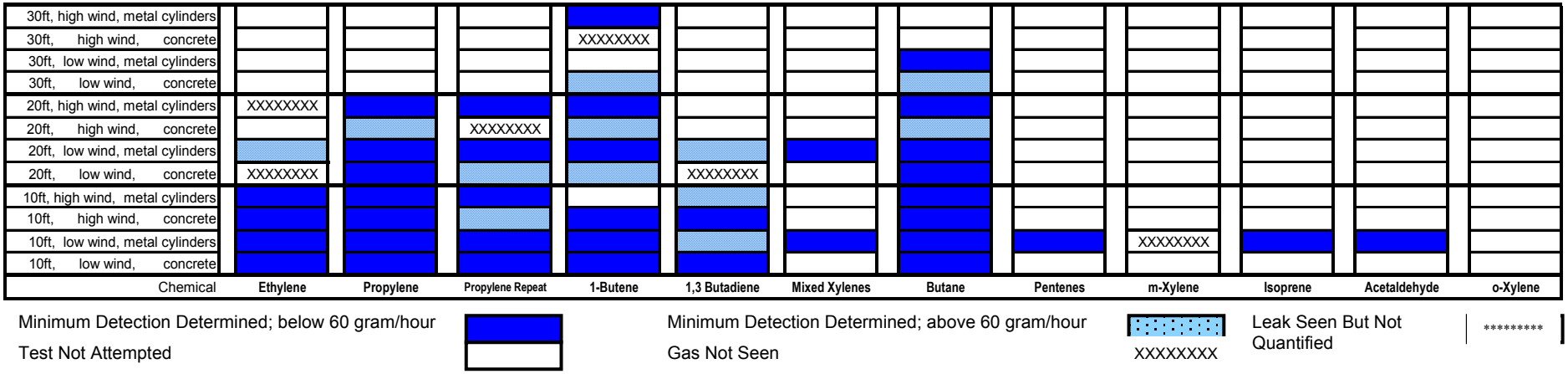

Exhibit 3-2. Long-wave BAGI test results.

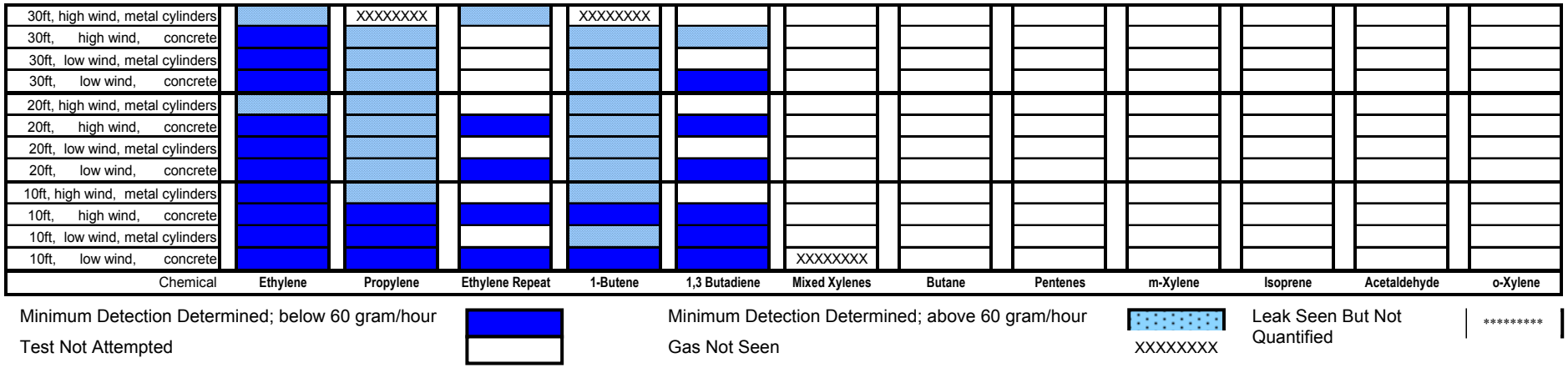

Exhibit 3-3. Mid-wave BAGI test results.

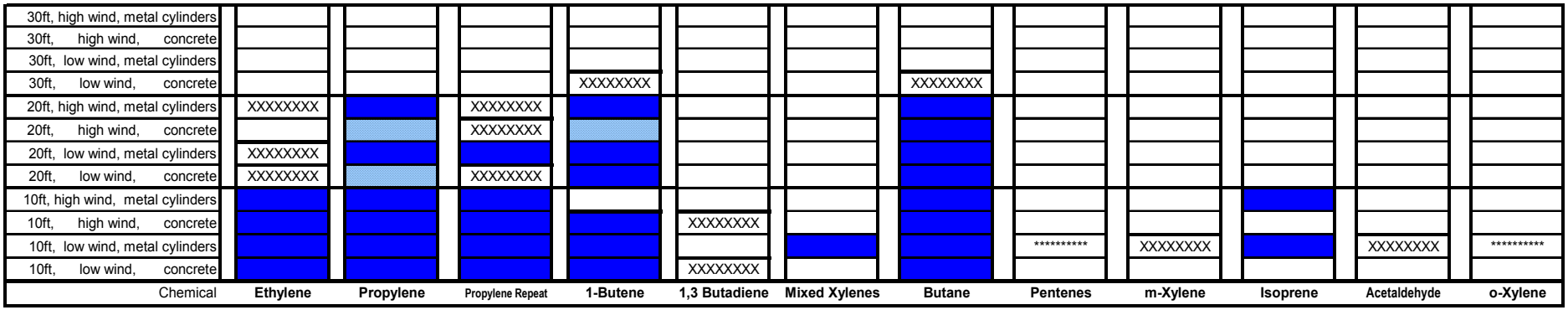

Exhibit 3-4. PIR test results.

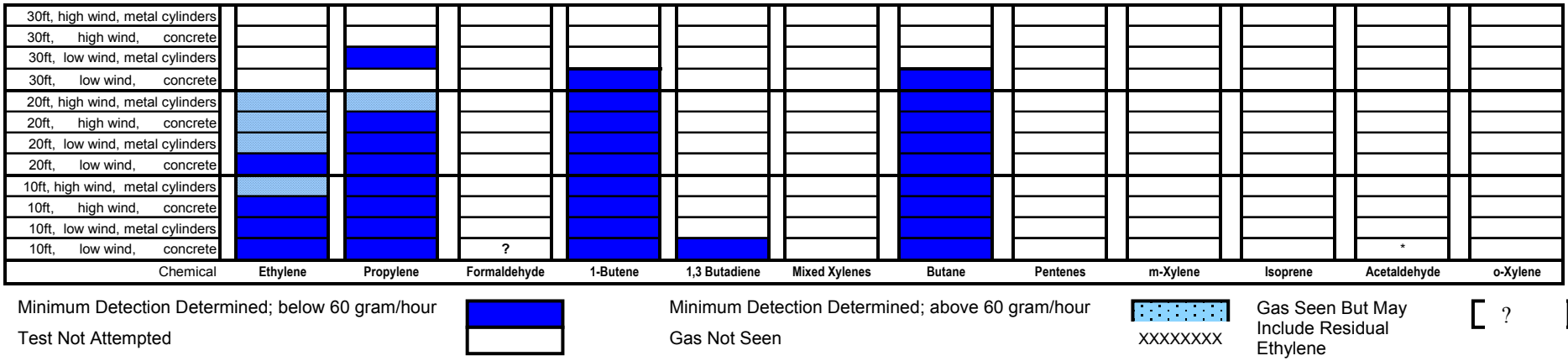

Minimum Detection Level Repeatability Results

Exhibits 3-5 to 3-8 shows repeat test runs for each camera for 10 foot, low wind speed, and concrete background tests. The repeat tests were included in the matrix to help determine how consistent the results were with the given camera-QA/QC team member combinations. When possible, at least three repeat test runs of a chemical were conducted on each camera. Because some cameras did not detect or did not attempt to detect certain chemicals, the repeat runs could only be performed on ethylene, propylene, 1-butene, 1,3 butadiene, and butane.

For all chemicals included in the IMSS repeatability tests, the minimum detection level standard deviations ranged from 2.6 to 4.4 grams per hour. The IMSS camera repeated test runs for the 10-foot, high wind speed, and concrete background test conditions. These repeats were performed after the first test run as these conditions produced an unexpectedly low flow meter reading. The repeats at these conditions were taken to explore the unexpected result, and ultimately the first test run at seven grams per hour could not be replicated.

Exhibit 3-5. IMSS minimum detection level repeatability.

	Minimum Detection Levels (grams / hour)					
	Ethylene	Propylene	1-Butene	1,3 Butadiene	Butane	Butane High Wind
	33	30	18	30	15	7
	34	25	14	26	15	14
	40	23	21	25	15	15
Different Day		22				
St. Dev.	3.8	3.6	3.5	2.6	0.0	4.4

10 ft, low wind speed, concrete background runs except where noted

The IMSS and mid-wave BAGI cameras were tested during the same week, and these two cameras completed the propylene test runs on one day and then repeated several propylene tests on a different day. Minimum detection level results for this chemical are separated by day.

Exhibit 3-6. Long-Wave BAGI minimum detection level repeatability.

	Minimum Detection Levels (grams / hour)			
	Ethylene	Propylene	1-Butene	1,3 Butadiene
	5	14	27	19
	5	31	30	19
	6		27	18
Different Day	5	28		
	8			
Total St. Dev.	**1.3**	**9.1**	**1.7**	**0.6**

10 ft, low wind speed, concrete background runs

Repeat runs for the long-wave BAGI give standard deviations of 0.6 to 1.7 grams per hour for all chemicals except propylene, which has one significant outlier of 14 grams per hour. This outlier caused the propylene standard deviation to equal 9.1 grams per hour. The remaining two repeat runs have a standard deviation of 2.1 grams per hour.

Exhibit 3-7. Mid-Wave BAGI minimum detection level repeatability.

	Minimum Detection Levels (grams / hour)			
	Ethylene	Propylene	1-Butene	Butane
	18	19	8	1
	24	20	7	1
	21	20	9	1
Different Day		8		
St. Dev.	3.0	5.9	1.0	0.0

10 ft, low wind speed, concrete background runs

For all the chemicals included in the mid-wave BAGI repeatability tests, the minimum detection level standard deviations ranged from 0.0 to 5.9 grams per hour. A propylene repeat test run performed on a different day than the other propylene repeat runs had a minimum detection level reduced by over 50%, and this result caused a large propylene standard deviation.

Exhibit 3-8. PIR minimum detection level repeatability.

	Minimum Detection Levels (grams / hour)				
	Ethylene	Propylene*	1-Butene	1,3 Butadiene	Butane
	16	6	7	17	4
	15	8	5	18	4
	12	7	4		8
			5		4
			5		4
Total St. Dev.	**1.9**	**1.0**	**1.3**	**1.0**	**1.6**

*first two runs are with 100mm lens

10 ft, low wind speed, concrete background runs

For all the chemicals included in the PIR repeatability tests, the minimum detection level standard deviations ranged from 1.0 to 1.9 grams per hour.

Repeatability/Consistency Across Flow Meters and Across Test Days

The information presented above provides data on the repeatability and consistency of the four cameras imaging several chemicals. In the section below, information is provided that examines the repeatability of long-wave BAGI ethylene tests, which were performed on three different flow meters and on three different test dates. Because the flow meters used for the other two cameras tested in August 2003 were not available in time for the entire long-wave BAGI tests, the long-wave BAGI camera tested under varying equipment. This section presents how the difference in test equipment affected the results. Exhibit 3-9 shows repeat test runs grouped by similar test conditions.

In Exhibit 3-9, results from the three different rotameters and the three different test dates are included. When grouped by similar test conditions, the results show significant, distinguishable differences between the test condition categories irrespective of rotameter or test date.

Some of the variance within a test condition group can be attributed to:

- Variation in the test conditions (i.e., low and high wind speeds were repeatable to about 0.3 miles per hour)
- Humidity differences between test dates
- Leak perception by the QA/QC test team member

Ultimately, the effect of testing under different rotameters and dates did not significantly affect trends in the results.

Exhibit 3-9. Long-wave BAGI repeat runs.

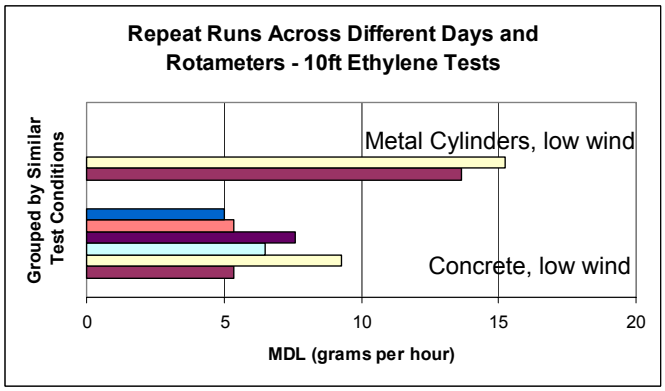

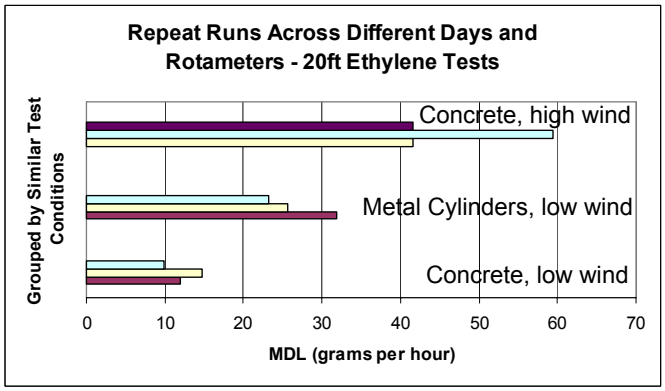

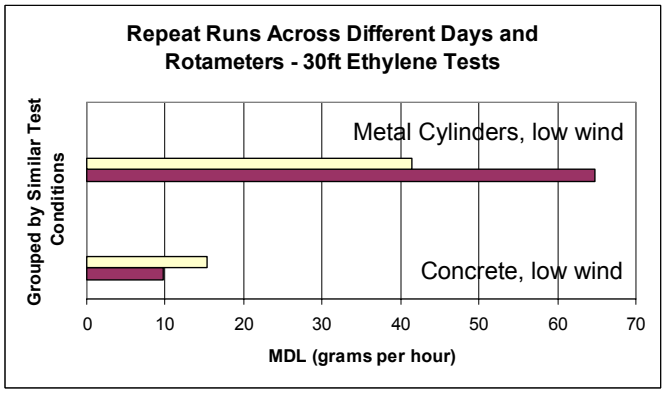

Effects of Camera Zooming

As described in Section 2, the long-wave and mid-wave BAGI cameras have the capability to adjust the focal distance of their lenses to obtain an optically zoomed-in view of the leak. This section explains the effects of camera zoom on minimum detection levels.

The long-wave BAGI camera tested mostly in its zoomed-out mode but imaged several leaks under zoom. Exhibit 3-10 presents cases where leaks were imaged for both a zoomed-in test and a zoomed-out test. The percent difference between the minimum detection level in a zoomed

versus non-zoomed mode for these nine cases ranges from 12% to 48%, with an average of 33%. In one set of test parameters, a leak could only be imaged under zoom.

Long-wave BAGI zoom test runs as shown in Exhibit 3-10 do not represent a true minimum detection level. The first three test condition categories in Exhibit 3-10 show zoomed minimum detection levels next to non-zoomed minimum detection levels. However, for the remaining categories, a zoomed test was performed at 2/3 of the non-zoomed minimum detection level, and the test team did not attempt to hone in on a true minimum. Thus, Exhibit 3-10 does not represent true differences between zoomed and non-zoomed-in gas imaging, but it does illustrate significantly increased sensitivity using the zoom feature.

Exhibit 3-10. Effects of camera zooming on Long-wave BAGI camera results.

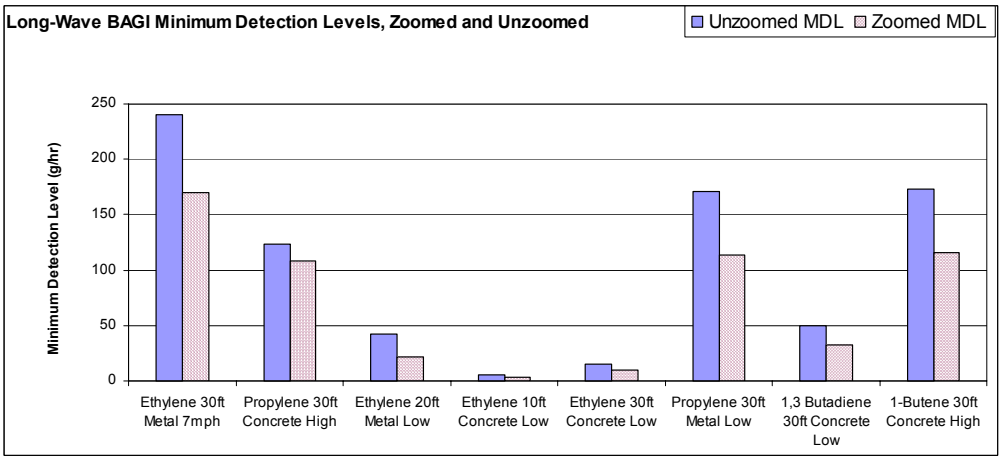

The mid-wave BAGI camera tested mostly in its zoomed mode. Two sets of test conditions were repeated for both a zoomed test and a non-zoomed test:

- 1-Butene, 20 foot distance, concrete background, low wind
- Propylene, 10 foot distance, metal cylinder background, low wind

These tests resulted in a 55% and 73% difference between zoomed and non-zoomed minimum detection levels, respectively. These results represent true minimum detection level determinations during the zoomed tests.

Because camera zoom has such a significant effect on the results, and because the cameras used zoom inconsistently, minimum detection levels cannot be directly compared between cameras.

Effects of Gas Delivery System Leak

As mentioned above, a leak in the gas delivery system occurred during the August 2003 test and was undetected for several test runs. Consideration was given to quantifying the gas delivery system leak that was discovered to affect IMSS butane tests. Methods to estimate the leak rate

were rejected as being too inaccurate. Therefore, we can only recognize that some IMSS butane camera results are uncertain.

Effects of Heated Gas Delivery Lines

During the August 2003 test, all tests were performed using heated lines to deliver the gas to the leaking component, with the exception of propylene tests performed with the IMSS and mid-wave BAGI cameras. The purpose of the heated lines was to ensure that low-volatility chemicals did not condense in the supply tubing. Exhibits 3-11 and 3-12 compare the non-heated line tests to other propylene tests with heated lines.

In Exhibit 3-11, IMSS propylene test results for the 10-foot distance, metal cylinder background conditions are displayed. The tests represent two different days of propylene tests with heated lines, and one day of tests without heated lines.

Exhibit 3-11. IMSS non-heated gas lines test results.

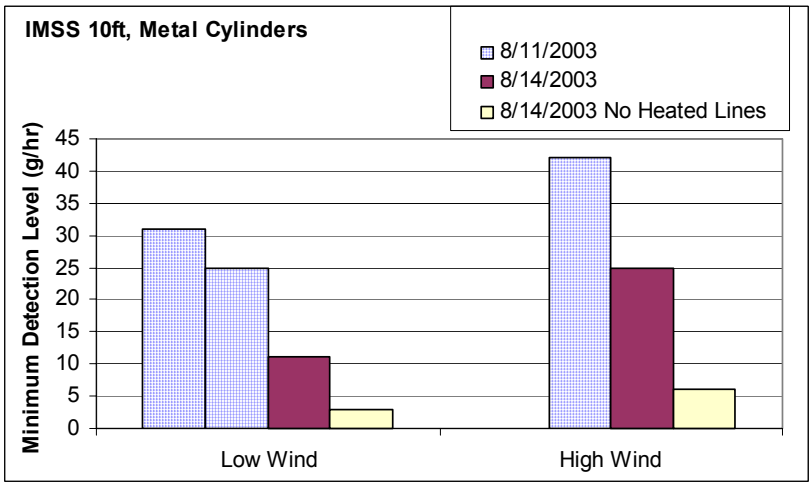

Within the same set of test conditions, the minimum detection level results varied. The non-heated lines results always produced the lowest detection levels, and these minimum detection levels were about four times less than with heated lines.

Although the IMSS camera could image the leak both with and without heated delivery lines, removing the chemical supply tubing heat source greatly increased IMSS detection sensitivity. The IMSS camera clearly imaged the heated delivery lines, regardless of whether or not gas was flowing through them. The lines appeared on the IMSS display much brighter than the surrounding area. Pacific Advanced Technology believes that inclusion of this strong infrared source in the field of view affected the image since during the tests the automatic gain control (AGC) of the camera system was turned on. This AGC function is similar to that used in commercial camcorders to automatically adjust the camera gain for different scene brightness without any adjustment required by the operator. However, this feature adjusts the gain on the camera for the average scene brightness, and is not optimum for a particular signal such as a very

weak leak signal. If there is a very strong (bright) infrared source, such as heaters in the scene, that source will have a large influence on the automatic gain setting for the scene, and will reduce the gain. The IMSS camera has a feature that allows the operator to turn off the AGC and manually adjust the camera gain for a setting that is more appropriate to image the dimmer leak signals. This adjustment feature was not used during the testing, and all tests were conducted with the IMSS camera AGC on. This reduced camera sensitivity when there was a bright source in the scene along with the leak.

A second possible explanation for the increased sensitivity of the IMSS camera without the heated lines is that the removal of the heating element lowered the leak gas temperature at the valve. In the tests, propylene was delivered to the valve at atmospheric pressure from a pressurized storage cylinder with gas at average room temperature. As the gas expanded from the cylinder, it would cool below room temperature. The heated supply line may have returned the gas temperature to near or above room temperature, which would be close to background temperature. Removal of the heat from the supply tubing would allow the gas to remain at a lower temperature relative to the background. A larger temperature difference between the gas and the background may have resulted in the observed increased IMSS detection sensitivity.

Exhibit 3-12 displays propylene tests for the mid-wave BAGI camera at the10-foot distance, metal cylinder background conditions. Within each of the two sets of test conditions, the minimum detection levels vary, and the non-heated line tests produce minimum detection levels that fall within the detection level range of the heated line results. Omitting heated lines had no consistent effect on mid-wave BAGI sensitivity.

Exhibit 3-12. Mid-Wave BAGI non-heated gas lines test results.

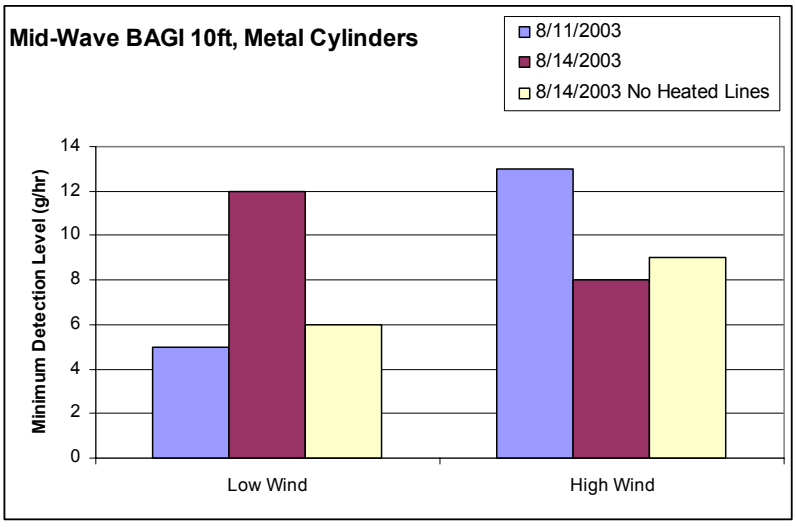

Measurement Error and Uncertainty

Table 3-1 contains estimates for measurement uncertainty in the primary test data.

Table 3-1. Measurement uncertainties.

Measurement	Uncertainty	Units
Lens-Camera Distance	± 0.005	ft
Wind Speed	± 0.3	mph
QA/QC Team Member Minimum Detection Level Determinations for all cameras	± 3.8	g/hr

STATISTICAL DATA ANALYSIS

The previous section provided test observations to:

- Quantify effects of leak perception on the four different imaging technologies;
- Quantify imaging consistency for each technology; and
- Quantify effects of several changes in test parameters, including flow meters, leak gas cloud temperature relative to background, and BAGI camera zooming.

This section contains results of a statistical regression on the test data to model minimum detection levels for different wind speeds, distances, backgrounds, and chemicals.

Regression Data

The entire test series data set included test run results (minimum detection levels) for the four cameras and permutations of distance, wind speed, background, and chemical test conditions. The data set included both test runs of successful gas imaging, where a minimum detection level was determined, as well as test runs where gas was not detected. Runs that resulted in a non-detection occurred in cases where:

- The combination of wind, distance, and background test conditions was rigorous enough to bring the imaging technology past its detection limits;
- The test chemical's absorbance spectra was such that a technology could not detect gas for any combination of test conditions; and/or
- The imaging technology successfully completed one test, and the following test at 2/3 of the determined minimum detection level resulted in a non-detection.

Test runs resulting in a minimum detection level determination were used for the regression discussed in the next section. Test runs resulting in non-detections helped to define boundaries for the regression.

Regression Methodology and Modeling

As per the test protocol, the objective of the test was to explore four parameters to generate an as-complete performance specification as possible in a laboratory setting for the gas-imaging cameras. The four parameters explored in the laboratory (and discussed in detail in Appendix B) are shown in Table 3-2.

Table 3-2. Protocol test parameters.

Parameter	Variables	Comment
Hydrocarbon	14 candidate chemicals	Absorbance surrogates allowed testing of 10 candidate chemicals to achieve results for all 14 chemical groups.
Wind Speed	0 to 2 miles per second 3 to 5 miles per second	One wind speed in each range selected for testing. Wind speeds in the lower range were typical of those found during normal weather conditions. The higher wind speed explores more extreme conditions than typically encountered in fugitive emissions monitoring.
Viewing Distance	10 feet 20 feet	Distance from the camera lens to the leaking component.
Background	Concrete wallboard Curved, painted metal surface	The concrete wallboard simulated concrete, gravel, and earth surfaces found at petroleum plants. A row of gas cylinders simulated pipes, vessels, and valves found at petroleum plants.

Of the four parameters evaluated for each camera, the chemical and the background are both qualitative variables whereas the wind speed and distance are quantitative variables. Below is a discussion of the model developed from these variables followed by a discussion of the model boundaries.

Model Development

The general linear model applied to estimate the minimum detection level (MDL) behavior of each camera was as follows:

$$\begin{aligned}\text{Ln(MDL)}_{\text{(for each camera)}} = \\ &a*\text{chemical} + \\ &b*\text{wind} + \\ &c*\text{distance} + \\ &d*\text{background} + \\ &e*(\text{interaction terms between chemical, wind, distance and background}) + \\ &f*(\text{Higher order terms of wind}) + \\ &g*(\text{higher order terms of distance}) + \\ &\text{error}\end{aligned}$$

In this general model, the function 'b' denotes the main effect of wind. The wind speed is either the target wind speed (0.66 or 2.0 m/s) or the actual wind speed. The model also considered higher order terms for wind speed (a quadratic and a cubic function) to determine if these higher order terms have a significant effect on MDL (or the log value of MDL). The function 'f' accounts for the effect of the higher order terms of wind. The function 'c' denotes the main effect of distance and the function 'g' accounts for the effects of the higher order terms of distance. The function 'e' represents the effect of the interaction between chemical, wind, distance and background.

The function 'a' represents the main effect of the chemical. Since 'chemical' is a qualitative variable, 'a' can be thought of as giving a different intercept for each chemical. Similarly, the function 'd' represents the main effect of background and can be thought of as giving a different intercept for each of the possible backgrounds. Since both chemical and background contribute to the value of intercept, it would be hard to distinguish their individual contribution or effect. Therefore, to provide a higher resolution to the model, it was considered best to estimate the behavior of each combination of camera and chemical rather than include a term for chemical on the right hand side of the model. With this in mind the model was reduced to the following form:

$$\text{Ln}(\text{MDL})_{\text{(for each camera and chemical)}} = b*\text{wind} + c*\text{distance} + d*\text{background} + e*(\text{interaction terms between wind, distance and background}) + f*(\text{Higher order terms of wind}) + g*(\text{higher order terms of distance}) + \text{error}$$

Preliminary analysis showed that the effect of the interaction terms as well as the higher order terms was insignificant on MDL.

Most of the variation in MDL (or log(MDL)) could be explained by the main effects of wind, distance and background. Therefore the final model was reduced to the following:

$$\text{Ln}(\text{MDL})_{\text{(for each camera and chemical combination)}} = b*\text{wind} + c*\text{distance} + d*\text{background} + \text{error}$$

The above model is linear in Log(MDL). The functions 'b' and 'c' provide the main effects of wind and distance respectively whereas the function 'd' provides different intercepts for different backgrounds. Table 3-3 lists the model assumptions.

Statistical analysis done for an earlier test of the long-wave BAGI camera[6] assumed that the coefficients for wind and distance would always be positive. In this report we do not make that assumption and allow the coefficients to be negative, as the model would fit the data better. In most cases the coefficients were indeed positive with a few exceptions where the slopes had a small negative value that could also have been caused by the normally distributed error term. Intuitively, the MDL value should increase with increase in either wind or distance.

Table 3-3. Model assumptions for Minimum Detection Level = f(wind, distance, background, chemical, camera.

Assumption	Reasoning
In (MDL) is linear function of wind speed	Previous report[7]; non-linear terms are orders of magnitude less than linear terms
In (MDL) is linear function of distance	Previous report[6]; non-linear terms are orders of magnitude less than linear terms
Each camera obeys the same model but has different coefficients	Each camera detects infrared light but in different capacities
Detection behavior depends on the background/chemical/camera combination (as opposed to the same behavior or slope for all chemicals tested under one camera/chemical combination)	Cameras use different wavelengths to detect different chemicals at different absorbance levels. Backgrounds are of different reflectivity.

Appendix F provides coefficients and intercepts for each combination of camera (IMSS, mid-wave BAGI, and long-wave BAGI), chemical, and background.

Model Boundaries

This section presents boundaries on wind, distance, and chemical for the minimum detection level prediction model.

- **Distance:** Testing was performed for all cameras between 10 and 30 feet. Although two cameras were able to image gas at 30 feet, distance limits varied by chemical. Therefore, upper distance bounds on the model validity are chemical-dependent. Lower distance bounds on the model were not approached, as the lowest distance parameter was 10 feet. The lower bound should approach 0 feet, a point where the valve consumes the image produced by a camera. The plots in Appendix G obey these chemical-specific boundaries.

- **Wind:** Testing was performed for three cameras (IMSS, mid-wave BAGI, and PIR) between 1.5 and 4.5 miles per hour; the long-wave BAGI camera tested between 1.5 and 6.5 miles per hour. These wind speeds represent constant, unidirectional airflow. Some cameras reached upper imaging boundaries with wind speed, but the upper bound is chemical-specific. The lower bound was not reached, and this value should approach but not reach zero wind speed, as no wind places the imaging conditions into a stagnant air

[6] Epperson, 2002.
[7] 'Report on Laboratory Test for Evaluating Backscatter Absorption Gas Imaging Technology', ICF Consulting, Prepared for U.S. EPA, May 2003

situation. Wind directions with a perpendicular component to the camera should adhere to the minimum detection level model.

- **Background:** Unlike distance or wind, background boundaries were not quantified in these tests. This model offsets predicted minimum detection levels based on the background type, and other background materials should adhere to the model.

- **Chemical:** Chemical species is not a quantified parameter in this model, but other species should adhere to the model: minimum detection levels depend in part on a chemical's infrared spectra. Candidate chemicals not explicitly tested were assigned spectral surrogates of tested chemicals. Results for a chemical that was not tested should approximate the results for its spectral surrogate. Appendix F provides mapping of non-tested chemicals to surrogate tested chemicals.

- **Ambient Test Conditions:** Boundaries were not explored for ambient temperature, humidity, or light sources (artificial or natural).

Minimum Detection Level Modeling Results

The regression results below are presented individually by camera. Propylene was selected as the main discussion chemical to provide an example of the statistical analyses. The propylene tests completed a large set of data for all four cameras, providing a large sample size for modeling. Certain cameras performed better on other chemicals than with propylene, and Appendix G contains results for all chemicals.

The regression results are used to estimate the expected value of the natural log MDL under a given set of conditions. Under the assumptions used in the regression modeling, that the error term is normally distributed, each predicted MDL for a given set of conditions would be detected fifty percent of the time.

If the wind coefficient, distance coefficient, or the intercept for any combination of camera and chemical is zero, it indicates that either the chemical was not tested or the data were insufficient to develop regression estimates (e.g., there were more unknown parameters than data points or the available data was tested at only one wind speed or distance). In that case, no MDL value can be determined and any coefficient estimated by the model is based on an incomplete model (less than full rank).

IMSS Results

This presentation of the IMSS camera results consist of a discussion of the regression terms followed by propylene minimum detection level plots. With the IMSS camera, there was sufficient data to conduct proper regression analysis for only propylene, 1,3-butadiene, ethylene, 1-butene and butane. For the other chemicals, either the camera did not see the chemical or there wasn't sufficient data collected and hence any regression values for these chemicals are meaningless.

IMSS Regression Terms

Models for the test results included a slope for wind speed, a slope for distance, and an intercept for each of the two backgrounds. The larger the term, the higher the predicted minimum detection level.

Exhibit 3-13 shows IMSS wind speed slopes for each chemical for which sufficient data was collected to develop a complete regression model. For other chemicals readers are encouraged to see Appendix F for values. The slopes ranged from 0.16 for ethylene to 0.44 for 1,3-butadiene. For ethylene, the 0.16 wind speed coefficient indicates that every unit change in wind speed will increase the minimum detection level by a multiplicative factor of $e^{0.16}$ if all other factors are held constant. This model is valid only for cases of constant, unidirectional wind speed.

Exhibit 3-13 also shows IMSS distance slopes for each chemical. Of the five chemicals listed above with sufficient data, butane was the most sensitive to distance increases with a coefficient of 0.8 and 1,3-butadiene was the least sensitive with a distance coefficient of 0.03. Infrared light attenuation over a distance is a function of the source intensity, not the chemical species.

Exhibit 3-14 shows IMSS intercepts for each chemical and both backgrounds. The different backgrounds track each other across chemicals, though no background is consistently higher than the other. A higher intercept value in Exhibit 3-14 indicates a higher minimum detection level for that background.

Exhibit 3-13. IMSS wind speed and distance coefficients.[8]

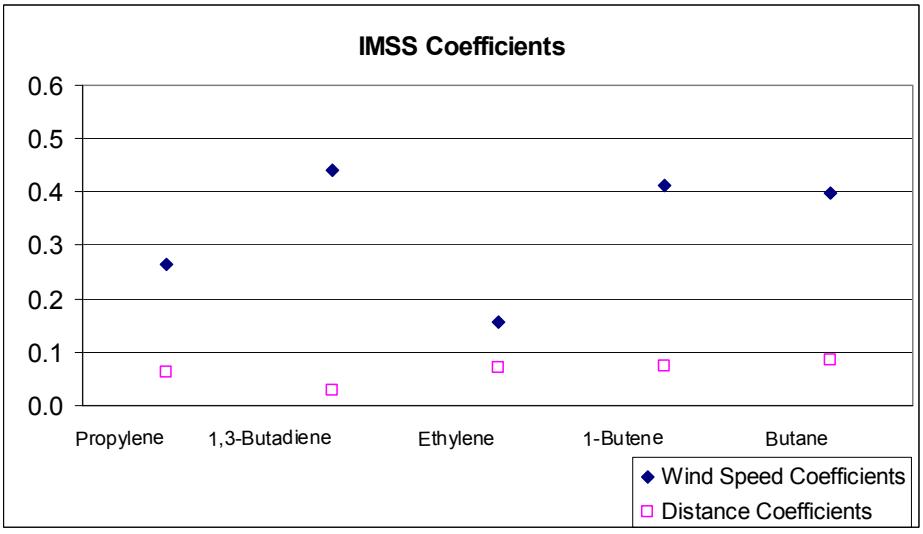

[8] Exhibit 3-13 plots wind speed and distance coefficients from the minimum detection level model.

Exhibit 3-14. IMSS background intercepts.

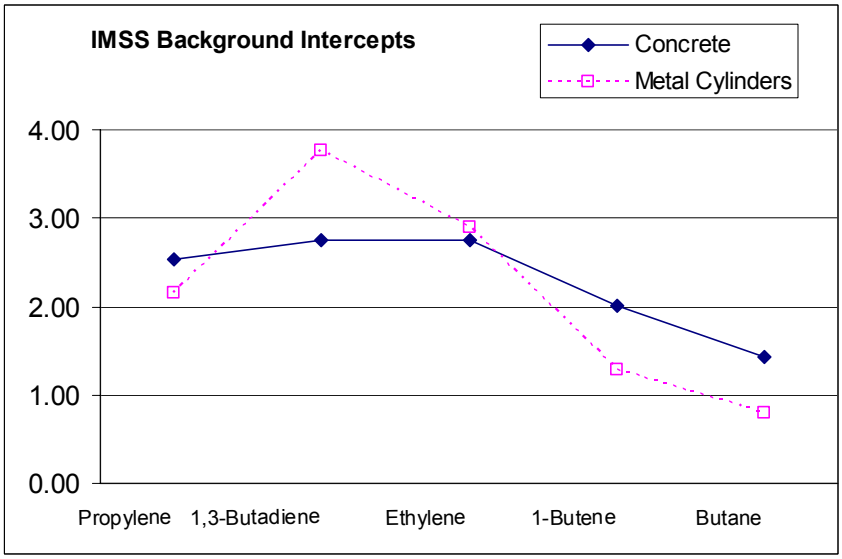

IMSS Minimum Detection Level Plots

This section discusses propylene-imaging results in detail to illustrate the findings extracted from minimum detection level plots. All other chemical statistical results are presented in Appendix G**.** The IMSS camera performed best on butane and 1-butene.

Exhibits 3-15 and 3-16 show IMSS propylene minimum detection level correlations versus wind speed at constant distances. Exhibit 3-15 illustrates results with the curved metal background. Exhibit 3-16 illustrates results with the concrete background. The plots contain the 60 grams per hour minimum detection level line for reference to the Method 21 mass flow rate equivalency for valves. Actual test data has been plotted as distinct points, while data regressions appear as bounded line segments.

Because the IMSS camera imaged propylene at the highest test wind speed, the upper wind speed boundary for the regression model was not determined. As expected, minimum detection levels at the 20-foot distance are higher than minimum detection levels at the 10-foot distance. Similarly, the plots show that minimum detection levels increase with wind speed.

Camera minimum detection level behavior is similar for both backgrounds, and the IMSS camera is more sensitive to propylene using the metal cylinder background. Minimum detection levels for both wind speeds and both distances remain below the 60 grams per hour reference line for the metal cylinder background. For the concrete background, the 20-foot regression line crosses the reference line at about a wind speed of two miles per hour.

The regression model for the minimum detection level imposed a constraint that wind speed slopes will be the same across different distances. Therefore, the 10- and 20-foot regression lines have the same slope, and the two line segments do not represent simple best-fit lines for the subsets of data points at the same distance.

Exhibit 3-15. IMSS propylene metal cylinders.

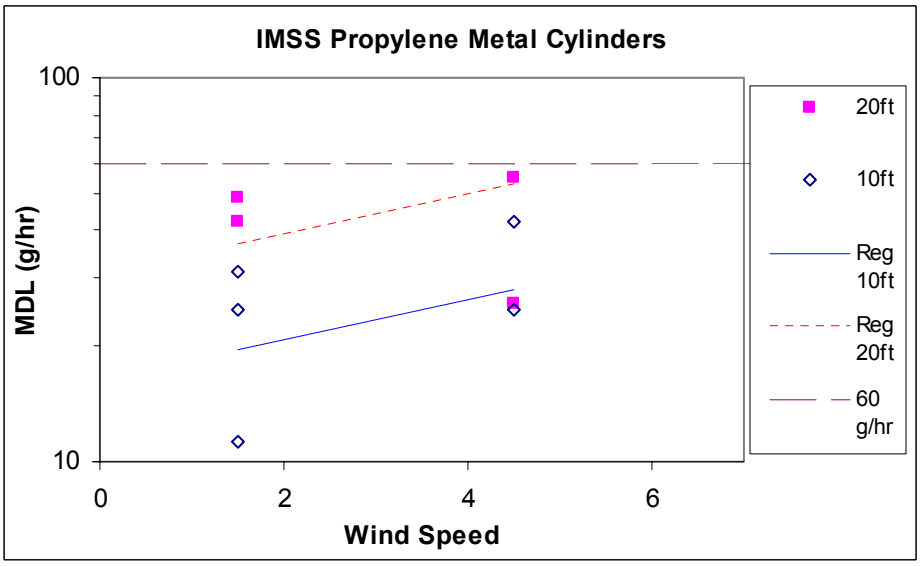

Exhibit 3-16. IMSS propylene concrete wallboard.

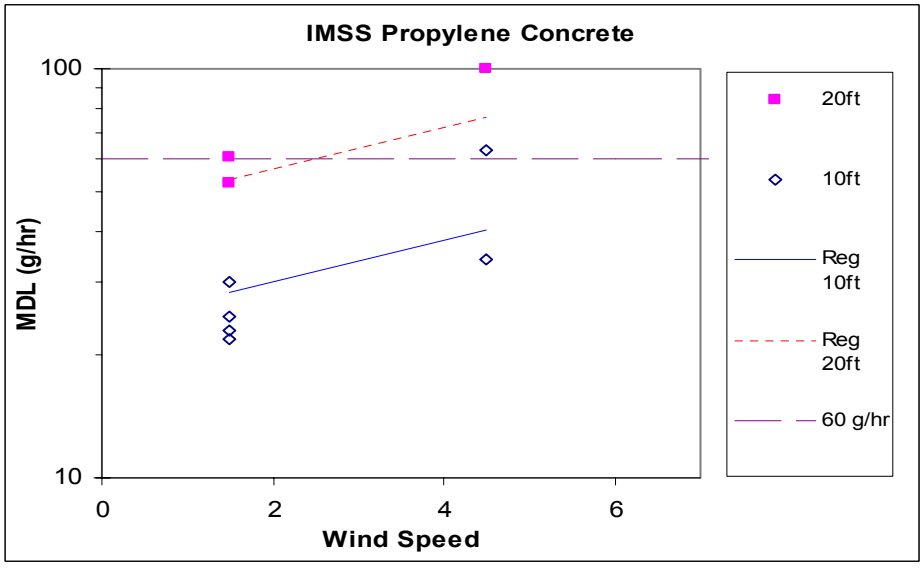

Exhibits 3-17 and 3-18 show IMSS propylene minimum detection level correlations versus distance at constant wind speeds. Exhibit 3-17 illustrates results with the curved metal background, while Exhibit 3-18 shows results with the concrete background. The plots contain the 60 grams per hour minimum detection level line for reference to the Method 21 mass flow rate equivalency for valves. Actual test data has been plotted as distinct points, while data regressions appear as bounded line segments.

Exhibit 3-17. IMSS propylene metal cylinders.

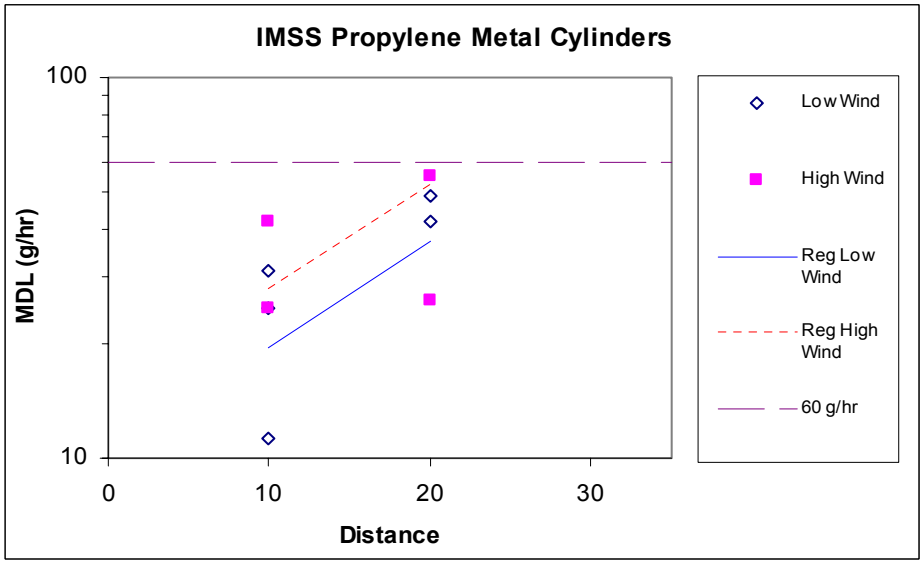

Exhibit 3-18. IMSS propylene concrete wallboard.

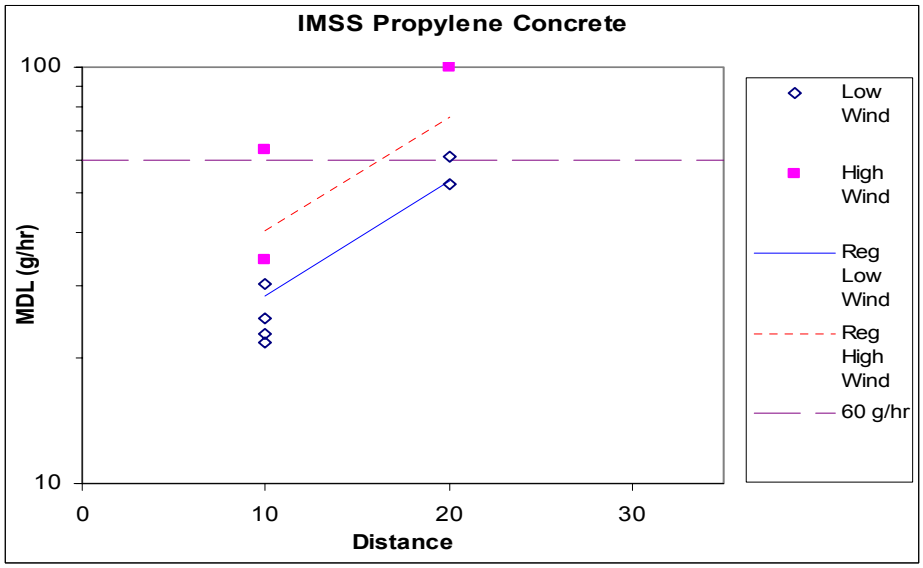

Because the IMSS camera did not image propylene beyond 20 feet, the upper distance boundary for the regression model was set to 20 feet. As expected, minimum detection levels at the high wind speed are higher than minimum detection levels at the low wind speed. Similarly, the plots show that minimum detection levels increase with distance.

Camera minimum detection level behavior is similar for both backgrounds, and the IMSS camera is more sensitive to propylene using the metal cylinder background. Minimum detection levels for both wind speeds and both distances remain below the 60 grams per hour reference line for

the metal cylinder background. For the concrete background, the high wind regression line crosses the reference line at about a 16-foot distance.

The minimum detection level model that regressed the test data imposed a constraint that distance slopes will be the same across different wind speeds. Therefore, the high- and low-wind speed regressions have the same slope, and the two line segments do not represent a simple best-fit line for the data points they model.

Long-wave BAGI Results

This presentation of the long-wave BAGI camera results consists of a discussion of the regression terms followed by the propylene minimum detection level plots.

Long-wave BAGI Regression Terms

Models for the test results included a slope for wind speed, a slope for distance, and an intercept for each of the two backgrounds. The larger the term, the higher the predicted minimum detection level. With the long-wave BAGI camera, there were sufficient data to conduct proper regression analysis for only propylene, 1,3-butadiene, ethylene and 1-butene. For the other chemicals, either the camera did not see the chemical or there weren't sufficient data collected and hence any regression values for these chemicals are meaningless.

Exhibit 3-19 shows long-wave BAGI wind speed slopes for each chemical for which sufficient data was collected to develop a regression model. For other chemicals readers are encouraged to see Appendix F for values. The slopes ranged from 0.21 for 1-butene to 0.46 for propylene. For 1-butene, the 0.21 wind speed coefficient indicates that every unit change in wind speed will increase the minimum detection level by a multiplicative factor $e^{0.21}$ if all other factors are held constant. This model is valid only for cases of constant, unidirectional wind speed.

Exhibit 3-19. Long-wave BAGI wind speed and distance coefficients.

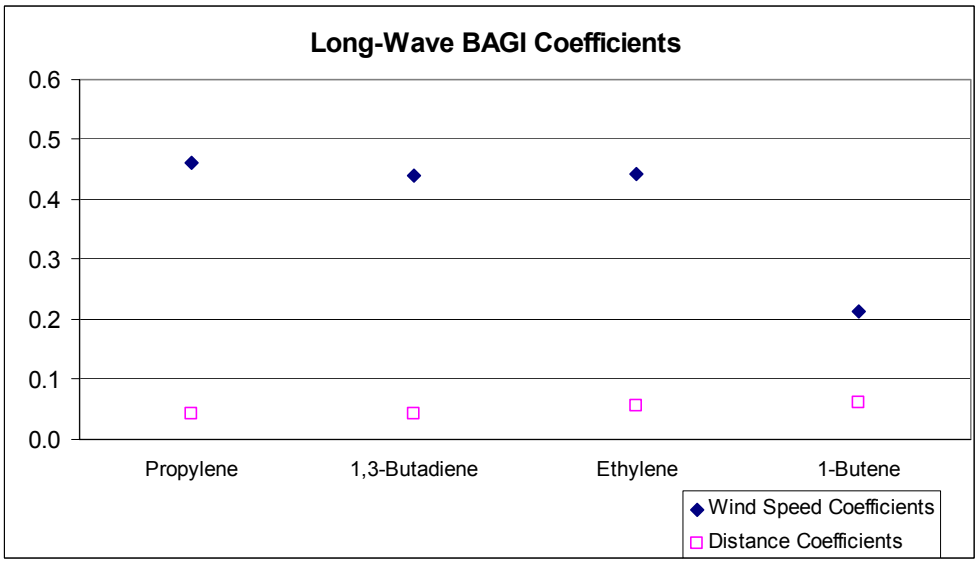

Exhibit 3-19 also shows long-wave BAGI distance slopes for each chemical. All four chemicals tested with the long-wave BAGI camera had distance slopes of less than 0.1.

Exhibit 3-20 shows long-wave BAGI intercepts for each chemical and both backgrounds. A higher intercept value in Exhibit 3-20 indicates a higher minimum detection level for that background. The two different backgrounds track each other across chemicals, and the metal cylinders consistently result in higher predicted minimum detection levels.

Long-wave BAGI Minimum Detection Level Plots

This section discusses propylene-imaging results in detail to illustrate the findings extracted from minimum detection level plots. All other chemical statistical results are presented in Appendix G. The long-wave BAGI camera performed best on ethylene.

Exhibit 3-20. Long-wave BAGI background intercepts.

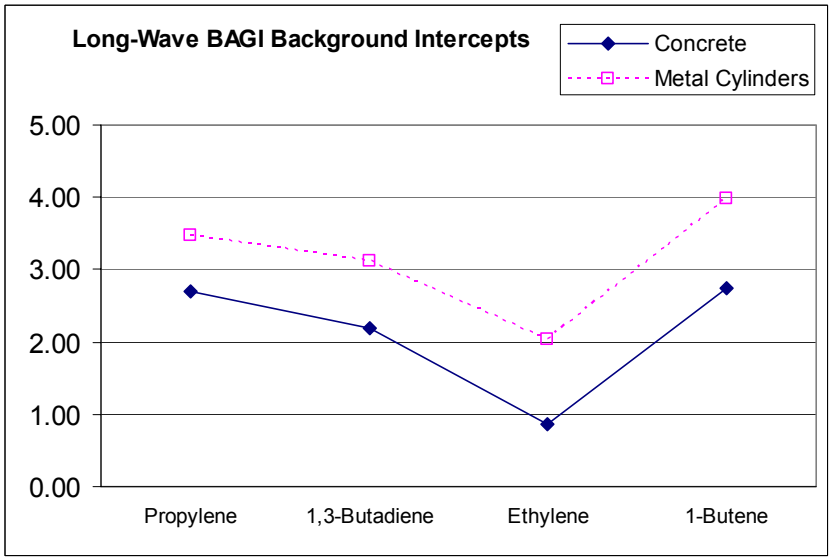

Exhibits 3-21 and 3-22 show long-wave BAGI propylene minimum detection level correlations versus wind speed at constant distances. Exhibit 3-21 illustrates results with the curved metal background, while Exhibit 3-22 shows results with the concrete background. The plots contain the 60 grams per hour minimum detection level line for reference to the Method 21 mass flow rate equivalency for valves. Actual test data has been plotted as distinct points, while data regressions appear as bounded line segments.

Because the long-wave BAGI camera imaged propylene at the highest test wind speed, the upper wind speed boundary for the regression model was not determined. As expected, minimum detection levels at the 20-foot distance are higher than minimum detection levels at the 10-foot distance, and detection levels at the 30-foot distance are higher than at 20 feet. Similarly, the plots show that minimum detection levels increase with wind speed.

Camera minimum detection level behavior is similar for both backgrounds, and the long-wave BAGI camera is more sensitive to propylene using the concrete background. Minimum detection levels for both wind speeds at the 10-foot distance remain below the 60 grams per hour reference line for the concrete background. The 20-foot, low wind speed test setup also has a predicted minimum detection level below 60 grams per hour. For the metal cylinder background, all regression lines remain above the reference line for the distance and wind speed region of interest.

The regression model for the minimum detection level imposed a constraint that wind speed slopes will be the same across different distances. Therefore, the 10- and 20-foot regression lines have the same slope, and the two line segments do not represent simple best-fit lines for the subsets of data points at the same distance.

Exhibit 3-21. Long-wave BAGI propylene metal cylinders.

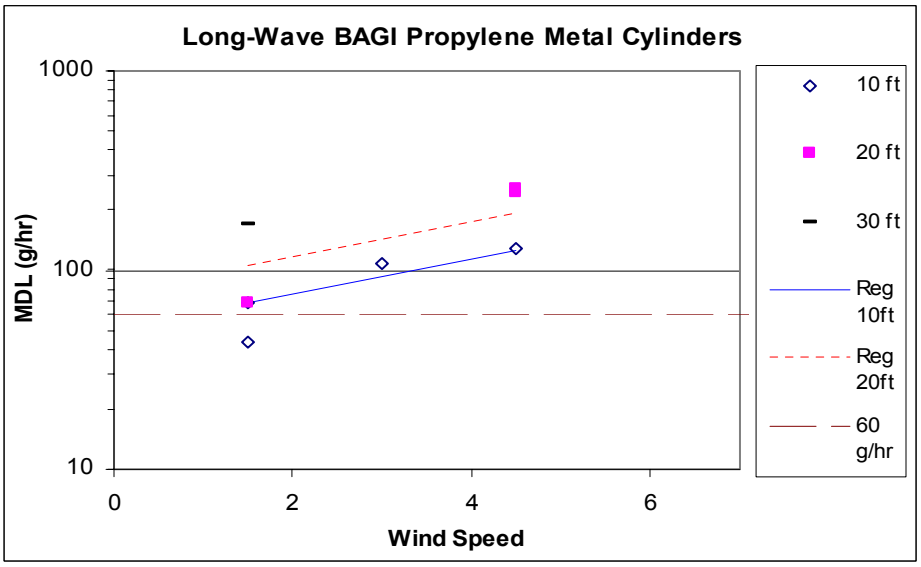

Exhibit 3-22. Long-wave BAGI propylene concrete wallboard.

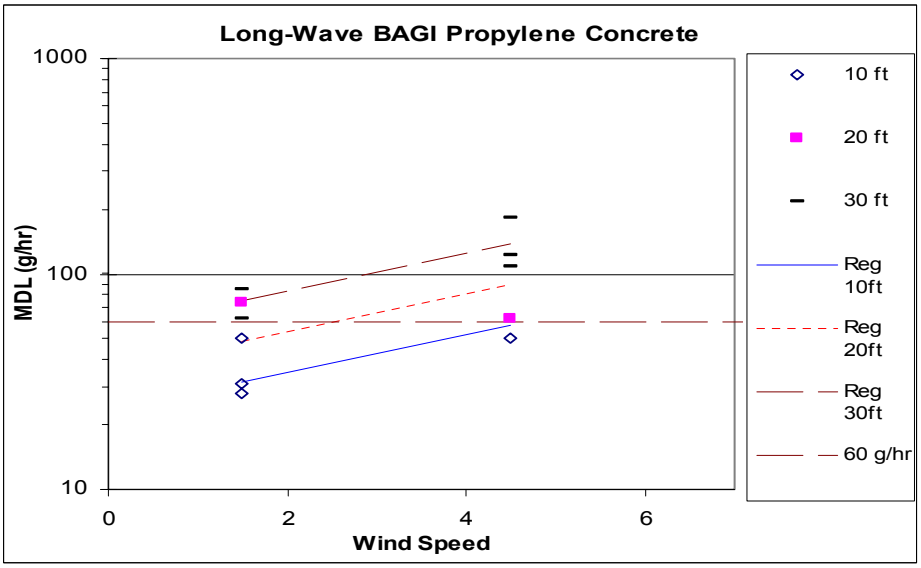

Exhibits 3-23 and 3-24 show long-wave BAGI propylene minimum detection level correlations versus distance at constant wind speeds. Exhibit 3-23 illustrates results with the curved metal background, while Exhibit 3-24 shows results with the concrete background. The plots contain the 60 grams per hour minimum detection level line for reference to the Method 21 mass flow rate equivalency for valves. Actual test data has been plotted as distinct points, while data regressions appear as bounded line segments.

In most cases, the long-wave BAGI camera imaged propylene at the highest test distance of 30 feet. The upper distance boundary for the regression model was set to 30 feet for all cases except the high wind line for metal cylinders in Exhibit 3-23. In this case, the camera did not image propylene at 30 feet, so the boundary was set to 20 feet. As expected, minimum detection levels at the high wind speed are higher than minimum detection levels at the low wind speed. Similarly, the plots show that minimum detection levels increase with distance.

Exhibit 3-23. Long-wave BAGI propylene metal cylinders.

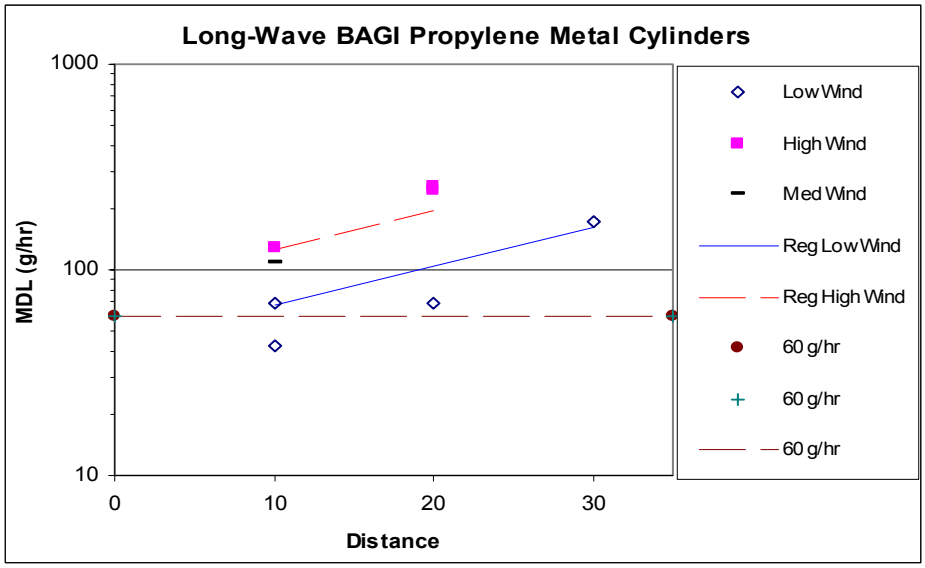

Exhibit 3-24. Long-wave BAGI propylene concrete wallboard.

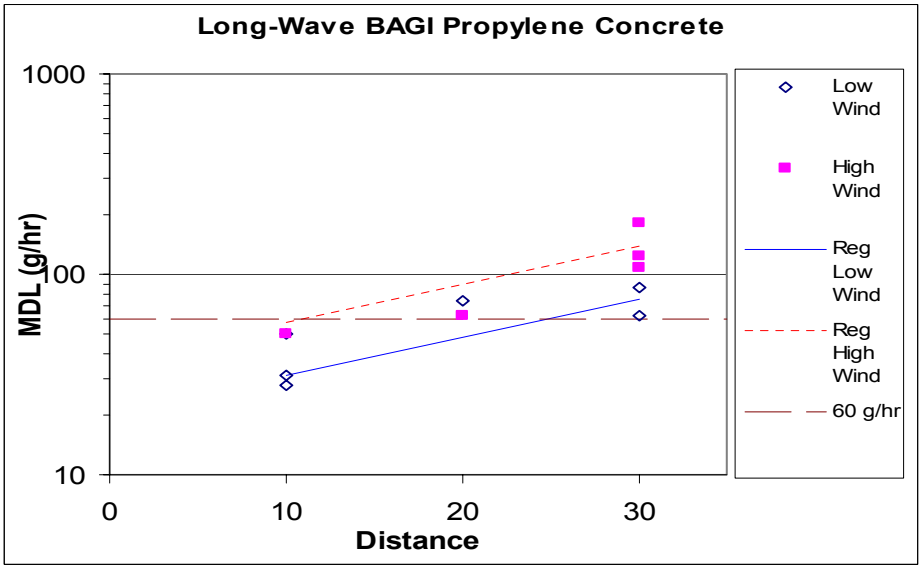

Camera minimum detection level behavior is similar for both backgrounds, and the long-wave BAGI camera is more sensitive to propylene using the concrete background. Minimum detection levels for the low wind speed remain below the 60 grams per hour reference line up to about 24 feet for the concrete background. For the metal cylinder background, all minimum detection level models were above the reference line.

The minimum detection level model that regressed the test data imposed a constraint that distance slopes will be the same across different wind speeds. Therefore, the high- and low-wind

speed regressions have the same slope, and the two line segments do not represent a simple best-fit line for the data points they model.

Mid-wave BAGI Results

This presentation of the mid-wave BAGI camera results consists of a discussion of the regression terms followed by the propylene minimum detection level plots.

Mid-wave BAGI Regression Terms

Models for the test results included a slope for wind speed, a slope for distance, and an intercept for each of the two backgrounds. The larger the term, the higher the predicted minimum detection level. With the mid-wave BAGI camera, there was sufficient data to conduct proper regression analysis for only propylene, ethylene, 1-butene and butane. For the other chemicals, either the camera did not see the chemical or there wasn't sufficient data collected and hence any regression values for these chemicals are meaningless. For ethylene, there was not enough data for tests with metal cylinders as background to form regression estimates.

Exhibit 3-25 shows mid-wave BAGI wind speed slopes for each chemical where sufficient data was collected to develop a complete regression model. For other chemicals, the readers are encouraged to see Appendix F for values. The slopes ranged from –0.02 for propylene to 0.51 for butane. For propylene, the -0.02-wind speed coefficient indicates that every unit change in wind speed will divide the minimum detection level by $e^{0.02}$ if all other factors are held constant. This model is valid only for cases of constant, unidirectional wind speed. Zero-value slopes in Exhibit 3-25 correspond to test chemicals that could not be detected or test chemicals with insufficient data to perform a regression.

Exhibit 3-25 also shows mid-wave BAGI distance slopes for each chemical. The slopes ranged from –0.08 for butane to 0.32 for ethylene.

Exhibit 3-26 shows mid-wave BAGI intercepts for each chemical and both backgrounds. A higher intercept value in Exhibit 3-26 indicates a higher minimum detection level for that background. The two different backgrounds track each other across chemicals, but no one background is consistently higher than the other across chemicals. With ethylene and metal cylinders as background, no intercept value was developed due to insufficient test data.

Mid-wave BAGI Minimum Detection Level Plots

This section discusses propylene-imaging results in detail to illustrate the findings extracted from minimum detection level plots. All other chemical statistical results are presented in Appendix G. The mid-wave BAGI camera performed best on butane.

Exhibit 3-25. Mid-wave BAGI wind speed and distance coefficients.

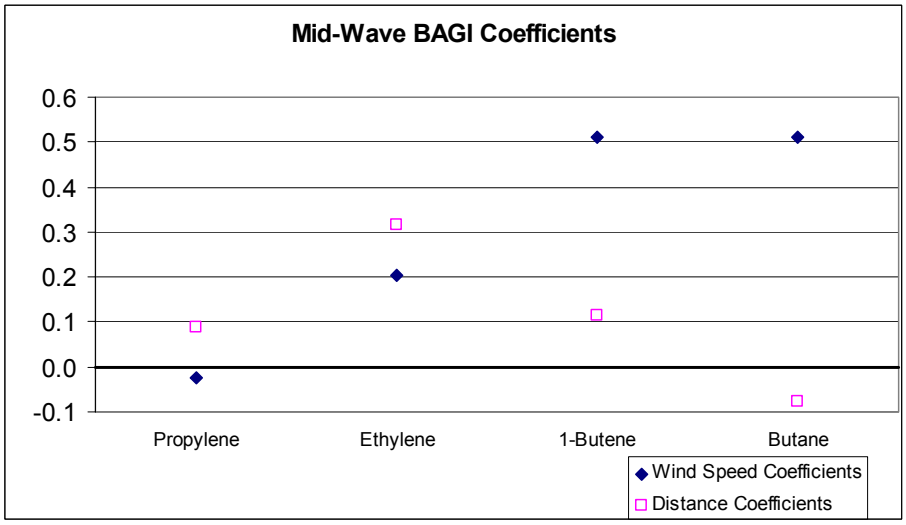

Exhibit 3-26. Mid-wave BAGI background intercepts.

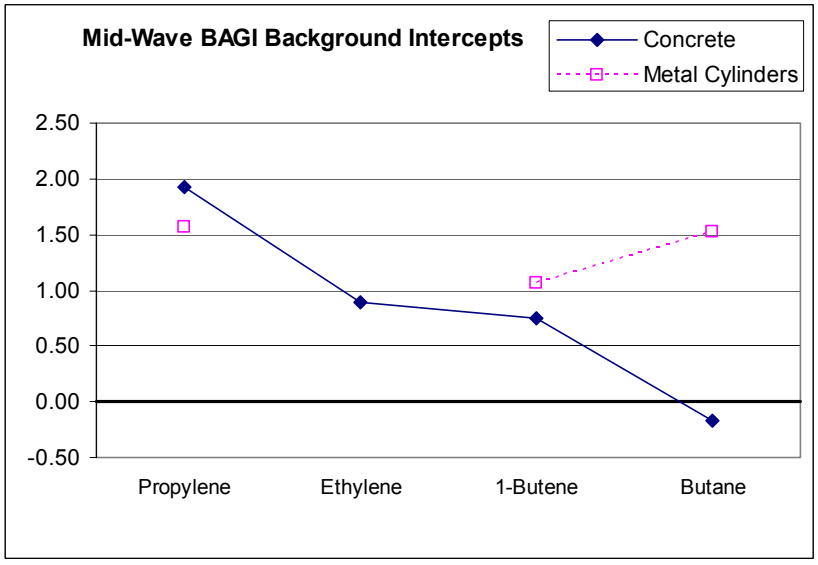

Exhibits 3-27 and 3-28 show mid-wave BAGI propylene minimum detection level correlations versus wind speed at constant distances. Exhibit 3-27 illustrates results with the curved metal background, while Exhibit 3-28 shows results with the concrete background. The plots contain the 60 grams per hour minimum detection level line for reference to the Method 21 mass flow rate equivalency for valves. Actual test data has been plotted as distinct points, while data regressions appear as bounded line segments.

Because the mid-wave BAGI camera imaged propylene at the highest test wind speed, the upper wind speed boundary for the regression model was not determined. As expected, minimum

detection levels at the 20-foot distance are higher than minimum detection levels at the 10-foot distance.

Exhibit 3-27. Mid-wave BAGI propylene metal cylinders.

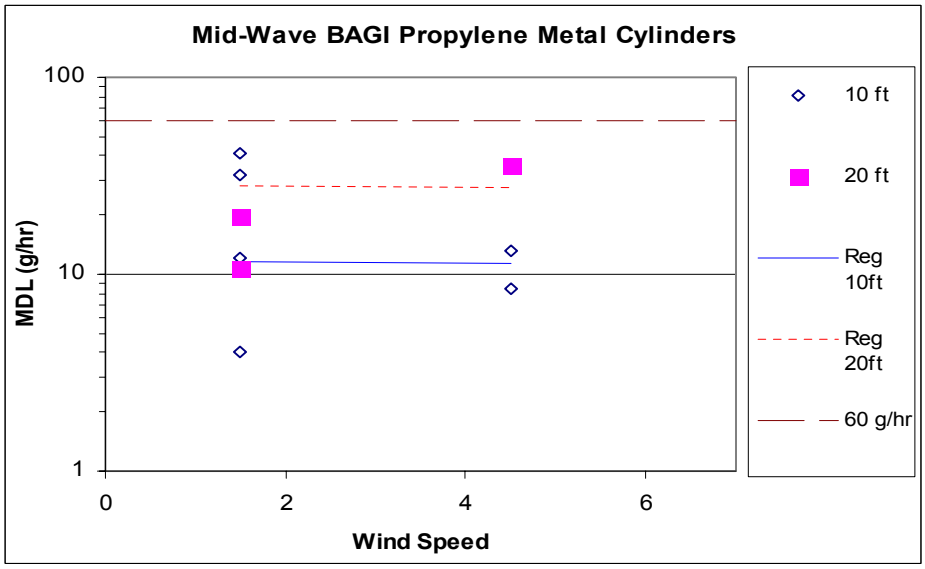

Exhibit 3-28. Mid-wave BAGI propylene concrete wallboard.

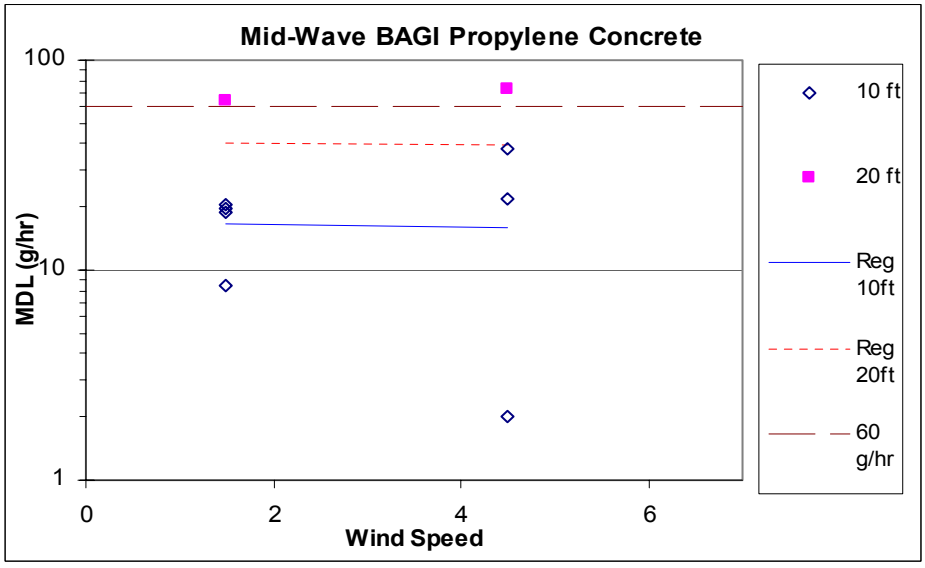

However, the prediction model lines show a slight decrease in minimum detection level as wind speed increases. This result is atypical of mid-wave BAGI minimum detection level trends, and all other wind speed plots in Appendix G show increasing detection levels as wind speed increases. One possible reason for the negative regression slopes is that the mid-wave BAGI tested propylene on two different test days. Previously it was concluded that tests spanning different days did not significantly affect results; however, the mid-wave BAGI laser power

varied over different test days. Some data points in Exhibits 3-27 and 3-28 represent minimum detection levels taken at 450 milliWatt laser power, while others represent a laser power of between 250 and 350 milliWatts.

Camera minimum detection level behavior is similar for both backgrounds, and the mid-wave BAGI camera is more sensitive to propylene using the metal cylinder background. Minimum detection levels for both wind speeds and both distances remain below the 60 grams per hour reference line for the metal cylinder background as well as for the concrete background.

The regression model for the minimum detection level imposed a constraint that wind speed slopes will be the same across different distances. Therefore, the 10- and 20-foot regression lines have the same slope, and the two line segments do not represent simple best-fit lines for the subsets of data points at the same distance.

Exhibits 3-29 and 3-30 show mid-wave BAGI propylene minimum detection level correlations versus distance at constant wind speeds. Exhibit 3-29 illustrates results with the curved metal background, while Exhibit 3-30 shows results with the concrete background. The plots contain the 60 grams per hour minimum detection level line for reference to the Method 21 mass flow rate equivalency for valves. Actual test data has been plotted as distinct points, while data regressions appear as bounded line segments.

Exhibit 3-29. Mid-wave BAGI propylene metal cylinders.

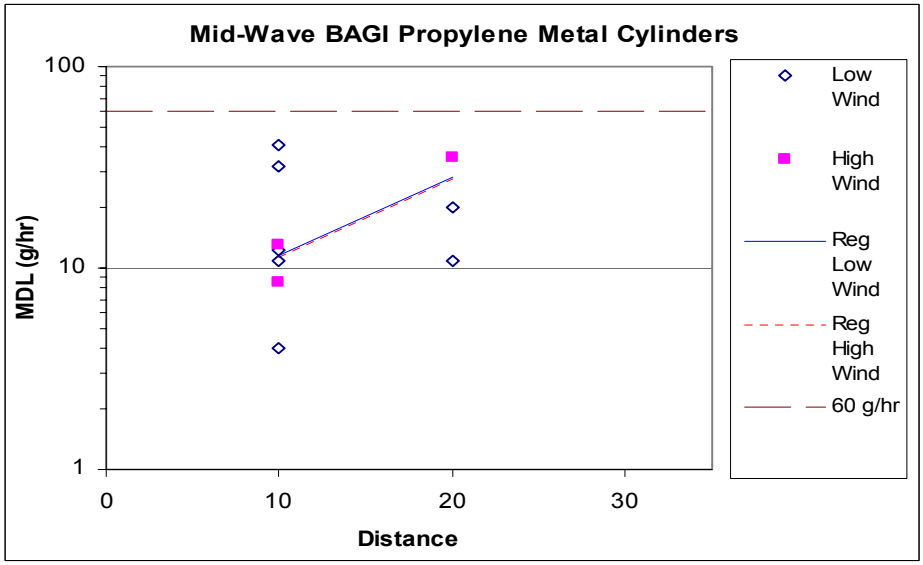

Because the mid-wave BAGI camera did not image propylene beyond 20 feet, the upper distance boundary for the regression model was set to 20 feet. As expected, minimum detection levels increase with distance. However, the predicted minimum detection level lines for high and low wind speeds are nearly superimposed, representing the almost flat detection level versus wind speed curves in Exhibits 3-27 and 3-28.

Camera minimum detection level behavior is similar for both backgrounds, and the mid-wave BAGI camera is more sensitive to propylene using the metal cylinder background. Minimum detection levels for both wind speeds and both distances remain below the 60 grams per hour reference line for the metal cylinder background as well as for the concrete background.

The minimum detection level model that regressed the test data imposed a constraint that distance slopes will be the same across different wind speeds. Therefore, the high- and low-wind speed regressions have the same slope, and the two line segments do not represent a simple best-fit line for the data points they model.

Exhibit 3-30. Mid-wave BAGI propylene concrete wallboard.

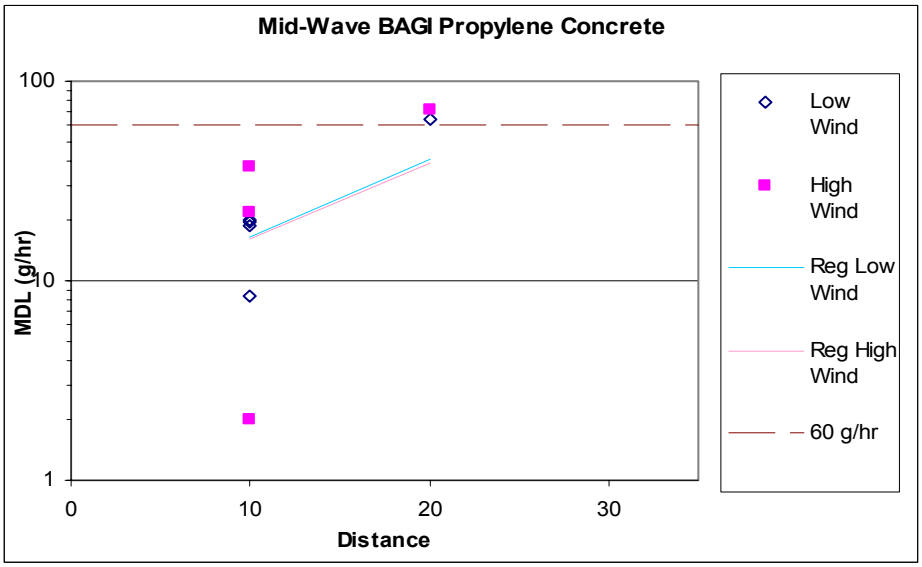

PIR Results

This presentation of the PIR camera results consists of a discussion of the regression terms followed by the propylene minimum detection level plots.

PIR Regression Terms

Models for the test results included a slope for wind speed, a slope for distance, and an intercept for each of the two backgrounds. The larger the term, the higher the predicted minimum detection level. With the PIR camera, there were sufficient data to conduct proper regression analysis for only propylene, ethylene, 1-butene and butane. For the other chemicals, either the camera did not see the chemical or there wasn't sufficient data collected and hence any regression values for these chemicals are meaningless.

Exhibit 3-31 shows PIR wind speed slopes for each chemical. The slopes ranged from -0.09 for butane to 0.76 for ethylene. For butane, the -0.09 wind speed coefficient indicates that every unit change in wind speed will divide the minimum detection level by $e^{-0.09}$ if all other factors are held constant. This model is valid only for cases of constant, unidirectional wind speed

Exhibit 3-31 also shows PIR distance slopes for each chemical. The slopes ranged from 0.007 for 1-butene to 0.08 for propylene, ethylene, and butane.

Exhibit 3-31. PIR wind speed and distance coefficients.

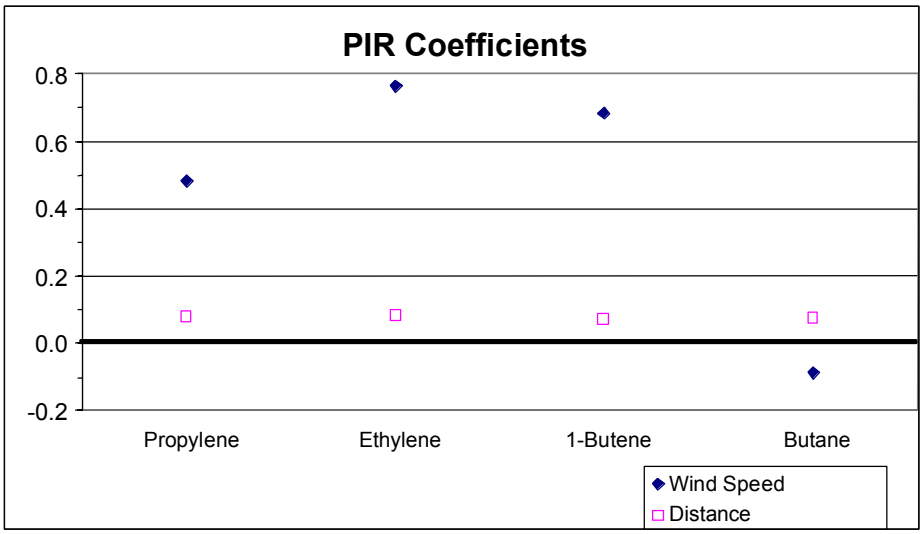

Exhibit 3-32 shows PIR intercepts for each chemical and both backgrounds. A higher intercept value in Exhibit 3-32 indicates a higher minimum detection level for that background. The two different backgrounds track each other across chemicals, and the metal cylinder background is consistently higher than the concrete across chemicals.

PIR Minimum Detection Level Plots

This section discusses propylene-imaging results in detail to illustrate the findings extracted from minimum detection level plots. All other chemical statistical results are presented in Appendix G.

Exhibit 3-32. PIR background intercepts.

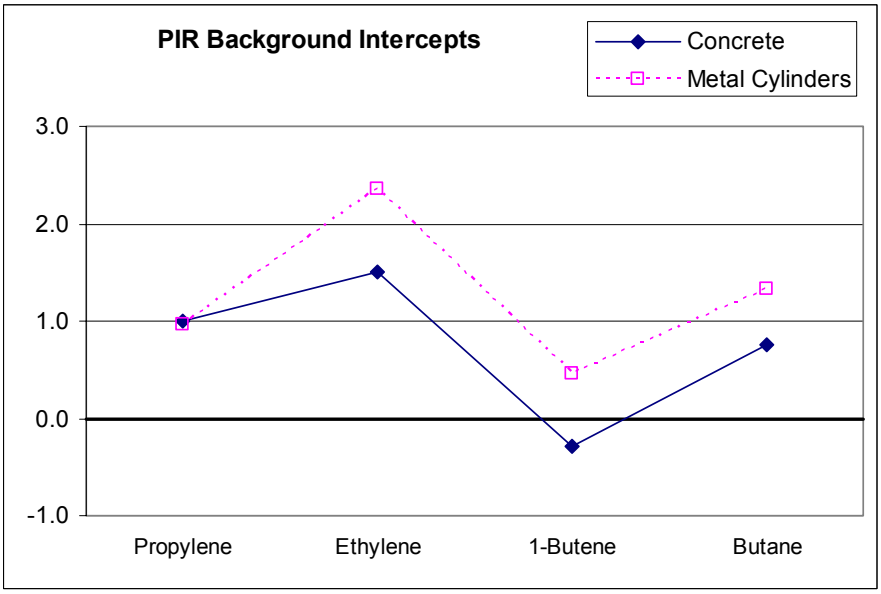

Exhibits 3-33 and 3-34 show PIR propylene minimum detection level correlations versus wind speed at constant distances. Exhibit 3-33 illustrates results with the curved metal background, while Exhibit 3-34 shows results with the concrete background. The plots contain the 60 grams per hour minimum detection level line for reference to the Method 21 mass flow rate equivalency for valves. Actual test data has been plotted as distinct points, while data regressions appear as bounded line segments.

Exhibit 3-33. PIR propylene metal cylinders.

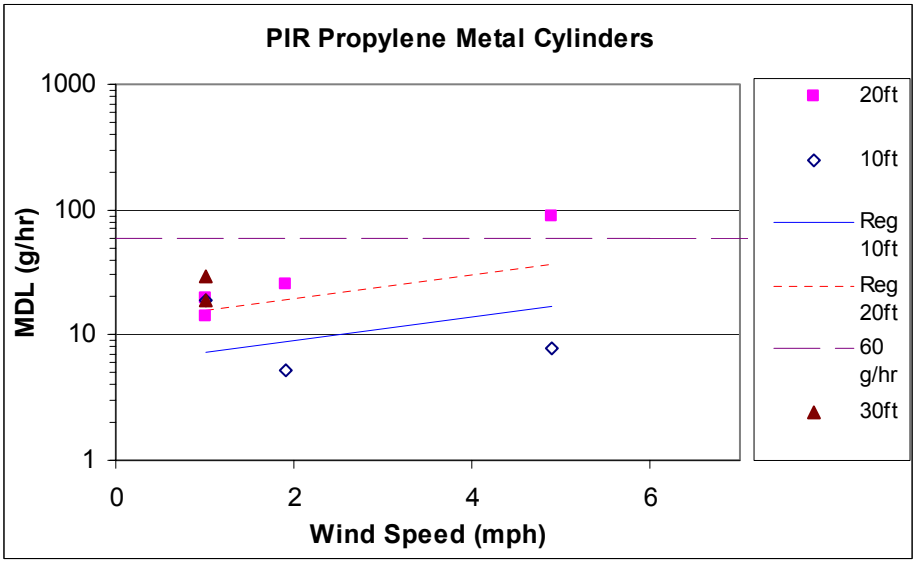

Exhibit 3-34. PIR propylene concrete wallboard.

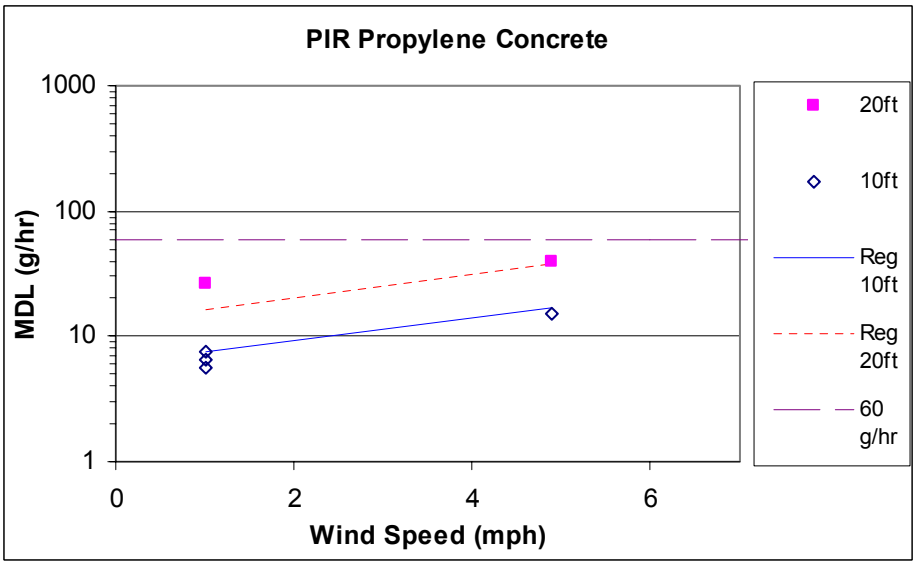

As expected, minimum detection levels at the 20-foot distance are higher than minimum detection levels at the 10-foot distance.

Camera minimum detection level behavior is similar for both backgrounds, and the PIR camera is nearly equally sensitive to propylene imaged against either background. Minimum detection levels for both wind speeds and both distances remain below the 60 grams per hour reference line for the metal cylinder background as well as for the concrete background.

The regression model for the minimum detection level imposed a constraint that wind speed slopes will be the same across different distances. Therefore, the 10- and 20-foot regression lines have the same slope, and the two line segments do not represent simple best-fit lines for the subsets of data points at the same distance.

Exhibits 3-35 and 3-36 show PIR propylene minimum detection level correlations versus distance at constant wind speeds. Exhibit 3-35 illustrates results with the curved metal background, while Exhibit 3-36 shows results with the concrete background. The plots contain the 60 grams per hour minimum detection level line for reference to the Method 21 mass flow rate equivalency for valves. Actual test data has been plotted as distinct points, while data regressions appear as bounded line segments.

As expected, minimum detection levels increase with distance, and the higher wind speeds give higher detection levels than the lower wind speeds.

Camera minimum detection level behavior is similar for both backgrounds, and the PIR camera is nearly equally sensitive to propylene on either background. Minimum detection levels for both wind speeds and both distances remain below the 60 grams per hour reference line for the metal cylinder background as well as for the concrete background.

Exhibit 3-35. PIR propylene metal cylinders.

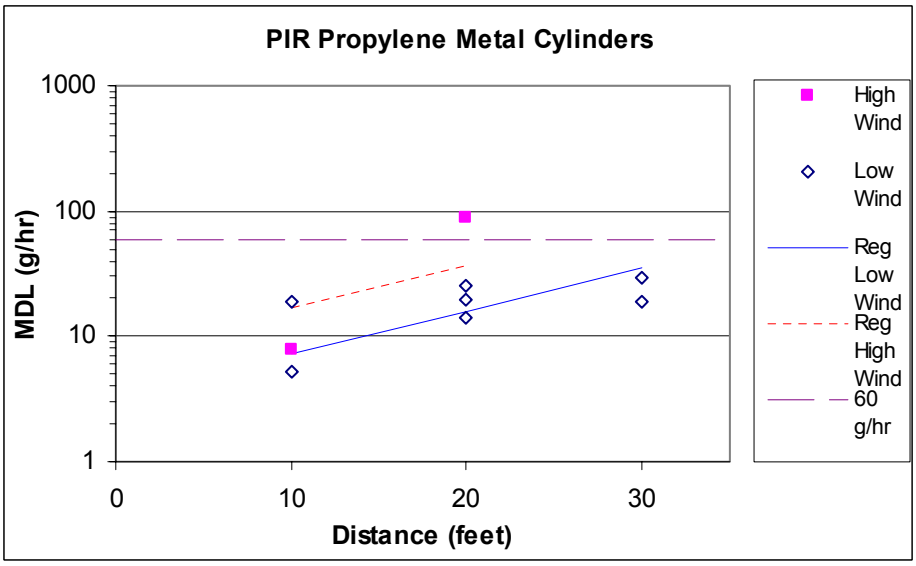

Exhibit 3-36. PIR propylene concrete wallboard.

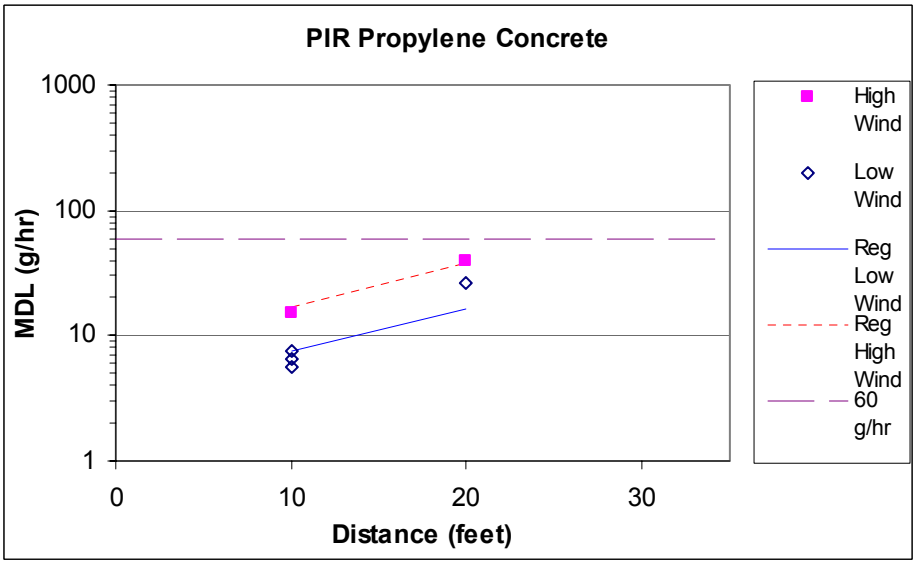

The minimum detection level model that regressed the test data imposed a constraint that distance slopes will be the same across different wind speeds. Therefore, the high- and low-wind speed regressions have the same slope, and the two line segments do not represent a simple best-fit line for the data points they model.

Camera Comparisons

This section provides a comparison of the four gas-imaging technologies evaluated – IMSS, long-wave BAGI, mid-wave BAGI and PIR. Selected test conditions are provided here for the

metal cylinder background and the four priority chemicals: 1,3 butadiene, 1-butene, ethylene, and propylene. The plots below have similar test conditions for each camera; however, each camera tested under different ambient conditions, and the long-wave BAGI camera tested without zooming.

To minimize the number of lines on a given plot, each exhibit in this section shows only portions of the regression models. The minimum detection level versus wind speed plots are limited to a 10-foot distance cases in this section. Furthermore, the minimum detection level versus distance plots are limited to the low wind speed cases in this section. Finally, the exhibits in this section show regression lines only. Additional plots showing distances at 20 and 30 feet, and high wind speeds are shown in Appendix G.

Exhibits 3-37 and 3-38 show camera comparisons for 1,3 butadiene. Exhibit 3-37 shows camera results for minimum detection level versus wind speed at only the 10-foot distance. Exhibit 3-38 shows camera results for minimum detection level versus distance at only the low wind speed.

The IMSS camera's detections were above 60 grams per hour but were made over a broader range of wind speeds and distances. The long-wave BAGI imaged 1,3 butadiene at only the 10-foot distance, so Exhibit 3-38 displays a point at that distance rather than a curve at multiple distances. The long-wave BAGI camera could detect 1,3 butadiene below a 60 grams per hour leak rate in the 10-foot, low wind speed case. The mid-wave BAGI camera did not image this chemical at any test conditions and the PIR camera only imaged this chemical with a concrete background.

Exhibit 3-37. 1,3 butadiene wind speed results.

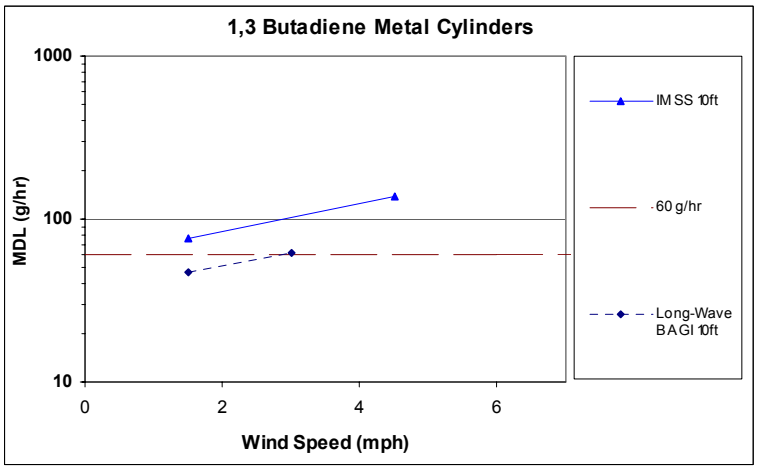

Exhibit 3-38. 1,3 butadiene distance results.

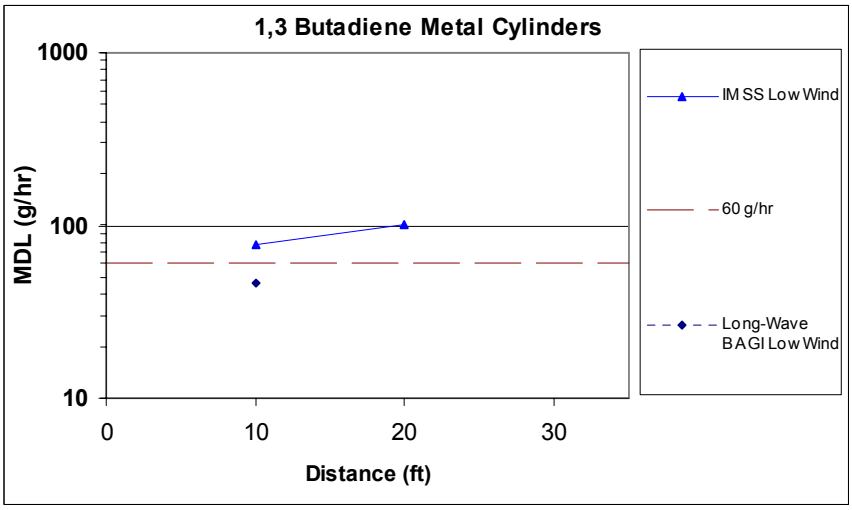

Exhibits 3-39 and 3-40 show camera comparisons for 1-butene. Exhibit 3-39 shows camera results for minimum detection level versus wind speed at only the 10-foot distance. Exhibit 3-40 shows camera results for minimum detection level versus distance at only the low wind speed.

The IMSS camera had detection levels below 60 grams per hour for two distances and low wind speed. The long-wave BAGI had broader detection ranges for wind speed and distance but did not image 1-butene below the 60 grams per hour reference line. The mid-wave BAGI camera had detection levels below 60 grams per hour for two distances and low wind speed. The PIR camera has detection levels below 60 grams per hour line for two wind speeds as well as two distances.

Exhibit 3-39. 1-Butene wind speed results.

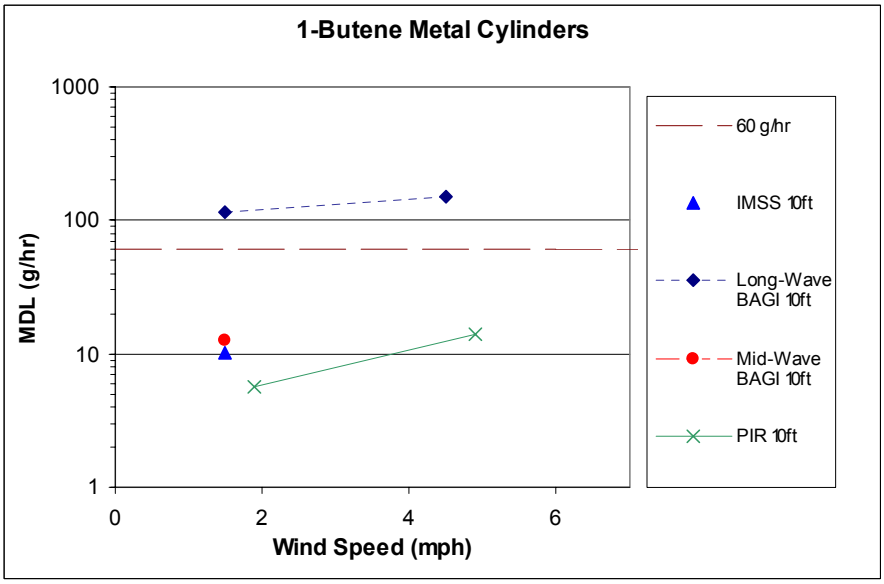

Exhibit 3-40. 1-Butene distance results.

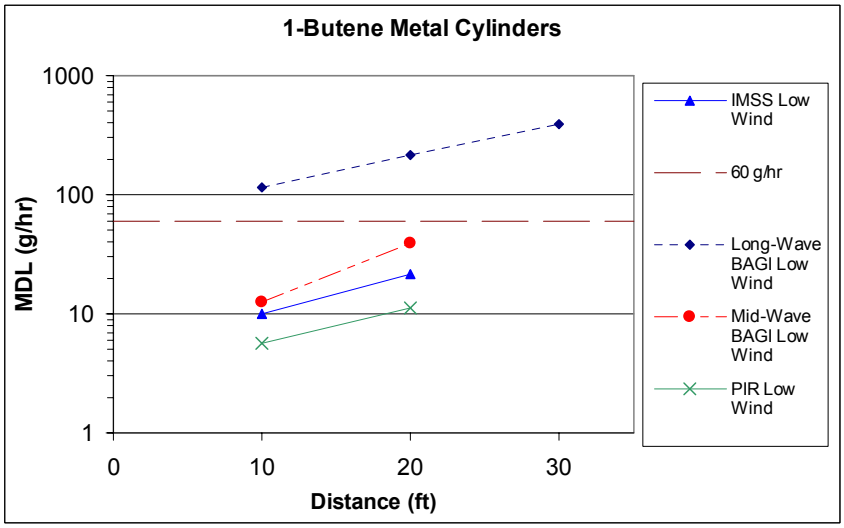

Exhibits 3-41 and 3-42 show camera comparisons for ethylene. Exhibit 3-41 shows camera results for minimum detection level versus wind speed at only the 10-foot distance. Exhibit 3-42 shows camera results for minimum detection level versus distance at only the low wind speed.

For wind speeds between 1.5 and 4.5 miles per hour, the IMSS camera detected ethylene below 60 grams per hour at 10 feet. The IMSS camera's predicted minimum detection level line crosses the 60 grams per hour reference line at about 15 feet for the low wind speed case.

Exhibit 3-41. Ethylene wind speed results.

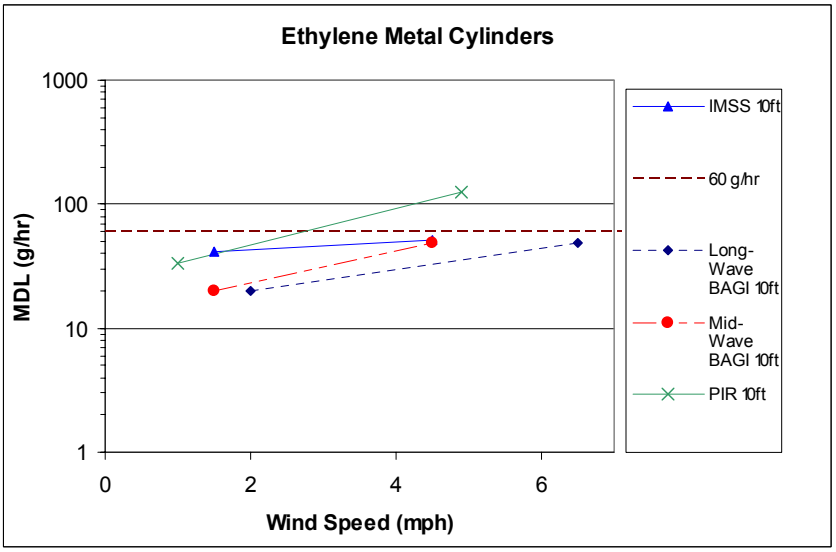

Exhibit 3-42. Ethylene distance results.

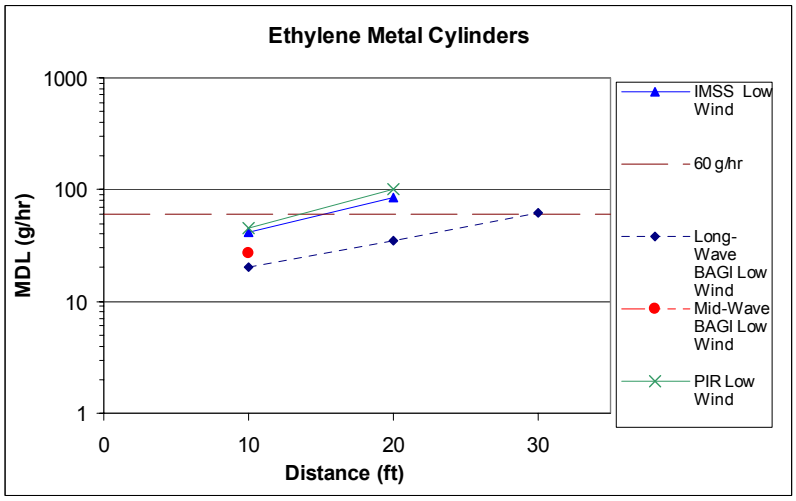

For wind speeds between 2.0 and 6.5 miles per hour, the long-wave BAGI detected ethylene below 60 grams per hour. The long-wave BAGI also detected ethylene below 60 grams per hour up to 30 feet for the low wind speed case.

For wind speeds between 1.5 and 4.5 miles per hour, the mid-wave BAGI camera detected ethylene below 60 grams per hour at 10 feet. The mid-wave BAGI camera's predicted minimum detection level line crosses the 60 grams per hour reference line at about 15 feet for the low wind speed case.

The PIR camera has detection levels below 60 grams per hour line for the low wind speed and 10 foot distance. The PIR camera's predicted minimum detection level crossed the 60 grams per hour line at about 3 miles per hour when imaged at 10ft distance.

Exhibits 3-43 and 3-44 show camera comparisons for propylene. Exhibit 3-43 shows camera results for minimum detection level versus wind speed at only the 10-foot distance. Exhibit 3-44 shows camera results for minimum detection level versus distance at only the low wind speed.

The IMSS camera could detect propylene below the 60 grams per hour level at wind speeds between 1.5 and 4.5 miles per hour and at distances between 10 and 20 feet. The long-wave BAGI camera's detections were made at leak rates higher than 60 grams per hour, but the distance detection range was the broadest of the imaging technologies, from 10 to 30 feet. The mid-wave BAGI camera could detect propylene below the 60 grams per hour level at wind speeds between 1.5 and 4.5 miles per hour and at distances between 10 and 20 feet. The PIR camera could detect propylene below the 60 grams per hour level at wind speeds between 1.5 and 4.5 miles per hour and at distances between 10 and 30 feet.

Exhibit 3-43. Propylene wind speed results.

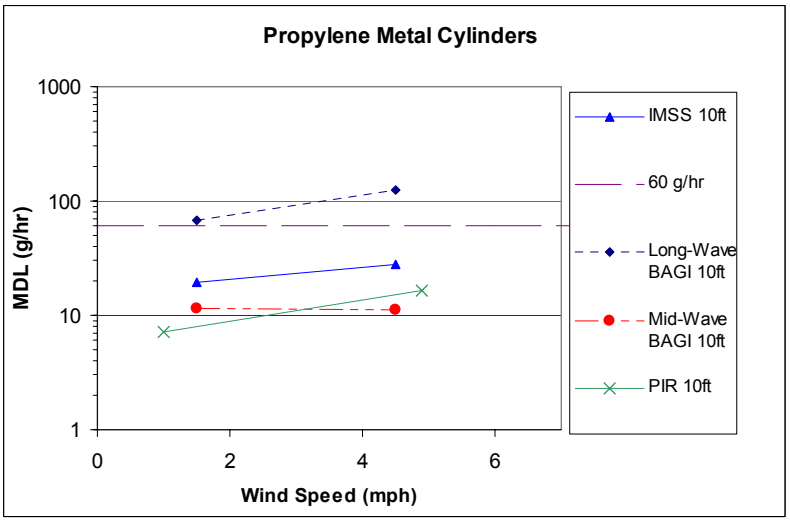

Exhibit 3-44. Propylene distance results.

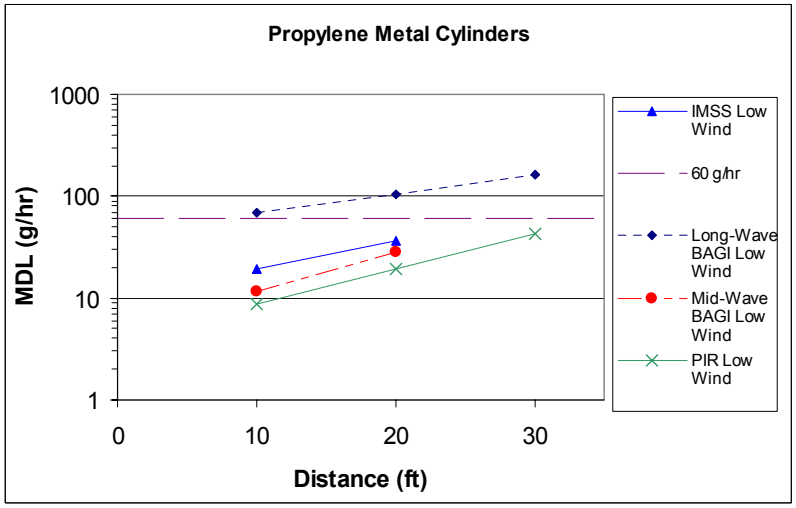

Appendix G shows results for all tested chemicals. The IMSS camera imaged butane, the only saturated hydrocarbon test chemical, below 60 grams per hour for all cases at 10 feet and for some cases at 20 and 30 feet. The IMSS camera also detected all six olefin test chemicals, and every tested olefin was detected at below 60 grams per hour for at least a 10-foot, low wind speed test case. Of the three aromatic test chemicals, the IMSS camera only imaged a leak stream of mixed xylenes, which also contained a large percentage of ethylbenzene. The IMSS camera was also the only technology to determine a minimum detection level for acetaldehyde.

The operator of the long-wave BAGI camera did not attempt to image butane, the only saturated hydrocarbon test chemical. The long-wave BAGI camera did not attempt to image certain chemicals because the operator did not believe the chemicals had sufficient infrared absorbance in the long-wave atmospheric window. Of the six olefin test chemicals, the long-wave BAGI

imaged four species at below 60 grams per hour for at least 10-foot, low and high wind speed cases. The remaining two test olefins, pentenes and isoprene, were not attempted with the long-wave BAGI camera. The three aromatic test chemicals were not imaged with the long-wave BAGI camera.

The mid-wave BAGI camera imaged butane, the only saturated hydrocarbon test chemical, below 60 grams per hour for all test cases up to and including 20-foot distances. For the olefin test chemicals, the mid-wave BAGI camera imaged four species at less than 60 grams per hour for at least 10-foot, low and high wind speed cases. The mid-wave BAGI camera could not detect 1,3 butadiene, and the pentenes leak was imaged, but the leak rate was not quantified.

QUANTIFICATION OF LEAKS OBSERVED WITH GAS IMAGING DEVICES

While Method 21 does not require that fugitive emissions be quantified, other regulatory programs do require the development of plant-wide emission inventories that include fugitive emissions. The gas-imaging cameras used in this study have not evolved to the point where they can provide a quantitative measure of a gas leak. As a result, mass emissions were quantified during the field study by either bagging components found to be leaking or using Method 21 screening results (which measure concentration) with correlation equations.

During the course of the laboratory evaluation, an effort was made to develop a technique to quantify fugitive emissions detected by the gas-imaging cameras. The test team considered several different approaches, which are discussed in this section of the report. While no approach proved to successfully quantify mass images as detected by gas-imaging cameras, the information provided below may provide a starting point for future investigations into quantification techniques.

Quantifying Mass Emissions as a Function of Distance

One approach evaluated considered the correlation of distance to mass emissions. While mass emission detection is influenced by several factors in addition to distance, a previous and rigorous evaluation of the BAGI technology that generated much more data on various factors assessed in this study showed clearly that for a particular chemical, distance is the predominant factor, followed by wind speed, and background.[9]

The principal behind this approach is as follows: the human eye can discern in an infrared image the presence of a hydrocarbon chemical leak plume against a background in proportion to the size and color density of the leak plume, relative to the background. Since the infrared image from some technologies is a black and white picture, discerning the leak plume is a matter of seeing a darker or lighter shade of gray against the varying shades of white to gray scale to black images of the background. In all cases, the movement of the plume in wind makes it considerably easier to detect the plume against the still background – as can be seen in several of the images included in this report, it is somewhat difficult to identify a small leak plume in a still

[9] Sandia National Laboratory and ICF Consulting, July 2003: *Report on Laboratory Test for Evaluating Backscatter Absorption Gas Imaging Technology*.

photograph. In general, the farther away the observer with the camera is, the smaller the plume image is in the camera viewer and the larger or darker the plume has to be to be observed.

Leaks that are above the minimum detection level for a particular chemical are progressively easier to observe because the plume size and/or density of the hydrocarbon forms a more contrasting image against the background. Under this approach, a camera operator must "back-up" to the distance from the leak where the image is barely perceptible. This would be the distance at which the mass emission is at the minimum detection level. Distance can be measured or estimated in the field and this measurement entered into a correlation equation to estimate the mass emission of the leak.

Limitations to a Distance-Based Approach

There are practical limitations by both types of technologies evaluated in this study to this approach. The BAGI technologies evaluated in this study create an infrared image by illuminating the scene with laser light of a frequency absorbed by the hydrocarbon of interest. Just as a flashlight cannot illuminate an airplane sufficiently for the human eye to detect in the night sky, the laser signals produced by the portable BAGI technologies tested in this study were not powerful enough to illuminate the leaking component beyond approximately 20 or 30 feet. A more powerful laser would extend the range of the BAGI technology – note that in another study where a more powerful mid-wave BAGI camera was employed from a van, leaks could be discerned from distances of 40 or 50 feet.[10]

In addition to the power of the laser, there must be a reflective background within range of the laser illumination beam for the BAGI technology to detect gases. For the man-portable cameras tested in this study, this means within 20 to 30 feet. A distant background and the sky appear black on a BAGI screen. Furthermore, certain other surfaces, such as ice, green vegetation, and steam plumes, absorb infrared light and appear dark or black. Also, highly reflective flat surfaces can reflect the laser beam away from the camera, creating a black image (e.g. flat plastic signs viewed from an oblique angle appeared black in field testing). In practice, the camera operator moving to a position where the equipment presents a bright, clear image against which a leak plume can be identified would overcome most of these background issues.

The practical effect of this limitation for BAGI technologies, insofar as this approach to quantification is concerned, is that as the camera operator "backs-up" to find the minimum detection level distance for a leak, the leaking component will become as dark as the plume before the minimum detection level is found due to the range limitation of the laser. In a way, this would be akin to "pegging" the instrument, which would represent an upper limit on determining the leak mass.

Passive technologies, such as the IMSS and PIR cameras evaluated in this study, do not effectively have an upper distance limit – in the field testing described in Section 4 of this report, some leaks were identified by the PIR camera from a distance in excess of 40 feet, and aerial

[10] U.S. EPA, November 1999: *April 1999 Refinery Test of a Gas Imaging System*. National Advisory Council on Environmental Policy and Technology (NACEPT), Petroleum Refining Sector Workgroup Equipment Leaks Project, ICF Consulting document no: 91069RP3.WPD. Fairfax, VA 22031.

applications of at least one of the passive technologies tested have identified large natural gas transmission pipeline leaks from a distance of 3.5 miles. The practical limitation of the minimum detection level distance correlation is the camera operator's ability to back-up far enough from the leak to reach the minimum perceptible leak image. It is conceivable that future technologies could be manufactured with optical demagnification (zoom out) ability that would allow a camera operator to determine a measure of minimum detection level without "backing-up."

In addition, passive IR technologies do not have the same background limitations as the BAGI technology. The sky and distant backgrounds may appear bright in the image, against which a hydrocarbon leak plume may contrast clearly. If the hydrocarbon plume radiance is lower (e.g. colder) than the background, the plume appears relatively darker. If the plume is more radiant (e.g. higher temperature) it appears relatively lighter. The limitation of passive IR is when the leak plume approaches the same radiance as the background. In the field tests conducted in this study, the highly variable equipment backgrounds in petroleum/petrochemical plants seemed to provide enough differential radiance that hydrocarbon leak plumes were found by the IMSS and PIR cameras as easily as the BAGI technologies. How this radiance variability would affect a correlation of minimum detection level distance requires more study.

The IMSS camera provided the camera operator with a false color image of the hydrocarbon leak plume, which contrasted quite well with typical hydrocarbon plant equipment. This can be seen in Figures 4-1 to 4-3. The false color image did not change brightness relative to the leak size, but rather "size." As the minimum detectable leak rate was approached, fewer pixels in the equipment image were falsely colored, until it was not possible to connect a few random and changing false color pixels with any particular leak source. This particular technology, in the state of development presented for these tests, produced considerable "noise" (false color images of movement in the equipment image not related to hydrocarbon leaks). When this technology is further developed with image stabilization, it could be superior to the other three technologies in its ability to identify leaks and correlate with the minimum detection level.

Alternative Technique

One alternative technique to this approach would be to define a specified distance for viewing a gas plume (e.g., 10 feet) and compare the plume size at this distance to a leak plume standard. For this alternative technique, three visual aids would be required for the comparison standard: size, color density, and some method for determining wind speed and direction. While this alternative technique would in theory be inherently quicker and easier than "backing up" to the minimum detection level distance, the angle of view of the plume may cause difficulties in comparing the plume with a plume standard. For example, in a parallel view (i.e. the plume moving directly toward or away from the camera operator), the plume would appear very thick, and absorb or radiate more infrared light per mass emission. With a perpendicular moving wind, the thickness of the hydrocarbon plume would be the least, and absorb or radiate the least amount of light relative to mass emission. In practice, wind currents are not steady and unidirectional in a typical plant environment, but rather wafting and swirling around in all directions. While the minimum detection level correlation equations were developed in a wind tunnel simulated environment and strictly perpendicular to the line of camera sight, the few field

data taken at minimum detection level distance correlated reasonably well with lab data regardless of wind direction.

Quantifying Mass Emissions by Differential Imaging

A second approach considered involved the concept of relative opacity measurement through differential imaging. In this approach, two laser beams could be directed to illuminate the equipment scene simultaneously – one tuned to a frequency strongly absorbed by the hydrocarbon plume and one not absorbed by the hydrocarbon. Comparing the strength of the two beams would allow for a direct comparison of how much infrared light energy had been absorbed, and therefore, what mass of hydrocarbon was present in the view.

While this approach has been tried with passive and active infrared imagers (and considered in the laboratory evaluation conducted in this study), there are many unknowns surrounding a leaking plume to objectively determine mass by this approach. The differential image of a gas plume is only represented in two dimensions in a camera viewer -- the operator only knows the vertical and horizontal dimensions of the plume; the plume thickness is an unknown. Since the optical density of the plume depends on the product of concentration times thickness, the mass density of the plume is only as good as one's guess of the thickness. Moreover, to determine the mass flux of the plume, one must determine the speed of the gas plume at the leak source.

Moving Forward

It remains clear that the ability to quantify emissions using a gas-imaging device is a desirable objective. This is due in part to limitations in calculating mass emissions using Method 21 screening values and correlation equations, particularly for nontraditional components for which correlation equations have not been developed. While a number of studies have been conducted to assess the accuracy of correlation equations across the entire population of fugitive components in a facility, it remains to be seen as to how accurate these equations are for calculating mass emissions from a smaller subset of components found to be leaking with gas-imaging.

Under Method 21, a hydrocarbon analyzer measures the concentration of a hydrocarbon leak by pulling a sample into a small probe at a single point. Most fugitive leaks occur from elongated cracks in imperfect mating surfaces between metal components and flexible gaskets. These cracks can be many feet long in flanges, vessel heads and manways. For valve stems, arguably the most common source of leaks, the "crack" may typically be only an inch of circumference around a valve stem, but this is still considerably longer than the analyzer probe is wide. As a result, the hydrocarbon analyzer measures a single spot in a leak that can range from a point source to a broad sheet of emission. Over a very large number of leaks, the statistical mean value can be reasonably accurate. But for a single leak, a pinhole leak of one gram per hour can give the same hydrocarbon analyzer concentration measurement as a heat exchanger bundle head or pipe flange of 1,000 grams per hour.

Optical leak imaging technologies view the entire leak plume. The size and density of the plume determines whether the camera operator sees the image. The size and density of the plume in the

camera view correlates well with distance from the leak. Therefore, a pinhole leak of one gram per hour does not present an image discernable by the camera operator from a reasonable viewing distance (e.g., 5 to 10 feet). Furthermore, a broad sheet of leakage that is in total 50 grams per hour may be visible to the optical gas-imaging camera operator, while at any single point it may register well below the "leak" threshold established for a Method 21 instrument.

4. FIELD EVALUATION OF GAS-IMAGING DEVICES

In this section of the report, the results of field studies conducted to measure and detect fugitive emissions using portable optical gas-imaging devices are presented. As discussed in earlier sections of this report, the use of gas-imaging devices, which provide a real-time, optical image of a leaking component, is of particular interest to federal and state regulatory agencies, as well as the petroleum and petrochemical industries, as a means to more cost effectively and accurately identify leaking hydrocarbons that contribute to air pollution. Both federal and state agencies are considering the acceptance of this class of technology as an alternative to the currently prescribed method of leak identification in federal and state air pollution prevention regulations.

The purpose of the field evaluation was to gain insight into the application of four optical gas-imaging devices for the detection of fugitive emissions of hydrocarbons from refinery and petrochemical plant process equipment and piping systems. Objectives of the evaluation included:

- Determining the mass emissions rate for various gases that each device could detect under normal refinery/chemical plant operating conditions; and

- Documenting (as appropriate) the apparent impact of external factors such as distance, angle of view, background objects, hydrocarbon type, and meteorological conditions on the ability of the gas-imaging devices to detect fugitive emissions.

Plant sites for the field study were chosen based on a list of chemicals of interest to the TCET. Prior to the field evaluation, three of the four gas-imaging cameras used in the field study participated in a laboratory study to determine, for each chemical of interest, the minimum gas detection level of each camera. A similar evaluation of the fourth camera was conducted following completion of the field study. The results of the laboratory study are discussed in Section 3 of this report.

Table 4-1 summarizes the chemicals of interest and identifies those seen by the gas-imaging cameras during laboratory and field testing.

Table 4-1. Summary of Chemical Species of Interest Viewed by Gas-Imaging Technologies.

Chemical Species of Interest	Tested in Lab	Tested in Field
Ethylene	X	x
Propylene	X	x
Acetaldehyde	X	
Isoprene	X	
all Butenes	X	x
1,3 Butadiene	X	x
all Pentenes	X	
all Xylenes	X	
all Butanes	X	
all Hexenes		x

Chemical Species of Interest	Tested in Lab	Tested in Field
Formaldehyde		
Toluene		
all Trimethylbenzenes		
all Ethyltoluenes		
All Pentanes		

In addition to the technical results of the field studies, this section provides information on the testing methodology followed for gathering and analyzing data. In addition, information on the field study test team and the roles and responsibilities of each are presented in this section.

FIELD STUDY TEST TEAMS

The project team conducted an evaluation of the four gas-imaging devices at two hydrocarbon plants located in the Houston/Galveston area between February 2 and 4, 2004.[1] The gas-imaging devices were used to detect fugitive emissions in a number of different process units covering several hydrocarbons. In general, components such as valves, pumps, heat exchangers and piping connectors were scanned for leaks.

At both sites, field study personnel were divided into six teams. These teams represented the following functions:

- Project Management;
- Gas Imaging;
- Method 21 monitoring
- Component Bagging;
- Data Analysis, Reporting, and Quality Assurance/Quality Control; and
- Plant Coordination.

During the field studies, at least one individual from the Project Management and Data Analysis teams accompanied the Gas Imaging team. A representative from the Method 21 monitoring team floated among the various Gas Imaging teams. In addition, personnel from the safety department at each facility escorted the project team and determined whether and where the gas-imaging devices could be safely used. A description of the functions and responsibilities of each team are as follows:

[1] In 2002, a field test to evaluate one optical imaging technology was conducted in the HGA at ethylene facilities designated as Sites A and B. In addition, other field evaluations were conducted in the 2002 study to assess the accuracy of fugitive emissions component counts. These evaluations were conducted at facilities in the HGA identified as Sites C through H. A copy of the 2002 study is available at www.harc.edu/harc/Projects/AirQuality/Projects/Status/H5.aspx. To provide a degree of consistency between the 2002 study and this study, the two facilities used in this study are identified throughout this report as Sites C_{04} and D_{04}.

- **Project Management Team:** The primary responsibilities of the Project Management team included the following:

    - Coordinate the design of test protocols that met the objectives of the statement of work;
    - Coordinate test activities and data collection of all other teams;
    - Interface with the TCEQ and plant personnel on the design and objective of the test;
    - Determine which leaking components were to be bagged;
    - Make decisions (in conjunction with plant personnel) regarding how the field study was to be conducted; and
    - Supervise/oversee the analysis and presentation of test results.

- **Gas Imaging Team:** The primary functions and responsibility of the Gas Imaging teams included the following:

    - Calibrate and operate their respective cameras and ensure that the equipment functioned at peak capability throughout the entire test period; and
    - Screen the areas selected by the Project Management team to determine the effectiveness of the camera to detect ethylene fugitive emissions.

- **Method 21 Team:** At both sites, the contractor providing leak detection and repair services to the facility were used for Method 21 monitoring.

- **Component Bagging Team:** The Component Bagging team gathered data required to determine the mass emissions rate and chemical composition of leaks. The team collected samples from both leaking components identified by the Gas Imaging team as well as leaks identified by Method 21 that were not identified by the camera. Team personnel performed gas chromatograph analyses on-site.

- **Data Analysis, Reporting, and Quality Assurance (QA)/Quality Control (QC) Team:** The responsibilities of the Data Analysis, Reporting and QA/QC team, included the following:

    - Observe that data collection and QA/QC activities were conducted according to the test protocol;
    - Gather and document environmental conditions, such as wind speed and direction, distance from the camera and leaking component, and time of day; and
    - Compile, analyze, and report on the data collected during the test.

- **Plant Coordination Team:** The Plant Coordination team coordinated testing plans and strategies between plant management and the Project Management team. The primary responsibilities of the Plant Coordination team were:

    - Facilitate all internal coordination for test activities and data collection plans; and

- Interface between field study and plant personnel during pre-test planning, testing, and post-test data analysis.

In addition to the field study teams, representatives from the TCEQ and EPA were present during part of the testing to observe gas imaging, Method 21 monitoring, and bagging operations.

FIELD DEMONSTRATION SITES

The field evaluation of the four gas-imaging cameras was carried out over three days at Sites C_{04} and D_{04}. On February 2 and 3, 2004, the project team was at Site C_{04} where chemicals such as ethylene, butane/butylenes, and hexene were present. On February 4, 2004, the project team was at Site D_{04} where propylene, butylene, and 1,3 butadiene were present.

Table 4-2 shows the process units monitored at Site C_{04}. As seen, Site C_{04} had an ethylene compressor shed. Of a total of 6 compressors in that shed, two operating compressors and their ancillary equipment were scanned for leaks. A total of 11 leaks were found in the compressor-shed region. The other units at Site C_{04} scanned for leaks included a 1-butene process unit, a series of process units containing ethylene, 1-butene, 1-hexene and higher alpha-olefins, and another area that had a 1-butene pump.

Table 4-2. Process Units Covered at Site C_{04}.

Surveillance Areas at Site C_{04}	Chemicals Detected	Camera Coverage
Ethylene compressor shed	Ethylene	All cameras
1-Butene area with double-pipe heat exchangers	1-Butene, 1-Hexene	All cameras
1-Butene pump	1-Butene	IMSS did not survey
Alpha olefin separation units	Ethylene, Alpha olefins	All cameras

Table 4-3 shows the process units monitored at Site D_{04}. At Site D_{04}, the equipment scanned included valves, pump seals, one ethylene compressor, heat exchangers, vessels and piping connectors involved in processing ethylene, propylene, and 1,3 butadiene among other hydrocarbons and chemicals that were not on the chemical list of interest.

Table 4-3. Process Units Covered at Site D_{04}.

Surveillance Areas at Site $_{04}$	Chemicals Detected	Camera Coverage
Propylene splitters	Propylene	All cameras
Ethylene compressor deck		No leaks found
Propylene pumps	Propylene	All cameras
Butadiene separation	1,3 Butadiene	Mid-wave and long-wave BAGI cameras elected not to survey

FIELD STUDY DATA COLLECTION PROTOCOL

Since the four gas-imaging cameras used in the field study are not currently intrinsically safe, a hot work permit was required to operate on-site. This was obtained at each facility prior to field monitoring. Once the permit was obtained, the field study teams were dispatched to the site areas designated by the Plant Coordination team. Prior to entering any process areas, plant personnel were consulted to ensure that the area was safe to work in and no plant operations were underway in the area that would restrict field study operations. Area supervisors were notified that field study teams were operating in the process area.

Gas Imaging and Method 21 Monitoring

To complete the surveys in the allotted time, the four cameras operated simultaneously at different processing areas at Sites C_{04} and D_{04}. Each camera surveyed a designated process area in an unlimited time period and then rotated to another designated process area. This allowed each camera operator the opportunity to locate leaks independently and without assistance or prior knowledge from other cameras. Camera operators were allowed discretion when surveying a process area to position their camera in any accessible area around the unit so as to view the equipment from any angle.

Accompanying each camera was a QA/QC/Data Collection team member. The QA/QC team documented the camera's leak detections (and non-detections of known leaks) with paper notes, by taking photographs of the leak source, documenting process units and equipment tag numbers on or near the source, and determining if the operator discovered the leak independently or with assistance. In general, after a camera operator completed a leak surveillance of a designated process area, known leaks that were not discovered were pointed out and the camera operator tried again to see the leak. In most cases, the camera operator videotaped both detected and non-detected known leaks as the equipment and leak appeared in the camera. In some cases, leaks that were falsely identified were videotaped for a visual record. QA/QC team members also recorded other relevant detection conditions including wind speed, viewing distance, and a description of the background behind a leak source. Leaks were verified by Method 21 readings in parts per million (ppm) of hydrocarbon present. All false detects by a camera were also verified by measuring the identified component with Method 21, finding zero leaking hydrocarbon. Selected leaks were measured for mass emissions using bagging techniques.

Mass Emissions Measurement

The gas-imaging technologies evaluated do not quantify the mass emissions rate of a leaking component. As a result, a second sampling team determined the mass rate and chemical speciation by bagging a representative sample of detected leaks. The bagging methodology is a measurement of the mass emissions from equipment leaks that has been used for several decades and is documented in the EPA's *Protocol for Equipment Leak Emission Estimates*.[2] The bagging methodology used at both sites is described in detail in Section 4 of the EPA protocol. After the

[2] U. S. Environmental Protection Agency. Protocol for Equipment Leak Emission Estimates. Research Triangle Park, NC. Publication No. EPA-453/R-95-017. November 1995.

field demonstration, bagging results were matched to camera imaging data using component ID tag numbers, written logs, and camera videotapes.

Analytical Procedures

The bag samples collected at both sites were quantitated using a Hewlett-Packard Model 5890 gas chromatograph (GC). Compound separation was accomplished with a 1/8" x 8' SP-1000 packed column. Samples were introduced into the GC using a 0.5 ml sample loop and air-actuated valve.

Samples were quantitated for ethylene, propylene, 1-butene, 1,3 butadiene, and 1-hexene. In addition, standards for the straight-chain alkanes (methane through hexane) were also analyzed to help assess relative retention times of the C_1 through C_6 alkenes and alkanes. Samples of ethylene, propylene, 1-butene, and 1,3 butadiene were quantitated using a five-point calibration curve while 1-hexene was quantitated based on a single concentration response factor. Therefore, quantitation of 1-hexene will have more uncertainty than the quantitation for the other four compounds.

The ethylene/propylene concentration curve was established by analyzing standards containing, nominally 100 ppm, 1,000 ppm and 5,000 ppm of each compound and then performing serial dilutions in a 100 ml gas-tight syringe with ambient air to challenge the curve and extend the range of the calibration. The 1-butene/1,3 butadiene concentration curve was established by using a single standard containing nominally 1,000 ppm of each compound. Serial syringe dilutions were then used to develop a calibration curve between 1,000 ppm and 20 ppm. Individual sample quantitation was then performed from a linear regression of the standard data. The concentration of 1-hexene was quantitated from the response factor from a single point 15-ppm standard. There were some unidentified C_4 compounds detected in a few of the samples, but in general, no other VOCs were found in any significant concentrations.

Data Collection and Compilation

Four primary types of data were collected during the plant surveys:

- Bagging data;
- Infrared camera data sheets;
- Infrared camera video recordings; and
- Visible light still images of leak sources

Several team members collected the field data. To ensure that the data was compiled into a consistent data set for reporting and analysis, several quality assurance/quality control (QA/QC) steps were taken. These steps are described below.

1. Field data was compiled into a single data set to create a master list of leak sources. Following each of the first two test days at Site C_{04}, the four QA/QC teams collaborated on a master list of leaks detected for that day. The Site D_{04} test was prematurely terminated because of weather so a master list could not be developed at the plant site and was created afterwards from the body of recorded data.

2. Once the master list of leak sources was compiled, still images and camera data sheets were matched with field data to the correct leak source from the master list.

3. Next, bagged leak data was matched to the correct source.

4. Finally, because each camera looked at (and recorded) leaks from potentially different directions and distances, the video segments from each camera were reviewed to verify that the data sheets correctly indicated a camera detecting the leaks identified on the master list.

In some instances, a camera did not have a data sheet or a video segment for a particular leak source, leaving a data gap. If the leak source was located in an area that the camera clearly had surveyed, the camera was assigned a "non-detect" for that source. In certain cases, a camera operator opted to bypass a particular leak source based on the knowledge that the camera could not image the predominant chemical species in the process area. In those cases, the camera was assigned a "non-detect" for that leak source.

In the data compilation, four assumptions were made:

1. All four cameras thoroughly surveyed all of the Site C_{04} areas except (2) below.

2. The IMSS camera did not survey a remote 1-butene pump area at Site C_{04}.

3. All four cameras thoroughly surveyed the Site D_{04} propylene areas.

4. The BAGI cameras did not survey the Site D_{04} butadiene area.

The resulting data set had 14 leaks that were detected by one or more cameras and bagged to give exact chemical speciation and mass leak rate. Cameras detected an additional 17 leaks but bagging data could not be connected to these sources. Finally, 35 leaks were identified by Method 21 and bagged for use in developing ethylene specific correlations (described in Section 6 of this report); the QA/QC teams did not know of these leaks and they were not detected by any camera.

The total leak rate in grams per hour for the 14 bagged and imaged leaks were determined by summing the mass leak rates for all chemical species present in the leak stream as determined from the bagging results. Determining which chemical(s) within a leak plume a camera actually imaged cannot be reported with confidence since operators adjusted detection wavelengths in the field and one camera's wavelength is proprietary. This creates a large degree of uncertainty in

determining which chemicals within a leak plume were being detected amongst the other species present in the leak.

Test Conditions

The weather on all three days of testing was windy, but the wind speed and direction within the plant areas was not steady; rather it was swirling and changing magnitude and direction throughout the test day. Wind speed and direction measurements were attempted with a hand-held anemometer, telltale, and compass but this data was highly irregular. Rain threatened all of the third day of testing; a thunderstorm eventually required the premature cessation of field activities.

Camera videos recorded the plant background, which was as typically variable as any petroleum refinery and petrochemical plant processing area. This background consisted of bare concrete pads and vessel supports, painted metal vessels, valves, pipes and piping connectors, and some unpainted metal equipment normally associated with pump seals and stainless steel tubing connectors. Most leaks were viewed against near background equipment. Some leaks were observed by the passive IR cameras against distant or sky backgrounds. Only the IMSS technology identified leaks that either could not be verified by Method 21 readings or were not a hydrocarbon leak (e.g., in one case, a cooling tower plume of water fog in the distant background was identified; in another case, an instrument air supply line leak was identified).

FIELD STUDY RESULTS

The field study resulted in the discovery of 66 leaks at the two test sites. The four infrared cameras imaged 31 leaks, while the Method 21/Bagging team discovered 49 leaks. Exhibit 4-1 provides a summary of leaks attributable to each survey method.

As seen in Exhibit 4-1, neither the Method 21/Bagging method nor the infrared camera survey method alone discovered all fugitives leaks at the test sites, and both methods found the same 21.2% of the total discovered leaks (14 leaks seen by both methods of a total of 66 leaks).

Exhibit 4-2 presents the same 66 leaks with respect to the infrared cameras. The leaks are tallied according to the measured leak rate, with successively larger leaks appearing near the right. The y-axis is a measure of leak count.

Exhibit 4-1. Leaks Discovered by Different Survey Methods.

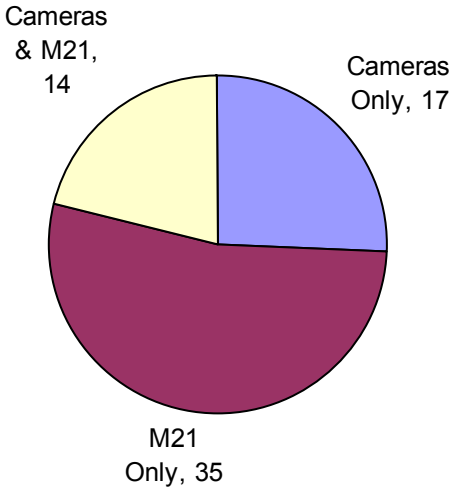

Exhibit 4-2. Leak Survey Summary by Leak Size.

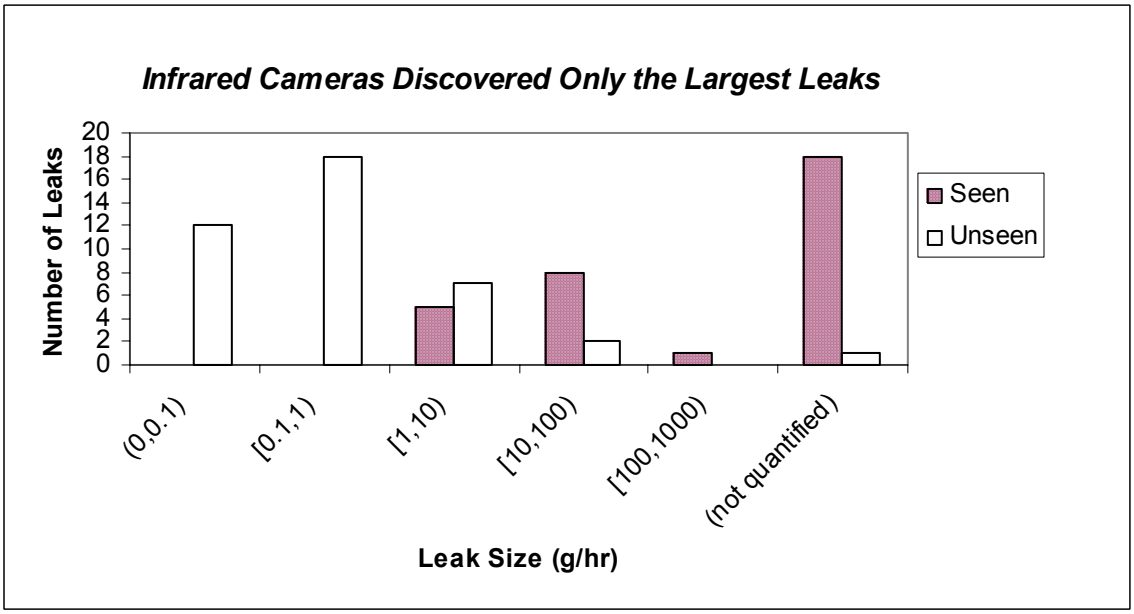

Exhibit 4-2 indicates that the infrared camera survey discovered only the larger leaks. The cameras discovered most of the fugitives emitting 1 gram per hour (g/hr) or higher, and the cameras did not discover any leaks measuring between 0 and 1 g/hr. The right-most column in Exhibit 4-2 shows leaks that were not measured during testing. Regardless of their size, the cameras successfully imaged all but one of the leaks that are not quantified which supports the conclusion that the infrared cameras do not detect most small leaks but do detect large leaks – the fugitives that are the most prominent source of emissions and the most-effective to repair. The 30 undetected leaks between 0 and 1 g/hr were emitting only 0.6 g/hr, so locating and repairing these leaks gave diminishing benefits compared to the more than 533.9 g/hr imaged by the cameras.

Survey Results by Camera

Exhibit 4-3 is a comprehensive summary of each camera's survey results. The exhibit shows the 49 measured leaks and each camera's performance on surveying the leaks. The leaks shown in Exhibit 4-3 include sources that are predominantly ethylene, butane, hexane, propylene, or butadiene. The y-axis lists the different cameras and is unitless. The x-axis shows measured leak rates on a logarithmic scale, so leaks are progressively larger moving to the right.

The left-most region of the x-axis is reserved for components considered to be non-leaking components. A camera that indicated the presence of a leak from these components, which could not be verified with Method 21, received a "false positive" for that component, and false positives are presented in Exhibit 4-3's zero region.

Hollow data points represent a measured leak that was not detected by a camera, while filled data points represent a measured leak successfully imaged by a camera. The *X* data points represent measured leaks discovered by the Method 21/bagging team but not discovered by any camera.

Exhibit 4-3. Performance Summary of Infrared Cameras.

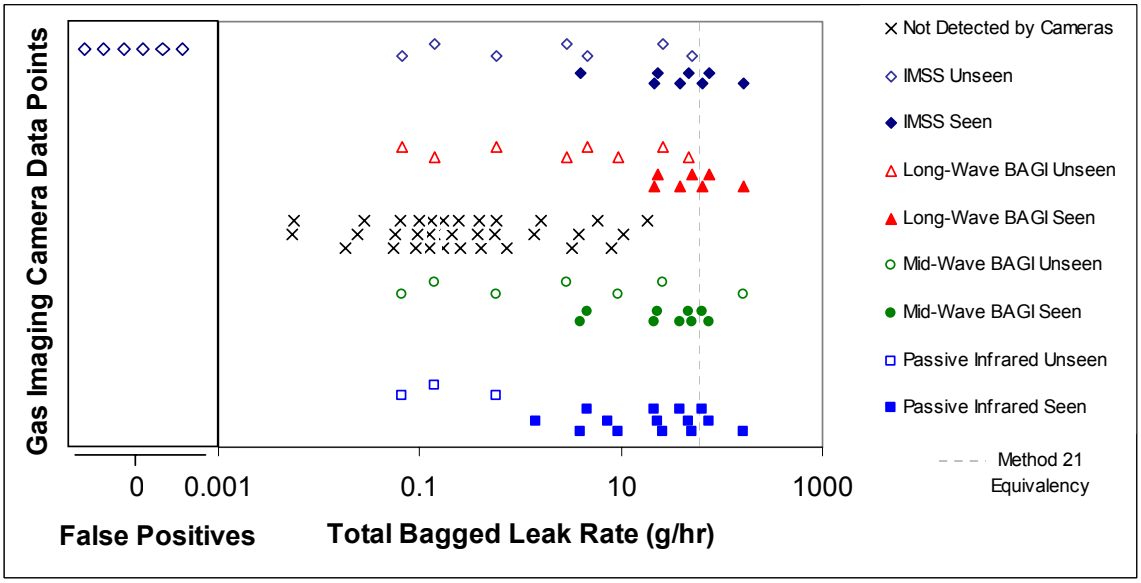

Exhibit 4-3 indicates that the gas-imaging camera survey discovered all of the large leaks, including all leaks at or above the 60 g/hr Method 21 equivalency leak rate. None of the cameras discovered any of the leaks emitting below 1.4 g/hr. Of the 42 leaks at or below 10 g/hr, the cameras detected five. In this field demonstration, the gas-imaging cameras detected 533.9 g/hr of the 595.4 g/hr of mass emissions determined by Method 21 and bagging, or approximately 90% of the bagged fugitive emissions from the demonstration sites.

Exhibit 4-3 also includes a vertical line marking the Method 21 equivalency leak rate for valves and other components. Three of the 49 leaks in Exhibit 4-3 emitted higher than the 60 g/hr Method 21 equivalency. The IMSS and long-wave BAGI cameras detected all leaks above 60

g/hr. The mid-wave BAGI and PIR cameras detected two of the three leaks above 60 g/hr. All four cameras detected numerous emissions sources below the Method 21 equivalency leak rate.

As apparent in Exhibit 4-2, Exhibit 4-3 shows that in general, the gas-imaging cameras do not detect the smallest leak sources and detect most of the larger leak sources. Each of the four cameras exhibits a region of non-detection followed by a region of detection where most but not all leaks are detected:

- The IMSS camera did not detect any leaks below 3.9 g/hr. Of the leaks larger than 3.9 g/hr, the IMSS camera did not detect three leaks.
- The long-wave BAGI camera did not detect any leaks below 21.7 g/hr. Of the leaks larger than 21.7 g/hr, the long-wave BAGI camera did not detect two leaks.
- The mid-wave BAGI camera did not detect any leaks below 3.9 g/hr. Of the leaks larger than 3.9 g/hr, the mid-wave BAGI camera did not detect three leaks.
- The PIR camera did not detect any leaks below 1.4 g/hr. Of the leaks larger than 1.4 g/hr, the PIR camera detected all leaks.

A camera with a larger region of detection missed more leaks within its region than a camera with a smaller region of detection, as shown in Exhibit 4-4.

Exhibit 4-4. Infrared Camera Detection and Non-Detection Regions.

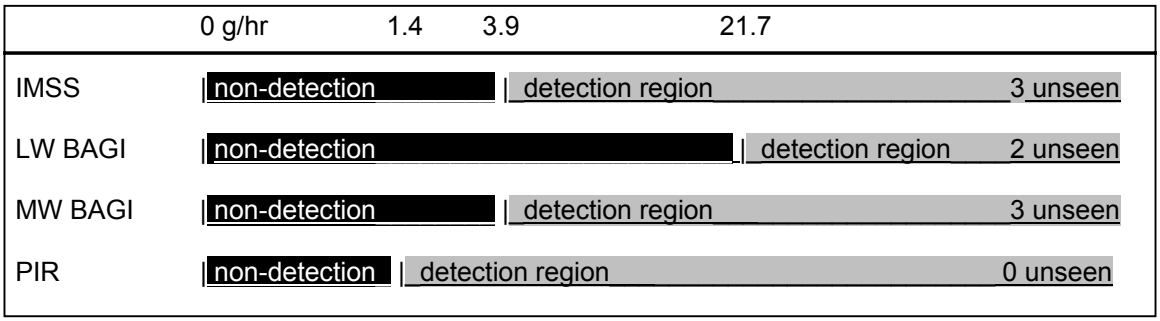

Exhibit 4-5 displays a subset of the leaks shown in Exhibit 4-4 and focuses only on leaks detected by the cameras. The exhibit shows a tally of detected leaks by each camera, as well as the total number of leaks discovered during the camera surveys. Exhibit 4-5 shows that no single technology detected all 31 leaks. Fewer leaks would have been discovered if only one technology had been evaluated instead of four. Exhibit 4-5 also differentiates between discovered leaks that were quantified and discovered leaks that were not quantified; the bagging method used to quantify leaks could not be performed on every leak source because of time constraints or leak sources that were not amenable to bagging (e.g. vent stack).

Exhibit 4-5. Gas-Imaging Camera Leak Detection Tally.

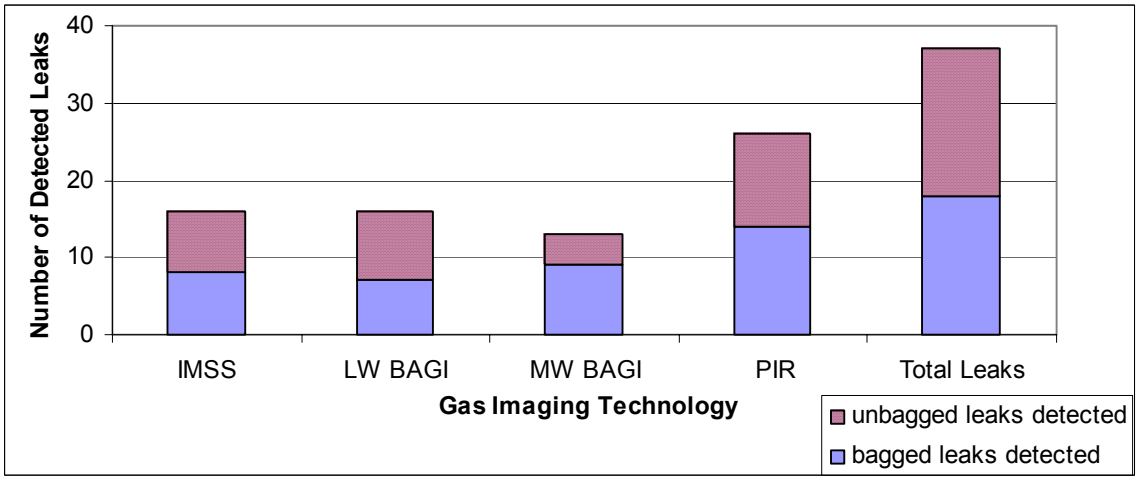

Survey Results by Species

Of the 49 leaks that were quantified, 30 leaks contained predominantly butene. Ethylene was the predominant species in 11 leaks, and the remaining leaks were primarily butadiene, hexene, or propylene. The species distribution of the leaks is shown in Exhibit 4-6.

Exhibit 4-6. Primary Mass Component of 49 Leak Sources.

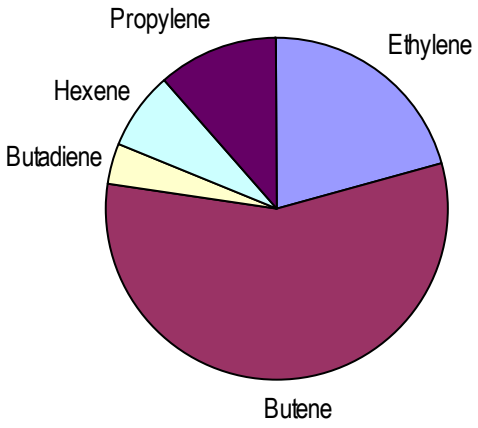

Since the majority of the leaks were composed of primarily butene or primarily ethylene, camera performance in the field survey can be evaluated by chemical species.

Butene Survey Results

Exhibit 4-7 shows the number of leaks that were predominantly detected by each of the four cameras, as well as the total number of butene leaks found in the camera survey.

Exhibit 4-7. Camera Survey Results for Butene.

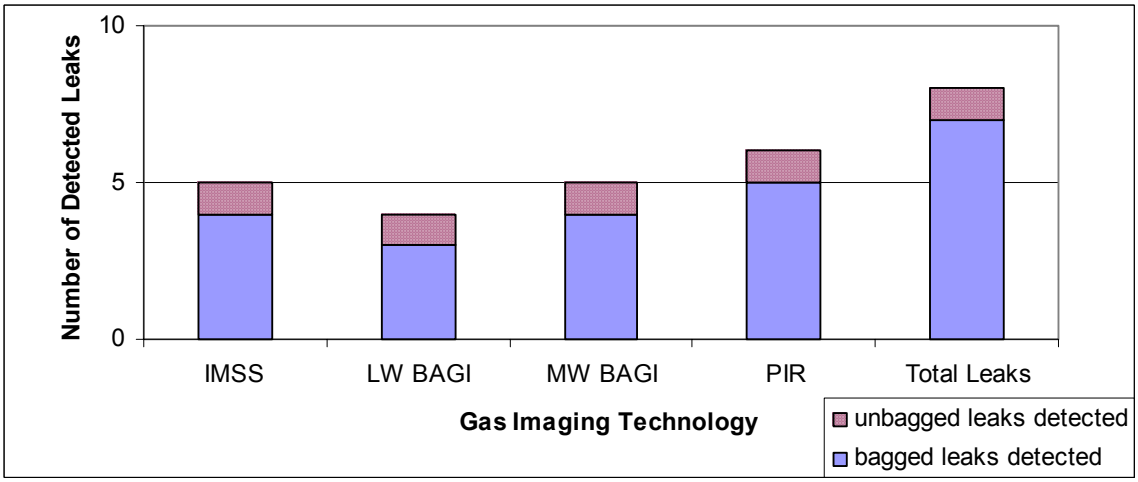

Exhibit 4-7 indicates that no single camera imaged all of the butene leaks found during the field study. Each camera imaged at least half of the butene leaks.

Exhibit 4-8 is a subset of Exhibit 4-3 and shows all butene leaks detected and measured by the cameras and by the Method 21/Bagging team. The y-axis separates the cameras and is unitless. The x-axis measures leak rates on a logarithmic scale. The leak rates shown in Exhibit 4-8 are the leak rates of pure butene or 1-butene. Other mass contributions to a predominantly butene leak were insignificant.

Exhibit 4-8. Survey Results for Butene.

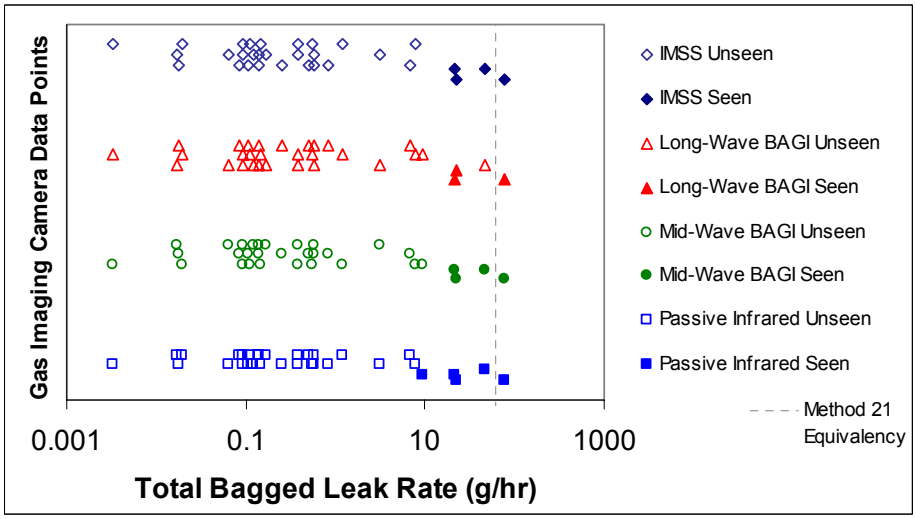

The butene-specific results mirror trends for the overall mass leak rate results; each camera's performance can be classified into a region of non-detection and a region of detection. All four cameras detected the one leak above the 60 g/hr Method 21 equivalency rate.

Exhibit 4-9 shows butene detections for each camera. Superimposed over each camera's butene performance is that camera's minimum detection level (MDL) determined from the Naperville MDL laboratory tests.[3]

Exhibit 4-9. Butene Detections by Camera.

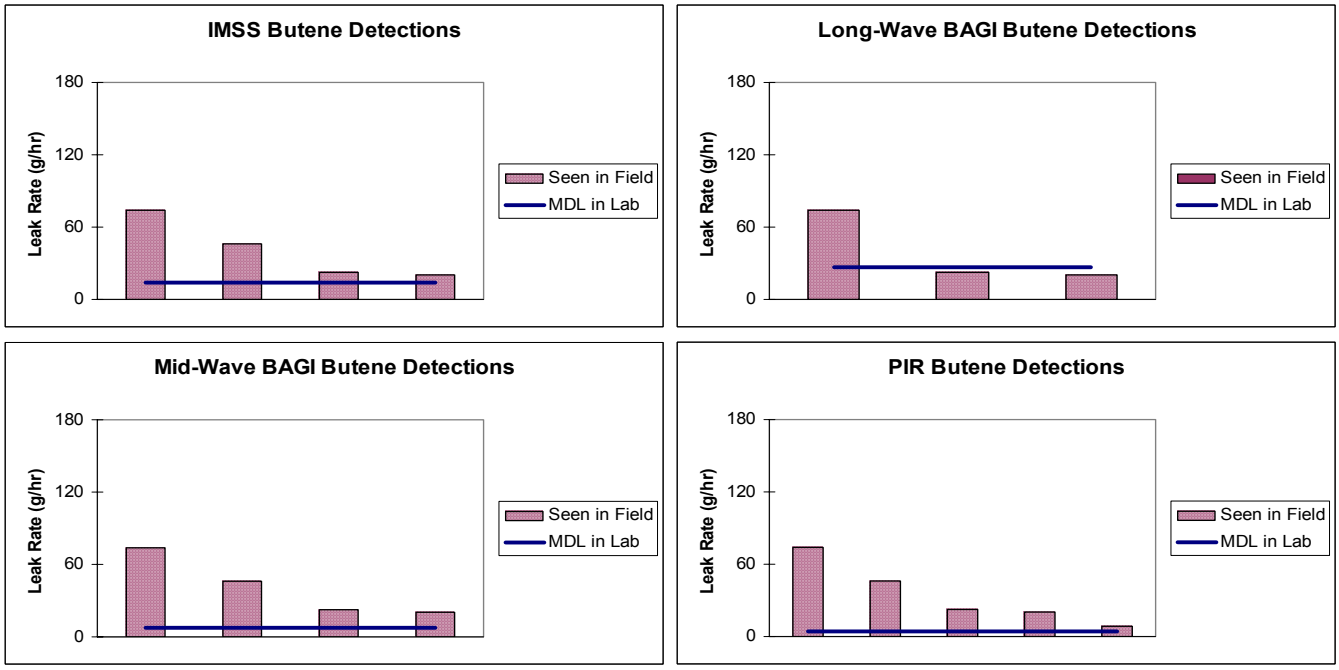

All butene leaks detected by the cameras were above each camera's MDL, with the exception of two leaks detected by the long-wave BAGI camera. The two leaks below the long-wave BAGI camera's MDL were smaller by 5 g/hr, which can be attributed to field conditions that were not replicated in the laboratory. Thus, the field survey results for butene do not conflict with MDL determinations in the laboratory.

Exhibit 4-10 shows butene leaks that were not detected by the cameras. Again, each camera's MDL for butene is included in the exhibit.

Exhibit 4-10 further affirms the MDL determinations from the laboratory experiments – most leaks that were not detected fell well below a camera's determined MDL. Most non-detected leak sources were measured to be several orders of magnitude below the corresponding MDL.

[3] The laboratory tests determined MDLs for various viewing parameters as described in Section 3 of this report. The MDLs used for comparison purposes here are the low wind, 10-foot distance, concrete background test conditions.

Exhibit 4-10. Butene Non-Detects by Camera.

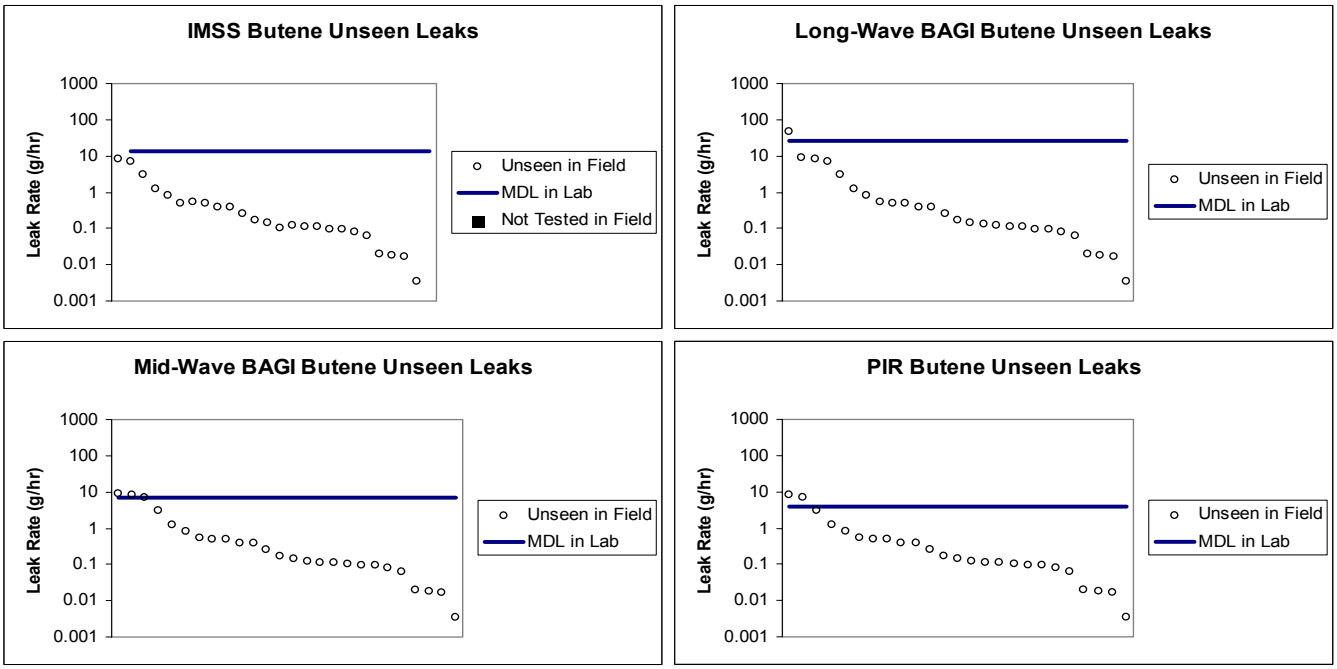

Ethylene Survey Results

Exhibit 4-11 shows the number of primarily ethylene leaks imaged by each of the four cameras, as well as the total number of ethylene leaks found in the camera survey.

Exhibit 4-11. Camera Survey Results for Ethylene.

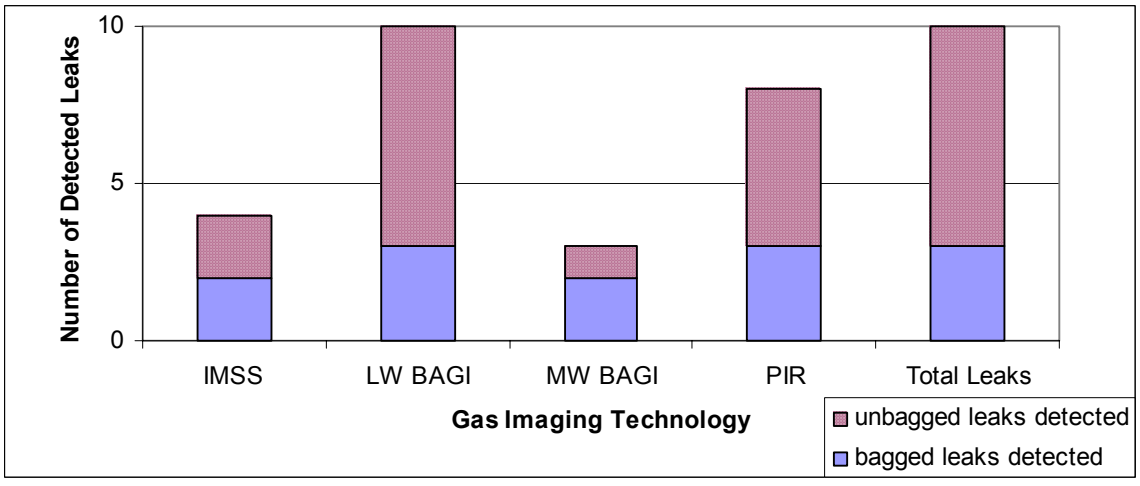

Exhibit 4-11 indicates that the long-wave BAGI camera imaged all ethylene leaks found during the field study. The PIR camera imaged all but two of the ethylene leaks. The mid-wave BAGI and IMSS cameras imaged less than half of the detected ethylene leaks.

Exhibit 4-12 is a subset of Exhibit 4-3 and shows all ethylene leaks detected and measured by the cameras and by the Method 21/Bagging team. The y-axis separates the cameras and is unitless. The x-axis measures leak rates on a logarithmic scale. The leak rates shown in Exhibit 4-12 are the leak rates of pure ethylene. Other mass contributions to a predominantly ethylene leak were insignificant.

Exhibit 4-12. Survey Results for Ethylene.

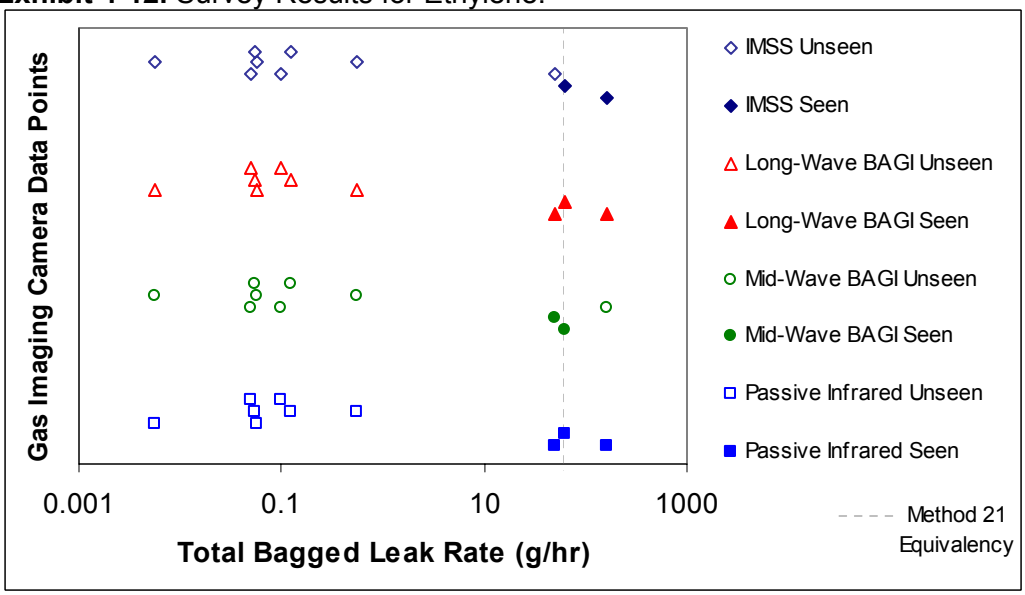

The ethylene-specific results mirror trends for the overall mass leak rate results – each camera's performance can be classified into a region of non-detection and a region of detection. Three cameras detected the two leaks above the 60 g/hr Method 21 equivalency rate; the mid-wave BAGI camera detected one of the two leaks.

Exhibit 4-13 shows ethylene detections for each camera. Superimposed over each camera's ethylene performance is that camera's minimum detection level (MDL) determined from the Naperville MDL laboratory tests.

All ethylene leaks detected by the cameras were above each camera's MDL; again the field survey results do not conflict with MDL determinations in the laboratory.

Exhibit 4-14 shows ethylene leaks that were not detected by the cameras. Again, each camera's MDL for ethylene is included in the exhibit.

Exhibit 4-14 again affirms the MDL determinations from the laboratory experiments – most leaks that were not detected fell well below a camera's determined MDL. Most non-detected leak sources were measured to be several orders of magnitude below the corresponding MDL.

Exhibit 4-13. Ethylene Detections by Camera.

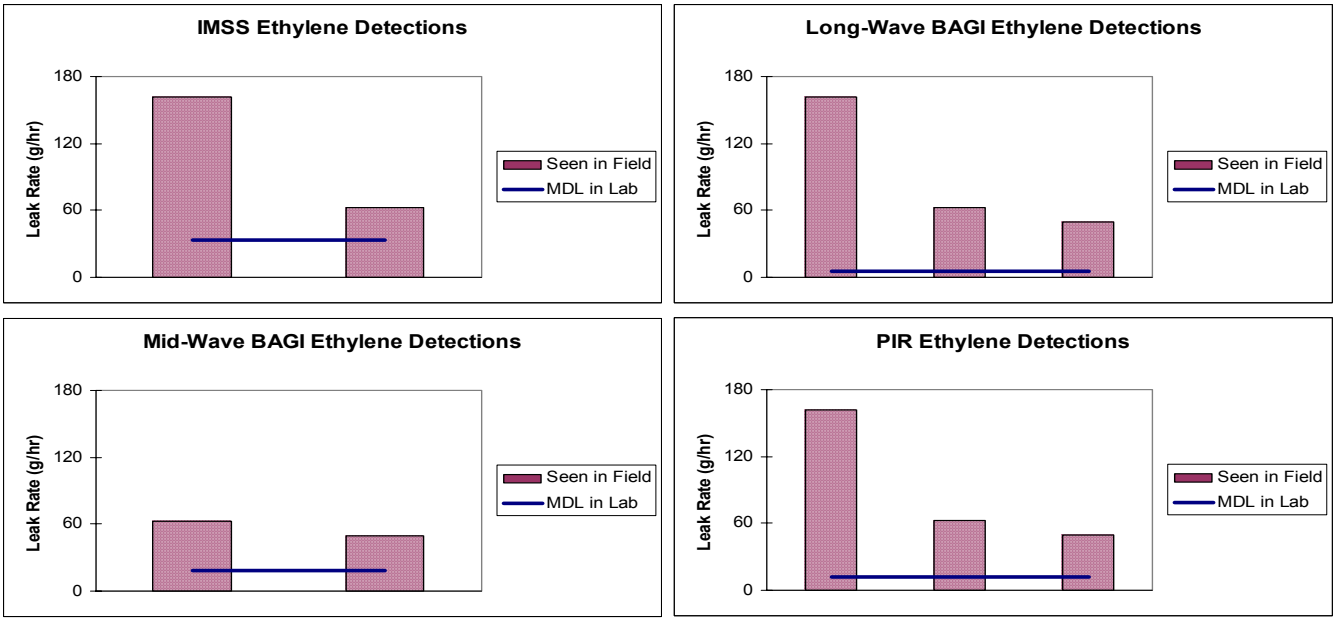

Exhibit 4-14. Ethylene Non-Detects by Camera

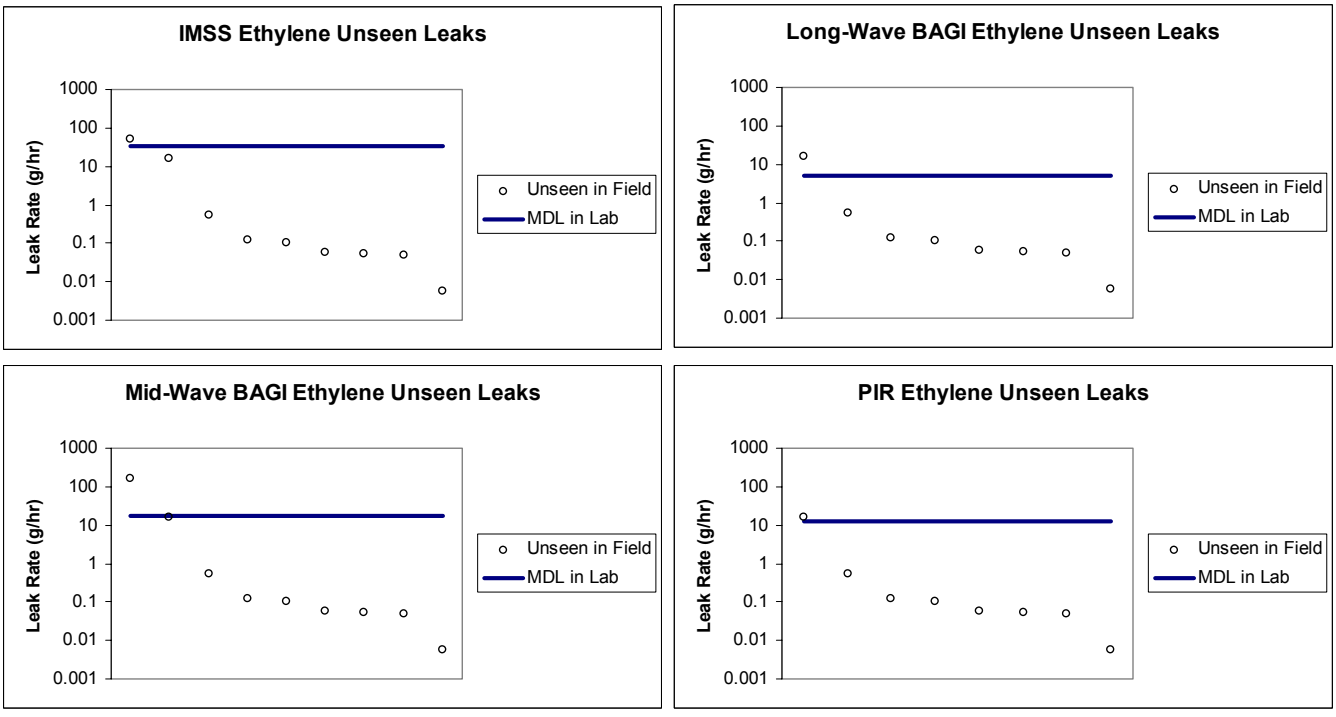

Qualitative Observations

The quantitative results presented above provide a summary of each camera's detection capabilities. Since the four cameras differ in their design, method of operation, and stage of development, qualitative aspects of each camera are discussed below.

Human perception of a camera's display of leak gas was the most subjective data collected during testing. Although each camera had an equal opportunity to survey a given area, each camera imaged leaks differently. Below is a discussion of leak imaging for each camera as observed in the field study.

IMSS Leak Imaging

During the field tests, the IMSS technology superimposed a computer processed false color (green) overlay of the gas plume on top of a visible light or infrared (IR) image of the equipment. Video output was sent to a small (about 2.5") video monitor attached to the side of the camera. The continuously processed false color image was updated at 70 hertz, but was approximately one second delayed from the real-time image of the equipment. For this reason, the camera in its state of development for the field study had to be stationary to match the leak image with the equipment image. Movement of the camera and/or movement of objects in the field of view (e.g. metal equipment tags blowing in the wind) created false color (same green as leaks) "noise" that was normally recognized by the camera operator as noise and not leaks.

False color noise was present throughout the entire IMSS testing: individual pixels; groups of pixels or horizontal lines the same green color as the gas flickered in the image as noise, and these blocks often recurred in the same part of the image. This required leaks to be larger than the pixilation in order to make a positive detection. Pixilation was also a function of the amount of vibration experienced by the camera. This characteristic of the camera probably contributed to the fact that several instances of false positive detects occurred. Through the three days of testing, the IMSS camera operator gained experience in adjusting the camera to still positions and in quickly recognizing noise from leaking gas images. The selected green false color leak images contrasted well with the background equipment images.

Long-Wave BAGI Leak Imaging

The long-wave BAGI camera produced a live motion, black and white image, with gas appearing as a dark, smoky plume. The long-wave BAGI image was viewable in the camera's eyepiece and was also sent to a small (about 2.5") monitor on a video recorder. The long-wave BAGI operator set brightness and contrast controls on the camera, similar in function to those found on a computer monitor. This technology could be slowly panned across the equipment without affecting the appearance of a plume of leaking gas.

Since distant background and other objects besides gas in the field of view could appear dark in the camera image, leak detections against objects that appeared brighter than the gas was necessary. Although the contrast between the dark gas and brighter portions of the background

was apparent, leak detection also depended on motion of the plume from airflow. Some plume motion helped to distinguish the gas from non-moving dark portions of the background.

Mid-Wave BAGI Leak Imaging

The mid-wave BAGI camera produced a live motion, black and white image, with gas appearing as a dark smoky plume similar to long-wave BAGI. The mid-wave BAGI image was viewable in the camera's eyepiece and was also sent to a small (about 2.5") monitor on a video recorder. The mid-wave BAGI operator set brightness and contrast controls on the camera, similar in function to those found on a computer monitor. This technology could also be panned across the equipment without affecting the appearance of a plume of leaking gas.

Since distant background and other objects besides gas in the field of view can appear dark in the camera image, leak detections against objects that appeared brighter than the gas was necessary. Although the contrast between the dark gas and brighter portions of the background was apparent, leak detection also depended on motion of the plume from airflow. Some plume motion helped to distinguish the gas from non-moving dark portions of the background. The Mid-Wave BAGI technology in this demonstration had a broader range of tunable IR wavelengths.

PIR Leak Imaging

The PIR camera produced a live motion, black and white image, with gas appearing as a dark smoky plume. Camera output was sent to a small (about 2.5") video monitor enclosed in a hood to reduce glare on the screen. The PIR operator set brightness and contrast controls on the camera, similar in function to those found on a computer monitor.

Since other objects besides gas in the field of view can appear dark in the camera image, leak detections against objects that appeared brighter than the gas was necessary. Although the contrast between the gas image and the background was normally apparent, leak detection also depended on motion of the plume from airflow. Some plume motion helped to distinguish the gas from non-moving dark portions of the background. As opposed to the BAGI technologies, distant or sky backgrounds did not necessarily appear as a black image.

Comparison of Gas Images

Figures 4-1 to 4-3 show a visible light image of a leak source found during testing (as recorded on a digital camera), followed by images of the same source as viewed from each of the gas imaging technologies. In some cases, the viewing angles and distances for the different technologies are different.

Visible light image of Leak M7 (digital camera)

Long-wave BAGI image of Leak M7

PIR image of Leak M7

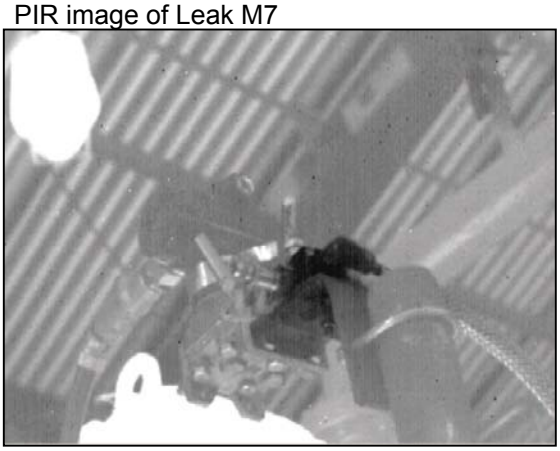

IMSS image of Leak M7

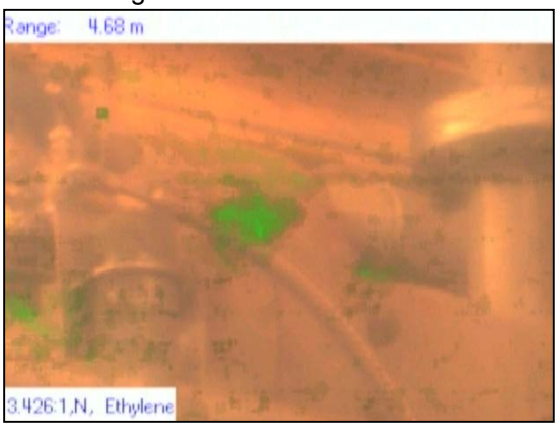

Mid-wave BAGI image of Leak M7

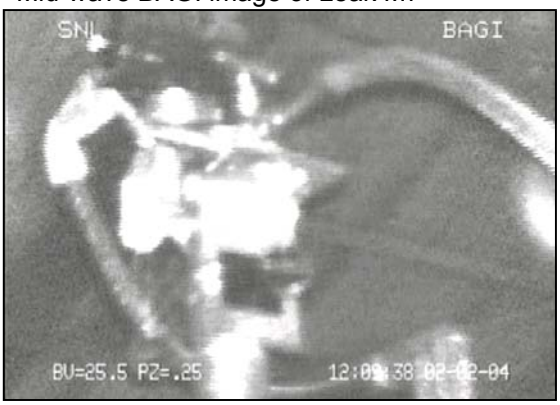

Figure 4-1. Comparison of Images of Leak M7.

Visible light image of Leak M12 (digital camera)

Long-wave BAGI image of Leak M12
(bag being constructed on lower flange)

PIR image of Leak M12

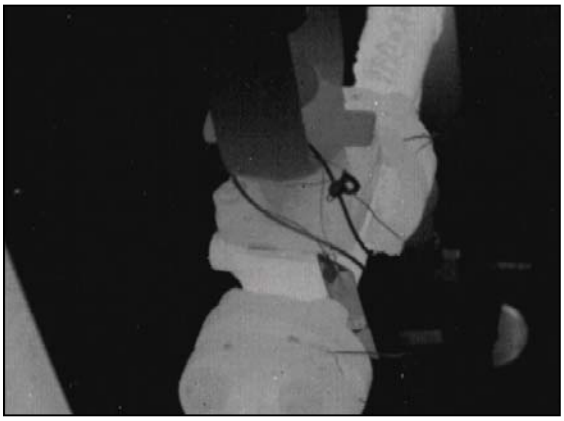

IMSS image of Leak M12

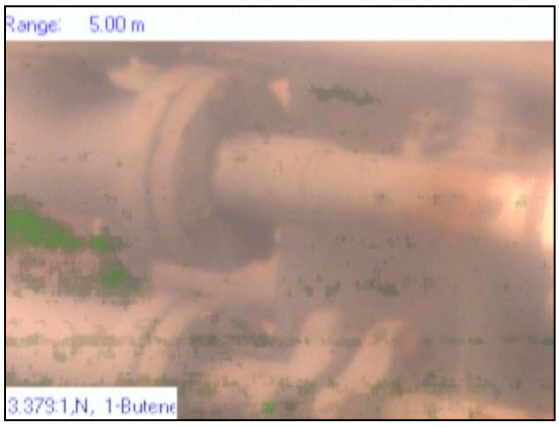

Mid-wave BAGI image of Leak M12

Figure 4-2. Comparison of Images of Leak M12.

Visible light image of Leak T2 (digital camera)

Long-wave BAGI image of Leak T2

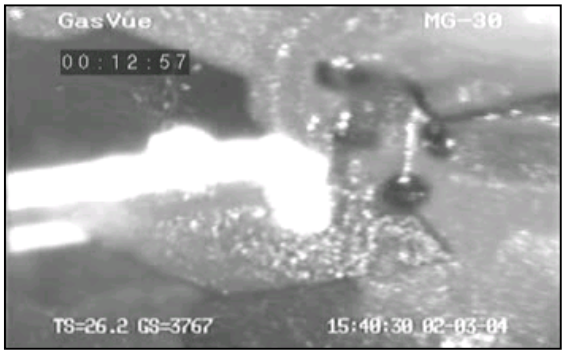

PIR image of Leak T2

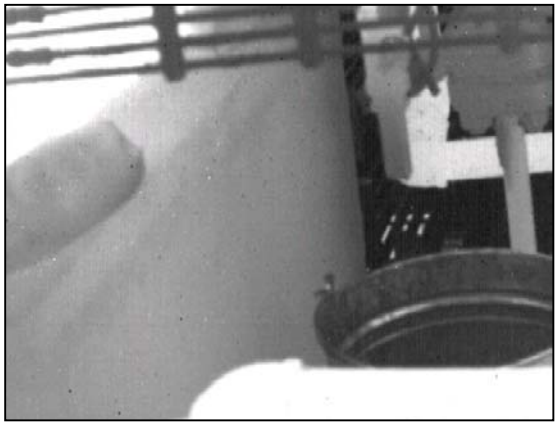

IMSS image of Leak T2

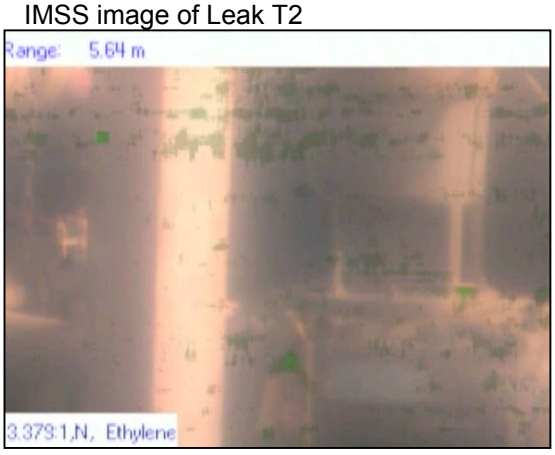

Mid-wave BAGI image of Leak T2

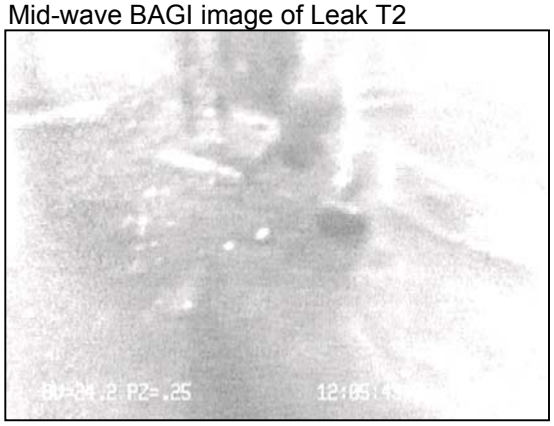

Figure 4-3. Comparison of Images of Leak T2.

Camera Portability

All four cameras provide portability for use within a plant environment. A major differentiating factor between the size and weight of the cameras was the power unit. The IMSS camera and the PIR cameras had small power units built into the camera and were capable of running on battery packs for considerable time. The PIR camera was presented in a shoulder–mounted configuration only with batteries carried in a backpack – this allowed the camera to go wherever the camera operator could go.

Due to its sensitivity to movement of any kind during use, the IMSS camera was operated on a non-wheeled tripod throughout the tests. The camera/tripod configuration was lightweight and easily carried from one place to another. During operation, the camera operator would view the image shown on the display in a hands-off mode to avoid any vibration. To pan an equipment area, the operator would reposition the camera direction and then again view the image in a hands-off position.

Both BAGI cameras had larger, considerably heavier power units that benefited from the use of a wheeled tripod. The camera itself could be shoulder-mounted within a limited radius of the tripod, restricted by the length of the power cable connecting the power unit and the camera unit. The use of the wheeled tripod limited the accessibility of the BAGI camera to components that were close to an accessible pathway. Both BAGI cameras could be shoulder operated for short periods (because of weight) with a battery/power-converter backpack for total portability.

5. PROTOCOL FOR THE USE OF GAS IMAGING AS AN ALTERNATIVE TO EPA METHOD 21

At it's most basic, leak detection and repair programs are rather simple – leaks from a defined population of components typically found in refineries, chemical plants, and other industrial facilities are found and repaired. In practice, the ability to manage large numbers of components in the changing dynamics of a refinery or chemical plant, effectively and efficiently detect leaks, repair them within a defined period of time to a point where they no longer emit volatile organic compounds above a defined threshold, and maintain information to credibly verify that these activities have taken place is anything but simple. As demonstrated in this study and other documented evaluations of gas-imaging devices for detecting fugitive emissions, the use of these types of devices for this application offer a promising alternative to EPA Method 21, the currently approved federal method for identifying and repairing leaking components.

In this section of the report, background information on the regulatory basis for allowing the use of gas-imaging devices as an alternative work practice to Method 21 is provided. In addition, efforts to demonstrate that the use of gas-imaging devices provides equal or better environmental protection to Method 21 are summarized. Following this, specific operational activities that should be considered for inclusion in a gas-imaging monitoring protocol are discussed. Finally, several issues that may arise from the use of gas-imaging devices as an alternative to Method 21 are raised for future consideration.

ALTERNATIVE WORK PRACTICES AND CONTROL EFFECTIVENESS

Current federal fugitive emissions regulations allow stakeholders to petition the EPA Administrator to recognize alternative work practices that provide equal or better environmental protection than that resulting from current requirements or methodologies.[1] To assist this recognition process, the EPA Steering Committee for Alternative Leak Detection Work Practices has developed a "demonstration protocol" to provide petitioners with a reasonable idea of what it will take for a new technology or work practice to achieve equivalent control effectiveness and be approved by the EPA. This demonstration protocol provides an optional "approval process" that includes a combination of laboratory testing, field testing, and mathematical analysis to quantify the performance of an alternative technology and determine if it can achieve equivalent fugitive emissions control to that achieved using Method 21. For the mathematical analysis, the EPA has developed Monte Carlo simulation software to help evaluate technologies or alternative work practices that may be proposed to meet the requirements of 40 CFR Part 60.8.[2]

[1] 40 CFR 60.8 (b) states in part that "performance tests shall be conducted in accordance with the test methods and procedures contained in each applicable subpart" unless the Administrator "approves the use of an equivalent method" or "approves the use of an alternative method the results of which he has determined to be adequate for indicating whether a specific source is in compliance".

[2] US EPA, "Monte Carlo Simulation Approach for Evaluating Alternative Work Practices for Equipment Leaks," OAQPS, Research Triangle Park, NC, 1999.

The EPA's Office of Air Quality Planning and Standards (OAQPS) is currently in the process of developing an alternative work practice that would allow the use of gas-imaging devices based in part on a 1999 study entitled "Monte Carlo Simulation Approach for Evaluating Alternative Work Practices for Equipment Leaks".[3] During the course of this project, discussions were held with OAQPS on the status of the EPA's efforts. In addition, the study team contributed comments to EPA on various drafts as they were circulated. The study team participated in these activities to ensure that the protocol developed as part of this study was consistent with that under development by EPA. While it should be noted that the EPA's efforts are in the draft stage of development and subject to modification prior to publication as a proposed rule change, many of the elements identified in the EPA protocol are relevant to the protocol being developed in this study.

In their latest draft protocol, the EPA has defined the detection sensitivity for the gas-imaging alternative work practice as shown in Table 5-1.

Table 5-1. Detection sensitivity levels associated with leak definitions from 500 to 10,000 ppmv (grams per hour).

Optical Imaging Frequency	Days	Detection Sensitivity Level (grams per hour)	
		Standard	Minimum
Bi-Monthly	60	60	6.0
Monthly	30	100	10.0

In the laboratory testing conducted as part of this study, minimum detection levels were established for a number of chemicals of interest to the TCET. As discussed in Section 3 of this report, the laboratory results matrix displayed minimum detection thresholds in two categories: thresholds at or below 60 grams per hour and thresholds above 60 grams per hour. The 60 grams per hour threshold was established based on the EPA's acceptance of that level as one that achieves environmental equivalency to Method 21.

ALTERNATIVE WORK PRACTICE PROTOCOL

The alternative work practice protocol encompasses four distinct areas: instrument specifications, daily instrument check, leak survey procedures, and recordkeeping. Each of these areas is discussed in more detail below.

Instrument Specifications

The instrument specification section of the protocol focuses on the establishment of procedures for ensuring a gas-imaging device is capable of detecting regulated chemical species at a level equal to or below the detection sensitivity level identified in Table 5-1. In the broadest sense, the purpose of this section of the protocol is to demonstrate that a gas-imaging device can provide an

[3] Epperson, David, "Monte Carlo Simulation Approach for Evaluating Alternative Work Practices for Equipment Leaks". Prepared for EPA Office of Air Quality Planning and Standards. ERG Project No. 8597.00.053. December 1999.

image of a component and the regulated chemicals that may be leaking from the component at a level below the environmental equivalency for Method 21.

To determine the regulated chemicals that a gas-imaging device can detect at or below the detection sensitivity level, testing on the device must be conducted prior to the introduction of the equipment into the field to determine the minimum detection level at a specified distance for all regulated chemical species that may be found in the facility.[4] The laboratory protocol developed in this study and shown as Appendix A provides one method for determining the minimum detection level. Once this testing has been completed and a list of regulated chemicals that can be detected below the sensitivity detection level prepared, use of the gas-imaging device in a facility can proceed.

In practice, an operator using a gas-imaging device to detect fugitive emissions will encounter chemical streams that are either pure streams (i.e., 100% of a particular chemical species) or mixed streams. For pure streams, the instrument specification requirement is relatively straightforward – for those regulated chemical species that the device can detect at or below the detection sensitivity level, an operator can use that device to monitor pure streams. Mixed streams, on the other hand, contain a number of different chemical species – some may be regulated and detectable below the detection sensitivity level and some may not. For these, the stream must be speciated to determine the percent composition of each chemical. Once the speciation has been completed, the detection sensitivity level must be lowered by an amount equal to the percent of the non-detectable chemical species in the stream. In the draft EPA protocol, this is determined by the following equation:

$$E_{adj} = (E_{rds}) \sum_{i=1}^{k} x_1$$

where:
- E_{adj} = Adjusted detection sensitivity in grams per hour
- x_1 = Mass fraction of detectable chemical(s) seen by the gas-imaging device
- E_{rds} = Standard detection sensitivity from Table 5-2 in grams per hour
- k = Total number of detectable chemicals emitted from the leaking equipment and seen by the gas-imaging device

To demonstrate how this adjusted detection sensitivity level would be determined, consider the following examples, which assume testing has been conducted to demonstrate that a gas-imaging device can detect ethylene and propylene at or below the sensitivity detection level shown in Table 5-1:

[4] The importance of testing to determine the minimum detection level at a specified distance is demonstrated in Exhibits 3-1 to 3-4. Using ethylene as an example, all four of the cameras tested in the laboratory were able to detect ethylene from a distance of 10 feet. When the monitoring distance was moved to 20 feet, the IMSS and mid-wave BAGI cameras were not able to detect ethylene below the detection sensitivity level; the PIR camera was only able to detect ethylene below the detection sensitivity level under the low wind, concrete background condition. The long-wave BAGI camera could detect ethylene below the detection sensitivity level at 20 feet and 30 feet under all conditions except the high wind, metal cylinder condition.

- If a stream contains 50% ethylene and 50% propylene (both of which can be detected by the camera at or below the detection sensitivity level), the detection sensitivity level remains at 60 grams per hour.

- If a chemical stream contains 50% ethylene, 25% propylene, and 25% of a chemical that is not detectable by the camera, the detection sensitivity level would be lowered by 25% to 45 grams per hour.

- If a stream contains 50 % ethylene and 50% of a chemical that is not detectable by the camera, the detection sensitivity level would be lowered by 50% to 30 grams per hour.

For a given facility, the chemical speciation determination only needs to be conducted once assuming the chemical composition of the process streams within that facility stays constant. For facilities with batch operations or chemical streams that change regularly, more frequent speciation determinations may be required.

Daily Instrument Check

Once it has been determined that a gas-imaging device is capable of detecting regulated chemical species at a level equal to or less than the detection sensitivity level, a daily instrument check of the device must be conducted each day that the device will be used for monitoring to ensure that the equipment is operating according to manufacturer's specifications.[5] To conduct the daily instrument check, the following steps are defined in the EPA draft protocol:

1. Start the gas-imaging device according to the manufacturer's instructions, ensuring that all appropriate settings conform to the manufacturer's instructions.

2. Use a gas that can be viewed by the gas-imaging device and that has a purity of no less than 98 percent.

3. Establish a mass flow rate by using the following procedures:

    a. Position a cylinder of gas in a secured upright position.

    b. Set-up the instrument at a recorded distance from the outlet or leak orifice of the flow meter that will not be exceeded in the actual performance of the leak survey.[6] Do not exceed the operating parameters of the flow meter.

[5] The laboratory results presented in Section 3 of this report demonstrate that wind conditions affect the ability of gas-imaging devices to detect fugitive emissions. It is also anticipated that other ambient factors, such as rain, relative humidity, and fog, may also affect the ability of these devices to detect leaks. Given the range of ambient conditions that exist in the State of Texas, it is recommended that the daily instrument check be conducted as close to the process area(s) where that day's leak survey(s) is to be conducted.

[6] While the EPA draft protocol requires that the distance from the outlet or leak orifice of the flow meter to the camera be measured and then not exceeded during the leak survey, it does not define a maximum distance for detecting leaks. Laboratory testing conducted in this study, as demonstrated in Exhibits 3-1 to 3-4, suggests that the maximum distance that cameras can reliably be expected to detect fugitive emissions is 20 feet.

c. Open the valve on the flow meter to set a flow rate that will create a mass emission rate equal to the emission rate as determined in the instrument specification demonstration for pure or mixed streams while observing the gas flow through the gas-imaging device viewfinder. When an image of the gas emission is seen through the viewfinder at the required emission rate, make a record of the reading on the flow meter.

Leak Survey Procedures

Once the daily instrument check has been completed, monitoring can begin. While conducting the leak survey, the following procedures should be followed:

1. The gas-imaging device operator must view each regulated component in accordance with the instrument manufacturer's operating guidelines and parameters.

2. During monitoring, the operator must maintain a distance between the gas-imaging device and the regulated component that does not exceed the distance used in conducting the daily instrument check.

3. When leaks are found in regulated components, repairs must be made within the number of days specified in the federal or state fugitive emission regulations applicable to the facility. Since the present generation of gas-imaging devices do not quantify identified leaks, a Method 21 screening should be conducted before a repair attempt is made on the component to meet current fugitive emission recordkeeping requirements in the State of Texas. All requirements under Method 21 for the quarterly performance evaluation and daily calibration of the hydrocarbon analyzer must be followed. Following the repair attempt, the gas-imaging device must be used to demonstrate that the leak has been successfully repaired.

Leak surveys under Method 21 are generally conducted by following an established monitoring run. The concept behind a monitoring run is to define a standard inspection interval for a given class or type of regulated components within a facility or process area. Using these classes of components, a fugitive emissions monitoring technician can then set the monitoring frequency by class to meet operational or regulatory constraints. Under this monitoring approach, the classes of regulated components are grouped either by monitoring frequency, location, component type, monitoring difficulty, or some combination of these criteria.

With gas imaging, a more appropriate method for grouping components may be by chemical species. Under this method, components would be grouped by process stream using information obtained during the instrument specification step. This is particularly relevant for gas-imaging devices that must be tuned to a specific wavelength corresponding to a unique chemical species.

Recordkeeping

Recordkeeping is an important element of a regulatory program intended to provide information that documents the successful completion of program requirements. For gas imaging, important documentation that should be recorded and retained include the following:

1. The detection sensitivity level used for the gas-imaging device.

2. The chemical speciation of process streams that is used to adjust the detection sensitivity level for mixed streams.

3. The analysis of the component population to determine the process stream associated with that component.

4. The daily instrument check.

5. All other recordkeeping requirements under applicable federal or state regulatory programs.[7]

In recent years, the requirement to use electronic time stamps as a means to document Method 21 monitoring has become more prevalent – both as a recordkeeping element of emerging regulations as well as standard operating procedures used by facility personnel and contractors. In the EPA's current draft protocol, a leak survey can be documented by using a video recording device, electronic recordkeeping, or written entry into a logbook. As part of this protocol, it is suggested that the State consider the requirement that all monitoring be conducted using a video recording device as the means for documenting leak survey results. This requirement serves two purposes. First, the use of a video recording device is consistent with the State's trend towards the use of electronic data to document monitoring – a video record of the leak survey provides a credible and verifiable record that each regulated component has been visited and screened, and that leaking components have been successfully repaired. Second, the use of a video recording device allows facility personnel to more efficiently repair leaking components by providing a visual image of where the leak is located thus increasing the effectiveness of repair activities and reducing the potential that small leaks are missed. This is particularly true for components that cannot be repaired immediately – maintenance personnel can use a video record of the leak at a later date to pinpoint the leak and focus repair activities.

A potential concern related to the requirement that video recording devices be used to document leak survey results is the management of the large quantity of videotape that will be generated with each leak survey. Efforts are underway to develop methods that can be used to catalog these video recordings. Ultimately, these efforts will simplify the process of using videotape as a means for documenting monitoring activities and increase the value of these visual records as a tool for better managing a facility's fugitive emissions program. A short-term solution may be

[7] For example, fugitive emission regulations in the State of Texas require facilities in ozone nonattainment areas to maintain records that include, but are not necessarily limited to, the identification of each process unit subject to fugitive monitoring, information on the types of components found within each process unit, and information on any components found to be leaking.

the incorporation of some type of "mile-post" signs placed at intervals throughout the process areas containing regulated components. These signs should be clearly visible and readable in a video recording, showing that the optical imaging device scanned all equipment from one marker to the next.

POTENTIAL ISSUES RESULTING FROM GAS IMAGING

The development, commercial introduction, and use of any new technology bring both opportunities and benefits as well as unique challenges. This holds particularly true for gas imaging. The regulatory approval of gas-imaging devices as an alternative work practice to Method 21 provides an opportunity for a "win-win-win" situation, a situation that is often an elusive goal of environmental regulations. For industry, the approval of an alternative work practice provides a potentially more cost-efficient and effective method to monitor fugitive emissions. For regulatory agencies, the use of gas-imaging devices as an alternative to Method 21 provides a more credible means for reducing a primary source of emissions from industrial facilities. For the public, the reduction of ozone precursors and other toxics from refineries and chemical plants through a more effective and credible monitoring procedure improves the health and well-being of those in communities near these facilities and others that may be exposed to these pollutants.

But challenges do exist that should be noted. It is not the intent of this discussion to provide a detailed explanation and/or solution to these challenges; rather the intent is to simply acknowledge that the challenges exist and suggest that further discussions be held to address the technical, regulatory, or strategic issues raised. Of note are the following:

- **Quantification of Fugitive Emissions** – Method 21 does not require that fugitive emissions be quantified – it simply requires that leaks over a defined threshold be identified and repaired. However, other regulatory programs do require the development of plant-wide emission inventories that include fugitive emissions. At present, fugitive emissions inventories are generally developed using the screening results from Method 21. The adoption of gas imaging as an alternative work practice may eliminate or greatly reduce the availability of Method 21 data. Coupled with the fact that the current generation of gas-imaging devices is not capable of quantifying fugitive emissions, the process for developing accurate fugitive emissions inventories needs to be addressed. In addition to the immediate issue of estimating fugitive emissions, the ability to compare emission inventories developed under different work practices (i.e., current versus alternative) over multiple years may complicate efforts to assess emission trends.

  Currently, there are at least four methodologies identified by the EPA that can be appropriately used to develop emission estimates for equipment leaks of volatile organic compounds and volatile hazardous air pollutants.[8] The only one of these methodologies that does not require screening data is the use of EPA average emission factors. This

[8] U. S. Environmental Protection Agency. Protocol for Equipment Leak Emission Estimates. Research Triangle Park, NC. Publication No. EPA-453/R-95-017. November 1995.

method, however, is the least accurate of the identified methodologies since measurements are not taken and the estimate is only based on the inventory of components. If other methodologies are used, screening data is required. This may result in the need to conduct both gas imaging as well as Method 21 screening. It is suggested that the TCEQ begin a dialogue with other interested stakeholders and evaluate various methods for estimating fugitive emissions.

A starting point for this dialogue may be a summary of alternative emission rate quantification methods developed by the American Petroleum Institute and discussed in an April 2004 paper entitled "Evaluation of Emissions Quantification Methods for Leak Detection and Repair (LDAR) Programs Using Optical Imaging Techniques". A copy of this paper is shown in Appendix H.

- **Identification of Fugitive Leaks from Nontraditional Components** – Work conducted in the field during this study and in previous studies identified leaks emanating from components that are not required to be monitored under current federal and state fugitive emission programs. While it is difficult to estimate the emissions resulting from these "nontraditional" leak sources since there are no directly applicable emission factors for these sources, they can represent a fairly significant source of emissions that are not included in a facility's fugitive emissions inventory – in a previous study, the potential to underestimate a facility's emission inventory as a result of the omission of nontraditional components ranged from 5% to 18%.[9]

  Method 21 monitoring will not find leaks from these components because Method 21 inspections are not routinely conducted on them. These components could be subject to measurements and/or repair if leaks were detected by sensory means (sight, smell, or hearing). Some types of equipment in this category include manways, heat exchanger heads, insulated components, buried components, sight glasses, and some instrumentation components (such as transmitters). The definitions of components covered in Method 21 and the federal and state fugitive emission regulations can be somewhat vague and open to interpretation. Because of this, some facilities may be routinely monitoring one or more of the nontraditional component types mentioned above while others are not monitoring them at all.

  Gas imaging has shown to be an effective means for identifying these nontraditional components. At present, the EPA is not considering the modification of current federal fugitive emission regulations to include these components under the alternative work practice. However, the ability to find these nontraditional components with gas imaging raises interesting questions about how these components should be treated. Some companies will choose to repair any and all leaks that are found with a gas-imaging device; others may not. It is not suggested at this time that state regulations be changed to include nontraditional components until further evaluations are conducted on the

[9] Houston Advanced Research Center. *Measurement and Assessment of Equipment Leak Fugitives in Industrial Ethylene and Other Chemical Sources.* 2003.

significance of these sources and the methods available to effectively repair these sources.

- **Adjustment of Emission Inventories** – The promise of gas imaging as an alternative to Method 21 is its ability to detect leaks wherever they exist in a facility. As discussed above, the use of gas imaging provides the opportunity to now detect leaks regardless of whether they are traditional or nontraditional. Work to date has shown that the potential exists for fugitive emission inventories to be underestimated. Once emission estimation methods are better understood and applied to facilities that use gas imaging, emission inventories will have to be adjusted to reflect fugitive emissions from all sources. How that process takes place requires more of strategic decision than a technical one. Again, it is suggested that the TCEQ engage interested stakeholders in a dialogue to address this issue.

CONCLUSION

The alternative work practice protocol suggested in this section takes advantage of the experience gained from the various field studies that have taken place over the last several years. Clearly technical and operational issues will arise as gas-imaging devices become more widely accepted by regulatory agencies and used by industry. Regulations should be adopted that provide the flexibility needed to adjust operating protocols as these issues are addressed. However, in whatever form the final regulatory language takes, the use of gas-imaging devices to detect fugitive emissions will provide clear and demonstrable improvements over Method 21.

6. CORRELATION EQUATIONS FOR HRVOC SERVICE

As part of this project, activities were conducted to gather mass emission rate data for use in developing emission correlation equations specific to highly reactive volatile organic compounds (HRVOC) service components. Using this data, regression equations were developed to predict Mass Emission Rates (MERs) for valves and connectors in all service categories. In this section of the report, these efforts are discussed.

BACKGROUND

Fugitive emission estimates are developed to meet requirements for permitting and emission inventories, and to meet various regulatory requirements [e.g., Superfund Amendments and Reauthorization Act of 1986 (SARA)]. In determining compliance with standards of performance or evaluating the effectiveness of individual programs of emissions reduction, estimating emissions from a given source is a key element. While testing for process emission sources is a relatively straightforward procedure, estimating emissions from widely dispersed fugitive emission sources can be somewhat more difficult.

Currently, four methodologies can be appropriately used to develop emission estimates for equipment leaks of volatile organic compounds and volatile hazardous air pollutants. These methods include the average emission factor method; the screening ranges emission factor method; the application of EPA correlation equations; and the development of new, site and/or industry-specific correlation equations.

All four methods require some level of data collection, data analysis, and/or statistical evaluation. The average factor method is the least complex and demanding, while developing site and/or industry-specific correlation equations is the most complex and data demanding. The end product of each methodology is an emissions inventory for equipment leaks organized by type of equipment and, in some cases, by service. (i.e., light liquid, gas, or heavy liquid).

DATA AVAILABILITY FOR HRVOC CORRELATION EQUATIONS

A previous project conducted for the Houston Advanced Research Center (HARC) performed field testing at two olefin manufacturing sites (Sites A and B) that resulted in data that could be used for the development of correlation equations specific to HRVOC service.[1] That study concluded that the Site A and B data gathered to characterize optical imaging technologies did not adequately cover lower screening value ranges. The work conducted as part of this study gathered additional mass emission data at two olefins-using facilities to complete the data needed for HRVOC correlation equations (identified in this report as Sites C_{04} and D_{04}).

[1] Houston Advanced Research Center. *Measurement and Assessment of Equipment Leak Fugitives in Industrial Ethylene and Other Chemical Sources.* 2003.

Table 6-1 presents a matrix of the data available for developing correlation equations.

Table 6-1. Data available in required screening value ranges.

Method 21 Monitoring Range (ppm)	Sites A & B		Sites C_{04} & D_{04}		Total	
	Connector	Valve	Connector	Valve	Connector	Valve
1 – 100			4	6	4	6
101 – 1000		2	7	7	7	9
1,001 – 10,000	3	4	6	2	9	6
10,001 – 100,000	7	9	1	1	8	10
> 100,000	4	5	11	5	15	10
Totals	14	20	29	21	43	41

DATA ADEQUACY

Chapter 2 of the EPA's 1995 *Protocol for Equipment Leak Emission Estimates* (EPA Protocol) provides guidelines for developing unit-specific correlation equations between Method 21 screening values and corresponding mass emissions data (i.e. component bagging data).[2] Among other things, these guidelines define the minimum amount of data required to develop new correlation equations. Specifically, the guidelines state:

> *"In developing new correlations, a minimum number of leak rate measurements and screening value pairs must be obtained according to the following methodology. First, equipment at the process unit is screened so that the distribution of screening values at the unit is known. Then, mass emissions data must be collected from individual sources that have screening values distributed over the entire range. The criteria for choosing these sources is as follows. For each equipment type (i.e., valves, pumps, etc.) and service (i.e., gas, light liquid, etc.), a random sample of a minimum of six components should be chosen for bagging from each of the following screening value ranges:*
>
> *Screening Value Range (ppmv)*
> *1 - 100*
> *101 - 1,000*
> *1,001 - 10,000*
> *10,001 - 100,000*
> *> 100,000*

The *Protocol for Equipment Leak Emission Estimates* goes on to state that there are two primary reasons for the six component minimum requirement when developing unit-specific correlation equations: 1) to ensure a high degree of confidence in the representativeness of the data, and 2)

[2] U. S. Environmental Protection Agency. Protocol for Equipment Leak Emission Estimates. Research Triangle Park, NC. Publication No. EPA-453/R-95-017. November 1995.

to accurately reflect the range of possible mass emission rates associated with a given screening value. As stated in the EPA's document:

> *"The importance of the first reason is self-evident: The more data collected, the better the representativeness. The importance of the second reason is that a given screening value does not necessarily have a "true" emissions rate. For a single screening value, the mass emissions may range over several orders of magnitude depending upon several factors, including the equipment type (i.e., gate valve versus ball valve versus plug valve, etc.) and operating parameters (i.e., chemical handled, temperature, pressure, etc.). This range of possible mass emission rates is accounted for when the correlation is developed, and it is important to obtain enough data to accurately reflect the range."*

The combined data collected at Sites A through D_{04} are sufficient to develop two correlation equations: one for connectors in all service categories and one for valves in all service categories. All of the minimum values for each screening range were met with the exception of connectors screening between 1 and 100 ppm. Optical imaging did not identify any components in this low range. The bagging team did some Method 21 surveys to try to find connectors in this range, but only four connectors could be found in this low range without expending an undue amount of time. The total data sets include more than the minimum 30 components, so this small deviation is not believed to compromise the validity of the correlation equations.

DEVELOPMENT OF CORRELATION EQUATIONS

Regression equations were developed to predict Mass Emission Rates (MERs) based on Screening Values (SVs, EPA Method 21 monitoring values expressed in ppmv). These regression equations had the following form:

$$Y_i = \beta_0 + \beta_1 X_i \qquad \text{Eq. 1}$$

where:

Y_i = Logarithm of the leak rate determined by bagging equipment piece *i*
X_i = Logarithm of the screening value for equipment piece *i*
β_0 = Intercept of the regression line; and
β_1 = Slope of the regression line.

Base 10 logarithms were used for all calculations.

In addition, a scale bias correction factor (SBCF) was computed according to the method described in the EPA protocol. The SCBF is used in the translation of the regression equation from log space to arithmetic space. The regression equation in arithmetic space has the following form:

$$Y'_i = \beta_0^{'} * X_i^{\beta_1} \qquad \text{Eq. 2}$$

where:

Y'_i = Predicted leak rate for equipment piece i (kg/hr)
X_i = Screening value for equipment piece i
$\beta_0^{'} = SBCF \times 10^{\beta_0}$ (β_0 = intercept of the log-space regression line); and
β_1 = Slope of the log-space regression line.

Regression equations were developed separately for connectors and valves. In both cases, two regression equations were developed using

- All the data collected for the subject component type, and
- Only those data pairs for which the screening value was less than 100,000 ppmv.

Table 6-2 gives the regression coefficients and SBCFs for each case and the current SOCMI coefficients for comparison.

Table 6-2. Comparison of TCEQ correlation equations to SOCMI correlation equations.

Case	β_0	β_1	SBCF	β'_0	R^2
Current Report Data					
All connectors	-5.476	0.6573	3.765	1.257E-05	0.577
Connectors for which SV < 100,000	-5.152	0.519	3.034	2.138E-05	0.414
All Valves	-5.423	0.624	2.143	8.091E-06	0.717
Valves for which SV < 100,000	-5.378	0.604	2.109	8.839E-06	0.647
SOCMI Data					
Connectors	-6.434	0.885	8.298	3.053E-06	0.525
Light Liquid Valves	-6.069	0.797	7.520	6.410E-06	0.677
Gas Valves	-6.529	0.873	6.315	1.870E-06	0.715
All Valves[3]	-6.262	0.827	7.351	4.021E-06	0.688

Figures 6-1 through 6-4 show the bagging data, regression lines, and 95% confidence intervals for four cases:

- Connectors – screening values below 100,000 ppm;
- Connectors – all data (including screening values above 100,000 ppm);
- Valves - screening values below 100,000 ppm; and
- Valves - all data (including screening values above 100,000 ppm).

Figures 6-5 and 6-6 show connector and valve data, respectively, with both TCEQ and SOCMI data points and regression lines.

[3] The regression for all SOCMI valves (i.e., both gas and light liquid service) was derived from the data given in Appendix B of the 1995 EPA report *Protocol for Equipment Leak Emission Estimates*, EPA-453/R-95-017.)

`

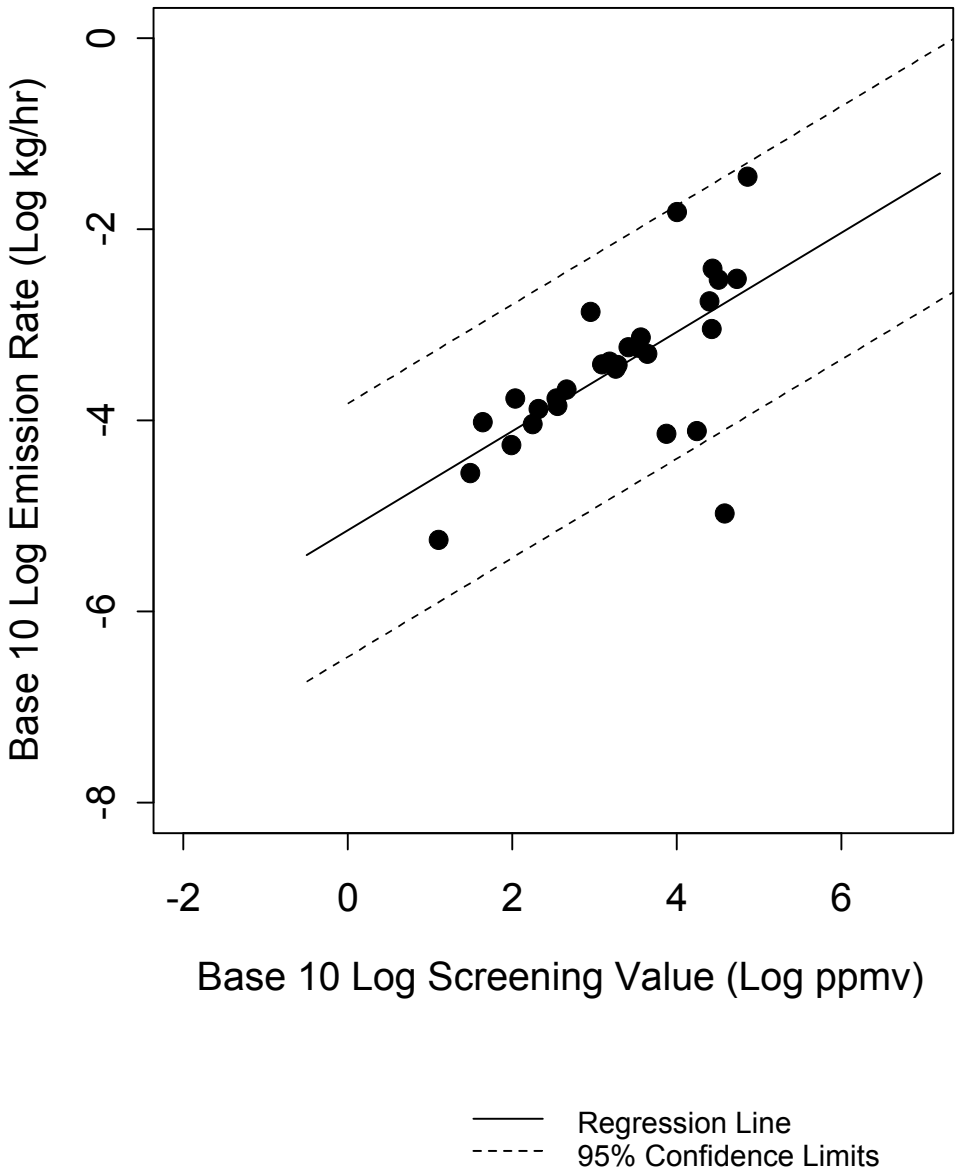

Figure 6-1. TCEQ data and regression line for connectors <100,000 ppm.

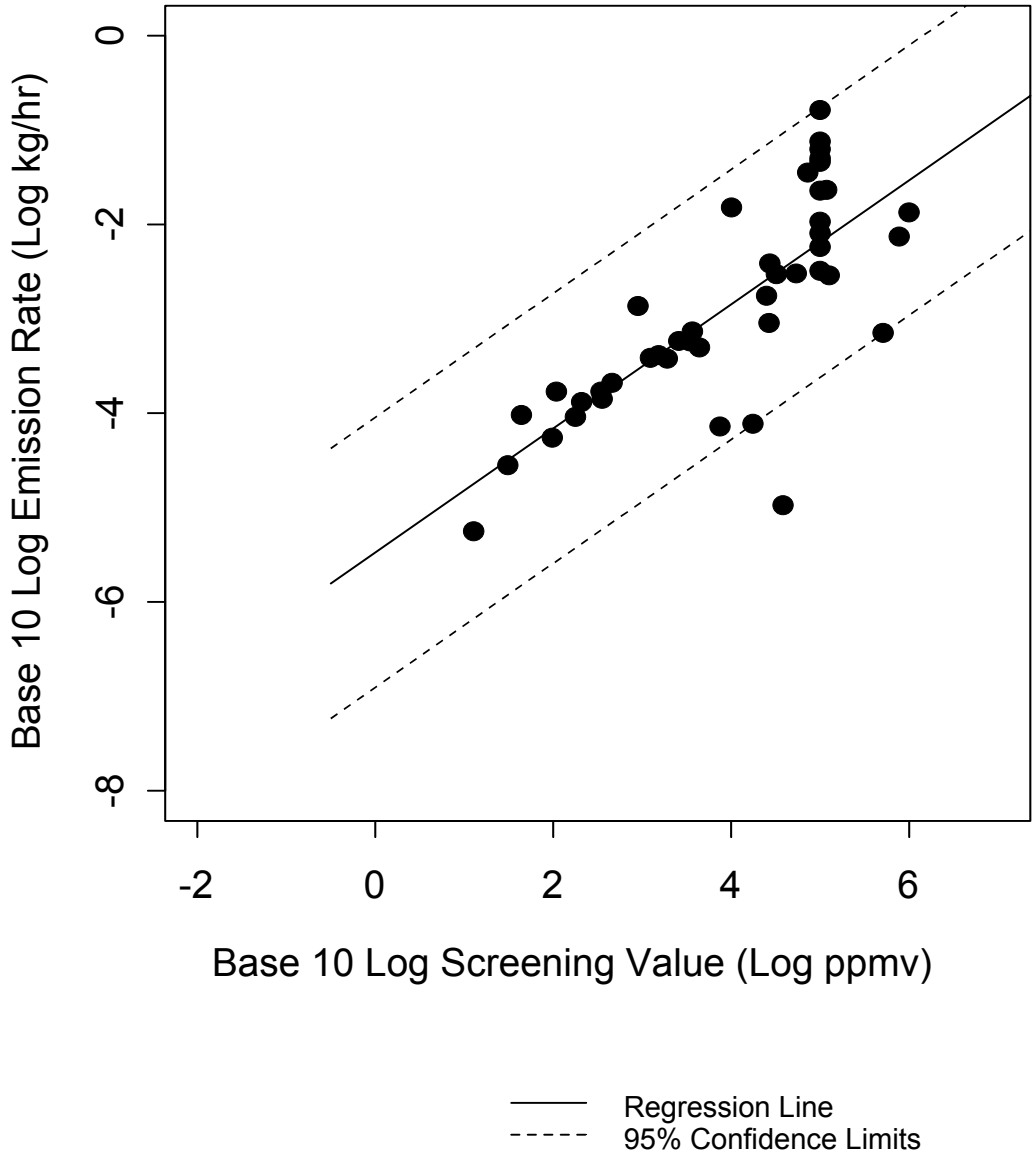

Figure 6-2. TCEQ data and regression line for all connectors.

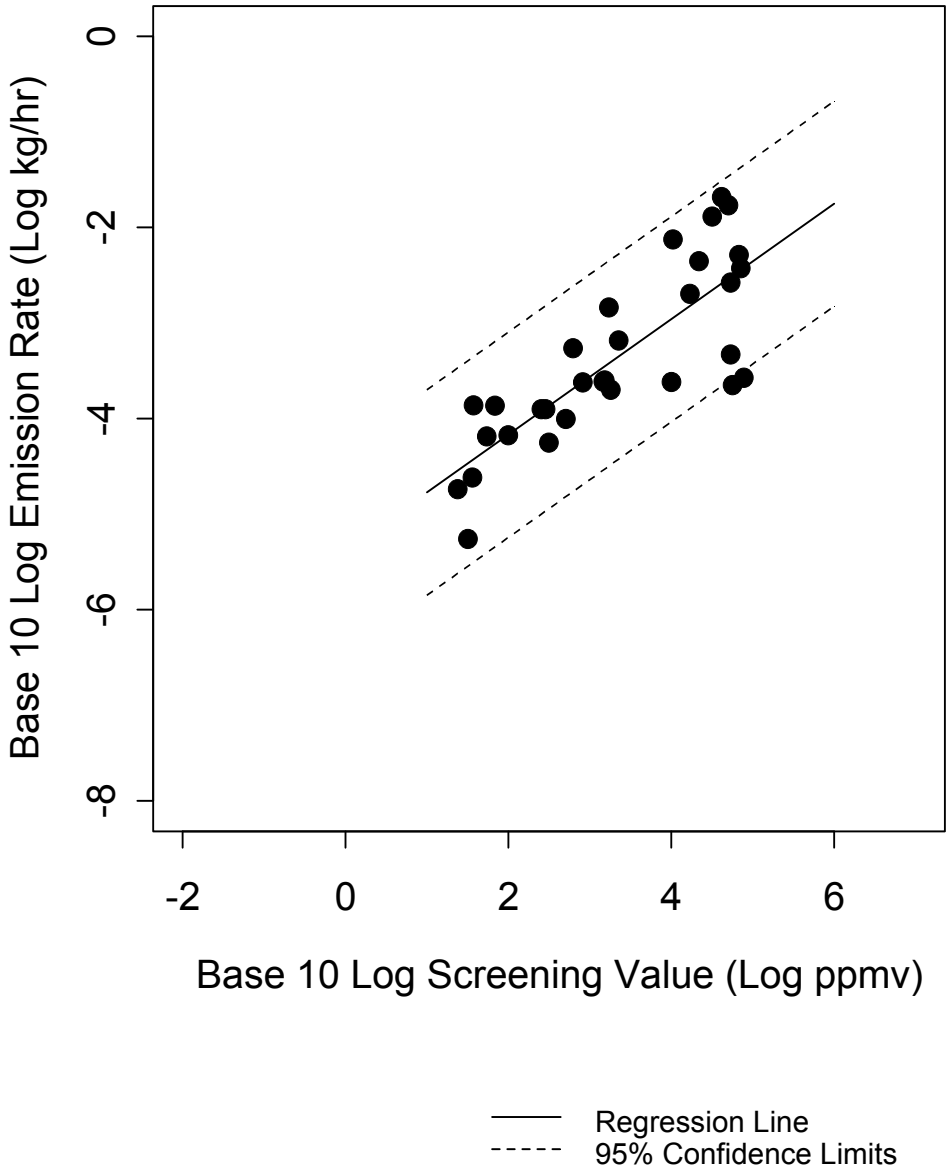

Figure 6-3. TCEQ data and regression line for valves <100,000 ppm.

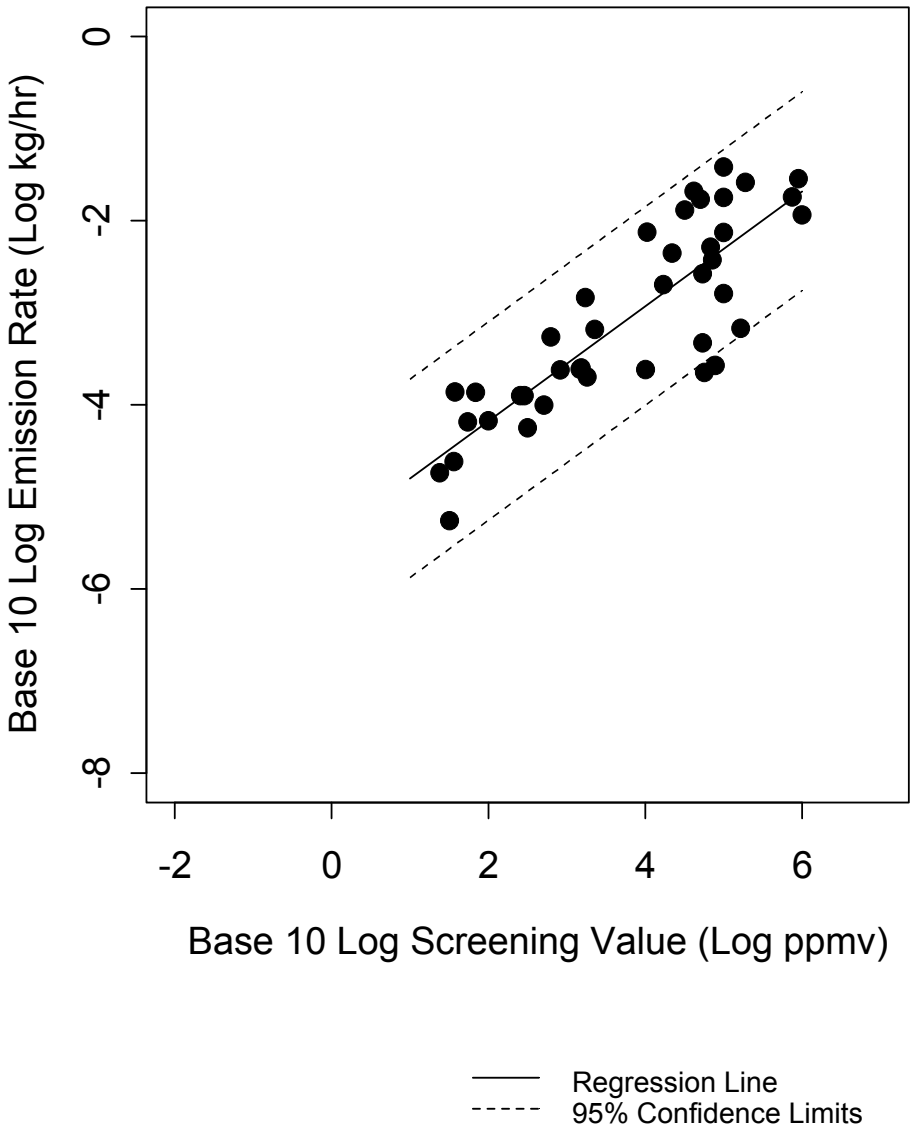

Figure 6-4. TCEQ data and regression line for all valves.

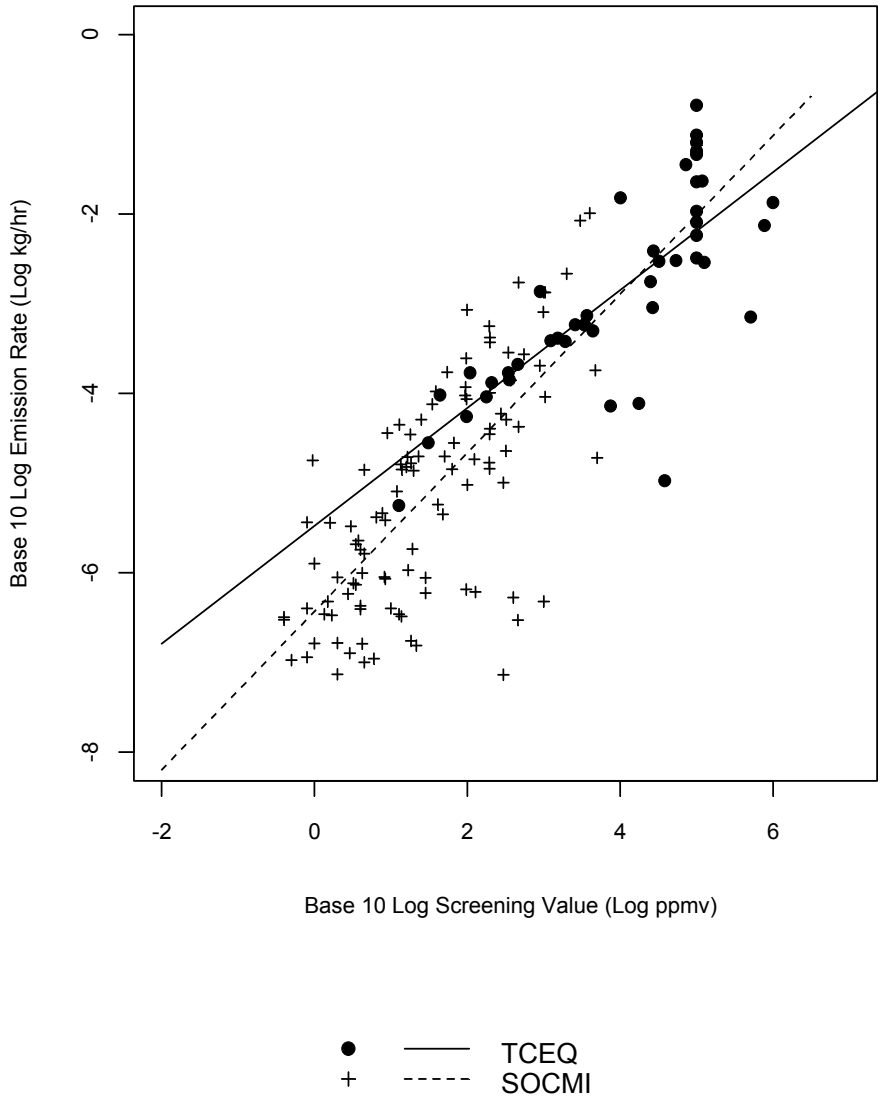

Figure 6-5. TCEQ & SOCMI data and regression lines for connectors <100,000 ppm.

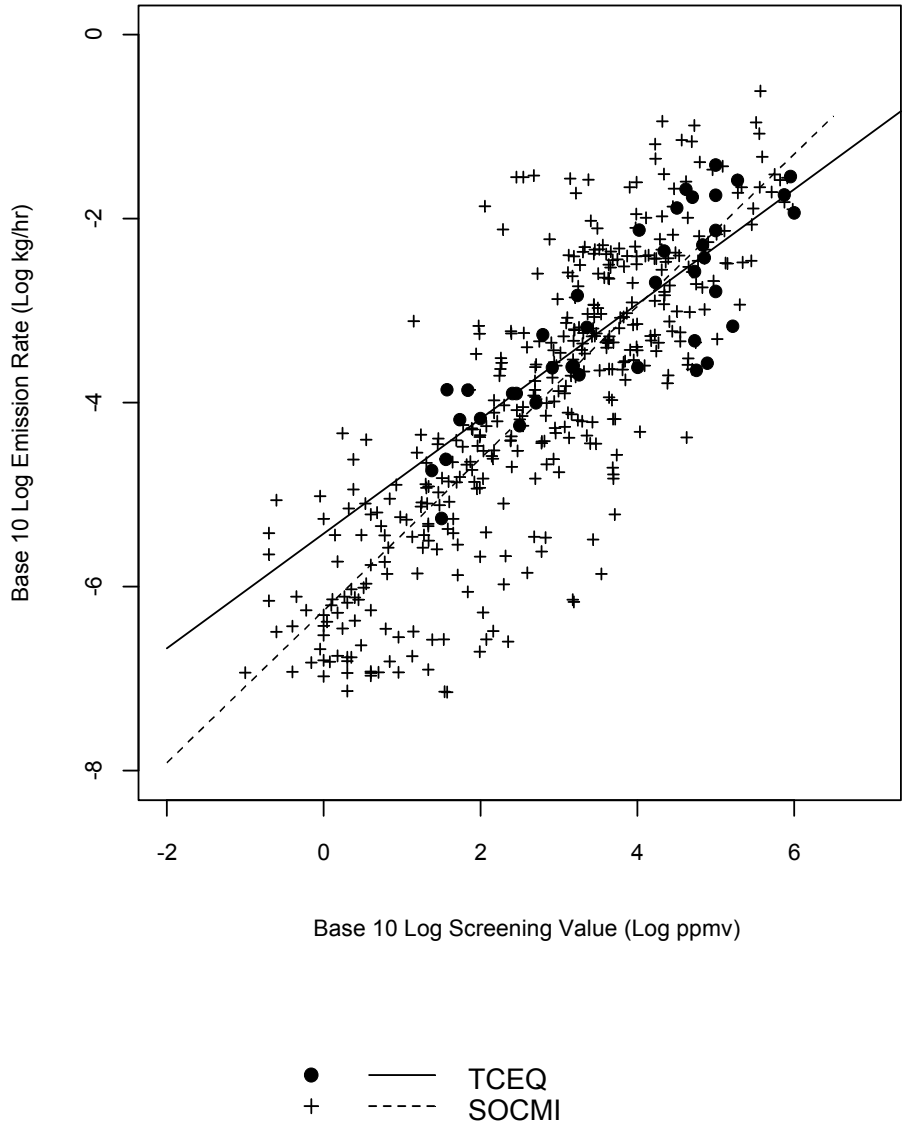

Figure 6-6. TCEQ & SOCMI data and regression lines for valves <100,000 ppm.

A statistical test was performed to determine whether the regression equations based on the current TECQ data were significantly different from the regression equations based on the SOCMI data. That is, if the regression equations derived from SOCMI data were used to predict the TCEQ leak rates, would the results differ significantly from predictions based on the regression lines derived from the TCEQ data itself? To test this question, the following method was used:

1. The current (TCEQ) data were converted to residuals against both the TCEQ and SOCMI regression lines by the following formula:

$$y_i = Y_i - Y_i^{'} = Y_i - \left(\beta_0 + \beta_1 X_i\right) \qquad \text{Eq. 3}$$

where:

y_i = residual leak rate for observation i
Y_i = logarithm of the observed leak rate (bagging data) for observation i
$Y_i^{'}$ = predicted log leak rate for observation i

and the other symbols are as for Equation 1.

For connectors, the residuals were computed against the regression line for the TCEQ data (SV < 100,000) and against the SOCMI regression line, resulting in two sets of residuals. For valves, the residuals were computed against the regression line for the TCEQ data (SV < 100,000) and against the regression line calculated for all SOCMI valves, resulting in two sets of residuals.

2. The Mean Squared Error was calculated for each of the four sets of residuals using the following formula:

$$MSE = \frac{1}{n-2}\sum_{i=1}^{n} y_i^2 \qquad \text{Eq. 4}$$

where:

MSE = Mean Squared Error
n = number of paired observations for connectors or valves
y_i = residual leak rate for observation i

3. The statistical significance of the difference between the MSE based on TCEQ curves and SOCMI curves was determined using an F-test as follows:

$$F = \frac{MSE_{SOCMI}}{MSE_{TCEQ}} \qquad (\text{df} = N_{TCEQ}, N_{TCEQ}) \qquad \text{Eq. 5}$$

where:

F = the F-value
MSE_{SOCMI} = the Mean Squared Error based on the SOCMI regression equation
MSE_{TCEQ} = the Mean Squared Error based on the TCEQ regression equation
N_{TCEQ} = number of paired observations in the TCEQ data set

This test was performed separately for connectors and valves. The computed F-values were compared to the 90% critical values for the respective degrees of freedom.

Table 6-3 summarizes the results of this analysis:

Table 6-3. Statistical test of TCEQ vs. SOCMI regression differences.

Case	n	MSE	F-Value	Significance
Connectors (SOCMI equation)	28	0.626	1.369	< 90%
Connectors (TCEQ equation)		0.457		
Valves (SOCMI equation)	30	0.346	1.312	< 90%
Valves (TCEQ equation)		0.264		

The mean squared error is slightly lower for the TCEQ equation in both cases, which would be expected since the TCEQ regression lines were set to minimize the MSE of these data sets. The differences between the two regression lines, however, are not statistically significant. In other words, the SOCMI regression lines predict the leak rates seen in the present data about as well as the regression lines derived from the present data.

DEVELOPMENT OF PEGGED EMISSION FACTORS

Pegged emission factors (PEFs) were computed for connectors and valves, based on the current (TCEQ) data for components screening >100,000 ppm, according to the method described in Appendix B of the EPA Protocol. Table 6-4 gives the pegged emission factors for the TCEQ data and the equivalent factors for SOCMI as reported in EPA Protocol, Table 2-13.

Table 6-4. TCEQ pegged emission factors vs. SOCMI and petroleum industry.

Case	n	Mean Log10 Mass Emission Rate (SV >= 100,000)	S^2	Scale Bias Correction Factor	Pegged Emission Factor, kg/hr
Connectors (TCEQ data)	15	-1.833	0.401	2.555	0.037541
Connectors (SOCMI)					0.22
Connectors (Petroleum Industry)	33	-2.493	0.920	9.245	0.029743
Valves (TCEQ)	9	-2.007	0.358	2.189	0.021530
Gas Valves (SOCMI)					0.11
Light Liquid Valves (SOCMI)					0.15
All Valves (Petroleum Industry)	99	-1.906	0.946	11.303	0.140429

The pegged emission factors based on the current testing are substantially lower than previously derived SOCMI and petroleum industry factors. Note that most of the difference comes from the scale bias correction factor (SBCF). The SBCF is a function of the number of data points and of the variability in the data, with higher variability resulting in a higher SBCF. The mean log10 mass emission rates compare reasonably well between the current TCEQ data and the petroleum industry data, with the TCEQ data for connectors actually showing a higher mean emission rate than the petroleum industry. The underlying data used to calculate pegged emission factors for SOCMI could not be located for comparison. The main difference in the final pegged emission factor is the SBCF, which is 3.6 times higher for the petroleum industry for connectors and 5 times higher for valves. These SBCF values are lower for the TCEQ data because the data show lower variability (see the values in the S^2 column of the table).

The higher variability of the data from the petroleum industry and SOCMI may be related to the use of dilution probes to make measurements over 10,000 ppm. Dilution probes can be calibrated to do a good job when reading a well-mixed gas sample, but LDAR readings in the field are seldom well-mixed samples. Leaks are typically pure hydrocarbons at the leak point, and the analyzer reading is a function of capture efficiency and dilution by the flow rate of the monitoring instrument. The dilution probe puts a restriction orifice in the sample flow path. This results in most readings that exceed 10,000 ppm without the dilution probe also reading over 100,000 ppm with the dilution probe. Modern electronic analyzers with digital readouts to 50,000 ppm (and greater with a data logger) might only read 12,000 on a component that would have read 100,000 plus on an OVA-108 with a dilution probe. This results in the inclusion of some lower mass emission rate samples in the pegged emission factor data pool, and it increases the variance of the data set. The increased variance then causes an increase in the SBCF and a higher calculated pegged emission factor. To a lesser extent, this same phenomenon is at least partly responsible for the differences between the TCEQ and SOCMI regression lines for the correlation equations.

RECOMMENDATIONS

The data collected for components in HRVOC service are adequate to develop emission correlation equations specific to this service. The resulting correlation equations are very close to the SOCMI correlation equations that are already available for emission estimating. Both correlation lines fall within the confidence intervals of the other correlation. A statistical analysis of the HRVOC and SOCMI correlation equations indicates that they are not significantly different.

The HRVOC correlations are of slightly lower slope than the SOCMI correlations, which will cause lower emission estimates than SOCMI for components with higher screening values. Since the majority of mass emissions are known to result from a relatively small group of components with high emission rates, the HRVOC correlation equations should result in a lower overall emission estimate than use of the SOCMI correlation equations.

It is recommended that TCEQ continue to advise facilities to use the SOCMI correlation equations to estimate emissions from HRVOC streams. In the interest of furthering the science of emission estimation, it is also recommended TCEQ forward the HRVOC data to EPA for inclusion in some future update of the SOCMI correlation equations.

If the correlation equations based on the new HRVOC data were to be used, it is recommended that the correlations based on all connector and all valve data be used. The correlations with all data (including components over 100,000 ppm) showed better correlation coefficients and lower mean squared errors, which indicates a better fit of the regression line to the data. The pegged emission factors for connectors and valves can also be used when readings greater than 100,000 ppm are encountered.

APPENDIX A

Literature Review Related to the Impact of Temperature and Emissivity on Passive Gas Imaging

LITERATURE REVIEW RELATED TO THE IMPACT OF TEMPERATURE AND EMISSIVITY ON PASSIVE GAS IMAGING

A thorough review of the existing literature on passive gas imaging was conducted in this study. Of particular interest in this review was the importance of the difference between the temperature of an observable gas and the background temperature (ΔT) when an attempt is made to detect the gas in the infrared spectral range.

Many of the identified papers relate to a comparison of the theoretical sensitivity of both passive and active infrared detection and gas imaging. Although the technology of thermal cameras has progressed over the last 30 or so years, the early studies and papers are instructive as they provide a basis for comparison. A great deal of the literature deals with the acquisition of spectral information, both quantitative as well as qualitative. When dealing with the current problem of gas imaging, the issues of quantitation are not as severe, generally, but surface when attempting to deal with detection limits. Additionally, much of the literature associated with the detection of vapor clouds deal with detection of hazardous, chemical threat clouds where not only is there a concern with the qualitative detection of the species but also a concern with the speed of detection and a reasonable assumption of the quantity of material. By the vary nature of these applications, many of the papers of interest deal with detection of these chemical vapors from significantly long (hundreds of meters) distances. Not only are the distances involved significant, the concentrations of the gases involved are orders of magnitude lower than required for industrial detection.

Detection of leaks from industrial processes, as a topic of interest in this study, by either passive or active gas imaging is a replacement or augmentation of current procedures involving man-carried hydrocarbon sniffing detectors that by their design require distances of a few feet (for the personnel involved) and 0 to 1 centimeters for the detectors. With gas imaging, these distances will more likely be between 5 and 20 feet. The criteria established hazardous cloud threat detection is more severe than the industrial requirements and can serve as a lower boundary.

Passive systems used for remote sensing run the range of simple thermal cameras, to thermal cameras with some level of spectral discrimination, and finally to Fourier Transform (FT) Infrared spectrometers either as stand-alone devices or used as a front end for thermal imaging. The discussions on FT-based systems deal with a generally greater optical throughput (Jacquinot's advantage) and the use of Felgett's advantage in noise reduction because of simultaneous measurement of the entire spectrum.[1,2,3,4,5] The

---

[1] Carter, Michael R., Charles L. Bennett, David J. Fields, John Hernandez, "Gaseous effluent monitoring and identification using an imaging Fourier transform spectrometer", SPIE Proceedings Substance Detection Systems, 2092, 1993, 16-26

[2] Haus, R., W. Bautzer, J. Heland, H. Mosebach, H. Bittner, T. Eisenman, "Mobile Fourier-transform infrared spectroscopy monitoring of air pollution", Appl. Opt, 33(24), 1994, 5682-5689

[3] Small, G. W., R.T. Kroutil, J.T. Ditillo, W.R. Loerop, "Detection of atmospheric pollutants by direct analysis of passive Fourier transform infrared interferograms", Anal. Chem, 60, 1988, 265-26

[4] Herget, W. F., J.D. Brasher, "Remote Fourier transform infrared air pollution studies", Opt. Eng., 19,

discussion of ΔT with respect to passive FTIR, although obviously germane to the detection of the observed spectra, has seen very limited use as an imaging device due to the complexity of the resulting image detection and analysis. Although the predicted noise equivalent concentration x length (NECL) for passive FTIR sensors based on assumed ΔT values of 0.1, 0.5, 1.0 and 5.0 ^{O}C of 1.1, 7, 11, and 70 mg/m^2 at small ranges, it was for species detection not imaging.[6,7] All of the estimations and modeling were derived using a Fourier transform passive spectrometer as the basis set for a passive system. As a consequence, no further discussions on FTIR passive imaging are included in this report.

Table A-1 is a synopsis of significant findings related to detection limits, delta temperature findings, and sensitivity relationships. Further discussions on each of the referenced articles are contained in the following paragraphs.

Table A-1. Summary of significant literature findings on passive gas imaging.

Author	ΔT (^{O}C)	Gas T (^{O}C)	Comments
Kanagawa, Ueda, Sumida, Nishio[8]	0-8 ^{o}C	292 - 300	Noise equivalent difference temperature (NEDT) is a function of the difference in background and gas temperatures as well as the difference in their emissivities
Polak, Hall, Herr[9]			Self-radiance of plume must be accounted for. Radiometric temperature of typical background results in a ΔT <10 ^{o}C
Flanigan			NEDT is a function of noise equivalent spectral radiance, the ΔT and frequency [10] [11] [12] Signal due to target (cloud) is not 1/R^2 dependent "as long as target fills Field of View" [10]
Flanigan[13]	0.1, 0.5, 1, 5		Noise Equivalent Concentration x Length = 1.1,

1980, 508-514

[5] Herget, W. F., "Remote and cross-stack measurement of stack gas concentrations using a mobile FT-IR system", Appl. Opt., 21, 1982, 635-641

[6] Flanigan, Dennis F., "Hazardous cloud imaging: a new way of using passive infrared", Applied Optics, 36(27), 1997, 7027-7036

[7] Flanigan, Dennis F., "Hazardous cloud imaging: A new way of using passive IR", Proceedings of SPIE-The International Society for Optical Engineering, 3082(Electro-Optical Technology for Remote Chemical Detection and Identification II), 1997, 14-21

[8] Kanagawa, Toshihide, Hirofumi Ueda, Kohichi Sumida, Takeshi Nishio, "Flammable gas imaging system using infrared adsorption", Proceedings of the International Gas Research Conference, 1995, 1058-1067

[9] Polak, Mark L., Jeffrey L. Hall, and Kenneth C. Herr, "Passive Fourier-transform infrared spectroscopy of chemical plumes: an algorithm for quantitative interpretation and real-time background removal", Applied Optics, **34**, 1995, 5406-5412

[10] Flanigan. 1997.

[11] Flanigan, Dennis F. "Prediction of the limits of detection of hazardous vapors by passive infrared with the use of MODTRAN", Applied Optics, 35(30), 1996, 6090-6098

[12] Flannigan, Dennis F., "Limits of passive remote detection of hazardous vapors by computer simulation", Proceedings of SPIE-The International Society for Optical Engineering, 2763 (Electro-Optical Technology for Remote Chemical Detection and Identification), 1996, 117-127

[13] Flanigan. 1986.

Author	ΔT (^{O}C)	Gas T (^{O}C)	Comments
			7, 11, 70 mg/m^2 Nominal □T of 1 ^{O}C is acceptable
Kulp, Powers, Kennedy[14]	5^{O}C		Adequate detection of gas cloud at 4.5 to 40 ppm
Reichardt, Devdas, Kulp[15 16]	5^{O}C		Active detection will be 10 times more sensitive than passive
Ljungberg, Jösson[17]	~2 – 30^{O}C		Most critical parameter is wind speed

NEDT Calculations

NEDT is a figure of merit for both active and passive systems. Rogalski describes the performance limits of infrared photon and thermal detectors and uncooled two-dimensional arrays of thermal detectors in a report that also discusses the use of NEDT as a figure of merit for focal plane arrays (FPAs).[18] The report states that NEDT is "the temperature change, for incident radiation, that gives an output signal equal to the rms noise level" and "the charge handling capacity of the readout, the integration time linked to the frame time, and dark current of the sensitive material become the major issues of IR FPAs". Rogalski calculates a NEDT (at 10 mm and background temperature of 300 K) for an array of HgCdTe photodiodes at 77K of 19.8 mK. For an array in the 10 μm range, Rogalski estimates that the scene contrast is about 2%/K of change in scene temperature and to obtain a pixel to pixel variation of apparent temperature less than 20 mK, the nonuniformity in response must be less than 0.04% across the array.

Many of the papers discussed below concern themselves with an estimation of the required ΔT necessary for passive detection. At the 1995 International Gas Research Conference, the results of a study on active and passive infrared imaging were presented.[19] These results graphically represented the variation of incident or received infrared energy with respect to gas concentration at various gas temperatures and a constant background temperature over a range of 292 to 300 K gas temperature (background at 300 K). The paper showed that the detectivity of a gas is related to the

[14] Reichardt, Thomas A., Wayne Einfeld, Thomas Kulp, "Review of Remote Detection for Natural Gas Transmission Pipeline Leaks", www.netl.doe.gov/scng/publications/t&d/tsa/NETL_review_2col_1.pdf

[15] Reichardt, Thomas A., Sanjay Devdas, Thomas J. Kulp, "Evaluation of Active and Passive Gas Imagers for Transmission Pipeline Remote Leak Detection", Presentation, Dec 2002, National Energy Technology Laboratory, http://www.netl.doe.gov/publications/proceedings/02/naturalgas/1-2.pdf

[16] Reichardt, Thomas A., Sanjay Devdas, Thomas J. Kulp, "Evaluation of Active and Passive Gas Imagers for Transmission Pipeline Remote Leak Detection", Final Report, Dec 2002, National Energy Technology Laboratory, www.netl.doe.gov/scng/projects/transmission/ngi/psr/pubs/psrFEW01-011123%202002%20Final%20Report.pdf

[17] Ljungbert, Sven-Ake, Owe Jösson, "Passive gas imaging – preliminary results from gas leak simulations a field study performed during real world conditions", Proceedings of Thermosense XXIV SPIE, 4710, 2002, 468-478

[18] Rogalski, A., "Competition of infrared detector technologies", Proc. SPIE VI Intl. Conf on Material Science and material Properties for Infrared Optoelectronics, Sizov, Gumenjuk-Sichevska, Kostyukevych, Eds, 5065, 2003, 23-38

[19] Kanagawa. 1995.

difference in background temperature and background emissivity and the gas temperature and gas emissivity. Unfortunately, the paper is very slim on details of the experiment or the theoretical basis for the conclusions.

The issue of passive detection is covered in a number of articles. In one, the difficulties in obtaining a significant difference between the plume temperature and the radiametric temperature of the background, removal of the spectral features of the background, correctly accounting for internal emission of the spectrometer elements when viewing cold backgrounds, and obtaining quantitative information about the plume are discussed.[20] The report observes that the radiometric temperature of the typical background is typically colder than or very close ($\Delta T < 10^{O} C$) to the plume temperature. The report goes on to say that the self-radiance of the plume must be taken explicitly into account.

A number of papers by Flanigan deal with the determination of the detection limits of hazardous vapors by passive infrared. [21,22] These determinations are involved in chemical cloud detection and identity using remote sensing generally looking downward from aircraft mounted systems. The distances between the detection systems and the target cloud involved are generally measured in hundreds of meters. This poses a significantly more involved, in some respects, basis in that the layers of atmosphere between the target cloud and the detection systems can be non-homogeneous in content and temperature, among other parameters. One paper states "ΔT is a measure of potential to sense vapors between the background and the space in front of the sensor. If the $T_{background} <> T_{boundary\ layer}$ [read cloud] then there can be a net transfer of energy and the intervening vapors (or aerosols) can be detected. ΔT will have a positive or negative value depending on whether the background is hotter or colder."

Flanigan has also shown that for a passive sensor when the gas image fills the field of view of a sensor, the light that is observed comes from the background, the target cloud and the atmospheric gases between the cloud and the sensor which can be expressed in terms of incident power as the following equation:

$$P_P = [T_A T_T N_{BG} + (1 - T_A T_T) N_T] A_C \Omega_S \qquad (6)$$

"where T_A is the atmospheric transmittance, T_T is the target cloud transmittance, N_{BG} is the radiance of the background, N_T is the radiance of a blackbody at the temperature of the target cloud, A_C is the collector area, Ω_S is the solid angle of acceptance of the sensor and is the transmittance of the optics. In normal conditions N_T and N_{BG} differ at most by a few percent. If $N_T = N_{BG}$, then $P_P = N_{BG} A_C T_0$, and the incoming radiation contains no information about the spectral properties of the gases. Therefore for detection to occur it is essential that $| N_{BG} - N_T | = \Delta N > 0$."[23]

---

[20] Polak. 1995.
[21] Flanigan. 1996,
[22] Flanigan. 1997.
[23] Flanigan. 1986.

The ambient air, target and background temperatures can be calculated from Plank's function. Generally, for small leaks, the temperature of the cloud can be assumed to equilibrate rapidly to the ambient air temperature. Therefore, the ΔT that needs to be examined is generally the temperature difference between the target cloud (atmosphere) and the radiametric temperature of the background, which also includes the emissivity of the background. "On a clear day, with a low-angle-sky background, the ΔT for passive operation can reach $20^{O}C$; however, given a 24-hour cycle and/or overcast weather, it is much safer to assume a limiting value of $1.0^{O}C$ to get 90% operational time.[24]

In a review of remote detection for natural gas pipeline leaks, Reichardt, Einfeld and Kulp provided a table that compares active and passive detection with comments on the limitations of each mode of detection.[25] In a 1998 companion paper, Kulp, Powers and Kennedy compared an active IR imaging system (BAGI) using a CO_2 laser source and a passive system using a bandpass filtered Ga:Si focal plane array.[26] In a controlled plume generation experiment, the passive system could "see" concentrations down to 4.5 ppm while at other times detection limits were in excess of 40 ppm. The range of detectabilities was attributed to the temperature differences of the target gas (ambient temperature) and the temperature of the 12-foot square target. Adequate detection was achieved when the ΔT was about $5^{O}C$ but degraded when the ΔT approached $0^{O}C$. Although the gas temperatures and target temperatures were logged over an extended period, the comparative data was only presented for two data points. They were able to conclude "since passive methods require a temperature/emissivity difference with the background, the detected gas will appear invisible at the temperature for which there is no net radiative heat transfer between the gas and the surroundings."

Experiments involving the leak detection of buried pipe were reported by Reichardt, Devdas and Kulp.[27] Active and passive systems were used to observe natural gas leaks from aircraft. "The passive detection limit is ultimately governed by the magnitude of the energy transfer between the gas plume and the ground surface. Given a relatively modest typical temperature difference of $5^{O}C$ between the ground and the air above the ground, the experimentally confirmed calculations predict that an active approach will be an order of magnitude more sensitive to detect natural gas leaks". "Passive methods allow nearly unlimited range with a simple instrumental configuration, these methods rely upon a thermal flux between the plume and the ground surface below it." They compared the system performance to theoretical predictions. "The source term for passive detection is a function of the concentration x cloud cross-section (C x L) as well as the emissivity of the background and the temperatures of the target plume and the background. Because the detector measures the radiant exchange, evaluation of the system performance is equivalent to characterizing the radiance sensitivity of the

---

[24] Flanigan. 1986.

[25] Reichardt, Thomas A., Wayne Einfeld, Thomas Kulp, "Review of Remote Detection for Natural Gas Transmission Pipeline Leaks".

[26] Kulp, T.J., P.E. Powers, R. Kennedy, "Remote imaging of controlled gas releases using active and passive infrared imaging systems", Proceedings of the Infrared Technology and Applications XXIII SPIE, 3061, 1998, 269-278

[27] Reichardt. 2002.

instrument." They used a camera (Model AE-173, Amber Engineering, Goleta, CA) (now Indigo Systems) that had a cooled InSb 256 x 256 array at 77K using f/2.3 100 mm effective focal-length lens. The optical signal was filtered at 3.4 mm and provided an on and off wavelength that was examined at 1 Hz. The absolute magnitude of optical signal was measured and compared to predictions between 30 ^{O}C and 55 ^{O}C. They examined or estimated sources of noise that included shot noise, dark current noise, offset noise, read noise, digitization noise which they estimated at 0.7% adding nonuniformity noise increased measured noise to1.5%. Images of plumes of 1,000-ppm m-butane were provided where ΔT's of 5, 10,14.5 and 21 ^{O}C.

Most of the above studies deal with the issue of NEDT. Driggers, Boylston, and Edwards cited that the ΔT required for the same instrument response in cooler environments is greater than those in warmer environments because the detectors used in infrared imaging respond to differential power and not just ΔT.[28] They calculated the Equivalent Temperature Differentials (EQΔT) for ambient ΔT s of 1.0, 3.0, 5.0 and 10.0 K in the range of 270 to 340 K (0-60 ^{O}C) for two infrared bands (8-12 μm and 3-5 μm). In the 3-5 μm region, the "EQΔT corresponding to an ambient ΔT of 1.0 ^{O}C varies from 0.4 ^{O}C to 2.3 ^{O}C over the 273 K to 333 K background temperature range."

In 1997, a conference on "State-of-the-Art and Future Plans for IR Imaging of Gaseous Fugitive Emission"[29] was held. Work continued in Sweden on a field study under "real-world" conditions[30] and reported by Ljundgberg and Jönsson. In their work, a FLIR AGEMA THV 100 camera operating in the 8-12 μm region looked at methane emissions from buried piping under controlled conditions. They measured leak source gas temperature, ambient surface temperature near the leak and the sky radiation temperature among other parameters. Delta Ts ranged from 2^{o} C to 30^{o} C with detection requiring at least a ΔT of 2^{o} C. In their experiment, the most critical parameter was wind speed.

Another passive system that has been used for gas imaging is a gas-correlation imaging system which uses a gas cell which is filled with the gas (gases) of interest that form a specific filter that effectively provides detection with a minimum of interference from other species.[31,32] The work of Sandsten and others documents the use of gas-correlation imaging using an Amega Thermovision 900 LW camera with a NEΔT of 80 mK. From the graph of ΔT's versus relative transmittance (6 different values of ΔT with a gas temperature of 294 K), they calculated an instrument response function and provided

---

[28] Driggers, Ronald G., Graves L. Boylston, George T. Edwards, "Equivalent temperature differences with respect to ambient temperature difference as a function of background temperature", Optical Engineering, 31(6), June 1992, 1357-1361

[29] Ljungberg, S. A., T. J. Kulp, T. G. McRae. "State of the art and future plans for IR imaging of gaseous fugitive emissions", SPIE Proceedings from Thermosense XIX: An International Conference on Thermal Sensing and Imaging Diagnostic Applications. 3056, 1997, 2-19

[30] Ljungbert, S. A., Owe Josson, "Passive gas imaging – preliminary results from gas leak simulations in a field study performed during real world conditions". Proceedings of Thermosense XXIV SPIE, 4710. 2002. 468-478.

[31] Sandsten, Jonas, Hans Edner and Sune Svanberg, "Gas Imaging by infrared gas-correlation imaging", Optics Letters, 23(23), Dec 1996, 1945-1947

[32] Sandsten, Jonas, Petter Weibring, Hans Edner and Sune Svanberg, "Real-time gas-correlation imaging employing thermal background radiation", Optics Express, 6(4), Feb 2000, 92-103.

error bars from which an estimate of the noise error associated with the measurements can be made. A ΔT of 1.2 K is estimated to correspond to a 0.1 unit change in relative transmittance between the reference cell and the filter cell. A transmittance of 1.0 corresponds to a ΔT of 0. The authors also provided an estimate of a sensitivity of 200 ppm for ammonia with a ΔT of 18 K. The background surface was measured with a non-contact thermometer with an accuracy of 1K.

In addition to the background temperature, the background emissivity, and the target cloud temperature, the target cloud emissivity may be an issue in observing the gas imaging. Tables for solid material emissivities exist.[33] Gas emissivity is an important issue in high temperature furnace operations.[34]

The results of the literature search indicates that there are a number of critical references that discuss the importance of the difference between the temperature of an observable gas and the background temperature when an attempt is made to detect the gas in the infrared spectral range. A significant number of these papers are a result of experimental and theoretical work associated with the long distance detection of chemical warfare agents using passive infrared spectrometry. The issue of detection is complicated by the physics of radiametric temperature and thermal temperature measurements. Emissivity of the background and potentially of the gas being observed, however, plays an important role.

The available literature does not directly address the minimum delta temperature associated with detection specifically for short distance work that is associated with leak detection using gas imaging. There is no debate that at a $\Delta T=0$ where the ΔT is a radiametric difference (power incident on the detector), there is no spectral information available and hence no imaging of the gas leak. However, there is no discussion that within the field of view that encompasses the gas image, this ΔT must be uniform or that in practice this ΔT is hardly ever uniform in time or space.

[33] An example is http://www.electo-optical.com/bb_rad/emissivity/matlemissivity.htm
[34] An example is http://coecs.ou.edu/William.H.Sutton/america_files/prinheat/radgas.htm

APPENDIX B

Laboratory Study Protocol

LABORATORY TEST PROTOCOL FOR EVALUATING OPTICAL IMAGING TECHNOLOGY

For:
TCET

By:
ICF Consulting
9300 Lee Highway
Fairfax, VA 22031-1207

July 24, 2003

LABORATORY TEST PROTOCOL
FOR
EVALUATING OPTICAL IMAGING TECHNOLOGY

This protocol outlines the procedures that Test Teams will follow to evaluate the capability of three portable optical imaging cameras to detect a set of specific chemicals that may be present at industrial facilities. The Test Teams will make every effort to adhere to this protocol. However, if any portion proves impractical due to unforeseen circumstances, TCET, Environ and the Test Teams will determine the best approach for completing the test.

The purpose of this laboratory test is to:

- Demonstrate the applicability of the gas-imaging technologies to detect leaks of 14 candidate chemicals:

  Ethylene (added at TCET request)
  Propylene
  Formaldehyde
  Acetaldehyde
  Isoprene
  all Butenes (butylenes)
  1,3, Butadiene
  Toluene
  all Pentenes
  all Trimethylbenzenes
  all Xylenes
  all Ethyltoluenes
  all Hexenes
  all Butanes
  all Pentanes

- Determine the minimum detection level of gas-imaging technologies.
- Collect data to begin to establish the sensitivity of optical gas-imaging technology to various factors that might be encountered during routine use at a chemical plant.

Three optical imaging cameras will be investigated during this test—two based on Backscatter Absorption Gas Imaging (BAGI) technology, and the Pacific Advanced Technology (PAT) gas leak detection camera based on Image Multi-spectral Sensing (IMSS).

2.1 Backscatter Absorption Gas Imaging (BAGI) Technology Cameras

Two BAGI technologies are currently available:

- A long-wave IR laser imager is a commercially available instrument, manufactured and marketed by Laser Imaging Systems (LIS) under the brand "GasVue®." It is applicable for detecting hydrocarbons absorbing in the 9 to 11 micron wavelength, which includes olefinic hydrocarbons such as ethylene and propylene, SF_6, rocket fuels, NH_3, and CFC's. It is currently used to detect SF_6 at electric power facilities.
- A mid-wave IR laser imager utilizes a mid-IR laser source developed at Sandia National Laboratory's (SNL) Livermore facility, in conjunction with a BAGI scanning camera purchased from LIS. It is suitable for hydrocarbons absorbing in the 3.1 to 3.6 micron wavelength, with potential extension to species absorbing in the 1.3 to 4.0 micron range. Examples of these hydrocarbons include methane, propylene, and butane.

In BAGI, a live video image is produced by illuminating the view area with laser light in the infrared frequency range. The reflected (backscattered) laser light is detected with a camera sensitive to that light. When the chosen laser wavelength is strongly absorbed by the gas of interest, a cloud of that gas is revealed as a dark image. Exhibit 2-1 shows how BAGI works. A video camera-type scanner both sends out the laser beam and picks up the backscattered infrared light. The camera converts this backscattered infrared light to an electronic signal, which is displayed in real-time as a black and white image on both the viewfinder and a video monitor. The same image will be seen whether the scanning is done in daylight or at night because the scanner is only sensitive to illumination coming from the infrared light source, not the sun. Also, because laser illumination is used, the measurement does not depend upon a temperature or emissivity difference between the background and the gas plume to be detected, as is necessary in a passive imaging measurement. However, the BAGI technology requires a reflective background relatively close (within ~30 feet) to the camera, unlike the passive imaging technology that can image a leak against the sky.

Exhibit 2-1. Schematic Description of BAGI Process

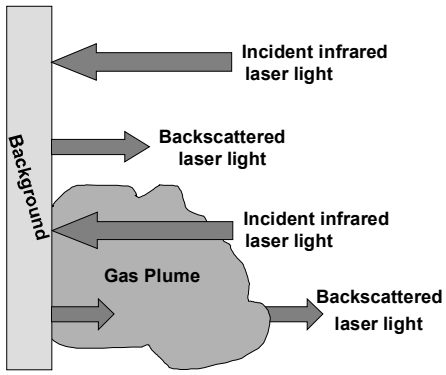

Source: As Adapted from McRae, Tom, *GasVue: A Rapid Leak Location Technology for Large VOC Fugitive Emissions*. (Presentation at the CSI Petroleum Refining Sector Equipment Leaks Group, Washington, DC, Sept. 9, 1997). See US Patent # 4,555,627

Note: Although this Exhibit shows the gas in contact with the background material, it is not a requirement that the gas be in contact with the background. The gas plume need only be between the background and the infrared camera.

Exhibits 2-2 and 2-3 show the visible light and infrared views of leaking components viewed with the two different BAGI imagers.

In their current state of development, these technologies make a visible image of vapor clouds of certain hydrocarbons and other chemical leaks that are invisible to the naked eye, but they do not yet quantify the mass emission rate of the leak cloud.

Exhibit 2-2 Leaking Valve Viewed with a Visible-Wavelength Camera and Long-Wave-IR BAGI Imager

Visible light view of leaking valve

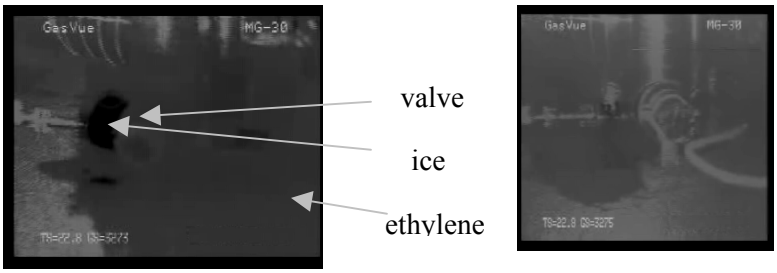

Infrared views of same leaking valve

Exhibit 2-3 Leaking Valve Viewed with a Visible-Wavelength Camera and Mid-Wave-IR BAGI Imager

Visible light view of leaking flange

Infrared view of leaking flange

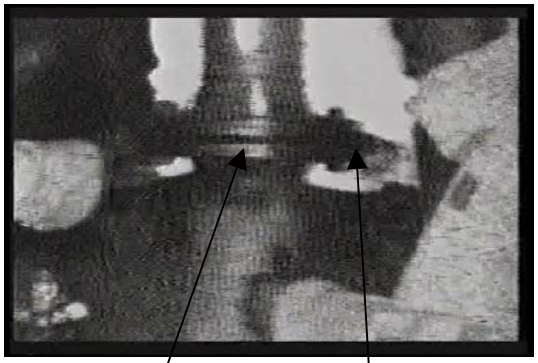

Three parameters that influence the performance of the two BAGI lasers are background, laser wavelength and atmospheric window.

Background. For the technology to visualize a leak, there must be a reflective, or backscattering, surface close behind the leak. It is not possible to visualize a gas plume against the sky or a distant background. It is also possible in many circumstances to image a leak against the component itself, with a distant or sky background appearing black. The operator knows that the imager is beyond detection range when the camera no longer produces a bright image of the components under inspection: the more distant the component or background, the darker the image. The operator can also switch the camera between infrared and visible light viewing to determine whether there is an adequate background surface behind the leak point being inspected.

Laser Wavelength. Gas leak detection sensitivity by optical imaging depends most strongly on the match between the laser wavelength and the wavelengths of strong absorption by the gas of interest. To produce an image in the viewfinder of a black cloud where the hydrocarbon gas is present, the gas cloud must be capable of absorbing the laser wavelength.

Wind speed, optical resolution, gas plume motion and viewing angle also affect detection sensitivity. The higher the wind speed, the more quickly the gas is dispersed as it leaves the leak source, and the less visible it becomes to the optical imager. However, some motion is beneficial for detecting a leak, as the human eye is particularly sensitive to movement. A stationary gas cloud is very difficult to distinguish against a non-uniform background.

Atmospheric Window. An "atmospheric window" is defined as a region of the spectrum where there is minimal or no light absorption by oxygen, nitrogen, carbon dioxide, and water vapor that are normally present in air. The major atmospheric windows in the infrared region are found in the 3 to 4.2 micron and in the 8 to 13 micron wavelength regions. A laser beam propagating through the atmosphere at wavelengths within these atmospheric windows will experience minimal attenuation.

However, laser light within these IR windows may still be attenuated by particulates in the air, including water droplets as in fog and steam. Consequently, these particulates will appear as dark clouds in the BAGI image as do the fugitive gases that absorb the laser light. However, since these particulates are also visible to the naked eye (while the fugitive gases are not), the BAGI operator can easily distinguish between the two types of cloud displays.

For example, if the cloud can be seen with the unaided eye AND with the BAGI camera – the cloud is likely particulates or steam. If the cloud can only be seen with the BAGI camera, it is likely gas.

2.1.1 Description and Operations of the BAGI Lasers

The two BAGI lasers, which weigh between 20 lbs and 30 lbs and are about the size of a TV camera, consist of two systems: a camera unit and a power/control unit. The camera portion of LIS's long-wave IR laser imager is connected to a mobile power pack that plugs into an external 110V AC outlet. The power pack converts AC to DC. The camera portion of SNL's prototype mid-wave IR laser plugs into a backpack borne power/control that is powered by a 28V lithium-ion battery. Battery lifetime while the mid-wave IR laser is operational is between 1 and 1½ hrs; batteries recharge in twelve hours. Batteries can be changed without shutting down the device. The mid-wave IR imager can also be operated on a 110 volt AC outlet through the power unit's 28 volt DC converter.

Both imagers can be operated in a shoulder-mounted position or with a tripod-mounted position (Exhibit 2-4). The tripod has a swivel fitting that permits the operator to move the instrument from left to right and up and down while scanning for leaks. A zoom lens allows the operator to adjust the focal distance to obtain a better view. The operator can record video of the image seen in the viewfinder. Both cameras have simple start up procedures requiring 10 – 15 minutes after power is switched on.

Exhibit 2-4 Laser Imagers shown in Shoulder- and Tripod-Mounted Operations

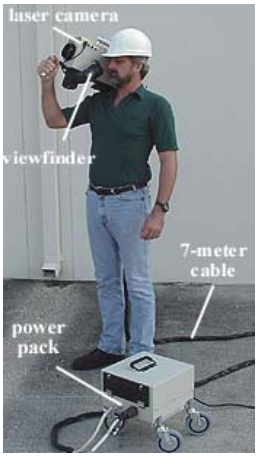

LIS Laser

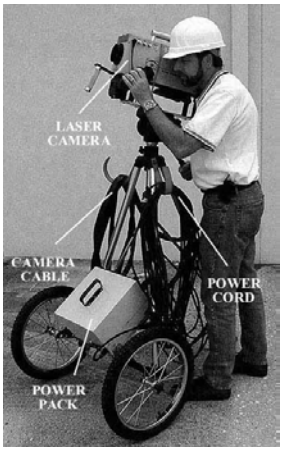

LIS Laser

Sandia Laser

2.1.2 Description of LIS's Long-Wave IR Laser

The CO_2 wave-guide laser operates in the 9-11 micron spectral region at 5W (US Patent 4,555,627). Use of such a low laser power is possible due to the unique optical arrangement shown at right which permits synchronous scanning of a laser beam and the instantaneous field-of-view (IFOV) of an infrared detector across the area of interest. The IFOV produced by the small (.005 cm X .005 cm), cooled IR detector and a collimating lens is scanned in a raster-like fashion across the target area by two scan mirrors, one for horizontal motion and another for vertical motion (in the same fashion as a television picture tube). As shown in Exhibit 2-5, the laser beam is directed onto, and scanned across the target area by these same two scan mirrors. This insures that the detector IFOV and the laser beam are in perfect synchronization, and that the laser only need irradiate that region of the target area viewed by the detector. In these long-range systems (>10 m), a beam expander is used to reduce the laser beam divergence so that it is less than the IFOV divergence. This keeps the laser power requirements to a minimum.

Exhibit 2-5 Long-Wave IR Laser's Synchro-Scan Optical Configuration

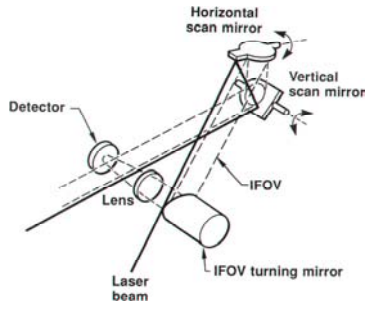

2.1.3 Description of Sandia National Laboratory's Mid-Wave IR Laser

Sandia National Laboratories (SNL) developed a new laser source that is effective for VOC emissions at refineries. The new laser device is an optical parametric oscillator (OPO), which uses the nonlinear optical crystal periodically poled lithium niobate (PPLN) as its active medium. An OPO is a laser-like device that consists of an optical cavity, which contains a nonlinear crystal (i.e., the PPLN). To operate the OPO, a beam from a separate laser (the pump laser) is focused into the PPLN crystal. Light from the pump laser is converted by the OPO into two new beams (called the signal and idler) whose frequencies add to that of the pump laser. The basic elements of the PPLN-based imager are shown in Exhibit 2-6. They consist of the pump laser, the OPO, and the raster scanner.

Exhibit 2-6. The Basic Elements of the PPLN-Based Imager

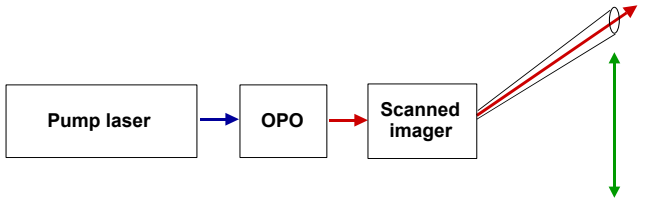

(1) The pump laser creates the initial laser radiation

(2) The OPO converts the pump light to the infrared

(3) The scanned imager creates the laser-illuminated image

2.2 The Image Multi-spectral Sensing (IMSS) Camera

The IMSS camera shown in Exhibit 2-7 is a hand-held, battery-operated device that is based on IMSS technology developed and patented by Pacific Advanced Technology (PAT)[1]. It is marketed under the Sherlock name. It weighs 12 pounds (including battery) and is 12(L) x 6(W) x 8(H) inches in size. It is a completely autonomous instrument, which includes an imbedded processor based on a Power PC, and a Linux operating system. The camera also contains special digital processing circuits with the ability to perform real-time processing algorithms using programmable FPGA. The camera can be controlled remotely over an Ethernet port. An IEEE 1394 FireWire interface allows high-speed data transfer to remote storage media such as FireWire removable drives.

Exhibit 2-7 IMSS Camera

2.2.1 The IMSS Principal

The IMSS is based on the principal of diffractive optics. As such, it is a combination of a diffractive imaging spectrometer and an adaptive tunable filter. Using a single lens, IMSS performs both imaging and dispersion. This enables a very small, lightweight, robust, and low-cost imaging spectrometer. The IMSS has a high throughput with a spectral resolution on the order of 6 wave numbers. Its noise equivalent spectral response NESR has been measured at 6 x 10^{-7} w/cm^2 - Fm-sr at the detector.

[1] US Patent 5,479,258 and 5,867,264

The basic concept of IMSS is shown in Exhibit 2-9, where it is compared with a monochrometer or dispersive spectrometer.

A conventional monochrometer has an entrance and exit slit and a dispersive element such as a prism or grading. Light coming through the entrance slit is dispersed onto the plane of the exit slit, and the exit slit is scanned through the dispersed light. To obtain fine spectral resolution, the dispersive spectrometer must reduce the size of the entrance and exit slits, and thus reduce the throughput of the instrument.

Exhibit 2-8 Operating the IMSS Camera

Exhibit 2-9 Basic Principle of IMSS

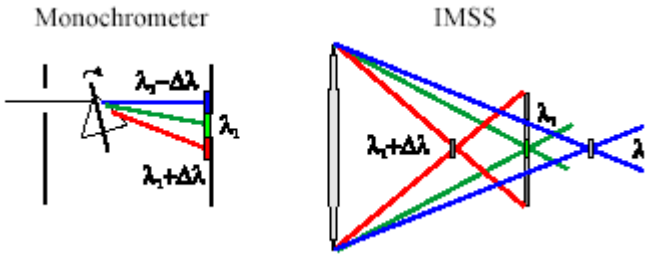

The IMSS uses the dispersive power of a diffractive optic to disperse the light along the optical axis, and the light gathering capability of the lens provides a very high throughput instrument. The fact that IMSS uses a single optical element to perform both imaging and throughput gives it the added advantage that no other spectral imaging approach has. It also provides the multiplexed advantage of image and dispersion with a single element. This allows high throughput, low cost, small size and an extremely robust instrument, which has very little optical alignment sensitivity. The fact that IMSS operates in a staring mode means that it does not require a spatial scanning and therefore can be field portable, and ideal for applications that require a small, light weight, robust instruments.

The IMSS camera collects spectral images in a band sequential mode as shown in Exhibit 2-10. Each frame of the camera is a spectral color, and subsequent frames can be different colors if the IMSS lens is scanned along the optical axis. Or, subsequent frames can be the same color as shown in Exhibit 2-11.

Exhibit 2-10 IMSS collects band sequential data

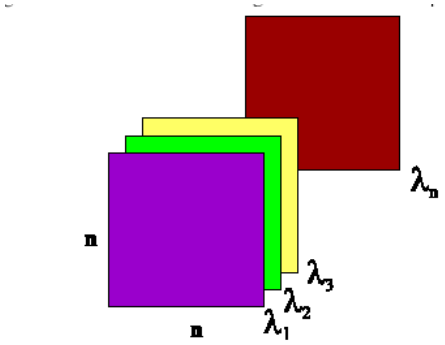

Exhibit 2-11 If desired, IMSS can collect only those spectral bands of interest

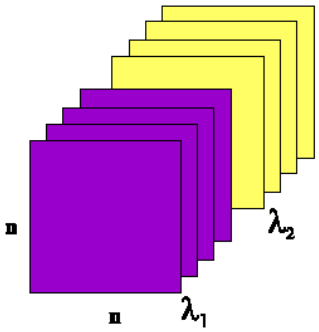

In this manner the IMSS imaging spectrometer is extremely adaptive and can collect only those spectral bands of interest, and can also dwell at a single spectral band indefinitely. This adaptability of IMSS makes it ideal for gas leak detection as compared to other spectral imaging techniques that require the collection of all spectral bands within the spectral free range of the instrument such as conventional dispersive instruments and FTIR spectrometers. For gas leak detection, certain spectral regions are of greater interest than others and thus there is no need to collect more than the necessary number of spectral bands. This saves time and necessary processing power. This ability also allows the IMSS to easily be adapted to numerous applications where real time spectral processing is of interest.

Exhibit 2-12 shows an IMSS image of a valve leaking methane at 0.1 scfm.

As the IMSS camera operates on passive IR imaging, the detection signal is generated by a difference in the IR radiance of the leak gas and the background behind the gas. The detection signal depends on the temperature difference between the gas and the background as well as the background's emissivity. In passive IR, a signal can disappear if a) the gas is imaged against a surface with an emissivity of 1, where the gas and the background have the same temperature; or b) A gas imaged against a surface with an emissivity lower than 1, where there is some nonzero difference in temperature between the gas and the background. While this test is not designed to explore temperature ranges or background types that produce these effects, as agreed with TCET and TCEQ, a brief discussion of the dependence of the signal on temperature and emissivity will be included in the test report. Additional information can be obtained from PAT.

Figure 2-12 IMSS images of a valve leaking methane at 0.1 scfm

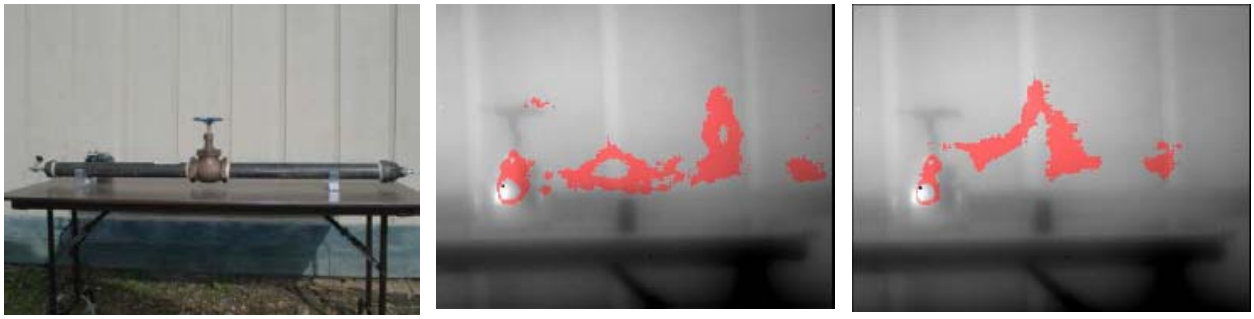

This section describes the test participants, equipment, and test parameters evaluated and test matrices for the test.

3.1 Test Teams

Six teams will participate in the test. Their respective roles and responsibilities are presented in the table below.

Team	Team Lead	Role/Responsibilities
Project Management Team	Environ Corporation – Michael Smylie	--design test protocol that meets the objectives of the statement of work -- coordinate test activities and data collection of all other teams -- supervise/oversee the analysis and presentation of test results
Sandia National Lab (SNL) Gas Imaging Team	Sandia National Laboratories – Tom Kulp	-- provide input to protocol design -- calibrate and operate the SNL BAGI camera, and ensure that the equipment functions at peak capability throughout the entire test period; -- record and maintain backup test data on their camera
Laser Imaging Systems (LIS) Gas Imaging Team	Laser Imaging Systems – Tom McRae	-- provide input to protocol design -- calibrate and operate the LIS BAGI camera, and ensure that the equipment functions at peak capability throughout the entire test period; -- record and maintain backup test data on their camera
Pacific Advanced Technology (PAT) Gas Imaging Team	Pacific Advanced Technology (PAT) – Bob Hinnrichs	-- provide input to protocol design -- calibrate and operate the IMSS camera, and ensure that the equipment functions at peak capability throughout the entire test period; -- record and maintain backup test data on their

Team	Team Lead	Role/Responsibilities
		camera
Test Facility Setup Team	Innovative Environmental Solutions – Jeff Panek	-- provide input to protocol design -- design test equipment (except cameras) and prepare lab for test -- operate test equipment (except cameras) -- record and maintain backup test data on all tests
Data Analysis, Reporting, and Quality Assurance (QA)/Quality Control (QC) Team	ICF Consulting – Don Robinson	-- design test protocol that meets the objectives of the statement of work -- observe that data collection and QA/QC activities are conducted according to the test protocol -- collect, compile, analyze, and report on the data collected during the test.

3.2 Test Equipment and Set-Up

Exhibit 3-1 shows an illustration of the test equipment set-up. The camera stand is on a track, which enables the operator to vary the viewing distance from 10 ft to 30 ft away from the component. The leak component lies between a fan and a hood, where the hood intake draws in leak gas in the same direction that the fan blows leak gas. As illustrated in Exhibit 3-2, placement of the fan and the hood limits flow of the leak gas to one direction. The component will be positioned so that the camera is directly ahead of the leak source, perpendicular to the fan/hood flow direction.

Exhibit 3-1 Test Equipment Set-up

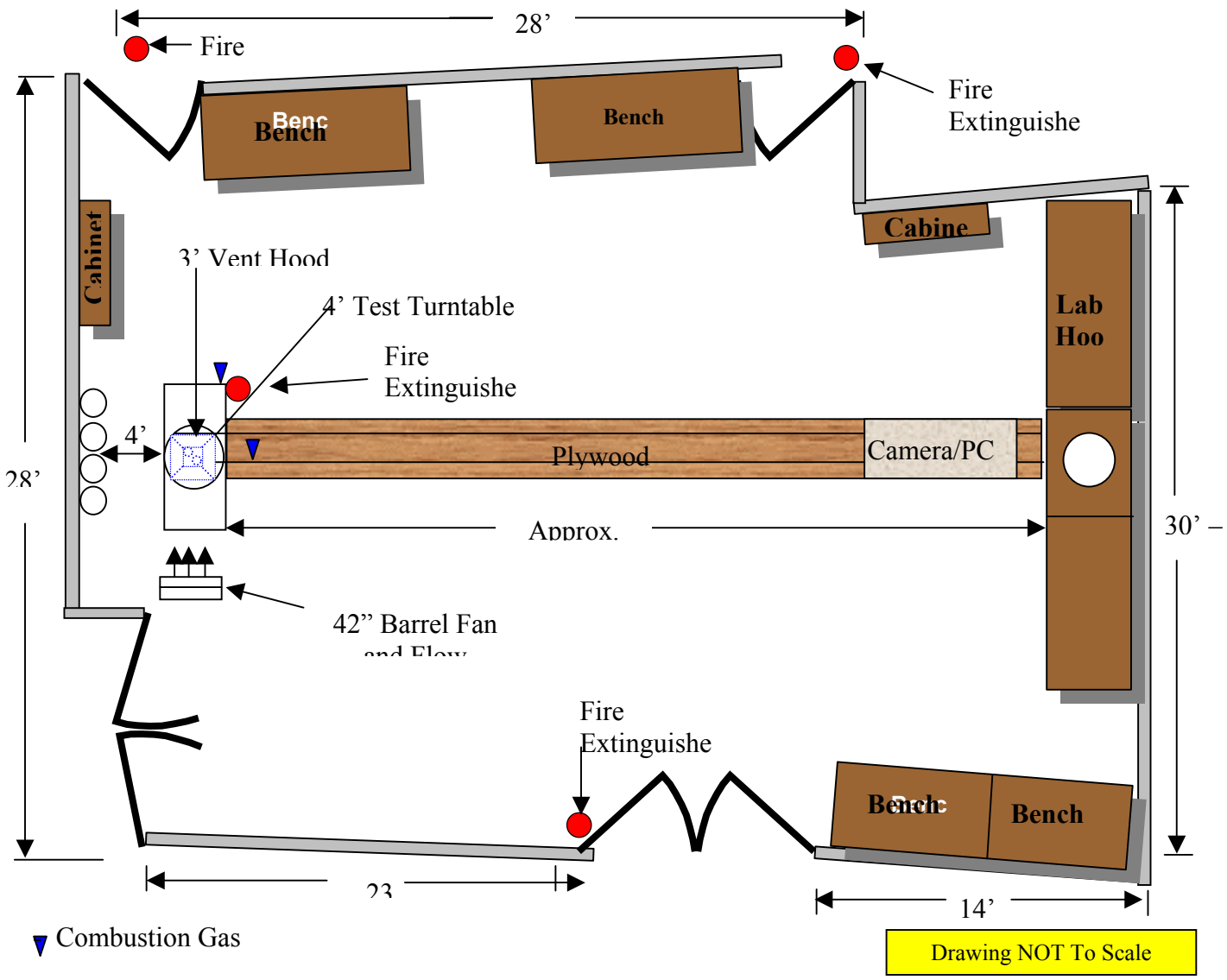

Exhibit 3-2 Air and Leak Flow

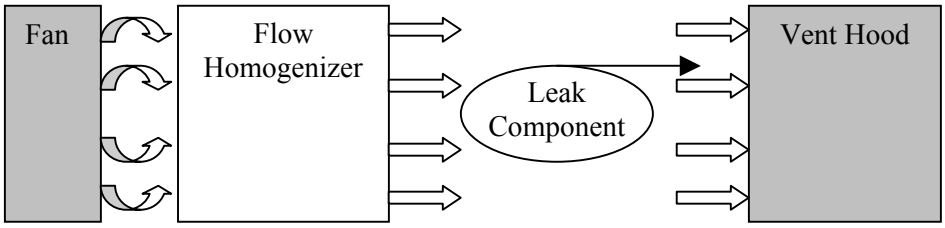

This test employs a variable-speed fan to simulate wind speed, and a flow homogenizer, illustrated in Exhibit 3-2, is positioned between the fan and the leak component. The flow homogenizer, a wooden frame completely filled in with about 7 inch lengths of 2 inch PVC pipe, is intended to limit rotational air flow caused by the fan.

Configuration of the fan/hood setup will employ a smoke wand to adjust hood flow. This will help to ensure undisturbed, uniform air flow across the leak component, which minimizes air flow variation over the test runs.

Leak Component

Exhibit 3-3 shows a 0.5 inch valve with removed stem packing used for imaging a leak source. The stem packing was removed to create a point leak that does not allow for the component to be pressurized. Leak gas is introduced to the component by a Cole Parmer A-03219-01 rotameter, and the downstream valve outlet is plugged so that all of the introduced gas exits the valve through the stem packing leak.

Exhibit 3-3 Leak Component

Rotameter calibration curves are available for air, and curves will be developed for butane, pentane, and xylene, which represent low, medium, and high molecular weight gasses used in this test.

Leak Backgrounds

Since background reflection is known to affect the performance of the BAGI cameras, two different background representative of typical chemical plant surfaces will be used for the tests:

1. Concrete Wallboard
2. A row of convex curved metal piping

Reflective Backgrounds

- Concrete Wallboard
- Convex curved metal piping

Both backgrounds may be positioned up to 4 feet away from the leak component.

Although background temperature is known to affect the performance of the IMSS camera, no variations in the two leak backgrounds will be conducted in these tests. Also, it is stipulated that the BAGI camera cannot image a leak against no, or distant, backgrounds; therefore, no tests will be conducted without a reflective background.

Hydrocarbons.

As all of the test cameras rely on gas absorption or emission spectra, the number of test chemicals can be reduced if two or more candidate chemicals share similar absorption/emission strengths at the same wavelength. Therefore, one candidate chemical will serve as a surrogate for others that share spectral absorption/emission properties, and the results of testing the surrogate chemicals will used to calculate the detection thresholds of all chemicals of interest. This allows for a more expansive test matrix on the surrogate chemicals, as the test time period per chemical increases when using

surrogates to shorten the test list. Using absorption/emission surrogates also allows the procedure to bypass a more toxic candidate chemical in favor of a less toxic candidate chemical with a similar absorption profile.

Since the BAGI lasers in this test operate at different wavelengths, two lists of surrogates are developed. An attempt was made to propose the same surrogate in both mid- and long-wave IR laser lists to minimize the number of chemicals. However, these same chemicals are surrogates for different other chemicals with each laser technology because of the different absorption characteristics of chemicals in the respective wave number ranges (e.g. propylene is a surrogate for pentene with the LIS laser, but not with the SNL laser).
On a molecular basis, one surrogate molecule has similar absorption/emission strengths at given wavelengths as a different molecule. Therefore, the leak rate equivalency of a surrogate gas is only valid in terms of volumetric leak rates. The minimum mass detection level of the surrogate will differ for the minimum mass detection level of the gas similar to the surrogate, as molecular weight adjustments are required.

The table below shows the 14 candidate chemicals in the left column. The middle column shows the list of surrogate chemicals for the LIS long-wave IR laser, and the right column shows the list of surrogate chemicals that will be tested for the SNL mid-wave IR laser and the PAT IMSS camera. The results from testing the surrogates will be applied to those chemicals not tested. This will provide results for all required candidate chemicals. With time available in the test program, after the below listed chemicals are characterized, a matrix of tests may be performed using formaldehyde or mixtures of chemicals typical in petroleum plant streams.

Candidate Chemicals	**LIS Long-Wave IR Laser Tested Chemicals**	**Sandia Mid-Wave IR Laser and PAT IMSS Tested Chemicals**
Acetaldehyde 1,3, Butadiene all Butanes all Butenes (Butylenes) Ethylene all Ethyltoluenes Formaldehyde all Hexenes Isoprene all Pentanes all Pentenes Propylene Toluene all Trimethylbenzenes all Xylenes	Ethylene 1,3-Butadiene 1-Butene for 2-Butene and for Isoprene O-Xylene for Toluene and Trimethylbenzene Propylene for 1-Pentene and for 2-Pentene m-Xylene	Ethylene Acetaldehyde 1,3-Butadiene 1-Butene Butane for Pentane and n-Hexane Isoprene 1-Pentene for 2-Pentene and Trimethylbenzene Propylene for 2-Butene O-Xylene for m-Xylene, p-Xylene, and Toluene

		Formaldehyde (as time permits)
Total: 15 Candidate Groups	**Total: 6 Test Groups**	**Total: 10 Test Groups**

Other Equipment

Exhibit 3-4 lists other equipment used to measure test parameters. Air temperature and humidity will be measured in the lab as well as outside of the lab near the ventilation intakes.

Exhibit 3-4 Other Test Equipment

Equipment	**Description**
The Outer Banks Weather Company BTC Anemometer	Measures fan speed across leak component
Kestrel propeller anemometer	Measures fan speed across leak component
Davis totalizing vane anemometer	Measures fan speed across leak component
Cole Parmer 8528-21 digital thermohydrometer	Air Temperature/Humidity probe
VWR Scientific 35519-050 Type J thermocouple	Temperature
Gas Omega HH23 Type J Thermocouple	Temperature
Foreground lighting: 2-300 watt incandescent and 2-250 watt IR bulbs Background lighting: 2 incandescent bulbs and 1 IR bulb	Available Room Lighting Options
Steel tape measure	Measures distances from camera lenses to leak component
Environics 4040 Gas Dilution System	Backup gas delivery to leak component assembly

3.3 Test Parameters, Variables & Matrix

The tests will explore four parameters to generate as complete a performance specification as possible in a laboratory setting.

Parameter	**Variables**	**Comment**
Hydrocarbon	14 candidate chemicals	Absorbance surrogates allow testing of 10 candidate chemicals to achieve results for all 14 chemical groups.
Wind Speed	0-2 m/s 3-5 m/s	One wind speed in each range will be selected for testing. Wind speeds in the lower range are typical of those found during normal weather conditions. The higher wind speed will explore more extreme conditions.
Viewing Distance	10 ft 20 ft	These are the distances from the camera lens to the leaking component.
Backgrounds	Concrete Wallboard Curved, painted metal surface	This background will simulate concrete, gravel and earth surfaces found at petroleum plants. A row of gas cylinders will simulate the pipes, vessels and valves found at petroleum plants.

Three tests (one for each camera) will be conducted over two weeks:

- Week 1 – Testing LIS's long-wave IR BAGI camera.
- Week 2 – the IMSS camera and SNL's mid-wave BAGI camera will be tested simultaneously. Both cameras will be mounted on the camera stand in a manner that will permit both cameras to screen the leak device at the same time.

The test matrix, presented below, anticipates 10 test runs for each of the tested chemicals. This results in 50 test runs using the 5-group surrogate list for the LIS laser and 80 test runs using the 8-group surrogate list for the SNL laser and IMSS camera. Each setting (e.g. TS1-1) will return 1 result. For each test run (e.g. TS1-1), the chemical flow rate will be adjusted until the operator determines the minimum mass detection level that can be observed from the leaking component. The minimum mass detection level *from the leaking component* is defined as the lowest leak rate where a gas cloud can be identified escaping from the component. For example, by this definition gas detected near the fume hood, but not extending to the leak site, would not characterize a camera's minimum mass detection level. The primary purpose of the optical imaging leak detection is to identify clearly the exact site and component that is leaking, out of a potential large array of potentially leaking components. To maintain consistency between operators and test runs, the imager operator will assist a QA/QC team member in making the official determination of the minimum mass detection level.

Number of Test Runs -

For LIS laser: 50 test runs, not including setup time and transition time between runs

For SNL laser and IMSS camera: 80 test runs, not including setup time and transition time between runs

Minimum Mass Detection Level -

The minimum detection level is the lowest leak rate for which a gas cloud can be clearly identified escaping from the leak location on the component. The gas cloud must be seen originating at the leak source. Gas detected elsewhere in the field of view, but not extending to the leak source, does not characterize a leak.

Because the screening methods of the IMSS and BAGI cameras differ, flow rate will be adjusted in discrete recorded intervals, e.g. at intervals of 0.5 g/hr. The minimum mass detection level (MDL) may be approached by either increasing the leak rate from zero or decreasing the leak rate from the maximum leak rate. The choice of increasing or decreasing gas flow is at the discretion of the equipment operators. The preferred approach is incrementally increasing gas flow from zero until all cameras participating in the test run reach their minimum detection threshold.

After identifying the minimum detection level for a test run, a camera will image a leak rate at 67% of the identified minimum detection level.

For each direction of the leak rate change, one complete set of test runs will be recorded in the following manner:

BAGI Camera Screening Procedures

- Screening is done by viewing the leak source through the viewfinder on the camera.
- A VHS recorder can simultaneously record the view that the operator observes.
- The operator will indicate when the minimum flow rate is reached, for the QA/QC officer to verify. The leak rate at the minimum detection threshold will be recorded on video. A

data collection sheet will be completed.

- The leak at one additional flow rate at 67% of threshold value will be set and recorded for 30 seconds on videotape. For example, if the leak threshold is determined to be 10 g/hr at 20 ft with wind speed 1 m/s, the Test Team will video tape a leak 7 g/hr which bracket the threshold. The purpose of recording threshold and an additional leak rates is to: (1) have sufficient data to bracket the threshold determined by the operator; and (2) have data that can be surveyed by an independent panel (at a later date if desired) to determine whether they detect the same threshold as the operator conducting the experiment.
- The flow rates, counter number and tape number will be recorded for each data point recorded.

IMSS Camera Screening Procedures

- Screening is done by taking digital pictures of the leaking device. The electronic image referred to as a "data cube" is then processed to create a false-color image of any detected gas leak.
- The operator will indicate when the minimum flow rate is reached, for the QA/QC officer to verify. The leak image at the MDL will be preserved, and a data collection sheet will be completed.
- The leak at one additional flow rate at 67% of threshold value will be photographed and processed. For example, if the leak threshold is determined to be 10 g/hr at 20 ft with wind speed 1 m/s, the Test Team will video tape a leak 7 g/hr which bracket the threshold. The purpose of recording threshold and an additional leak rates is to: (1) have sufficient data to bracket the threshold determined by the operator; and (2) have data that can be surveyed by an independent panel (at a later date if desired) to determine whether they detect the same threshold as the operator conducting the experiment.

The test runs and direction of change in leak rate (reducing or increasing the flow rate) will be selected at operator discretion until the entire matrix is complete.

Test Matrix – Determining the Mass Leak Detection Threshold

Test Set 1 (TS1)			
Test Run	**Lens-Valve Distance (ft)**	**Wind Speed (m/s)**	**Background**
TS1-1 TS1-2	10 20	0-2 0-2	Concrete Concrete

Test Set 2 (TS2)			
Test Run	**Lens-Valve Distance (ft)**	**Wind Speed (m/s)**	**Background**
TS2-1 TS2-2	10 20	3-5 3-5	Concrete Concrete

Test Set 3 (TS3)			
Test Run	**Lens-Valve Distance (ft)**	**Wind Speed (m/s)**	**Background**
TS3-1 TS3-2	10 20	0-2 0-2	Metal Cylinders Metal Cylinders

Test Set 4 (TS4)			
Test Run	**Lens-Valve Distance (ft)**	**Wind Speed (m/s)**	**Background**
TS4-1 TS4-2	10 20	3-5 3-5	Metal Cylinders Metal Cylinders

For purposes of exploring the reproducibility of the results, TS3-1 will be repeated a total of three times for four chemicals of high interest:

(1) 1-3 Butadiene
(2) 1 Butene
(3) Ethylene
(4) Propylene

The three TS3-1 runs will occur in non-sequential order: other test runs must occur between taking a TS3-1 run. Run order is left to the discretion of the operators.

Additional available lab time will be used to perform several test runs at a viewing distance of 30 ft. This provides three distance data points to confirm the relationship of MDL with distance as found in previous tests.

A sample data collection sheet is presented in Exhibit 3-4. All data will be recorded on-site as test run is completed.

Exhibit 3-4

Project Title: TCET Optical Imaging Testing

Date: _____, **Time:** _____AM PM **Test Run:** _____

Camera (*circle one*)**:** PAT IMSS SNL Laser LIS Laser

Operator: _____ **Lens-Valve Distance** (*circle one*)**:** 10ft , 20 ft, 30 ft

Background (*circle one*)**:** Concrete Curved Painted Metal

Wind Speed: _____ units:_____

Leak Detected (*circle one*)**:** Yes No **Flow Rate** _____ units:_____

Leak Comments/Observations:_____

_____

Leak Detection Threshold _____ units:_____ **Pressure** _____ units:_____

Leak Set by: Reducing flow Increasing flow

Time/Date Stamp at: Start of Test: _____ **End of Test**: _____

(number displayed by recorder indicating location on the tape)

BAGI Tape Number (s): _____ *(assuming several tapes used to capture the entire test)*

IMSS Data Cube Identifier (s): _____

Data Point	Mass Rate (g/hr)	Counter No. at Start	Counter No. at End	Tape/Data Cube Number
Threshold				
67% of Threshold				

Other Observations: _____

4.0 Test Boundaries

This section describes boundary conditions for parameters that may affect results and any bearing the boundaries might have on the design of the test, sample collection or decision-making.

Parameter	Comment
Wind Speed and Direction	Two wind speeds between 0 and 5 m/s will be examined. The use of the fan and homogenizer will create streamlined air flow not typical in nature, but repeatable over the test runs.
Daylight Variation, Night Conditions, Precipitation	The test does not include evaluating the performance of the optical devices in rain, snow, or under varying light conditions. Tests that examine lighting variations to mimic bright sunshine or overcast daytime conditions may be done at the discretion of the test team and included in the test results.
Hydrocarbons	Surrogate chemicals are used to represent other chemicals with similar absorption at similar wave numbers. Hence, experimental data on every candidate chemical will be limited. Time available, tests of mixtures of the chemicals may be done at the discretion of the test teams and included in the results.
Viewing Distance from Leak	The test is designed for viewing distances between 10 and 30 ft from the leak source. The Test Team will record any distances outside these boundaries at which measurements are taken.
Ambient Temperature and Humidity	The test facility's climate control system is limited, so temperature and humidity will be measured but not actively manipulated or controlled. Temperature and humidity variations are minimized by testing two cameras simultaneously and testing the third camera the immediately prior week.
Operator Determination of Minimum Detection Limit	Minimum detection limit determination depends in part on operator perception. Each camera will take data recordings of its respective view to allow review of the minimum detection limit as determined by the operator and verified by the QA/QC person.
Leak Component	One valve will be modified to emit leaks for this test. Other components such as flanges, threaded connectors, etc, found at chemical facilities are not examined because of time constraints. The nature of leaks (pinpoint versus cracks) which may influence a leak's detectability will also be excluded because of time. These variables will be present and thus examined during field testing during the next phase of this effort.
Viewing Angle	The leak component is viewed from only one angle with respect to the gas cloud, component, and background (i.e. directly perpendicular to the leak component). The influence of viewing angle will be examined during field testing.

Parameter	Comment
Background and Leak Gas Temperature Differential	The dependence of leak gas detection on the delta T between the background and leak gas is an acknowledged performance parameter of passive detection imagers but will not be investigated as part of this test. A brief discussion of the dependence of the detection signal on this temperature differential will be included in the test report.

5.0 Quality Assurance (QA) and Quality Control (QC)

This section details QA/QC procedures for the test, test equipment, and cameras.

5.1 QA Procedures

QA procedures are as follows:

- The Project Management Team will develop a test protocol that meets objectives of statement of work.
- The Project Management & QA/QC Teams will ensure that the test is conducted in accordance with the Test Protocol.
- The QA/QC Team will observe that the data is collected correctly (e.g. data sheets completed as experiments are conducted) and maintain a logbook to record procedures witnessed and any deviations from the test protocol.

5.2 Test QC Procedures

QC procedures consist of equipment calibration and document management.

5.2.1 Equipment Calibration

The respective gas imaging teams are responsible for calibration of their cameras.

5.2.1.1 Calibrating/Startup of the BAGI Cameras

Below are descriptions of calibration and startup procedures for the Sandia and LIS laser imagers

Sandia Imager Calibration and Startup

Wavelength Calibration.

To insure that the portable imager is optimized for detection of a specific gas or group of gases, such as the hydrocarbons found in refinery leaks, the wavelength of the signal beam will be measured and adjusted prior to data collection. Using propane as an example, if the signal beam is tuned to a

wavelength of 1.5555nm, the idler beam that illuminates the scene will be tuned to the peak absorption wavelength of the propane CH-stretch. Since the absorption of propane is the highest at this point the black cloud in the collected image will be the darkest possible. If the wavelength is off in either direction, the gas cloud in the image may not be as intense or may not be seen at all.

Laser Power Monitor of the SNL laser

Using a portion of the signal beam the OPO power will be monitored before data is collected. The signal beam power directly correlates to the idler power that is used to illuminate the scene. As the idler power increases, the range of the imaging system will increase, allowing the operator to view gas leaks that are farther away. The minimum operating power for the OPO is ~270mW of 3 μm light. This will allow for reasonable images at distances up to 15 ft. Based on previous testing, at an operation power of 500mW the working distance increased to 30 feet.

Start-up Procedure of the SNL laser:

1. Connect to 28V DC power supply. Leave the control box and imaging unit turned off until the crystal oven comes to temperature (175° C). This takes 5-10 minutes.
2. Turn on the control box. This activates the seed laser and the TEC control for the fiber amplifier.
3. Do a visual/power check that the seed laser is going through the OPO properly.
4. Turn on the scanner (switch is on the side of the shoulder mounted imager).
5. Wait for the built-in 3 minute delay before turning on the fiber amplifier (switch is on the back of the shoulder mounted imager). When the fiber amplifier is turned on there should be red light in the OPO cavity.
6. Measure the wavelength of the idler beam. For hydrocarbon detection, the wavemeter should read 1.5555 μm. Make necessary adjustments by turning the knob at the top of the oven translation stage.
7. Measure the OPO power using the built in power meter. It should read between 140 and 160mV. A higher reading is always okay.
8. If the output power is lower than 140mV, first check the polarization of the light going into the OPO by adjusting the waveplates in front of the seed laser and OPO. If the polarization is maximized and the power is still low, adjustments of the fiber port's z-axis may be made.
9. Remove all diagnostics and put the blue cover on the system.
10. Complete a final system check by looking at a leak of a known rate and substance. Make adjustments to scanner gain and phase if necessary.

LIS Imager Calibration and Startup

Calibration of the LIS Laser

The GasVue® camera will be calibrated for all relevant wavelength at the factory just prior to shipment to BP Naperville. On-site calibration verification will be performed using the Q-branch absorption of ethylene gas.

Start-up Procedure for the LIS Laser

Typical start-up and shut-down of the system is accomplished by the following steps:

1. See that the AC power cord is connected to the proper power source, and the viewfinder (or an auxiliary TV monitor) is connected.

2. Insert the key in the key switch on the Power Pack, and turn clockwise. The Power Pack cooling fan will start, and the WAIT mode self-check display will come up on the video monitor. The RED shutter indicator on the top of the Laser Camera should also come on.

3. After the WAIT mode has transitioned to the OPERATE mode, press the "LASER OFF" button on the Laser Camera to clear any CAUTION or FAULT messages that may be displayed on-screen. NOTE: In normal operation, the "SCANNER FAULT" should always appear and require clearing. Also, some CAUTION messages may remain displayed until the system reaches its operational set point. If the "SCANNER FAULT" message does not appear, turn off the key switch, wait a few seconds, and then re-start the system.

4. Next press the "LASER ON" button switch to start the laser. The GREEN indicator on the top of the Laser Camera should come. After a five second delay, the laser will come on. Using the "DISPLAY" button, call up page #1 of the PARAMETERS screen. After about five minutes, check that all system parameters are within their appropriate operational ranges, and that all "CAUTION" messages have disappeared. If all parameters seem OK, press the "DISPLAY " button until you return to the OPERATE screen.

5. Using the "DISPLAY" button, call up the GAS SELECTION screen, and adjust the GS= and TS= settings for the gas of interest. If all parameters seem OK, press the "DISPLAY " button until you return to the OPERATE screen.

6. Point the Laser Camera at an object or surface about 5-10 meters away. Adjust the "CONT" control knob fully counter-clockwise (lowest CONTRAST position), and then adjust the "BRIGHT" control to get the best image of the objects being viewed. Next increase the "CONTRAST" setting if the image appears too dark. In general, you will not have to further adjust the "BRIGHT" setting; only adjustments to the "CONTRAST" setting will be required for your leak inspections.

7. Your GasVue system is now ready for leak location use.

8. Normal shutdown of the system is accomplished by turning the key counter-clockwise to the straight-up position.

5.2.1.2 Calibrating/Startup of the IMSS Camera

The IMSS camera is factory calibrated and needs no further calibration in the field. It recalibrates itself automatically when it is turned on, and does not need a factory calibration unless the camera is disassembled for a repair.

There also is no formal startup procedure. The camera needs about 9 minutes for the Dewar to cool down the focal plane array. The camera will automatically provide an image once it is cooled down. An external PC computer will interface to the camera and provide a display of the gas, store the test data, images, etc. The PC software requires about 2-3 minutes to load and initialize, so the camera startup requires about 12 minutes.

5.2.1.3 Rotameter Calibration

The Cole Parmer A-03219-01 rotameter has an air calibration curve, and three additional curves corresponding to low, medium, and high molecular weight gases (relative to the test gases) will be developed for the test. Butane will be used to check the rotameter against either a wet gas meter, dry gas meter, or bubble meter.

5.2.1.4 Calibrating Other Equipment

Other test equipment such as the flow meter, rotameters, anemometers, etc, will be calibrated according to manufacturers' instructions. The AQ/QC Team will obtain verification of calibration procedures.

5.2.2 Document Management

The Test Team will retain originals of the data collection sheets; recorded video and QA/QC log and include copies of these documents in Appendices of the Test Report.

6.0 Reporting and Data Reduction Requirements

The Test Team will prepare a report that report includes the following sections:

- Executive Summary;
- Test Matrix;
- Sampling Technology and Procedures;
- QA/QC Procedures;
- Test Results;
- Test Data and Calibration Sheets;
- List of Participants; and
- Appendices.

APPENDIX C

Absorbance Spectra

ABSORBANCE SPECTRA FOR TESTED CHEMICALS

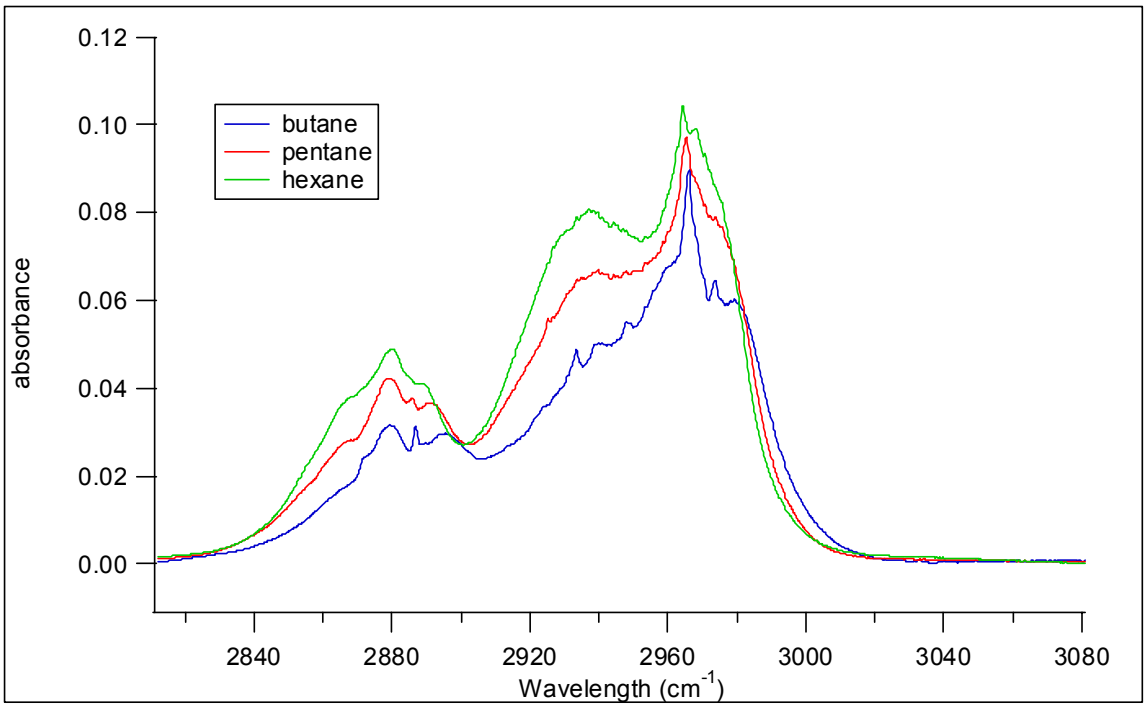

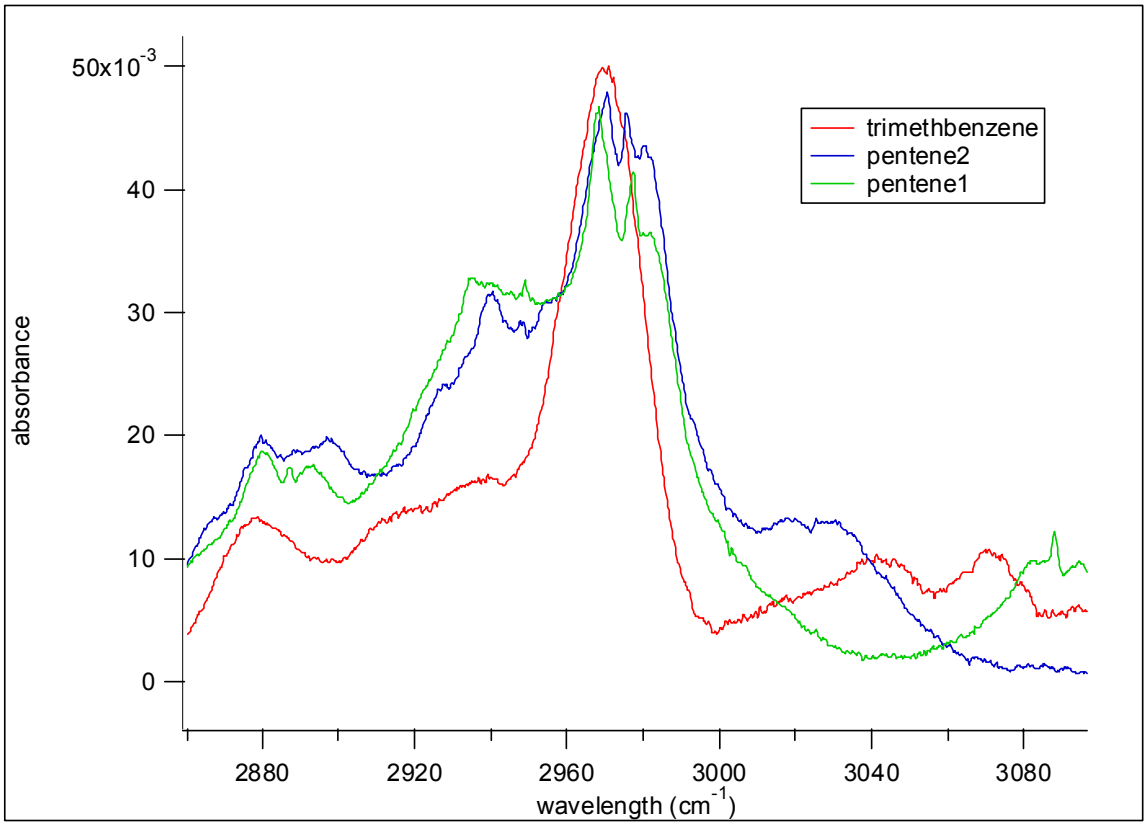

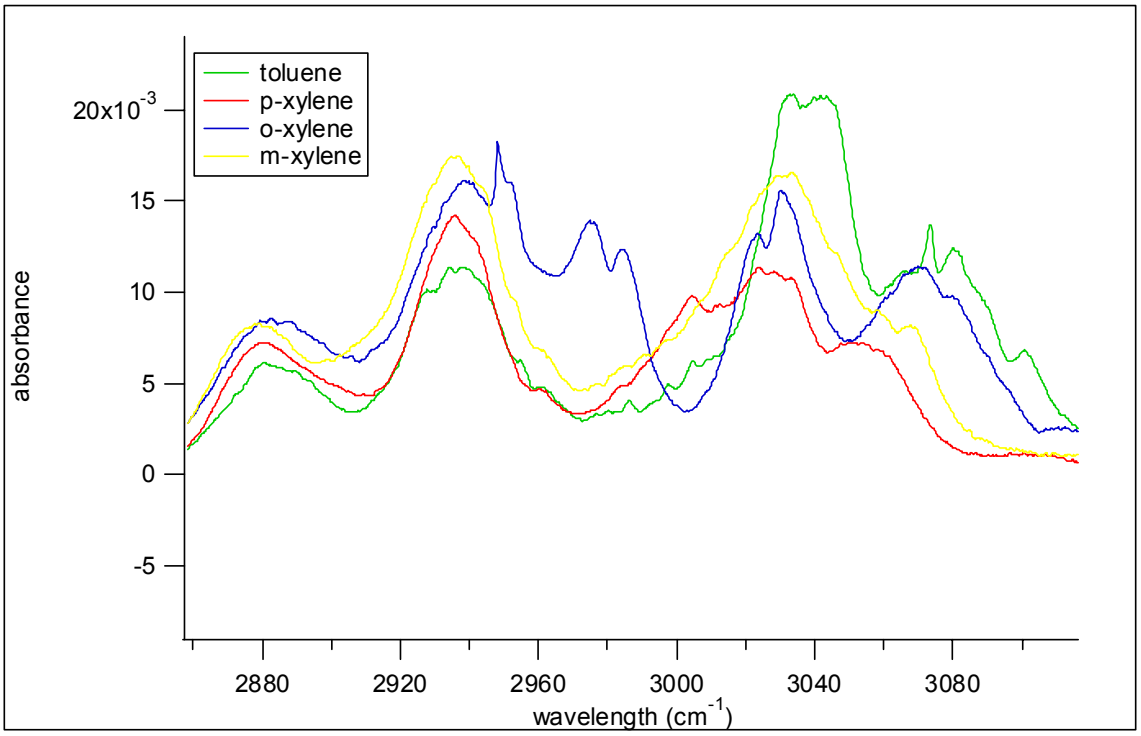
toluene
p-xylene
o-xylene
m-xylene
20x10-3
15
10
5
0
-5
absorbance
2880
2920
2960
3000
3040
3080
wavelength (cm-1)

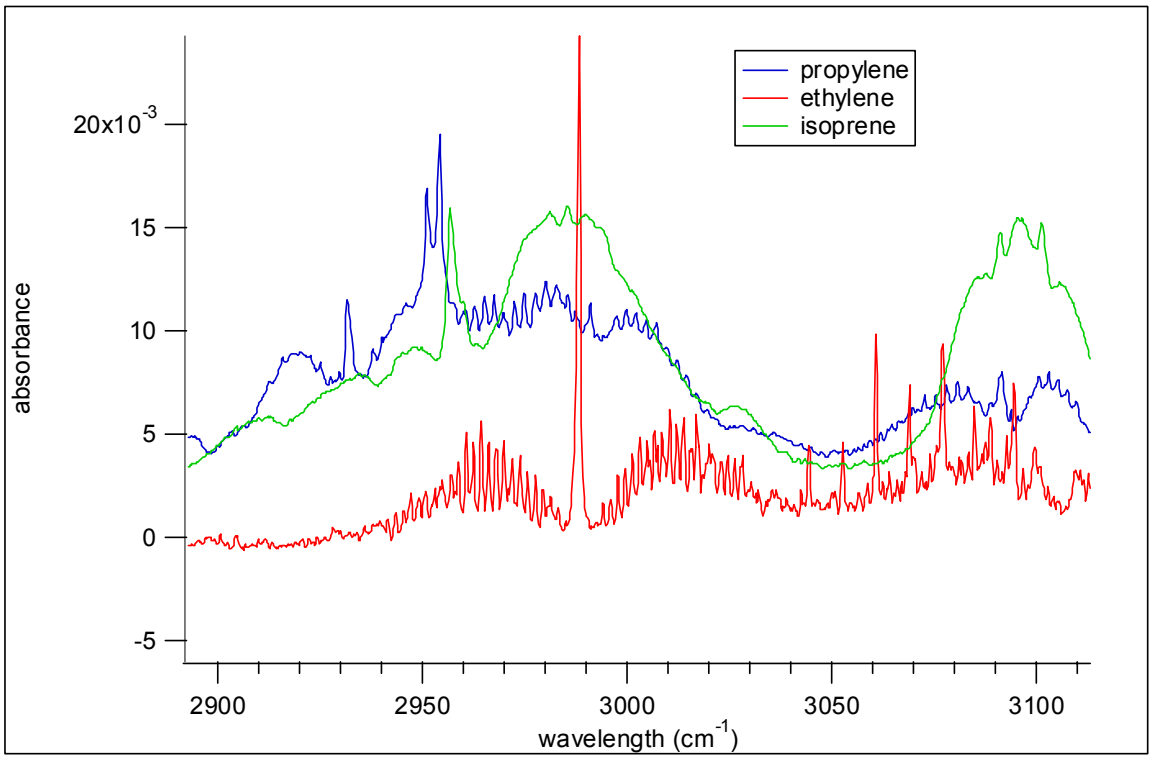
propylene
ethylene
isoprene
20x10-3
15
10
5
0
-5
absorbance
2900
2950
3000
3050
3100
wavelength (cm-1)

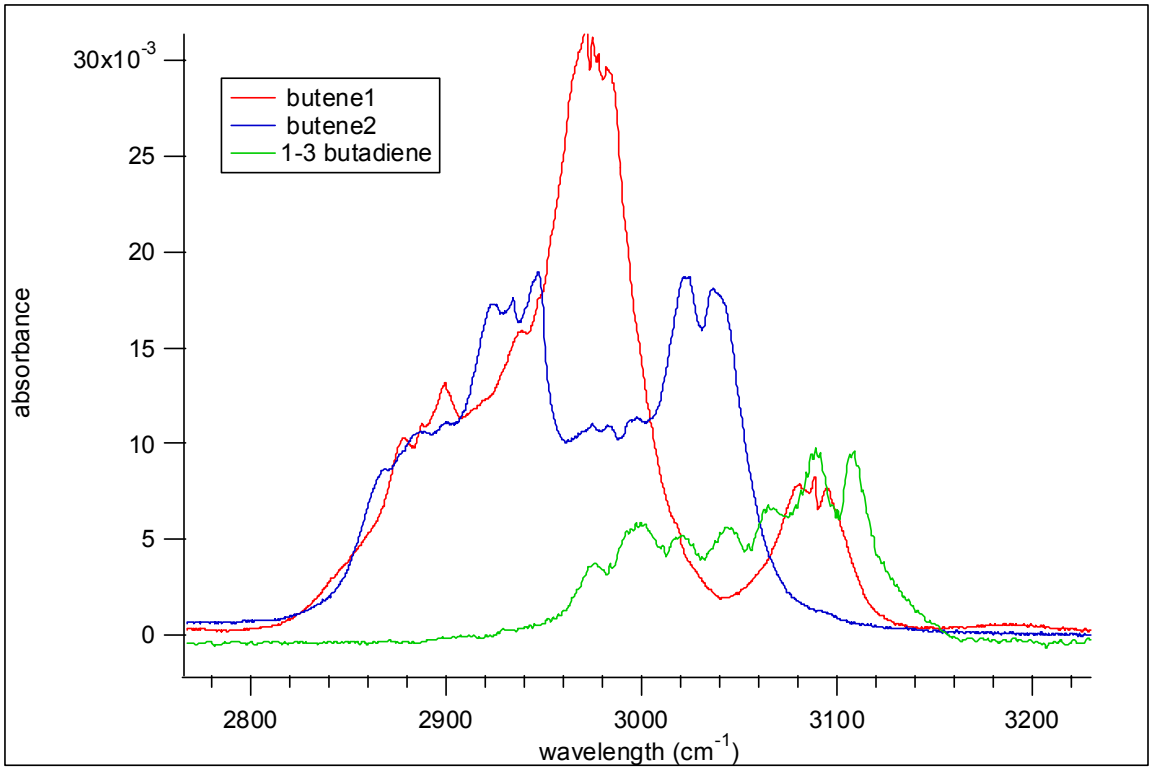
30x10-3
25
20
15
10
5
0
absorbance
butene1
butene2
1-3 butadiene
2800
2900
3000
3100
3200
wavelength (cm-1)

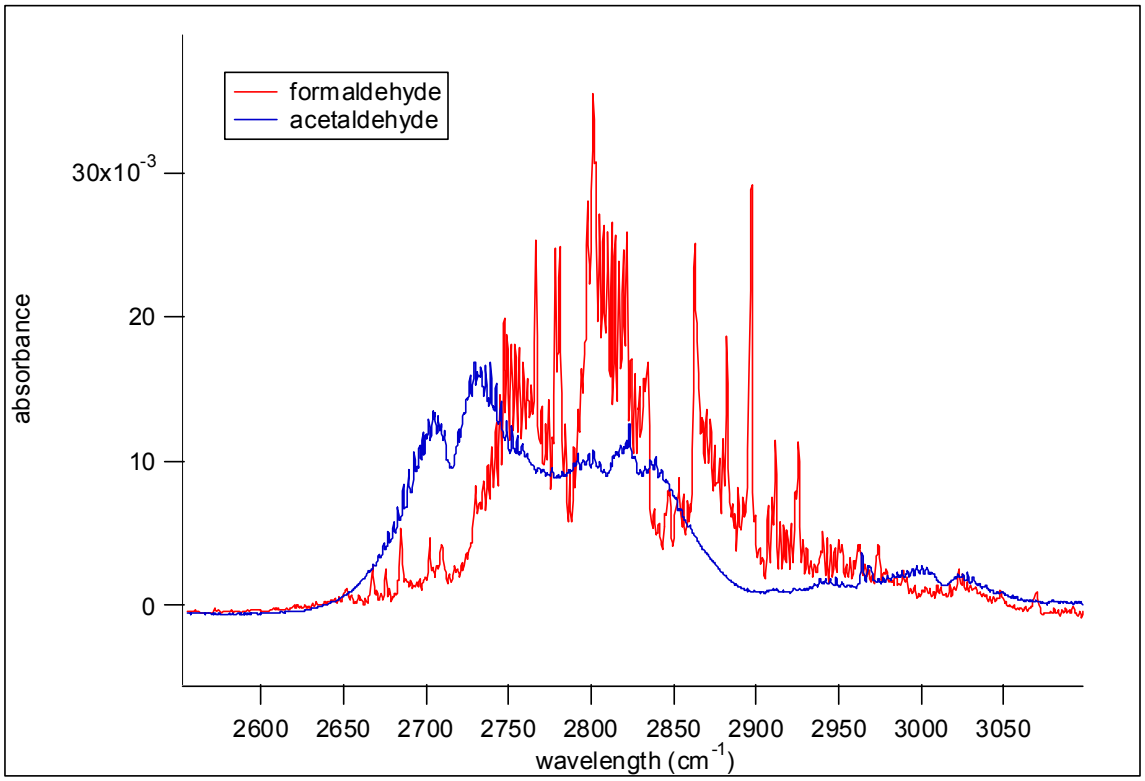
formaldehyde
acetaldehyde
30x10-3
20
10
0
absorbance
2600
2650
2700
2750
2800
2850
2900
2950
3000
3050
wavelength (cm-1)

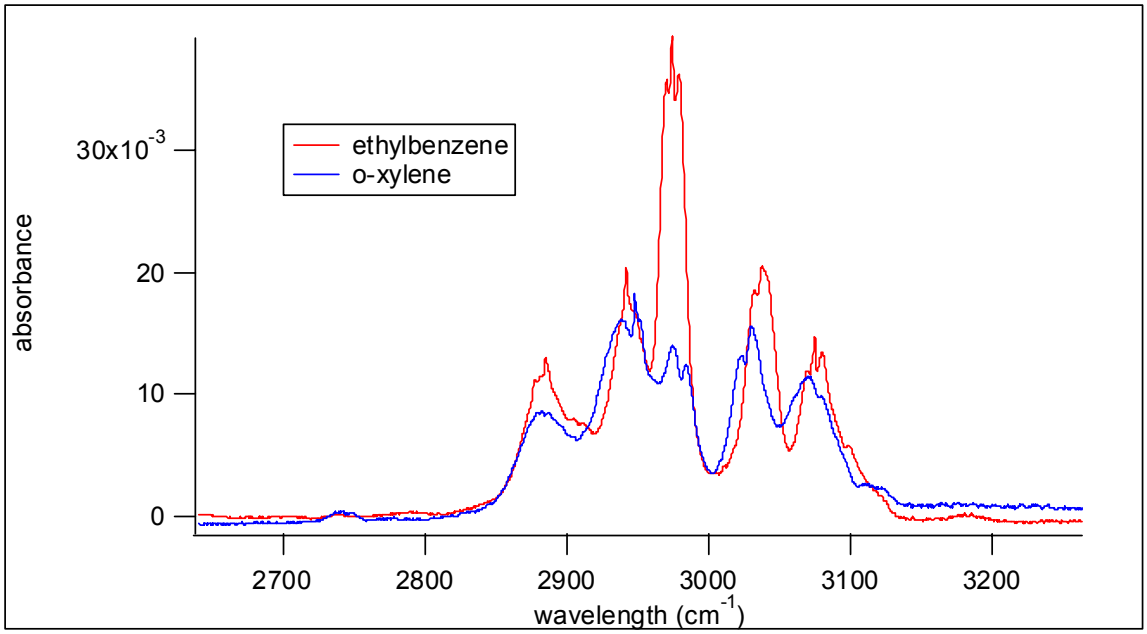
ethylbenzene
o-xylene
absorbance
30x10-3
20
10
0
2700
2800
2900
3000
3100
3200
wavelength (cm-1)

APPENDIX D

Spectral Surrogates

SPECTRAL SURROGATES

This surrogate chemical proposal reduces the number of chemicals to 10 from a starting list of 18, which includes the multiple isomers in the TCET list of 14 chemicals. No spectral data was provided for ethyltoluene and hexene, so neither could be grouped. Should these two chemicals be of particular interest to TCET, each would have to be included, raising the total number to twelve chemicals.

Two lists, one for the CO2 laser and a second for the PPLN laser and the PAT technology are included because several of the chemicals are below reasonable detection range at the higher wavenumbers of the CO2 laser (e.g. aliphatics). An attempt was made to propose the same surrogate in both CO2 and PPLN laser lists to minimize the number of chemicals. However, these same chemicals are surrogates for different other chemicals with each laser technology because of the different absorption characteristics of chemicals in the respective wavenumber ranges (e.g. propylene is a surrogate for pentene with the CO2 laser, but not with the PPLN laser).

Overlapping of the test matrix for all three technologies could be done with propylene, o-xylene and 1,3-butadiene. Further overlapping of the tests could also be performed on 1-butene and m-xylene, however, this would be duplicating data on the PPLN and PAT technologies that is generated using propylene and o-xylene. Binary mixtures that would be commonly found in refinery streams could include propylene and 1-butene for the CO2 laser camera, and propylene and butane for the PPLN laser camera.

LIS (CO2) Laser List

The chemicals listed first are viewed as a suitable surrogate for others listed, preference given to gases over liquids, and less toxic chemicals over more toxic. There appears to be no good surrogates for m-Xylene and Butadiene. Either Toluene or o-Xylene would be a suitable surrogate for the other plus Trimethylbenzene. Either 1 or 2-Butene, or a mixture of both, would be a suitable surrogate for the other plus Isoprene.

1. CO2 Laser wavenumber ranges (regions within which the chemicals must absorb most strongly). The CO2 Laser produces a beam with these four wavenumber ranges simultaneously.
    i. 930-953
    ii. 970-985
    iii. 1031-1055
    iv. 1073-1081
2. Surrogate Groups (relative absorption) @ wavenumbers within the CO2 laser ranges
    i. Propylene (.009) for 1-Pentene(.008) and 2-Pentene(.009) @ 940/931/972
    ii. O-Xylene(.004) for Toluene(.005) and Trimethylbenzene(.004) @ 1054/1034/1032
    iii. 1-Butene(.004) for 2-Butene(.004) and Isoprene(.005) @ 979/976/985
    iv. m-Xylene(.001) @ 1043
    v. 1,3-Butadiene(.003) @ 977

SNL (PPLN) Laser List also applicable to the PAT technology

The chemicals listed first are viewed as suitable surrogates for others listed, preference given go gases over liquids, less toxic chemicals over more toxic, and a similar chemical as recommended on the CO2 Laser list above.

A. PPLN Laser wavenumber ranges (regions within which the chemicals must absorb strongly). The PPLN Laser is somewhat tunable to narrow bands over the range, but produces a beam that varies plus/minus a few wavenumbers within the tuned band.
    a. 2868-3028
    b. best atmospheric window through water vapor is 2960-2969
B. Surrogate Groups (relative absorption) @ wavenumbers within the PPLN laser range
    a. Butane(.081) for Pentane(.096) and n-Hexane(.102) @ 2965
    b. 1-Pentene(.046) for 2-Pentene(.048) and Trimethylbenzene(.05) @ 2971
    c. Propylene(.02) for 1-Butene(.021) and 2-Butene(.019) @ 2954-2947
    d. O-Xylene(.015) for m-Xylene(.017) and p-Xylene(.014) @ 2934-2937
    e. Acetaldehyde(.0039) @ 2868
    f. Formaldehyde(.01 & .02-.03) @ 2868-83 & 2911-12
    g. Isoprene(.015) @ 2977-93
    h. Toluene(.015-.017) @ 3025-28
    i. 1,3-Butadiene(.0058 @ 3002

APPENDIX E

Additional Information on Laboratory Materials and Methods

ADDITIONAL MATERIALS AND METHODS

This appendix contains additional information on the test materials and methods, including other secondary data collected for each test run, test equipment details, and other quantitative test observations.

Other Collected Data

- Rotameter Outlet Temperature (F): a thermocouple was placed at the rotameter outlet to measure gas temperature. This corresponds to the temperature attained by the first of two heaters used in the delivery system

- Valve Temperature (F): a thermocouple was placed inside the delivery line near the leak component to measure delivery temperature. This corresponds to the temperature attained by the second of two heaters used in the delivery system. For the second week of testing, a thermistor was attached to the exterior of the valve for temperature measurements.

- Background Temperature (F): a thermocouple was placed on either the concrete wallboard or the metal cylinders, depending on which background was being tested at the time. For the second test week, a thermistor was attached to the backgrounds in addition to the thermocouple. The thermistor readings closely track the thermocouple readings across the test runs, and only the thermocouple readings are reported on the electronic data sheet.

- Room Temperature (F): a thermocouple was placed near the leak component but not in the direct path of the fan or the leaked gas. Temperature measurements conducted on August 15 showed that the maximum temperature difference between two points in the lab was 1.4^{o}F.

- Room Humidity (%): the room temperature instrumentation also provided a humidity reading.

- Ambient Pressure (in Hg): a pressure gage was hung near the fan, but outside of the fan's path.

- Date

- Camera Operator

- QA/QC/Data Collection Team Member

- Cylinder paint: background cylinders are empty helium containers with blue paint. Airgas distributed the cylinders but could not provide more information on the paint type.

Equipment

Below is a list of measured parameters and the equipment used to collect data on those parameters.

Delivery Pressure:	Ashcroft model Q8962 0-30 psi and 0-30 in Hg

Wind Speed:	Maximum® Anemometer model BTC (cup anemometer. not used in data collection) Kestrel 2000 digital anemometer
Control Desk Pressure Gages:	Haenni KI16 0-11 bar 0-160 psi Three gages, same model
Gas Outlet Temperature:	Cole Parmer Digisense Thermocouple model 8528-20 Omega SRTD-1 Thermistor
Background Temperature:	Cole Parmer Digisense Thermocouple model 8529-00 Omega SRTD-2 Thermistor
Ambient Temperature and Humidity:	Digital Thermohygrometer
Ambient Pressure:	Taylor pressure gage
Leak rate:	KI 10410 (smaller KI rotameter) KI 10610 (larger KI rotameter) GF 6541 1200 (smaller GF rotameter) GF 6540 1216 (larger GF rotameter)
Light Intensity:	Sekonic Light Meter

Additional Test Observations

Test Conditions Charts: The exhibits below show changes in ambient room temperature and humidity as well as changes in background temperatures for the two test weeks.

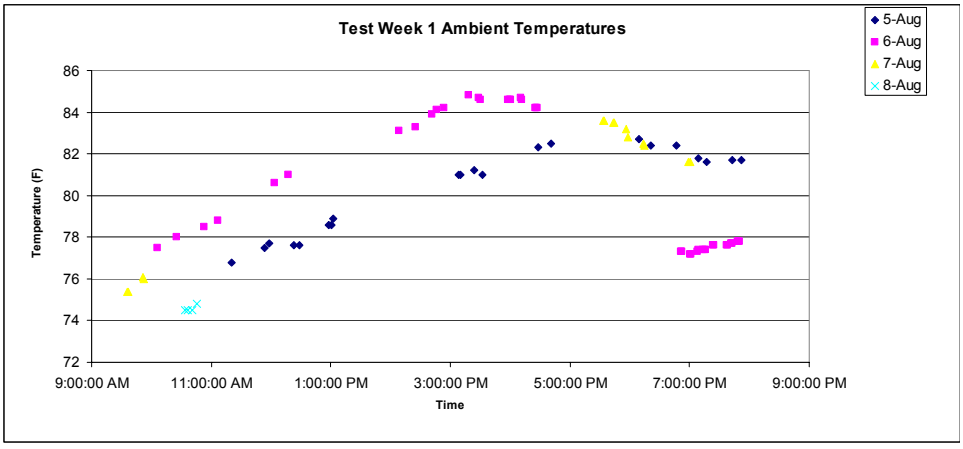

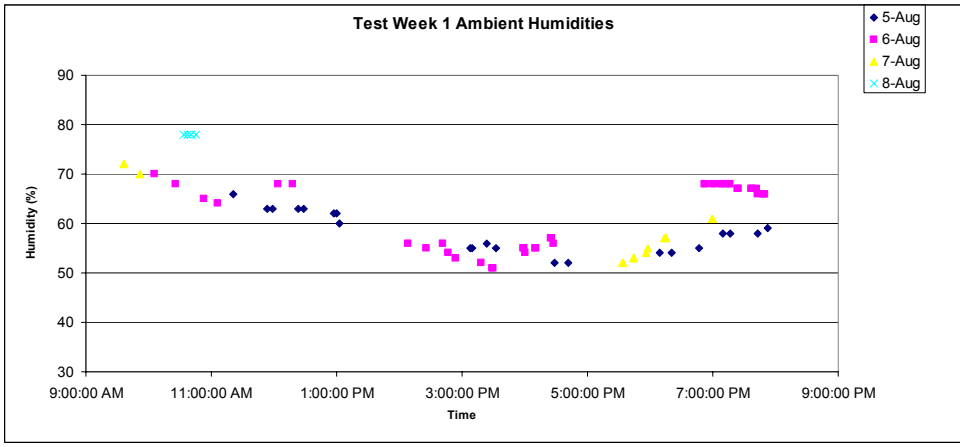
Test Week 1 Ambient Humidities
5-Aug
6-Aug
7-Aug
8-Aug
90
80
70
60
50
40
30
Humidity (%)
9:00:00 AM
11:00:00 AM
1:00:00 PM
3:00:00 PM
5:00:00 PM
7:00:00 PM
9:00:00 PM
Time

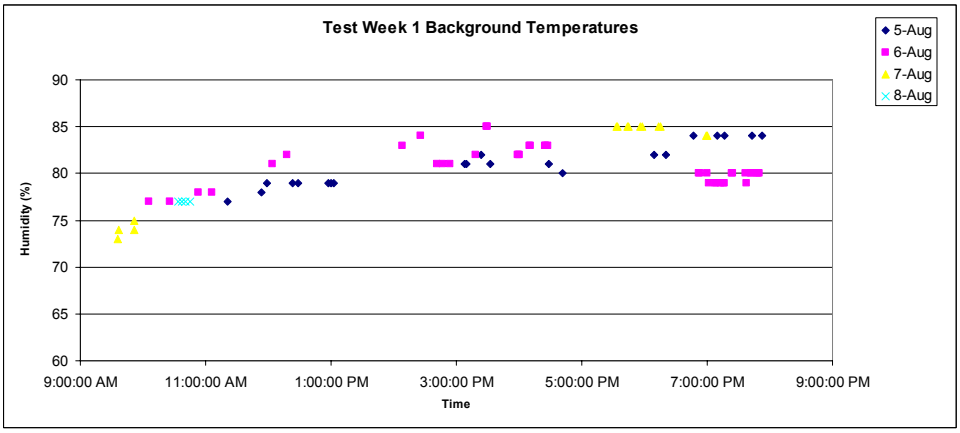
Test Week 1 Background Temperatures
5-Aug
6-Aug
7-Aug
8-Aug
90
85
80
75
70
65
60
Humidity (%)
9:00:00 AM
11:00:00 AM
1:00:00 PM
3:00:00 PM
5:00:00 PM
7:00:00 PM
9:00:00 PM
Time

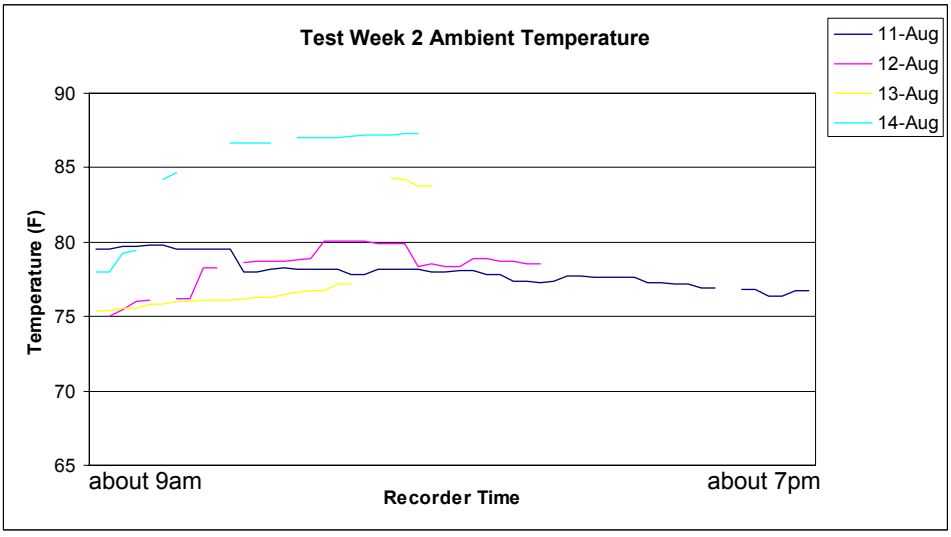
Test Week 2 Ambient Temperature
11-Aug
12-Aug
13-Aug
14-Aug
90
85
80
75
70
65
Temperature (F)
about 9am
about 7pm
Recorder Time

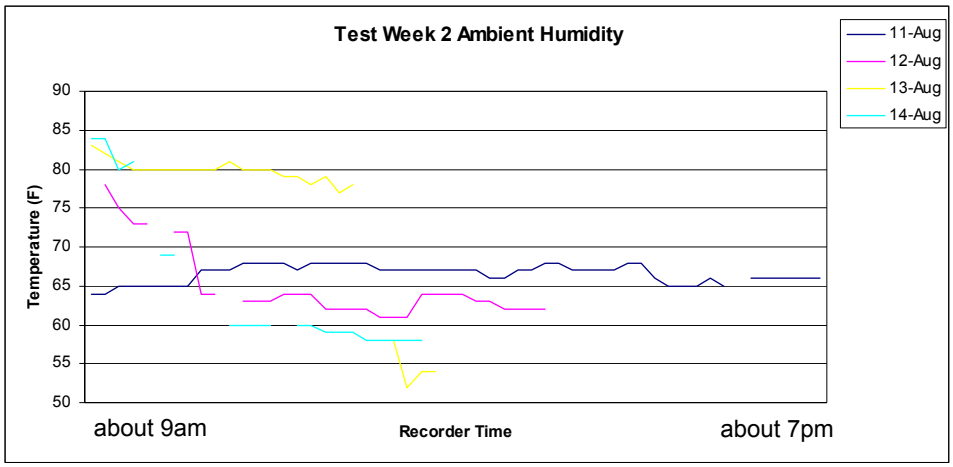
Test Week 2 Ambient Humidity
11-Aug
12-Aug
13-Aug
14-Aug
90
85
80
75
70
65
60
55
50
Temperature (F)
about 9am
Recorder Time
about 7pm

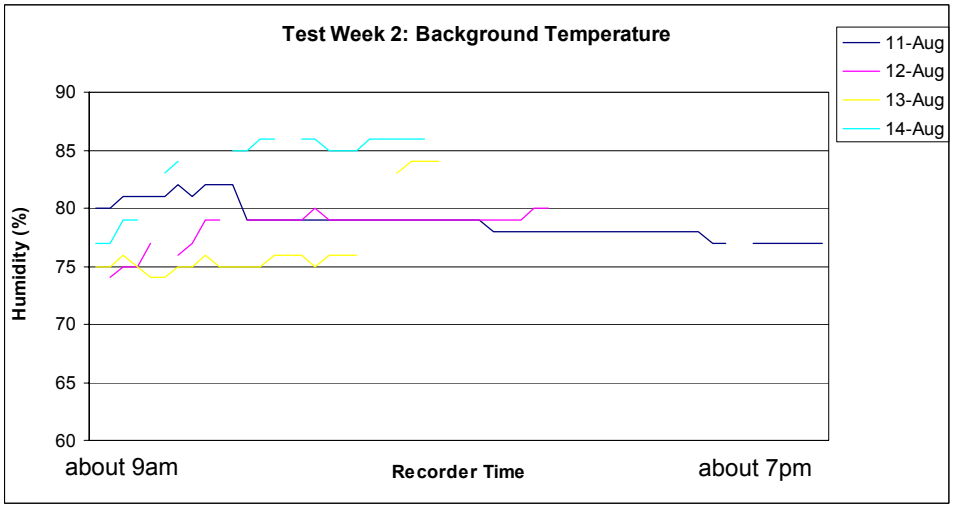
Test Week 2: Background Temperature
11-Aug
12-Aug
13-Aug
14-Aug
90
85
80
75
70
65
60
Humidity (%)
about 9am
Recorder Time
about 7pm

Field of View Measurements:

Two vertical poles were positioned at the edge of each camera's field of view, and the distance between the poles was measured at 10, 20, and 30 feet from the leak component

IMSS Field of View Measurements

10ft	20 inches
20ft	39 inches
30ft	57 inches

Long-wave BAGI Field of View Measurements

10ft	36 inches
20ft	60 inches
30ft	105.5 inches

Mid-wave BAGI Field of View Measurements

10ft	18 inches
20ft	39 inches
30ft	60 inches
10ft zoom	14.5 inches
20ft zoom	30 inches
30ft zoom	47.5 inches

Camera Wavelength Settings:

The long-wave BAGI camera infrared wavelength settings for each chemical are provided below.

ethylene = 10.5321 microns
propylene = 10.7640 microns
1-butene = 10.7640 microns
1,3 butadiene = 10.7640 microns

APPENDIX F

Prediction Models

PREDICTION MODELS

Equation for each camera is of the form

ln(MDL)i= Aij + Bi * Wind Speed + Ci * Distance

where

i	stands for the three cameras (IMSS, Long-Wave BAGI and Mid-Wave BAGI)
j	stands for combination of chemical and background (e.g Propylene - Concrete, Propylene-Metal Cylinders)

distance co-efficients are unique for each camera,

Coefficients and Intercepts from Regressions Analysis

Note Blackened cell indicates insufficient data to predict behavior

Wind Speed Coefficients

Chemical	Background	IMSS	Long-Wave BAGI	Mid-Wave BAGI
Propylene	Concrete	0.27	0.46	-0.02
1,3-Butadiene	Concrete	0.44	0.44	x
Ethylene	Concrete	0.16	0.44	0.20
1-Butene	Concrete	0.41	0.21	0.51
Mixed Xylenes	Concrete	4.65	x	0.00
Butane	Concrete	0.40	x	0.51
Acetaldehyde	Concrete	0.00	x	x
Pentenes	Concrete	0.00	x	x
Propylene No Heated Lines	Concrete	x	x	x
o-Xylene	Concrete	x	x	x
m-Xylene	Concrete	x	x	x
Isoprene	Concrete	0.00	x	0.44
Propylene	Metal Cylinders	0.27	0.46	-0.02
1,3-Butadiene	Metal Cylinders	0.44	0.44	x
Ethylene	Metal Cylinders	0.16	0.44	0.20
1-Butene	Metal Cylinders	0.41	0.21	0.51
Mixed Xylenes	Metal Cylinders	4.65	x	0.00
Butane	Metal Cylinders	0.40	x	0.51
Acetaldehyde	Metal Cylinders	0.00	x	x
Pentenes	Metal Cylinders	0.00	x	x
Propylene No Heated Lines	Metal Cylinders	x	x	x
o-Xylene	Metal Cylinders	x	x	x
m-Xylene	Metal Cylinders	x	x	x
Isoprene	Metal Cylinders	0.00	x	0.44

Distance Coefficients

Chemical	Background	IMSS	Long-Wave BAGI	Mid-Wave BAGI
Propylene	Concrete	0.06	0.04	0.09
1,3-Butadiene	Concrete	0.03	0.04	x
Ethylene	Concrete	0.07	0.06	0.32
1-Butene	Concrete	0.08	0.06	0.11
Mixed Xylenes	Concrete	0.02	x	0.33
Butane	Concrete	0.08	x	-0.08
Acetaldehyde	Concrete	0.24	x	x
Pentenes	Concrete	0.36	x	x
Propylene No Heated Lines	Concrete	x	x	x
o-Xylene	Concrete	x	x	x
m-Xylene	Concrete	x	x	x
Isoprene	Concrete	0.37	x	0.23
Propylene	Metal Cylinders	0.06	0.04	0.09
1,3-Butadiene	Metal Cylinders	0.03	0.04	x
Ethylene	Metal Cylinders	0.07	0.06	0.32

R-Square Values for each Camera and Chemical

Chemical		IMSS	Long-Wave BAGI	Mid-Wave BAGI
Propylene		0.9897	0.9960	0.9149
1,3-Butadiene		0.9994	0.9978	
Ethylene		0.9995	0.9920	0.9899
1-Butene		0.9937	0.9941	0.9772
Mixed Xylenes				
Butane		0.9918		0.6867
Acetaldehyde				
Pentenes				
Propylene No Heated Lines				
o-Xylene				
m-Xylene				
Isoprene				
Mixed Xylenes	Concrete			
Butane	Concrete	1.42		0.74
Acetaldehyde	Concrete			
Pentenes	Concrete			
Propylene No Heated Lines	Concrete			
o-Xylene	Concrete			
m-Xylene	Concrete			
Isoprene	Concrete			
Propylene	Metal Cylinders	2.16	3.48	1.57
1,3-Butadiene	Metal Cylinders	3.76	3.12	
Ethylene	Metal Cylinders	2.90	2.04	
1-Butene	Metal Cylinders	1.29	3.98	1.07
Mixed Xylenes	Metal Cylinders			
Butane	Metal Cylinders	0.80		1.52
Acetaldehyde	Metal Cylinders			
Pentenes	Metal Cylinders			
Propylene No Heated Lines	Metal Cylinders			
o-Xylene	Metal Cylinders			
m-Xylene	Metal Cylinders			
Isoprene	Metal Cylinders			

APPENDIX G

Model Plots

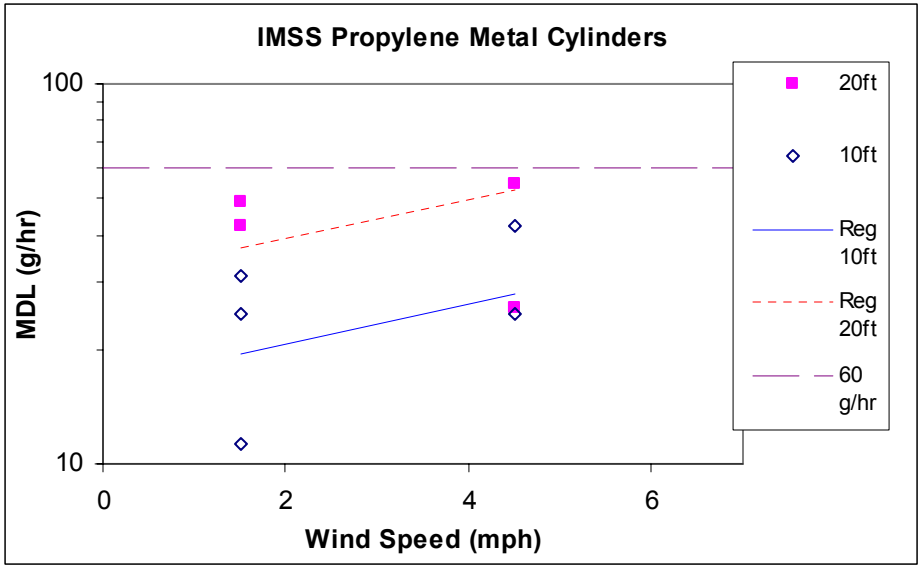
IMSS Propylene Metal Cylinders
100
10
MDL (g/hr)
0
2
4
6
Wind Speed (mph)
20ft
10ft
Reg 10ft
Reg 20ft
60 g/hr

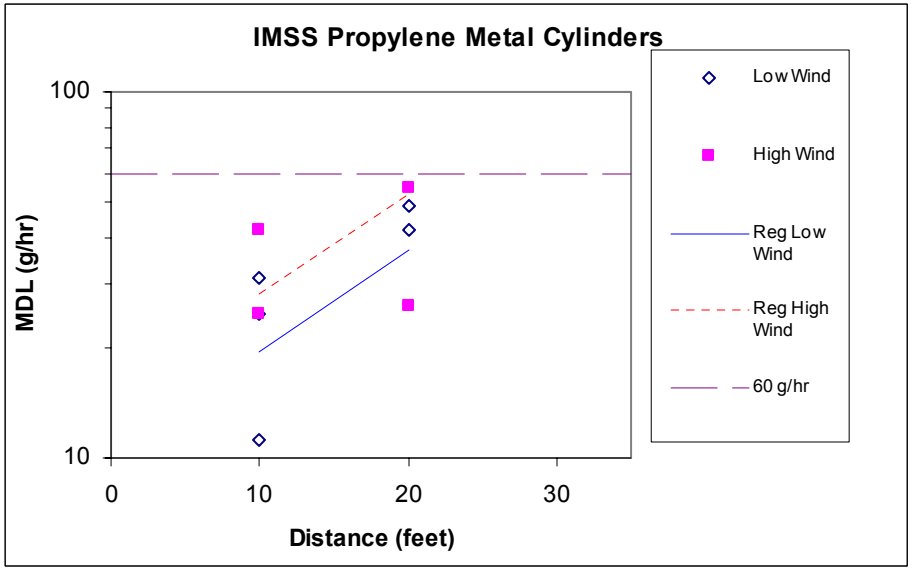
IMSS Propylene Metal Cylinders
100
10
MDL (g/hr)
0
10
20
30
Distance (feet)
Low Wind
High Wind
Reg Low Wind
Reg High Wind
60 g/hr

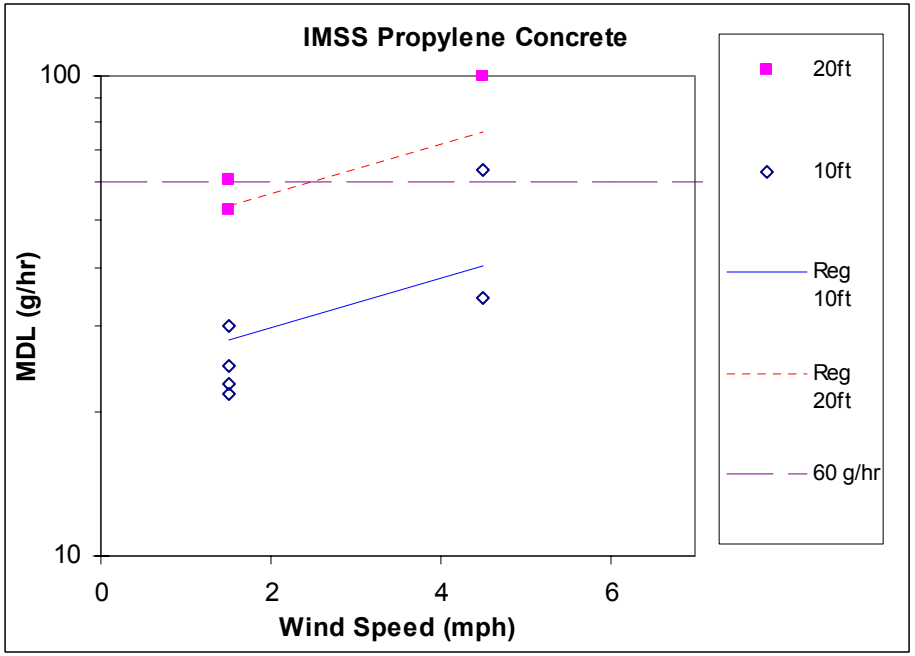
IMSS Propylene Concrete
100
10
MDL (g/hr)
0
2
4
6
Wind Speed (mph)
20ft
10ft
Reg 10ft
Reg 20ft
60 g/hr

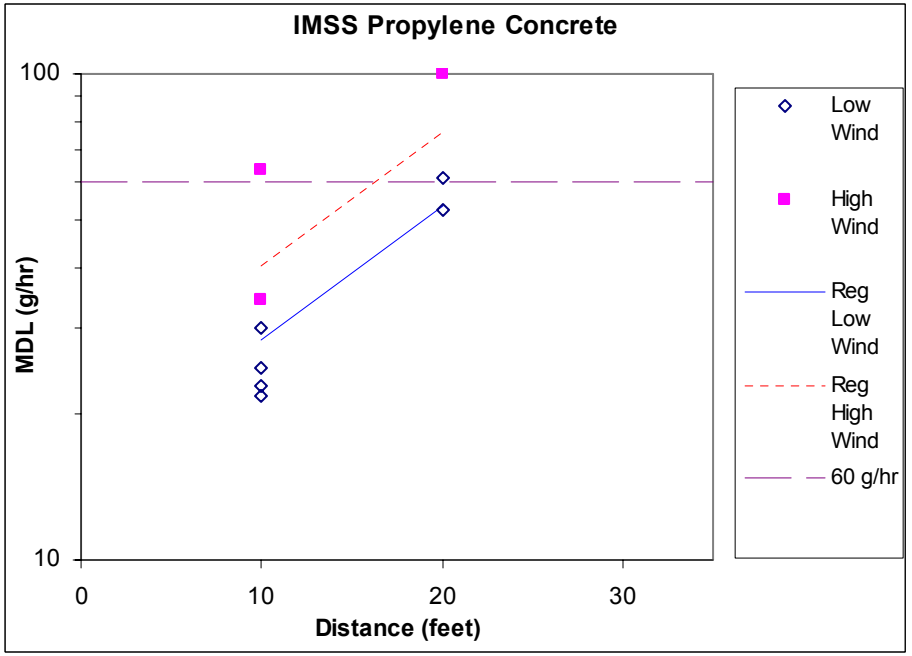
IMSS Propylene Concrete
100
10
MDL (g/hr)
0
10
20
30
Distance (feet)
Low Wind
High Wind
Reg Low Wind
Reg High Wind
60 g/hr

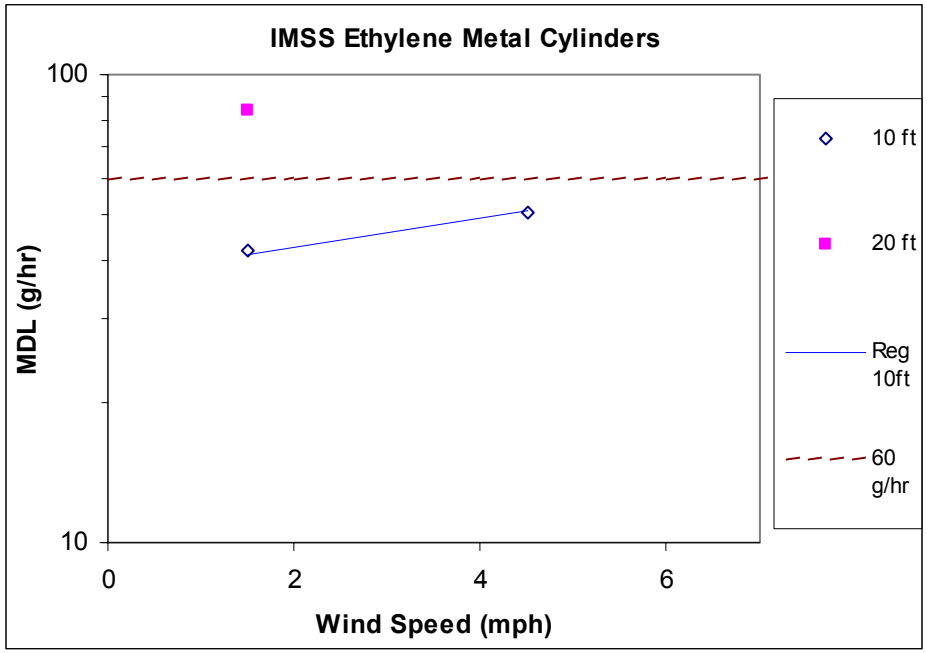
IMSS Ethylene Metal Cylinders
100
10
MDL (g/hr)
0
2
4
6
Wind Speed (mph)
10 ft
20 ft
Reg 10ft
60 g/hr

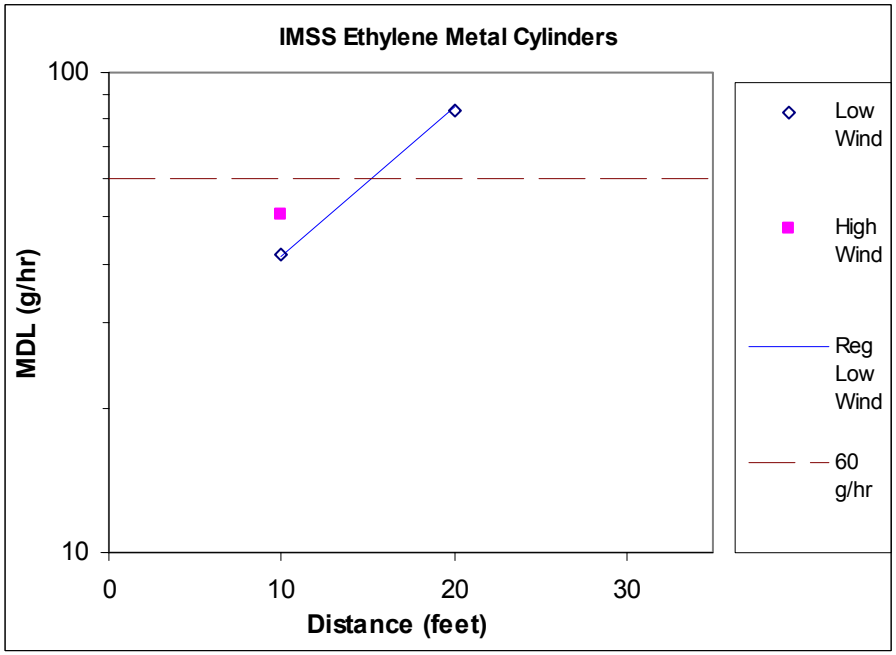
IMSS Ethylene Metal Cylinders
100
10
MDL (g/hr)
0
10
20
30
Distance (feet)
Low Wind
High Wind
Reg Low Wind
60 g/hr

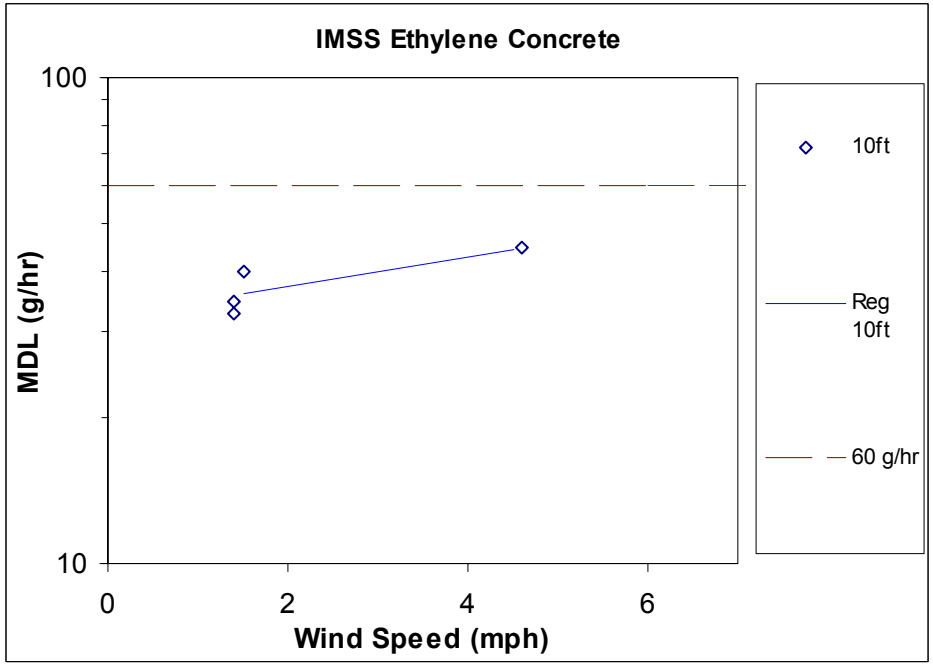
IMSS Ethylene Concrete
100
10
MDL (g/hr)
0
2
4
6
Wind Speed (mph)
10ft
Reg 10ft
60 g/hr

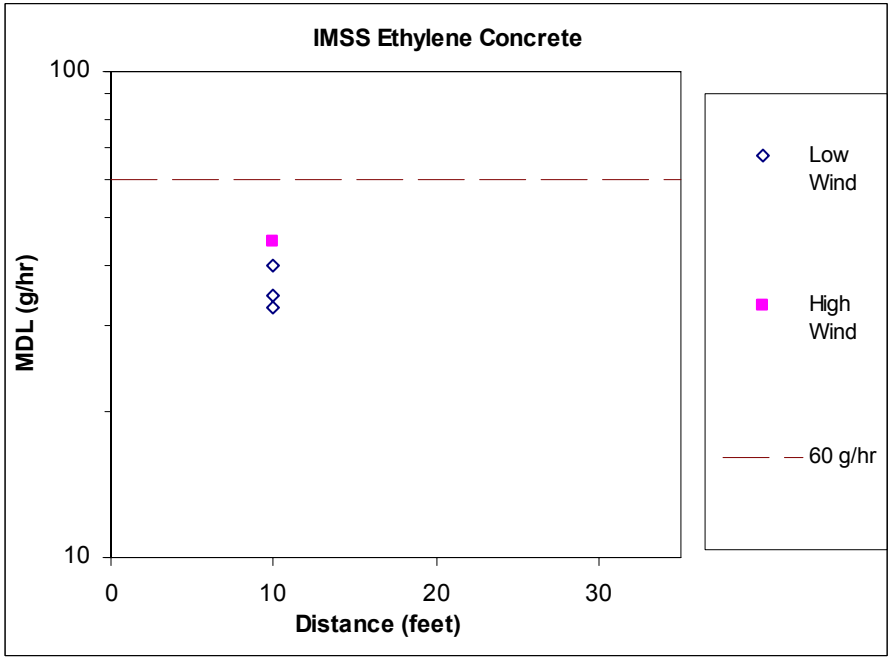
IMSS Ethylene Concrete
100
10
MDL (g/hr)
0
10
20
30
Distance (feet)
Low Wind
High Wind
60 g/hr

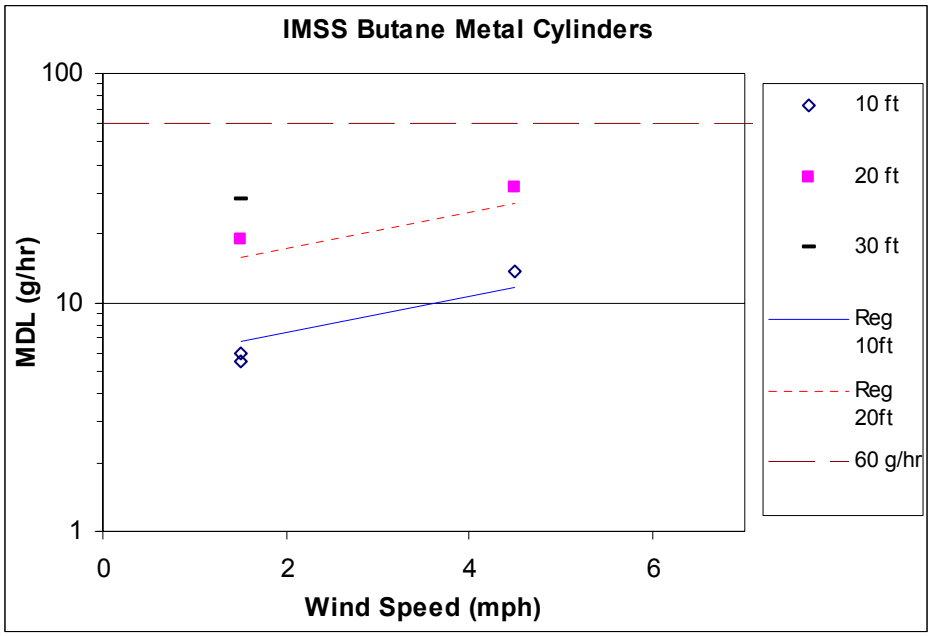
IMSS Butane Metal Cylinders
100
10
1
MDL (g/hr)
0
2
4
6
Wind Speed (mph)
10 ft
20 ft
30 ft
Reg 10ft
Reg 20ft
60 g/hr

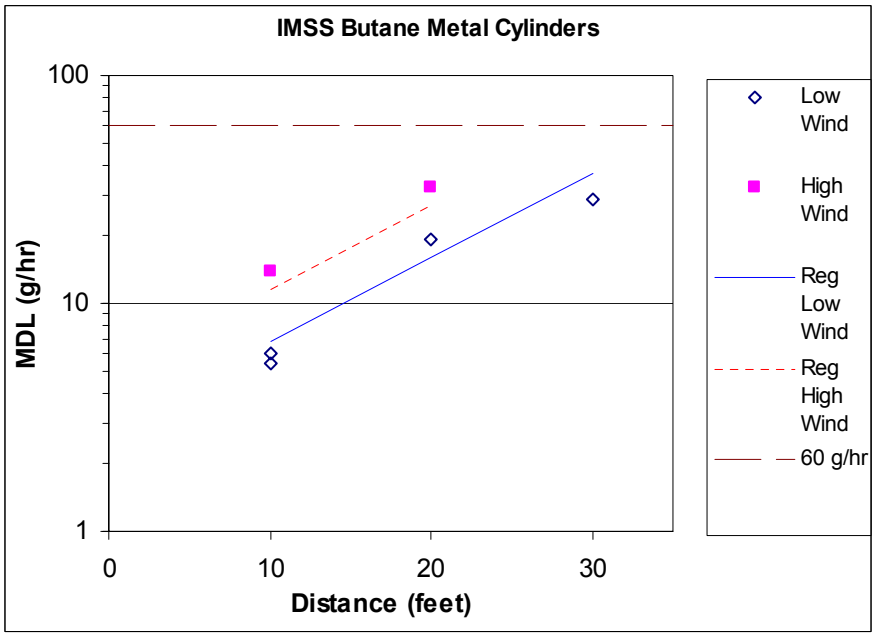
IMSS Butane Metal Cylinders
100
10
1
MDL (g/hr)
0
10
20
30
Distance (feet)
Low Wind
High Wind
Reg Low Wind
Reg High Wind
60 g/hr

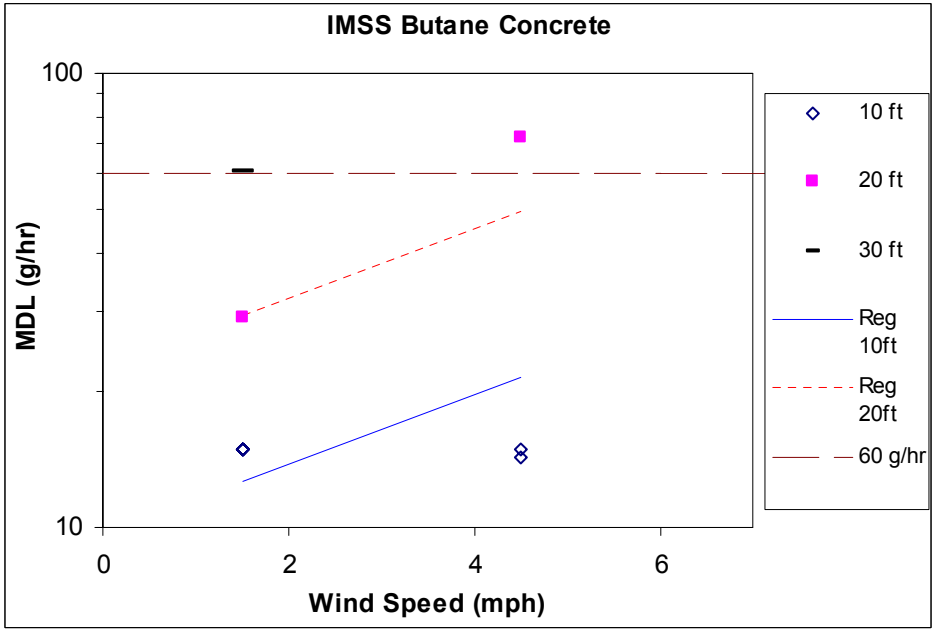
IMSS Butane Concrete
100
10
MDL (g/hr)
0
2
4
6
Wind Speed (mph)
10 ft
20 ft
30 ft
Reg 10ft
Reg 20ft
60 g/hr

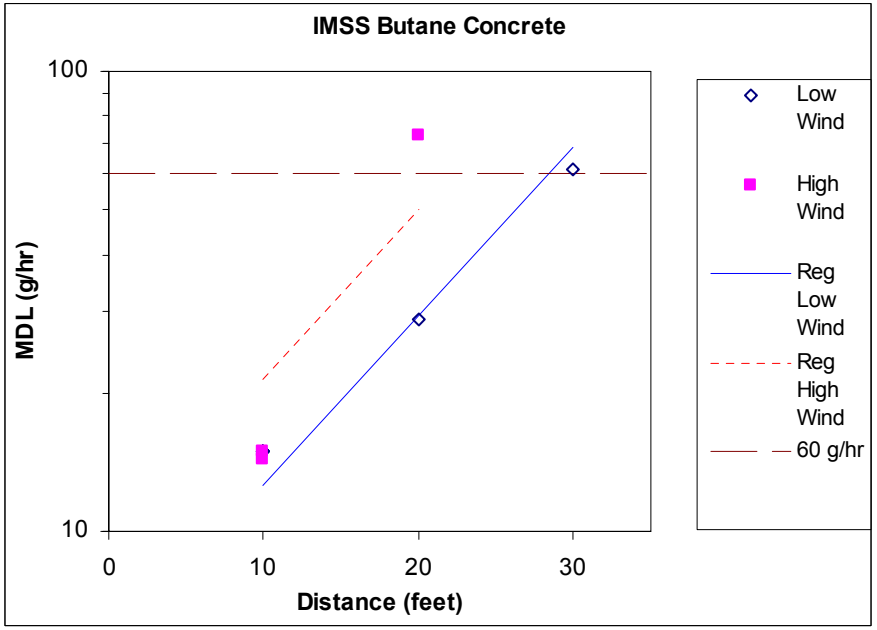
IMSS Butane Concrete
100
10
MDL (g/hr)
0
10
20
30
Distance (feet)
Low Wind
High Wind
Reg Low Wind
Reg High Wind
60 g/hr

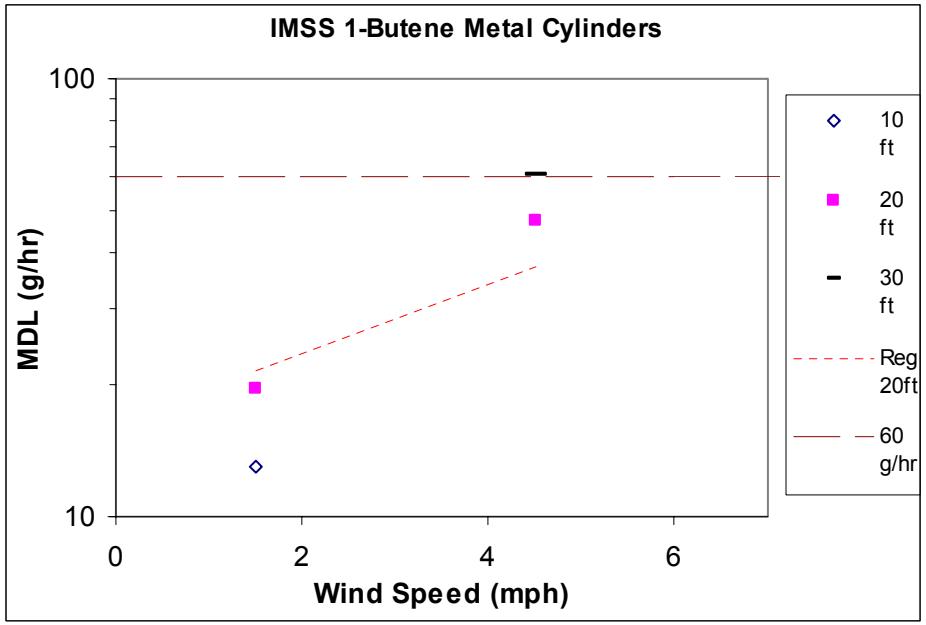
IMSS 1-Butene Metal Cylinders
100
10
MDL (g/hr)
0
2
4
6
Wind Speed (mph)
10 ft
20 ft
30 ft
Reg 20ft
60 g/hr

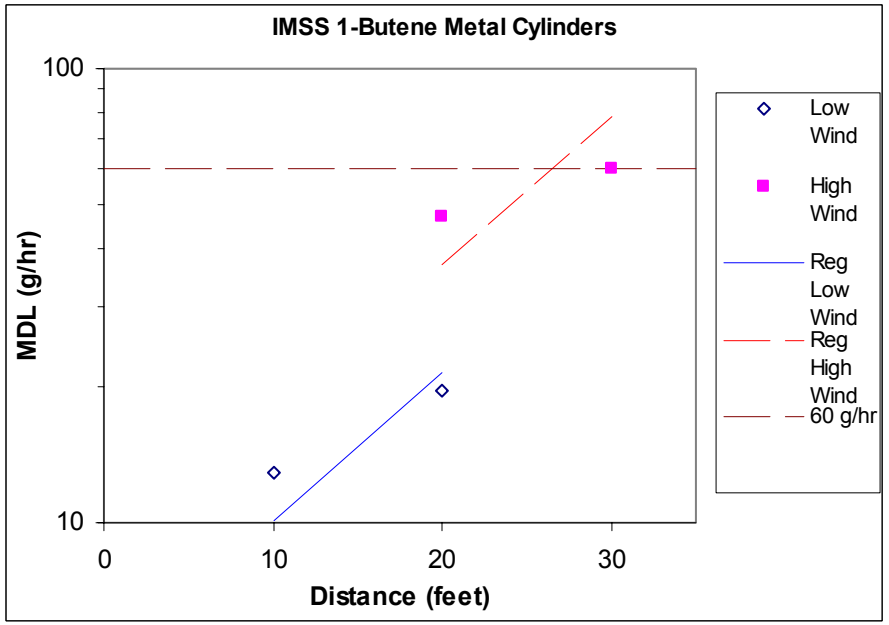
IMSS 1-Butene Metal Cylinders
100
10
MDL (g/hr)
0
10
20
30
Distance (feet)
Low Wind
High Wind
Reg Low Wind
Reg High Wind
60 g/hr

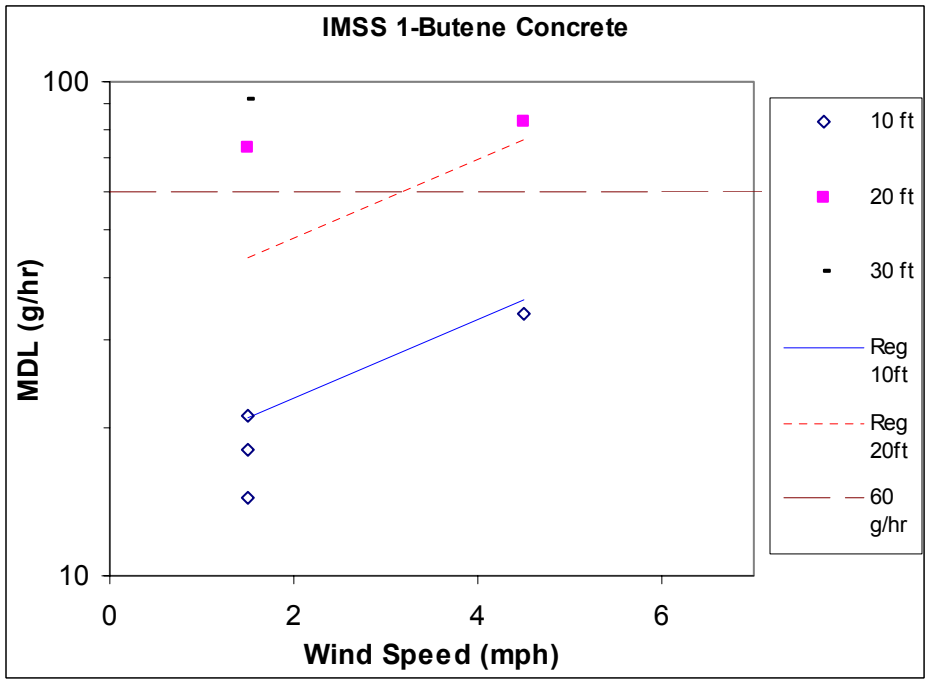
IMSS 1-Butene Concrete
100
10
MDL (g/hr)
0
2
4
6
Wind Speed (mph)
10 ft
20 ft
30 ft
Reg 10ft
Reg 20ft
60 g/hr

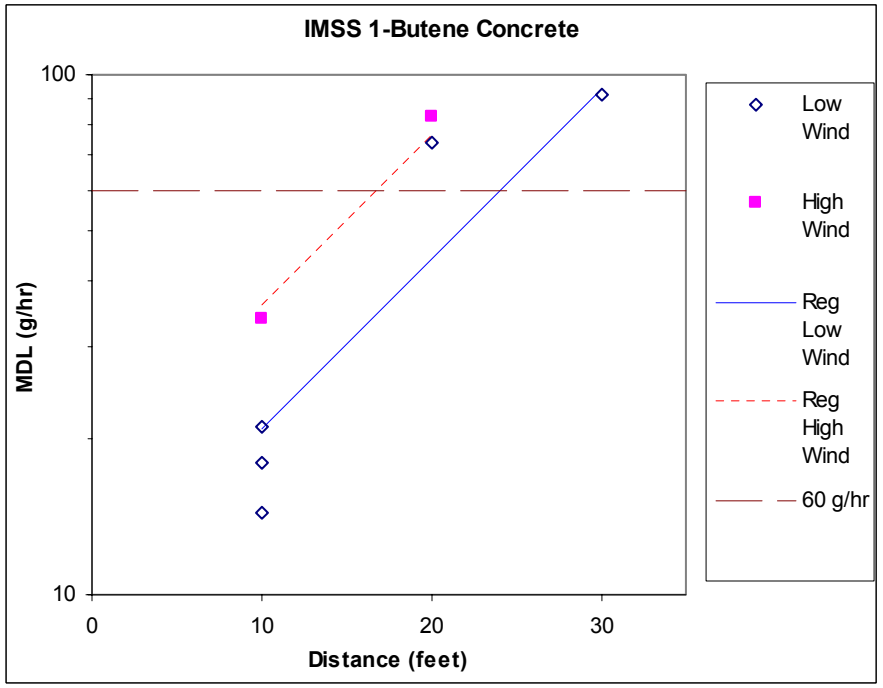
IMSS 1-Butene Concrete
100
10
MDL (g/hr)
0
10
20
30
Distance (feet)
Low Wind
High Wind
Reg Low Wind
Reg High Wind
60 g/hr

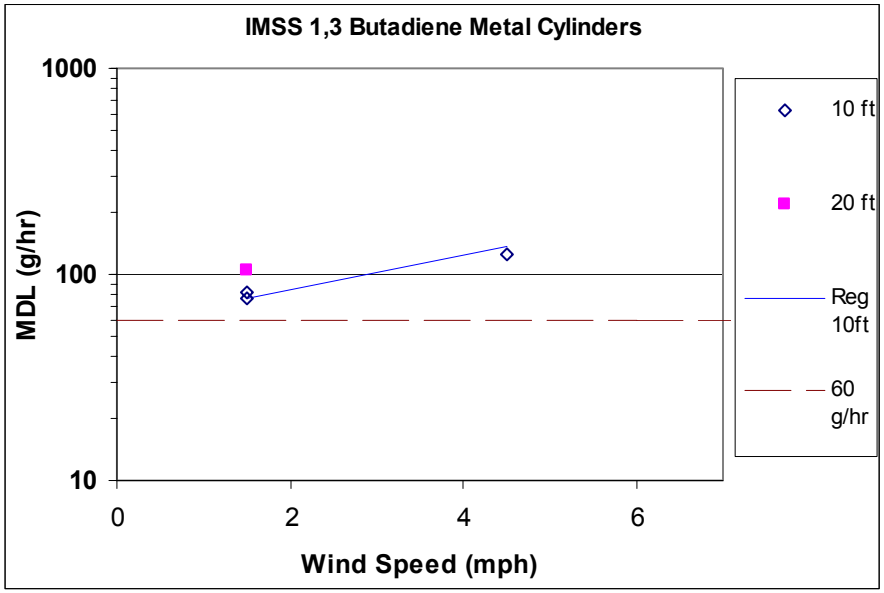
IMSS 1,3 Butadiene Metal Cylinders
1000
100
10
MDL (g/hr)
0
2
4
6
Wind Speed (mph)
10 ft
20 ft
Reg 10ft
60 g/hr

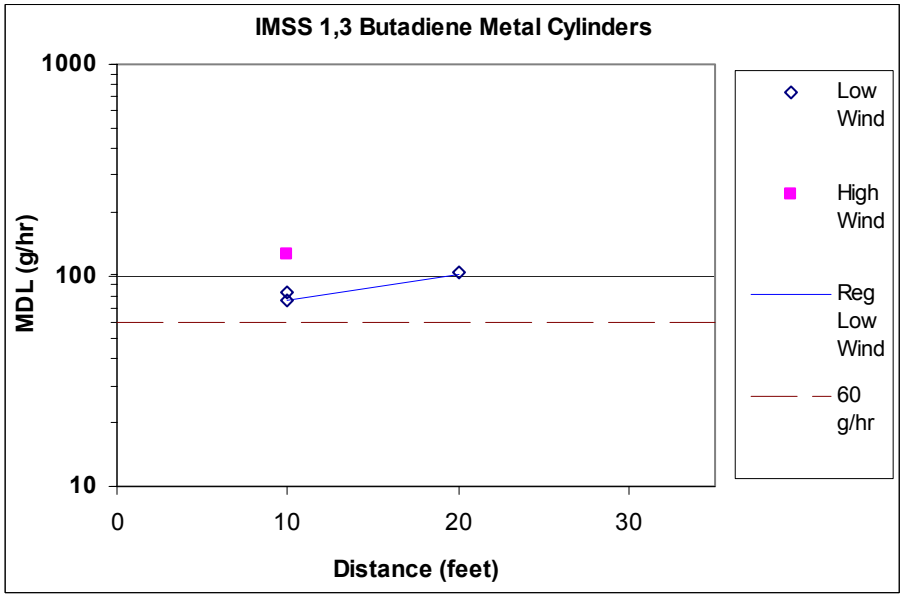
IMSS 1,3 Butadiene Metal Cylinders
1000
100
10
MDL (g/hr)
0
10
20
30
Distance (feet)
Low Wind
High Wind
Reg Low Wind
60 g/hr

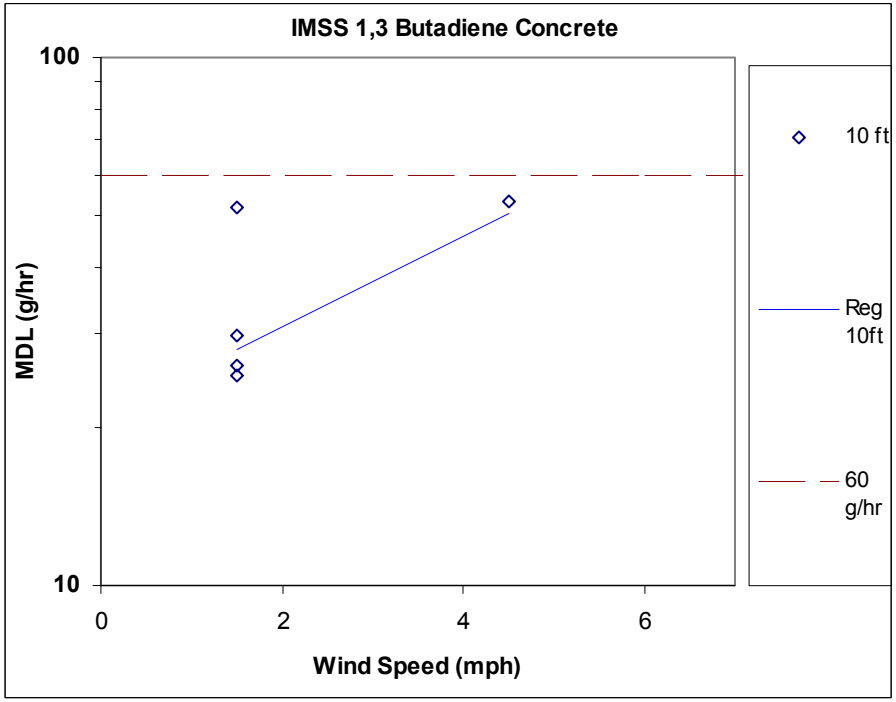
IMSS 1,3 Butadiene Concrete
100
10
MDL (g/hr)
0
2
4
6
Wind Speed (mph)
10 ft
Reg 10ft
60 g/hr

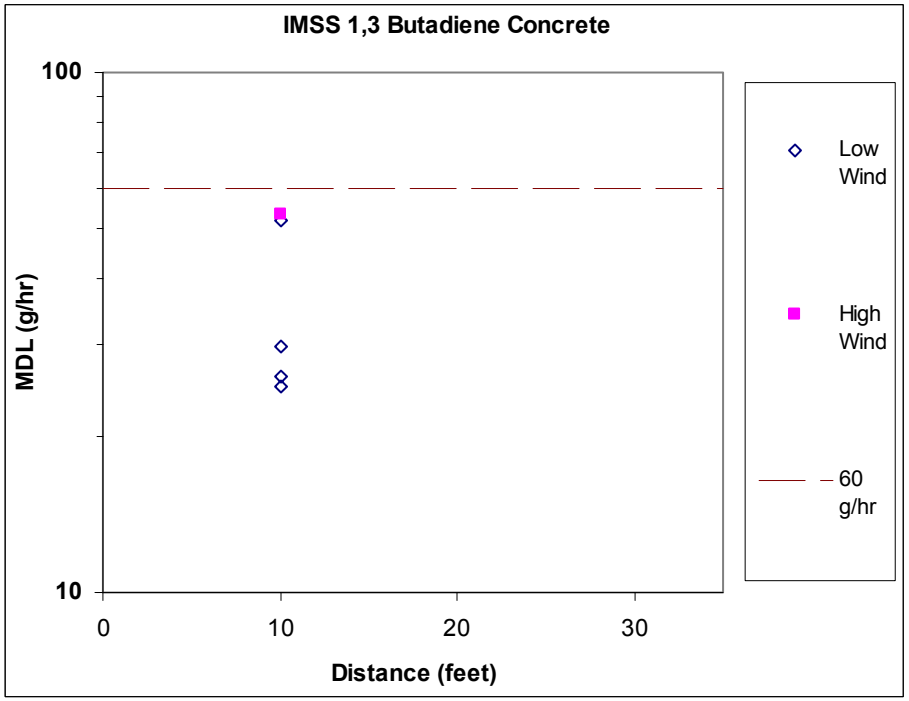
IMSS 1,3 Butadiene Concrete
100
10
MDL (g/hr)
0
10
20
30
Distance (feet)
Low Wind
High Wind
60 g/hr

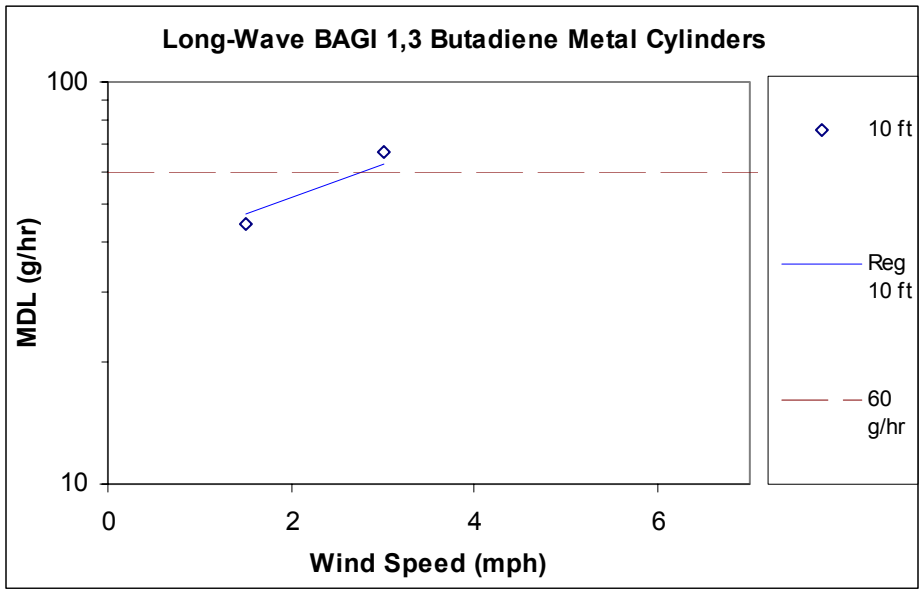
Long-Wave BAGI 1,3 Butadiene Metal Cylinders
100
10
MDL (g/hr)
0
2
4
6
Wind Speed (mph)
10 ft
Reg 10 ft
60 g/hr

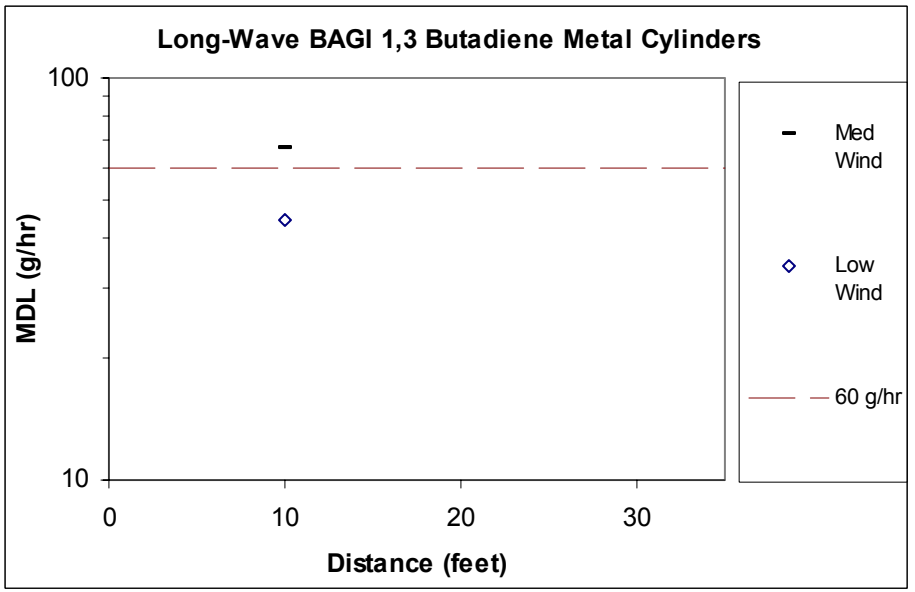
Long-Wave BAGI 1,3 Butadiene Metal Cylinders
100
10
MDL (g/hr)
0
10
20
30
Distance (feet)
Med Wind
Low Wind
60 g/hr

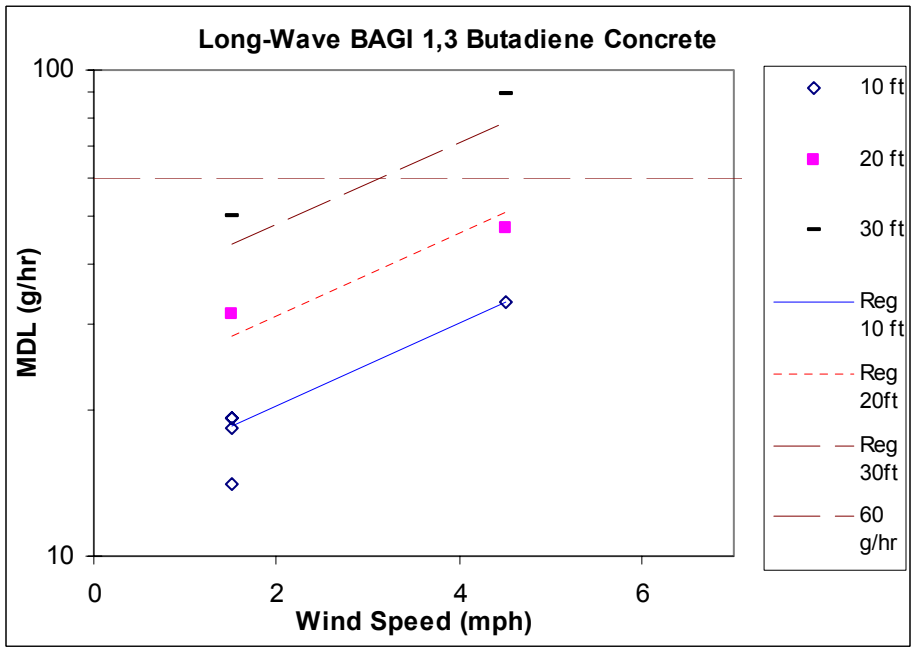
Long-Wave BAGI 1,3 Butadiene Concrete
100
10
MDL (g/hr)
0
2
4
6
Wind Speed (mph)
10 ft
20 ft
30 ft
Reg 10 ft
Reg 20ft
Reg 30ft
60 g/hr

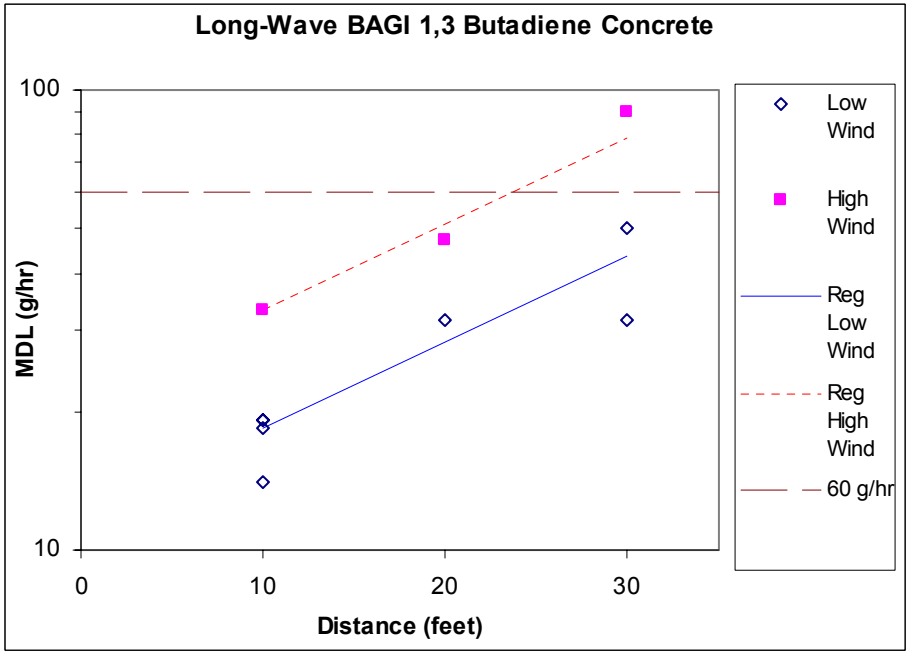
Long-Wave BAGI 1,3 Butadiene Concrete
100
10
MDL (g/hr)
0
10
20
30
Distance (feet)
Low Wind
High Wind
Reg Low Wind
Reg High Wind
60 g/hr

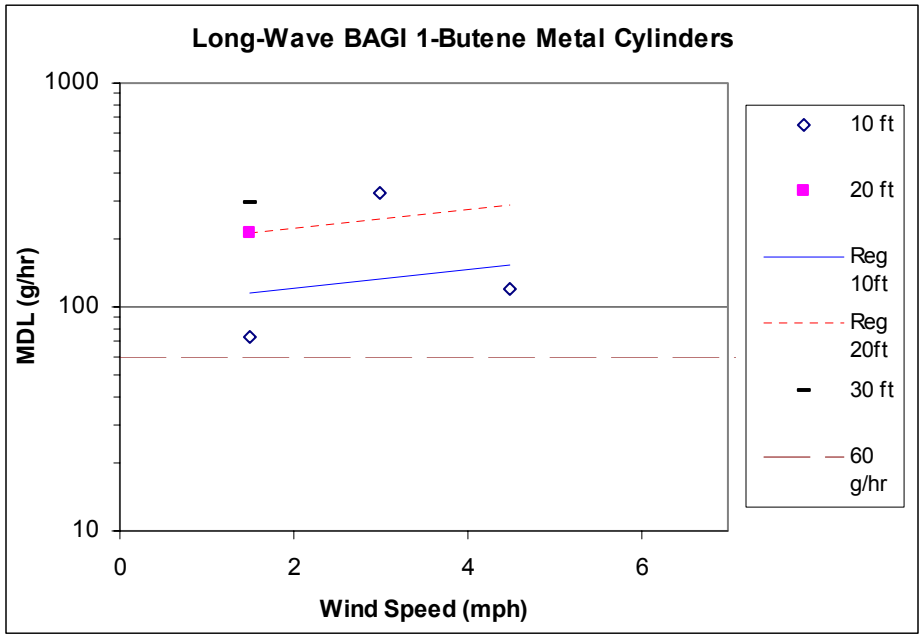
Long-Wave BAGI 1-Butene Metal Cylinders
1000
100
10
MDL (g/hr)
0
2
4
6
Wind Speed (mph)
10 ft
20 ft
Reg 10ft
Reg 20ft
30 ft
60 g/hr

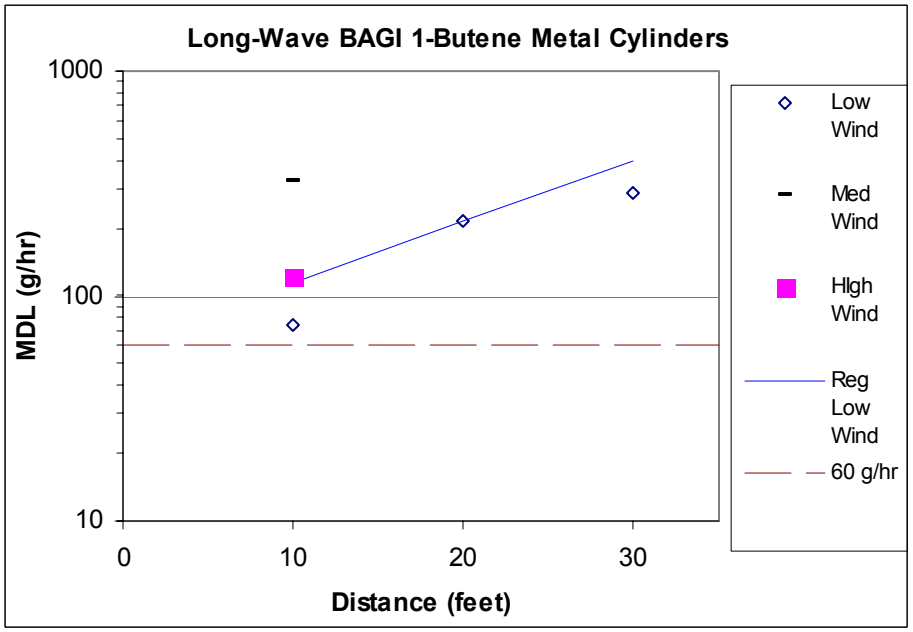
Long-Wave BAGI 1-Butene Metal Cylinders
1000
100
10
MDL (g/hr)
0
10
20
30
Distance (feet)
Low Wind
Med Wind
Hlgh Wind
Reg Low Wind
60 g/hr

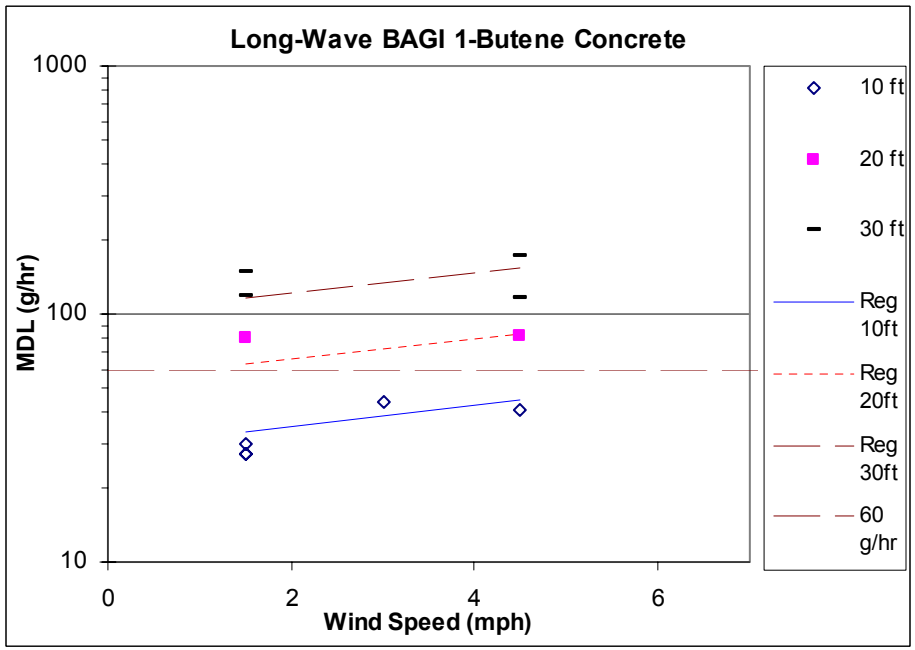
Long-Wave BAGI 1-Butene Concrete
1000
100
10
MDL (g/hr)
0
2
4
6
Wind Speed (mph)
10 ft
20 ft
30 ft
Reg 10ft
Reg 20ft
Reg 30ft
60 g/hr

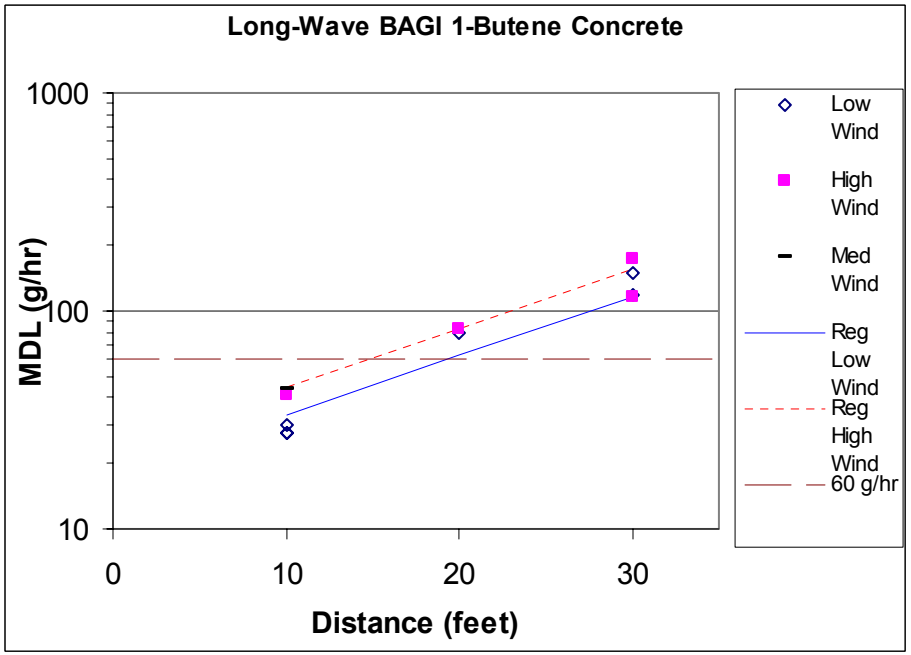
Long-Wave BAGI 1-Butene Concrete
1000
100
10
MDL (g/hr)
0
10
20
30
Distance (feet)
Low Wind
High Wind
Med Wind
Reg Low Wind
Reg High Wind
60 g/hr

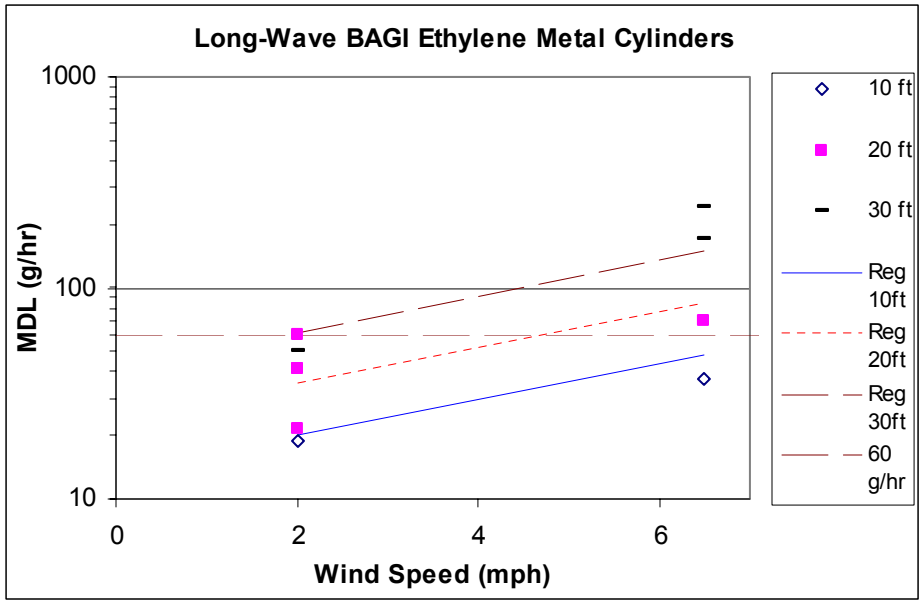
Long-Wave BAGI Ethylene Metal Cylinders
1000
100
10
MDL (g/hr)
0
2
4
6
Wind Speed (mph)
10 ft
20 ft
30 ft
Reg 10ft
Reg 20ft
Reg 30ft
60 g/hr

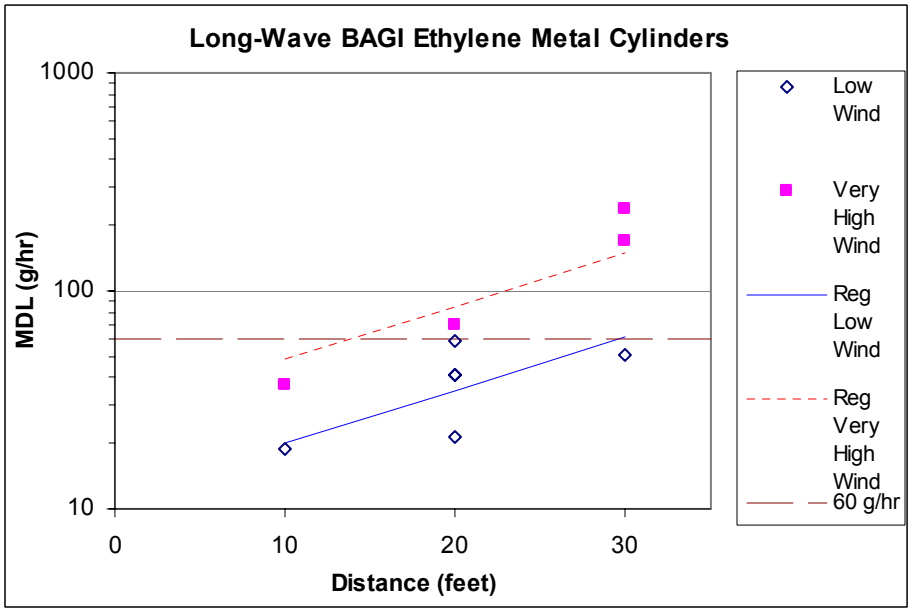
Long-Wave BAGI Ethylene Metal Cylinders
1000
100
10
MDL (g/hr)
0
10
20
30
Distance (feet)
Low Wind
Very High Wind
Reg Low Wind
Reg Very High Wind
60 g/hr

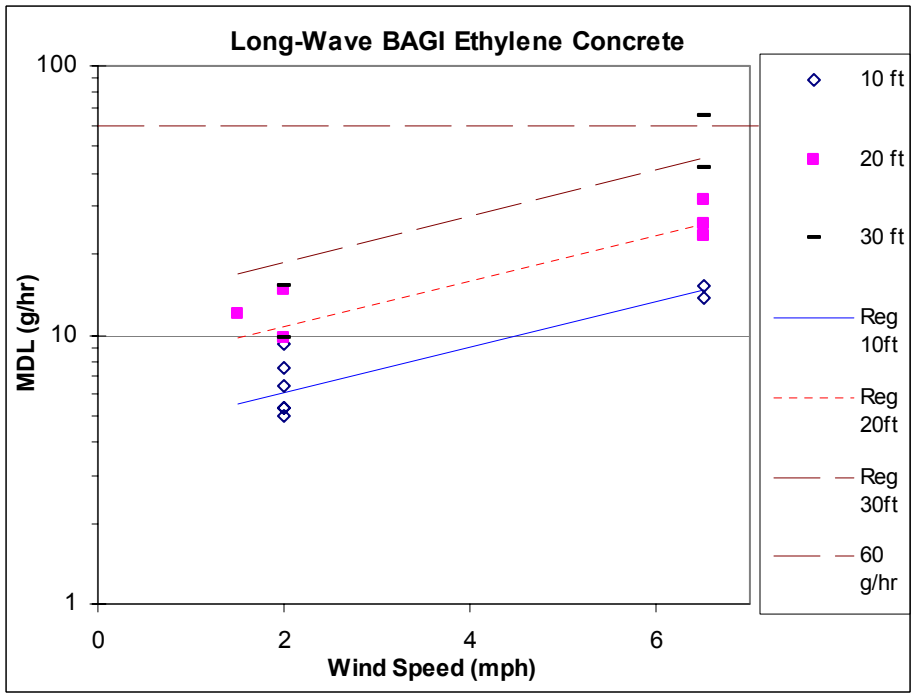
Long-Wave BAGI Ethylene Concrete
100
10
1
MDL (g/hr)
0
2
4
6
Wind Speed (mph)
10 ft
20 ft
30 ft
Reg 10ft
Reg 20ft
Reg 30ft
60 g/hr

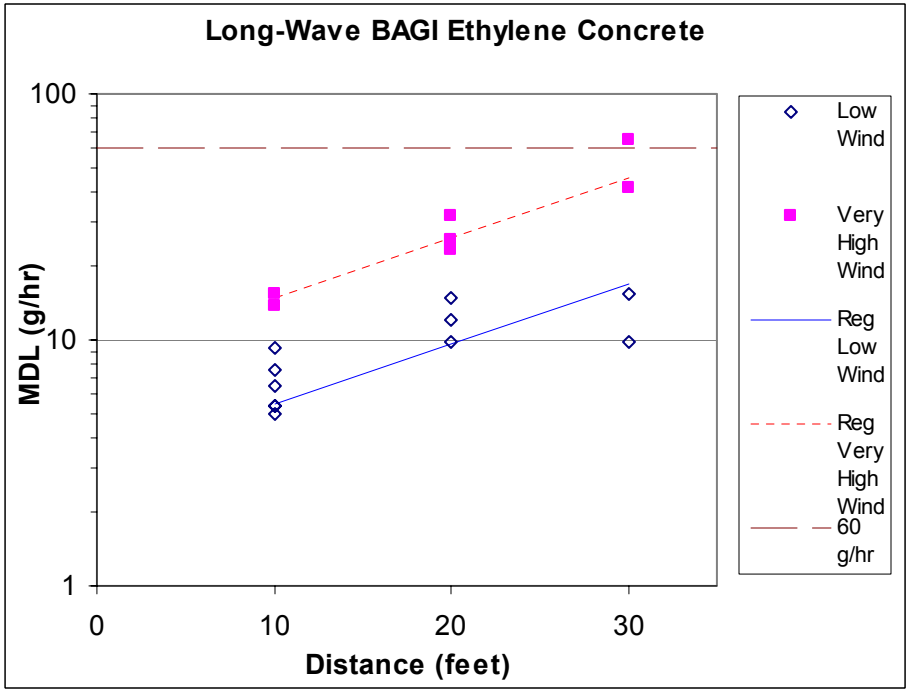
Long-Wave BAGI Ethylene Concrete
100
10
1
MDL (g/hr)
0
10
20
30
Distance (feet)
Low Wind
Very High Wind
Reg Low Wind
Reg Very High Wind
60 g/hr

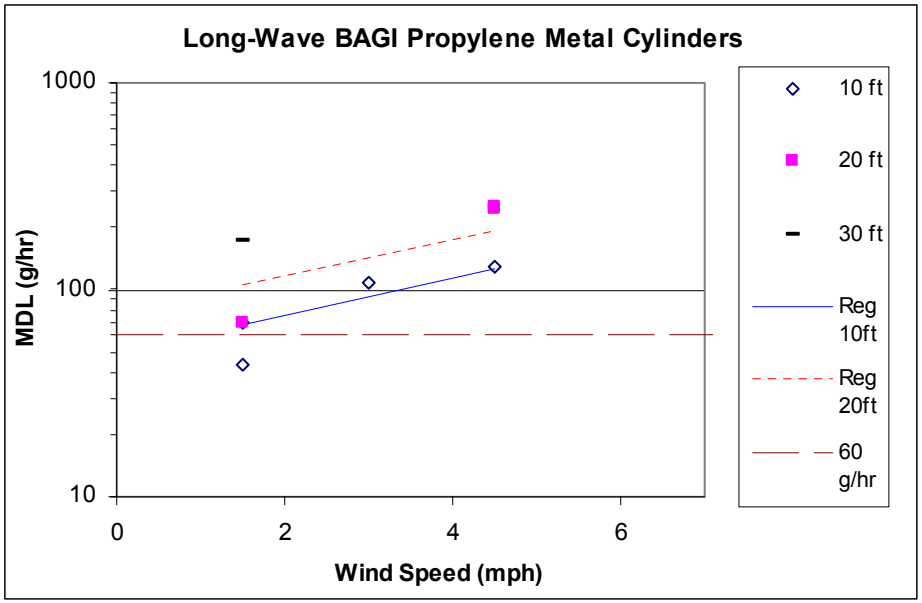
Long-Wave BAGI Propylene Metal Cylinders
MDL (g/hr)
1000
100
10
0
2
4
6
Wind Speed (mph)
10 ft
20 ft
30 ft
Reg 10ft
Reg 20ft
60 g/hr

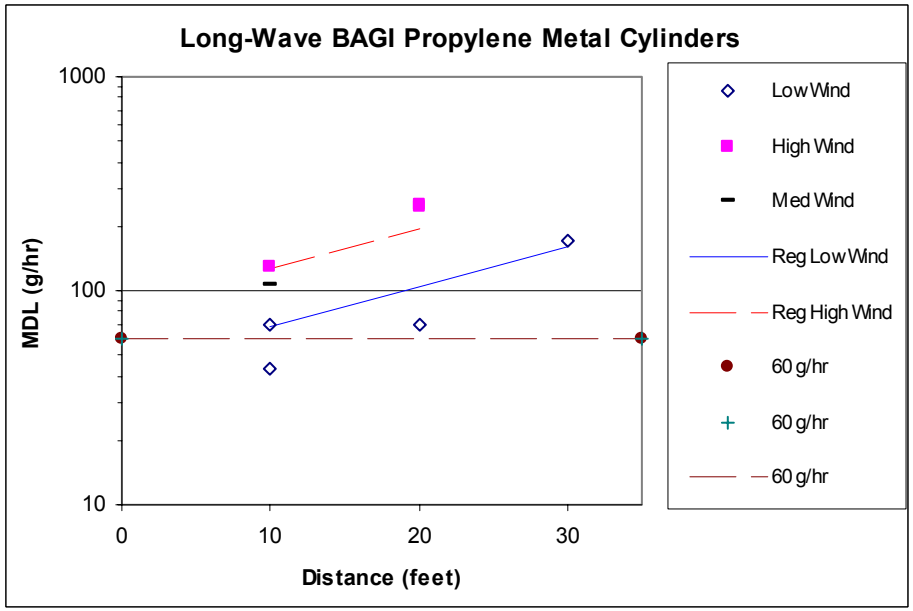
Long-Wave BAGI Propylene Metal Cylinders
MDL (g/hr)
1000
100
10
0
10
20
30
Distance (feet)
Low Wind
High Wind
Med Wind
Reg Low Wind
Reg High Wind
60 g/hr
60 g/hr
60 g/hr

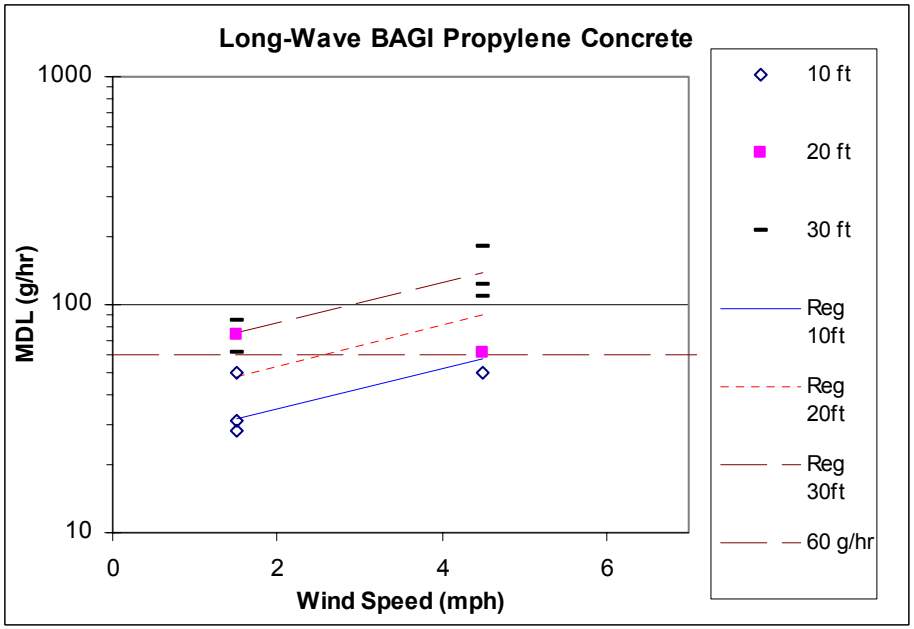
Long-Wave BAGI Propylene Concrete
MDL (g/hr)
1000
100
10
0
2
4
6
Wind Speed (mph)
10 ft
20 ft
30 ft
Reg 10ft
Reg 20ft
Reg 30ft
60 g/hr

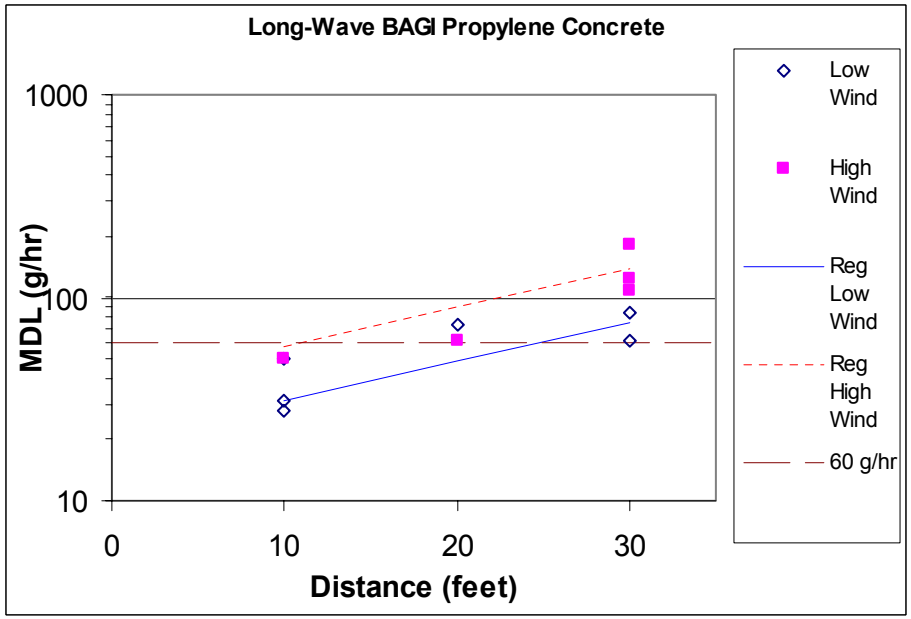
Long-Wave BAGI Propylene Concrete
MDL (g/hr)
1000
100
10
0
10
20
30
Distance (feet)
Low Wind
High Wind
Reg Low Wind
Reg High Wind
60 g/hr

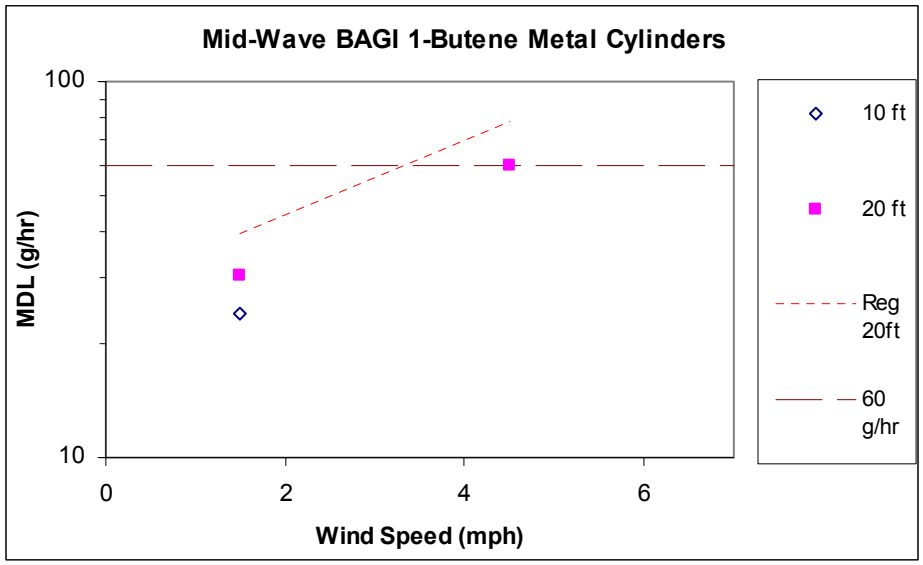
Mid-Wave BAGI 1-Butene Metal Cylinders
100
10
MDL (g/hr)
0
2
4
6
Wind Speed (mph)
10 ft
20 ft
Reg 20ft
60 g/hr

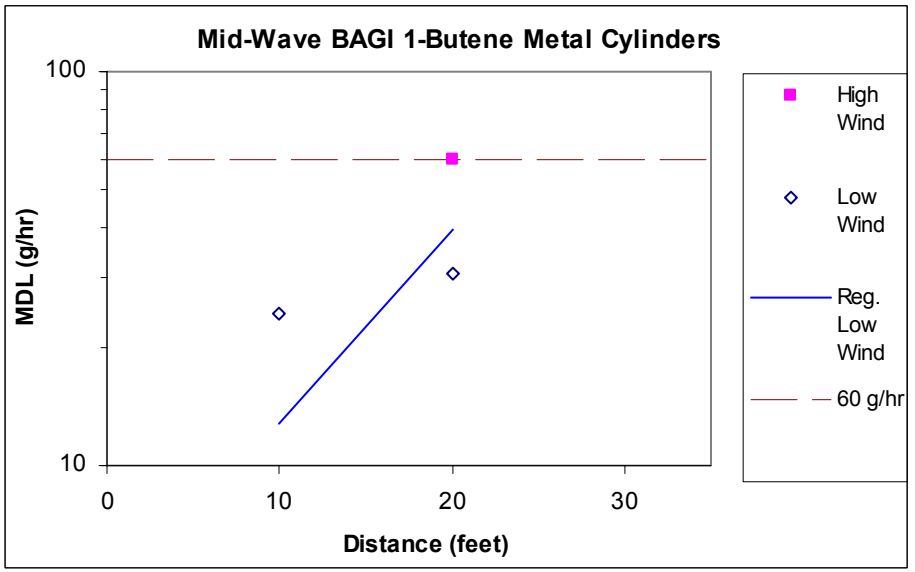
Mid-Wave BAGI 1-Butene Metal Cylinders
100
10
MDL (g/hr)
0
10
20
30
Distance (feet)
High Wind
Low Wind
Reg. Low Wind
60 g/hr

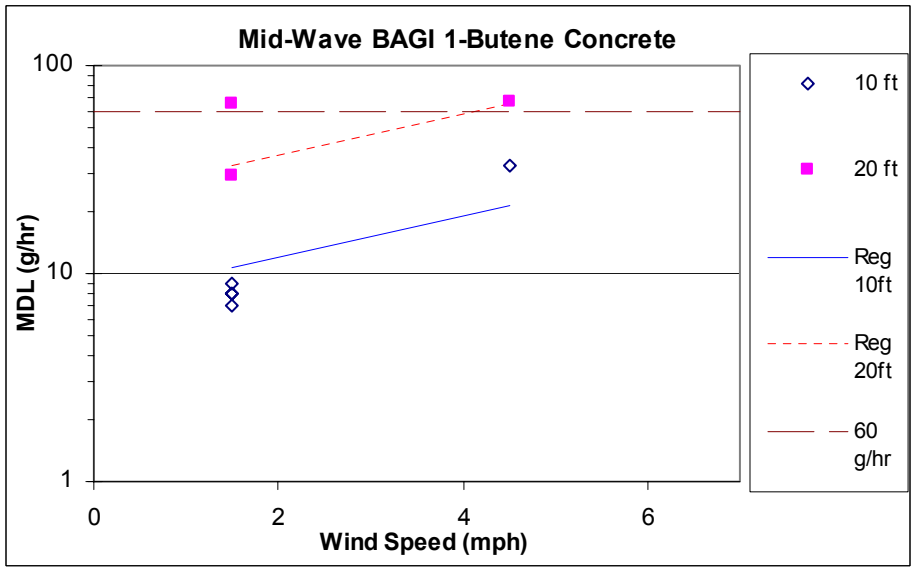
Mid-Wave BAGI 1-Butene Concrete
100
10
1
MDL (g/hr)
0
2
4
6
Wind Speed (mph)
10 ft
20 ft
Reg 10ft
Reg 20ft
60 g/hr

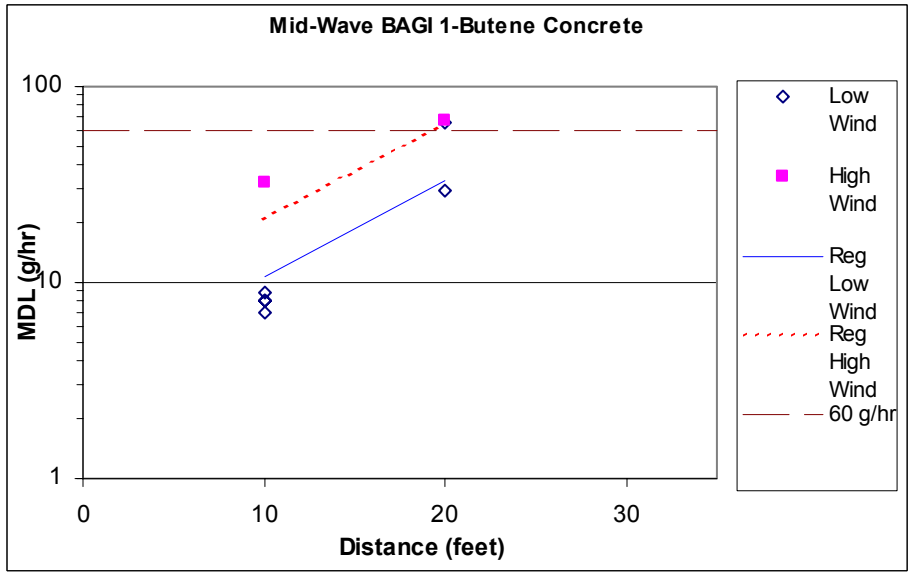
Mid-Wave BAGI 1-Butene Concrete
100
10
1
MDL (g/hr)
0
10
20
30
Distance (feet)
Low Wind
High Wind
Reg Low Wind
Reg High Wind
60 g/hr

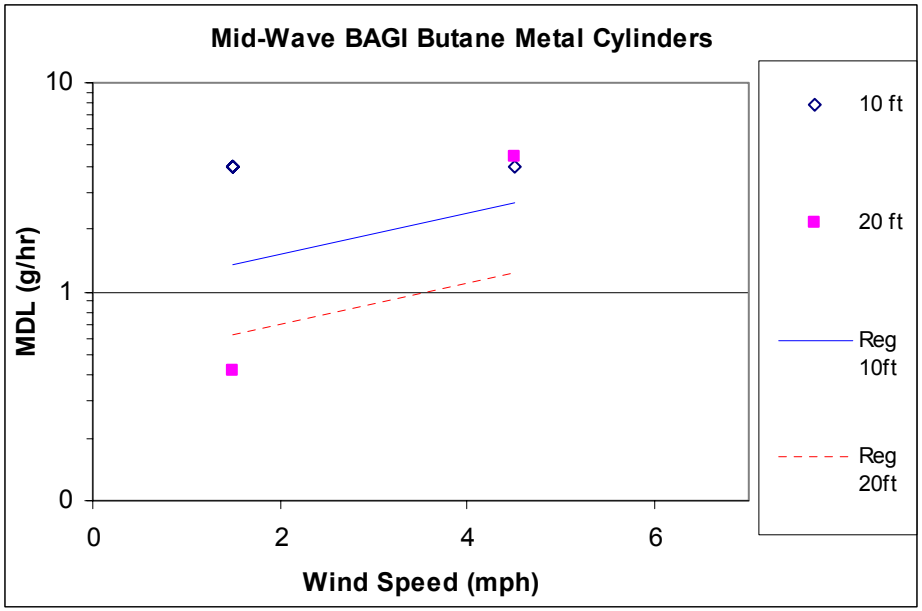
Mid-Wave BAGI Butane Metal Cylinders
MDL (g/hr)
10
1
0
0
2
4
6
Wind Speed (mph)
10 ft
20 ft
Reg 10ft
Reg 20ft

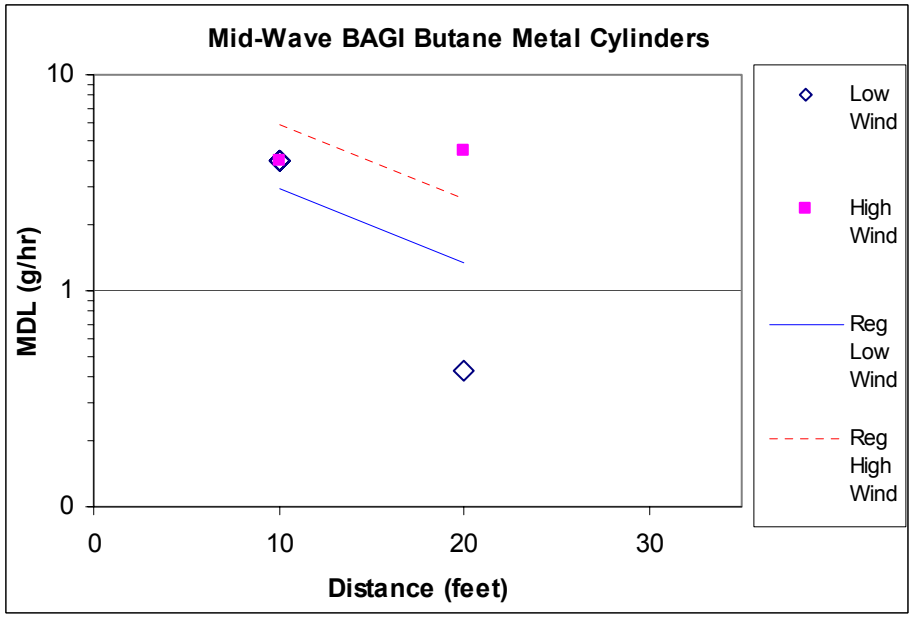
Mid-Wave BAGI Butane Metal Cylinders
MDL (g/hr)
10
1
0
0
10
20
30
Distance (feet)
Low Wind
High Wind
Reg Low Wind
Reg High Wind

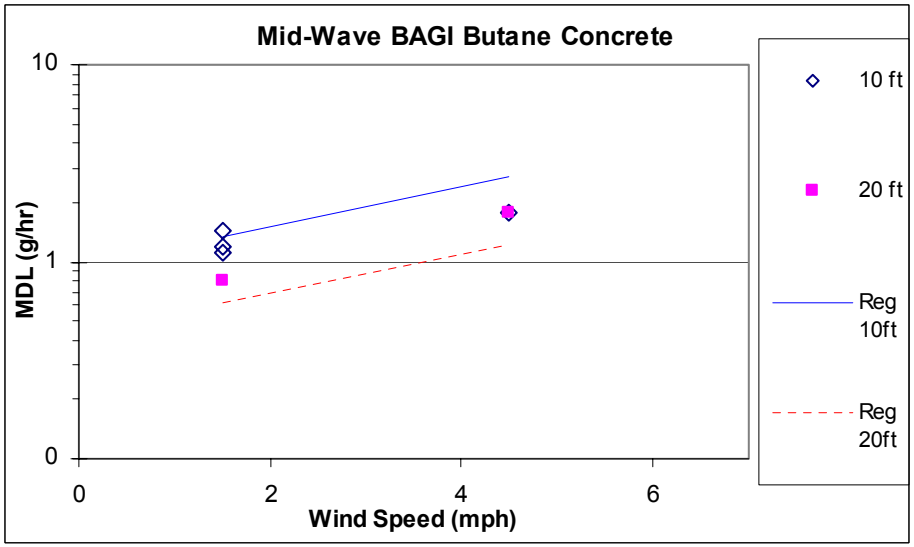
Mid-Wave BAGI Butane Concrete
MDL (g/hr)
10
1
0
0
2
4
6
Wind Speed (mph)
10 ft
20 ft
Reg 10ft
Reg 20ft

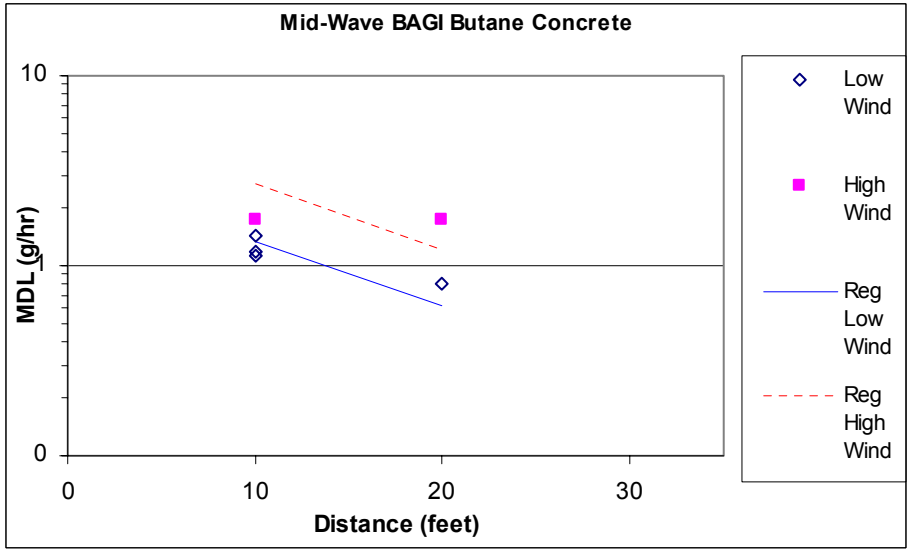
Mid-Wave BAGI Butane Concrete
MDL (g/hr)
10
1
0
0
10
20
30
Distance (feet)
Low Wind
High Wind
Reg Low Wind
Reg High Wind

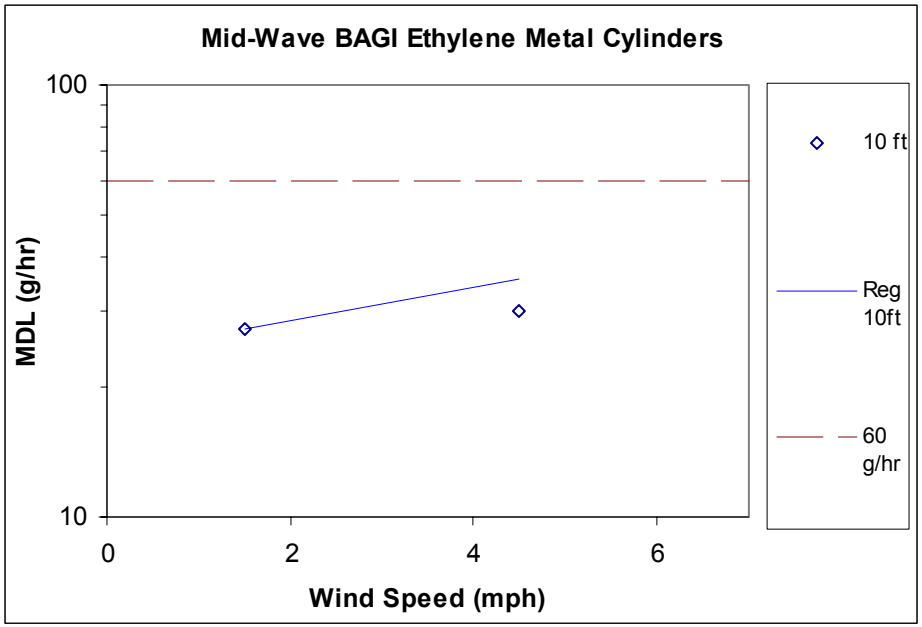
Mid-Wave BAGI Ethylene Metal Cylinders
100
10
MDL (g/hr)
0
2
4
6
Wind Speed (mph)
10 ft
Reg 10ft
60 g/hr

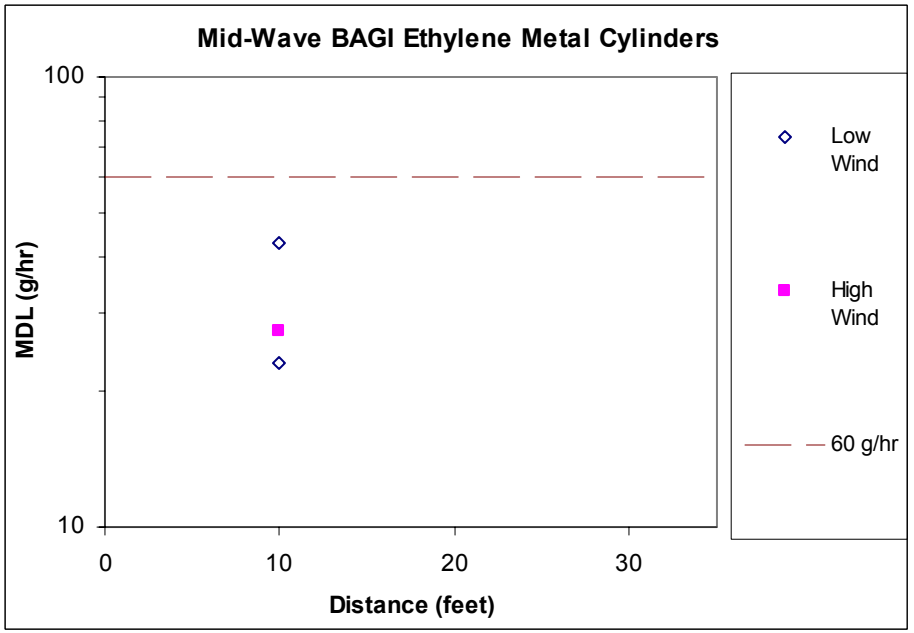
Mid-Wave BAGI Ethylene Metal Cylinders
100
10
MDL (g/hr)
0
10
20
30
Distance (feet)
Low Wind
High Wind
60 g/hr

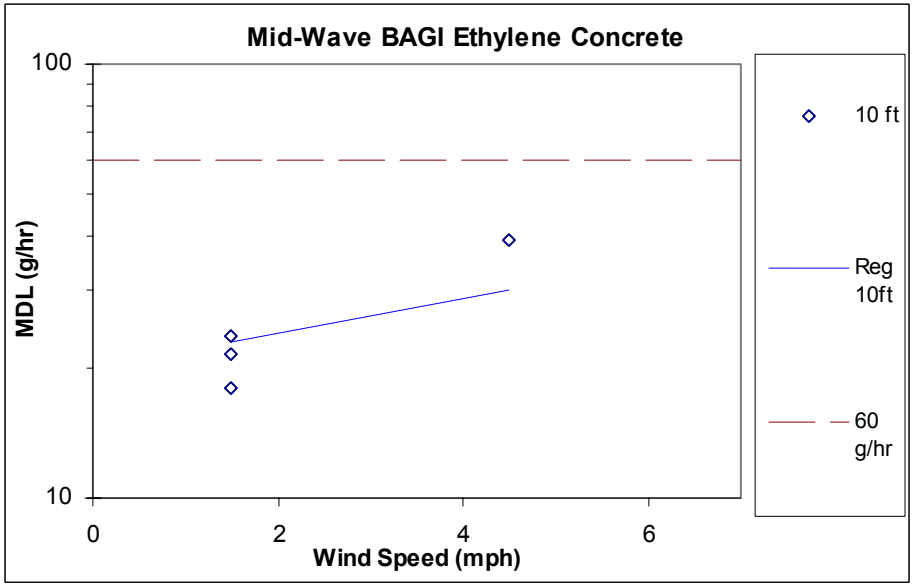
Mid-Wave BAGI Ethylene Concrete
100
10
MDL (g/hr)
0
2
4
6
Wind Speed (mph)
10 ft
Reg 10ft
60 g/hr

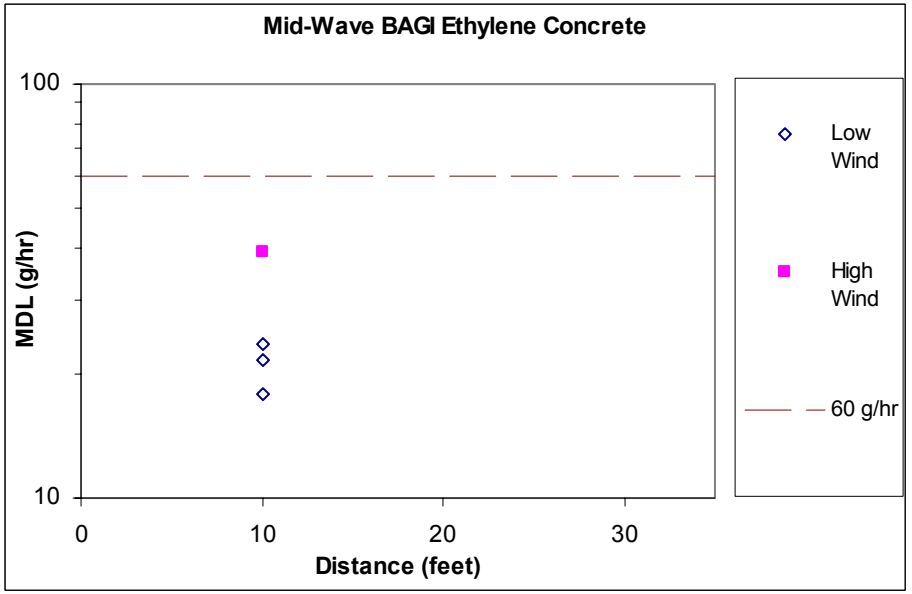
Mid-Wave BAGI Ethylene Concrete
100
10
MDL (g/hr)
0
10
20
30
Distance (feet)
Low Wind
High Wind
60 g/hr

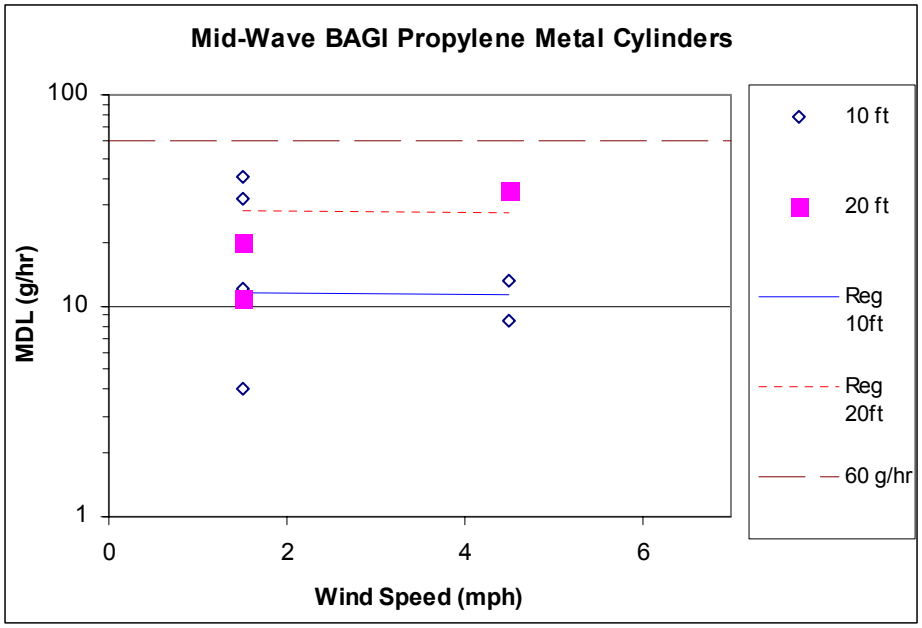
Mid-Wave BAGI Propylene Metal Cylinders
MDL (g/hr)
100
10
1
0
2
4
6
Wind Speed (mph)
10 ft
20 ft
Reg 10ft
Reg 20ft
60 g/hr

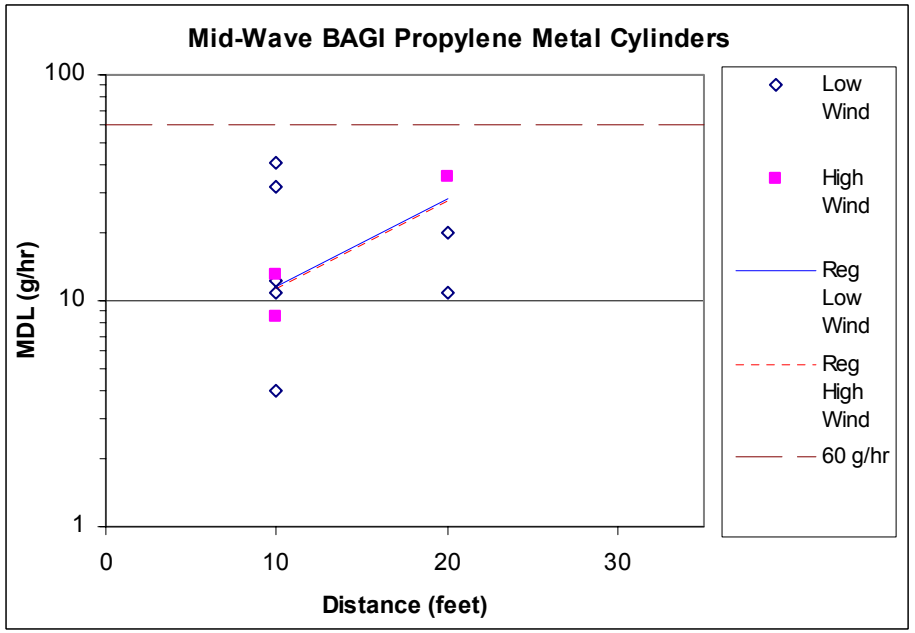
Mid-Wave BAGI Propylene Metal Cylinders
MDL (g/hr)
100
10
1
0
10
20
30
Distance (feet)
Low Wind
High Wind
Reg Low Wind
Reg High Wind
60 g/hr

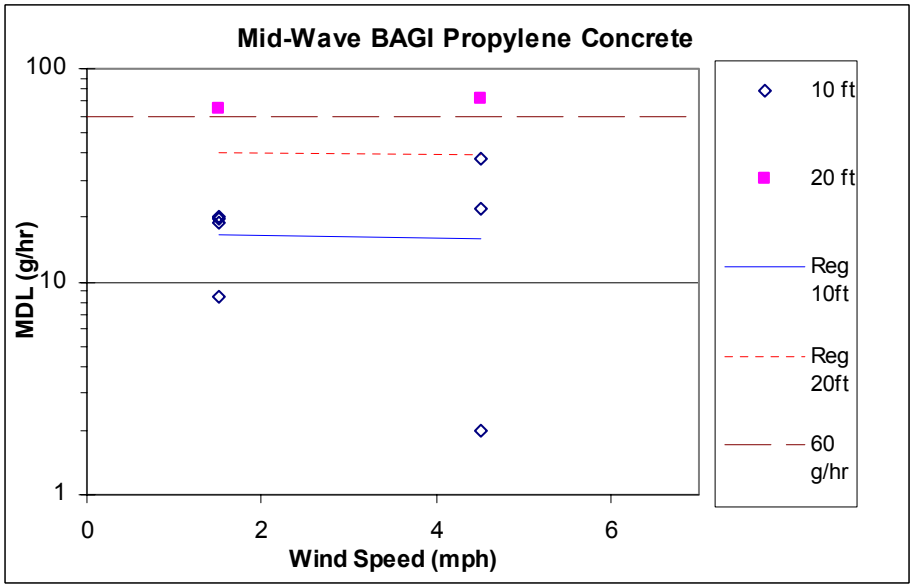
Mid-Wave BAGI Propylene Concrete
MDL (g/hr)
100
10
1
0
2
4
6
Wind Speed (mph)
10 ft
20 ft
Reg 10ft
Reg 20ft
60 g/hr

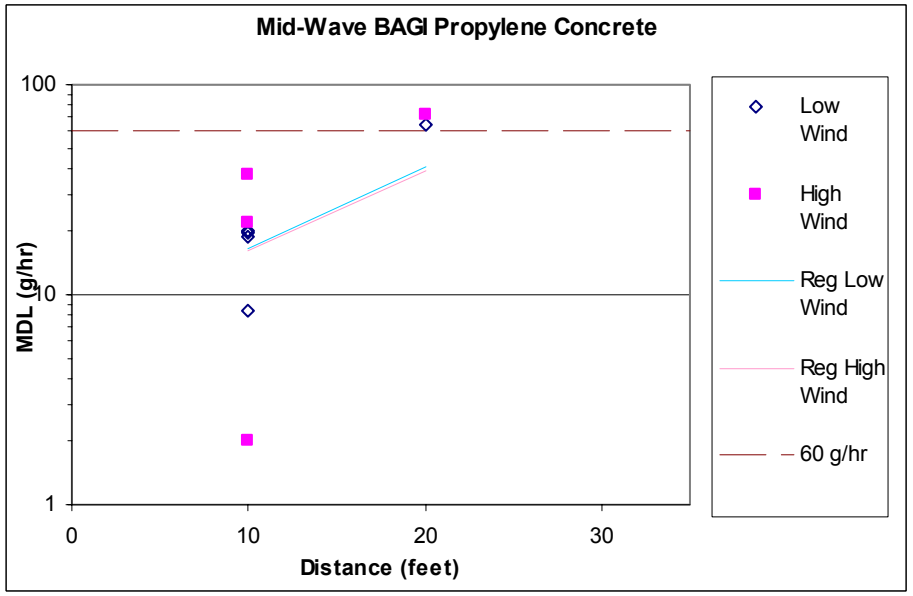
Mid-Wave BAGI Propylene Concrete
MDL (g/hr)
100
10
1
0
10
20
30
Distance (feet)
Low Wind
High Wind
Reg Low Wind
Reg High Wind
60 g/hr

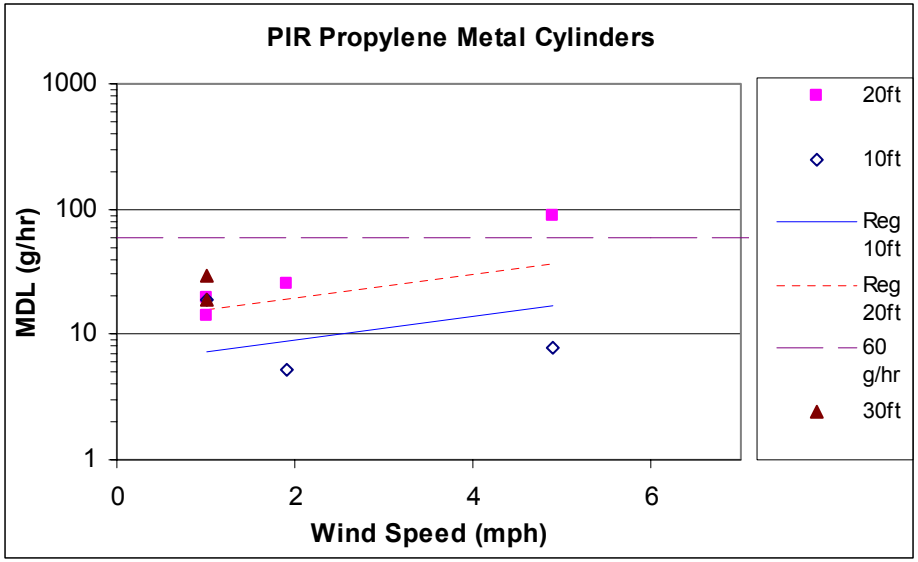
PIR Propylene Metal Cylinders
MDL (g/hr)
1000
100
10
1
0
2
4
6
Wind Speed (mph)
20ft
10ft
Reg 10ft
Reg 20ft
60 g/hr
30ft

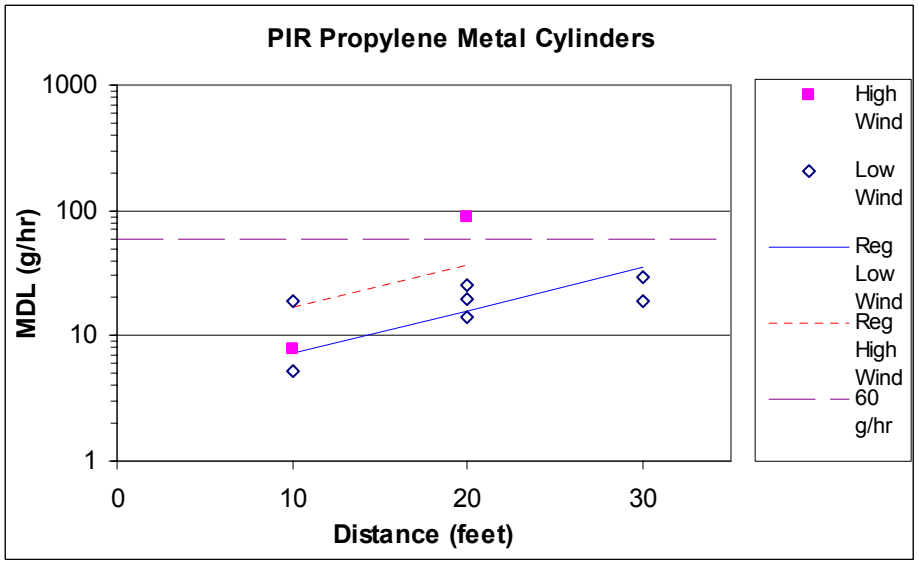
PIR Propylene Metal Cylinders
MDL (g/hr)
1000
100
10
1
0
10
20
30
Distance (feet)
High Wind
Low Wind
Reg Low Wind
Reg High Wind
60 g/hr

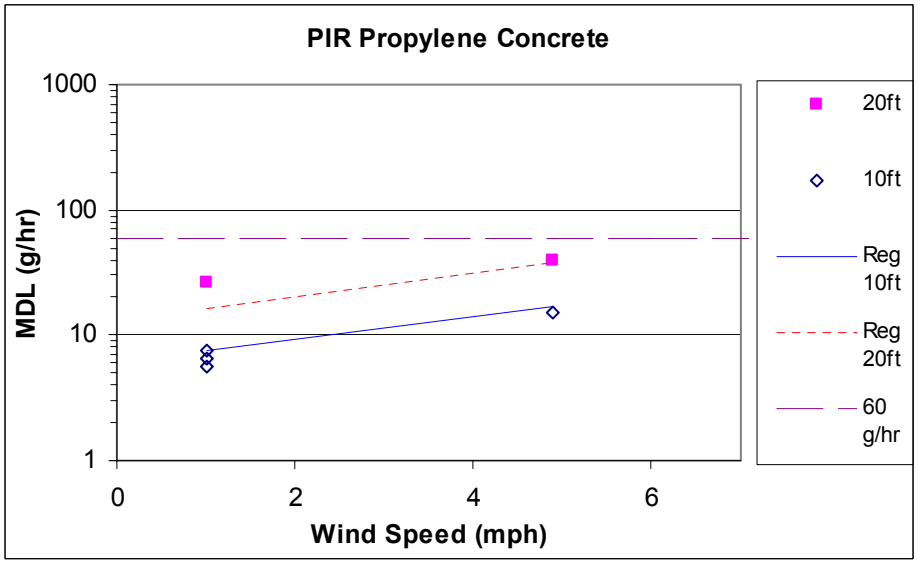
PIR Propylene Concrete
MDL (g/hr)
1000
100
10
1
0
2
4
6
Wind Speed (mph)
20ft
10ft
Reg 10ft
Reg 20ft
60 g/hr

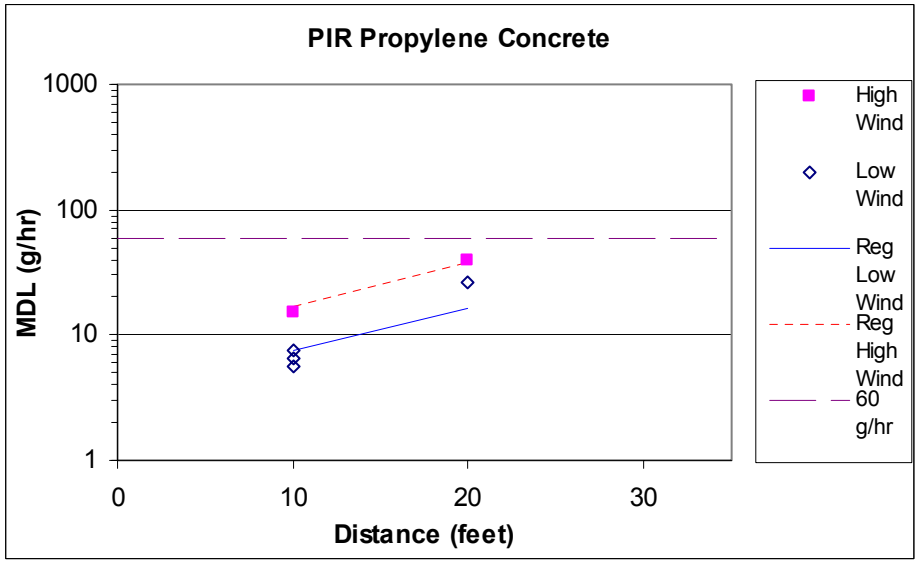
PIR Propylene Concrete
MDL (g/hr)
1000
100
10
1
0
10
20
30
Distance (feet)
High Wind
Low Wind
Reg Low Wind
Reg High Wind
60 g/hr

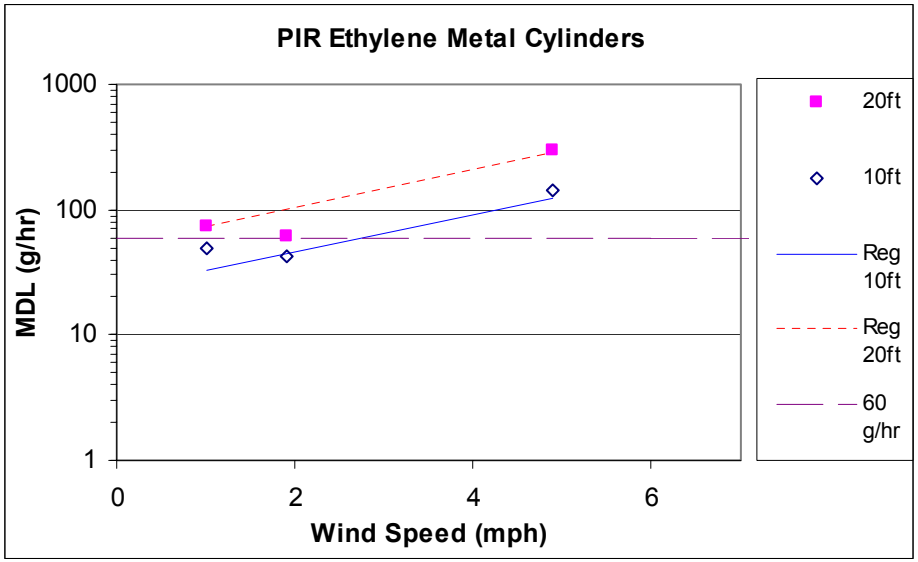
PIR Ethylene Metal Cylinders
MDL (g/hr)
1000
100
10
1
0
2
4
6
Wind Speed (mph)
20ft
10ft
Reg 10ft
Reg 20ft
60 g/hr

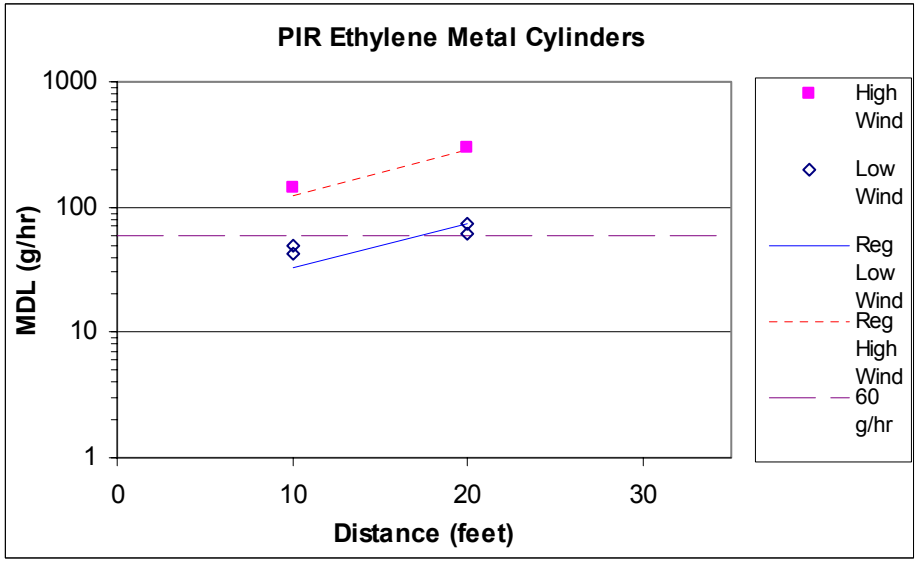
PIR Ethylene Metal Cylinders
MDL (g/hr)
1000
100
10
1
0
10
20
30
Distance (feet)
High Wind
Low Wind
Reg Low Wind
Reg High Wind
60 g/hr

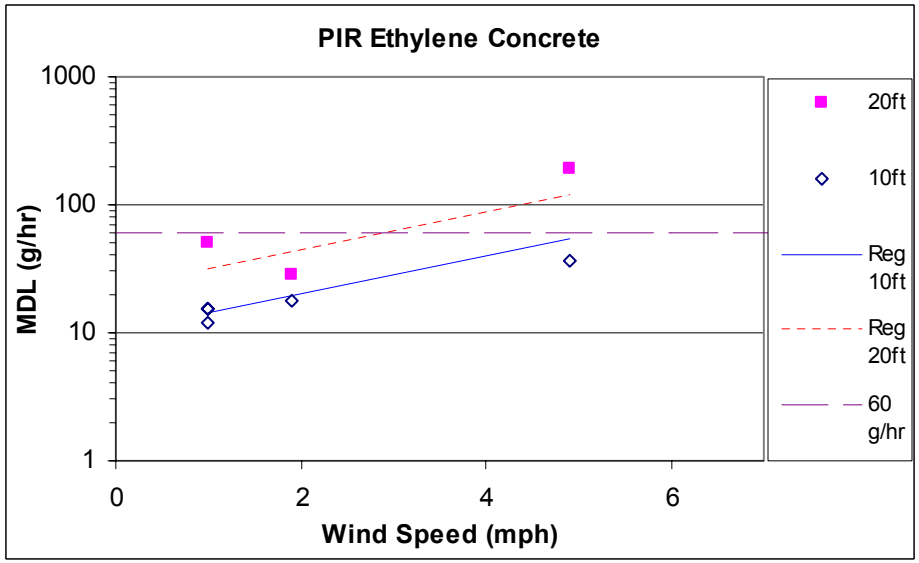
PIR Ethylene Concrete
MDL (g/hr)
1000
100
10
1
0
2
4
6
Wind Speed (mph)
20ft
10ft
Reg 10ft
Reg 20ft
60 g/hr

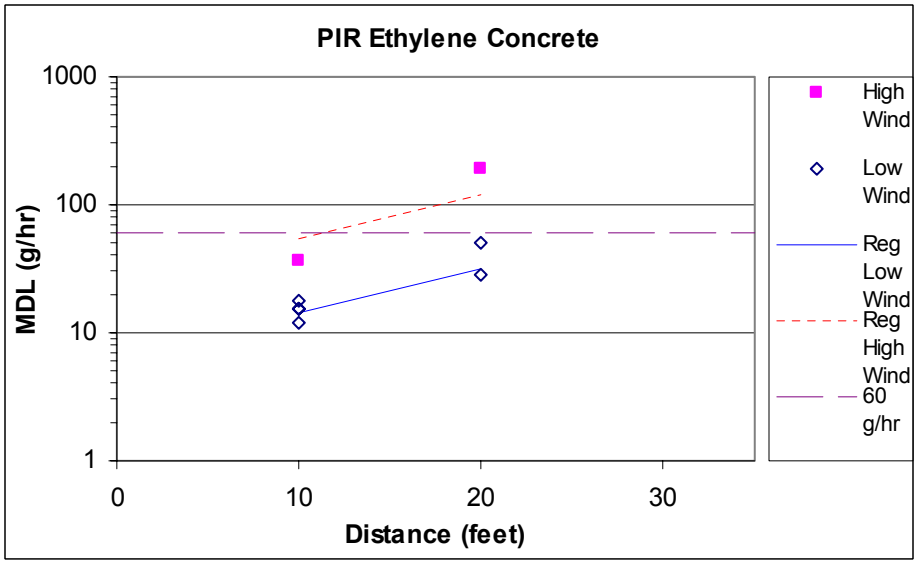
PIR Ethylene Concrete
MDL (g/hr)
1000
100
10
1
0
10
20
30
Distance (feet)
High Wind
Low Wind
Reg Low Wind
Reg High Wind
60 g/hr

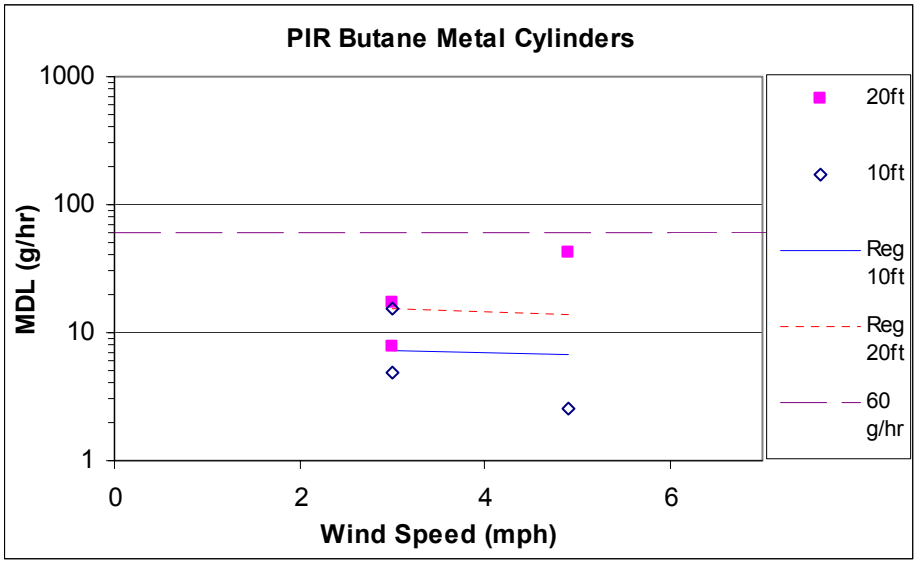
PIR Butane Metal Cylinders
MDL (g/hr)
1000
100
10
1
0
2
4
6
Wind Speed (mph)
20ft
10ft
Reg 10ft
Reg 20ft
60 g/hr

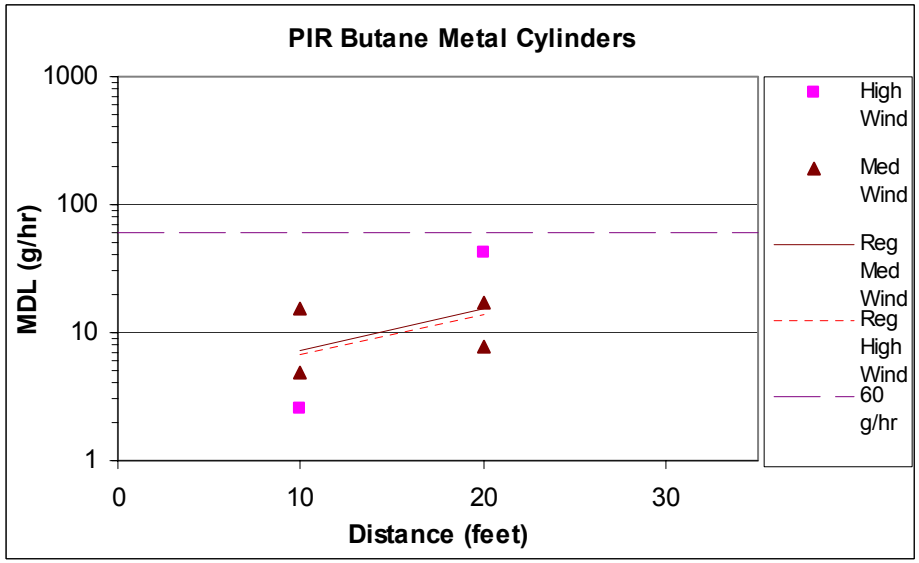
PIR Butane Metal Cylinders
MDL (g/hr)
1000
100
10
1
0
10
20
30
Distance (feet)
High Wind
Med Wind
Reg Med Wind
Reg High Wind
60 g/hr

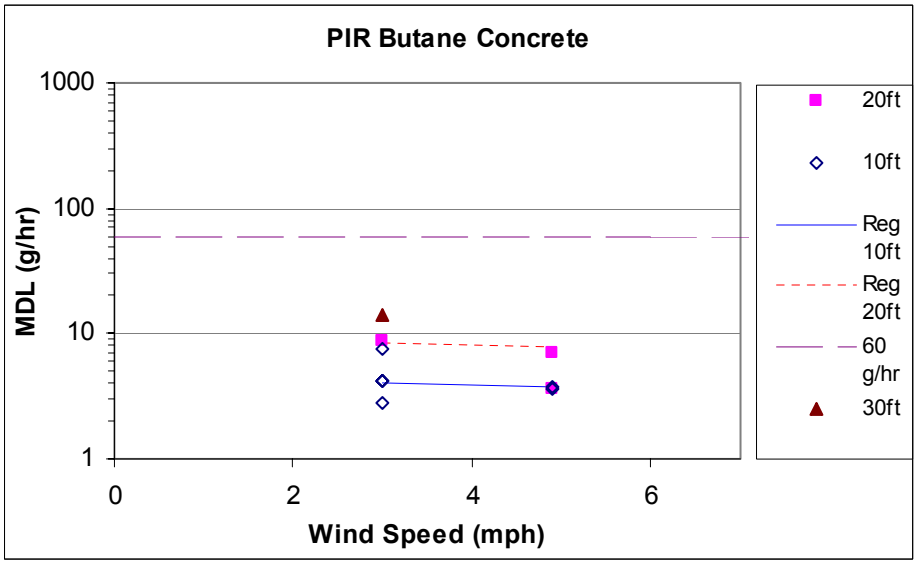
PIR Butane Concrete
MDL (g/hr)
1000
100
10
1
0
2
4
6
Wind Speed (mph)
20ft
10ft
Reg 10ft
Reg 20ft
60 g/hr
30ft

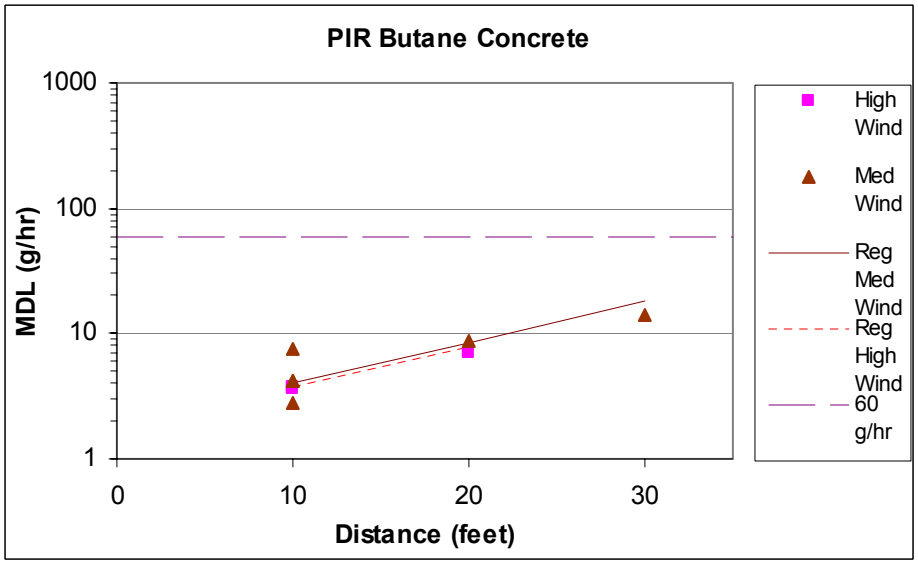
PIR Butane Concrete
MDL (g/hr)
1000
100
10
1
0
10
20
30
Distance (feet)
High Wind
Med Wind
Reg Med Wind
Reg High Wind
60 g/hr

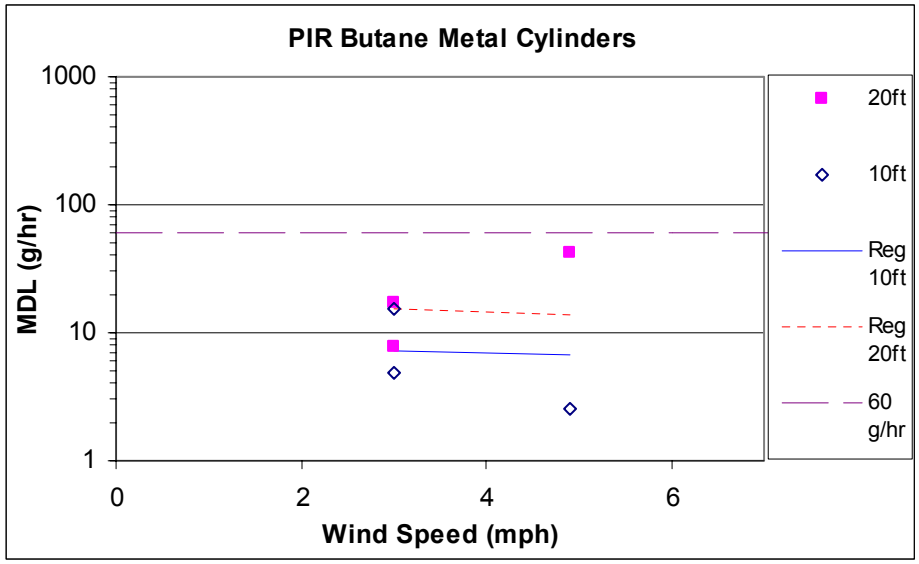
PIR Butane Metal Cylinders
MDL (g/hr)
1000
100
10
1
0
2
4
6
Wind Speed (mph)
20ft
10ft
Reg 10ft
Reg 20ft
60 g/hr

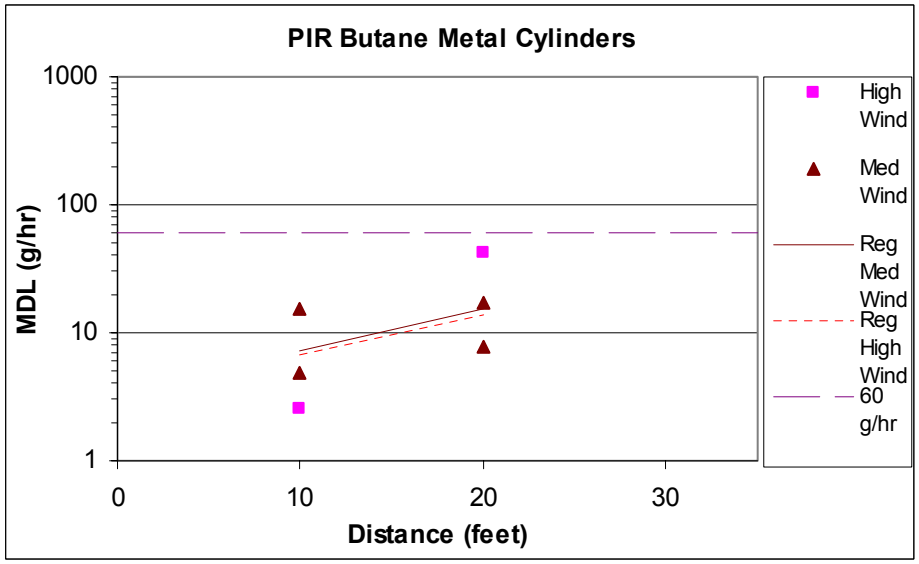
PIR Butane Metal Cylinders
MDL (g/hr)
1000
100
10
1
0
10
20
30
Distance (feet)
High Wind
Med Wind
Reg Med Wind
Reg High Wind
60 g/hr

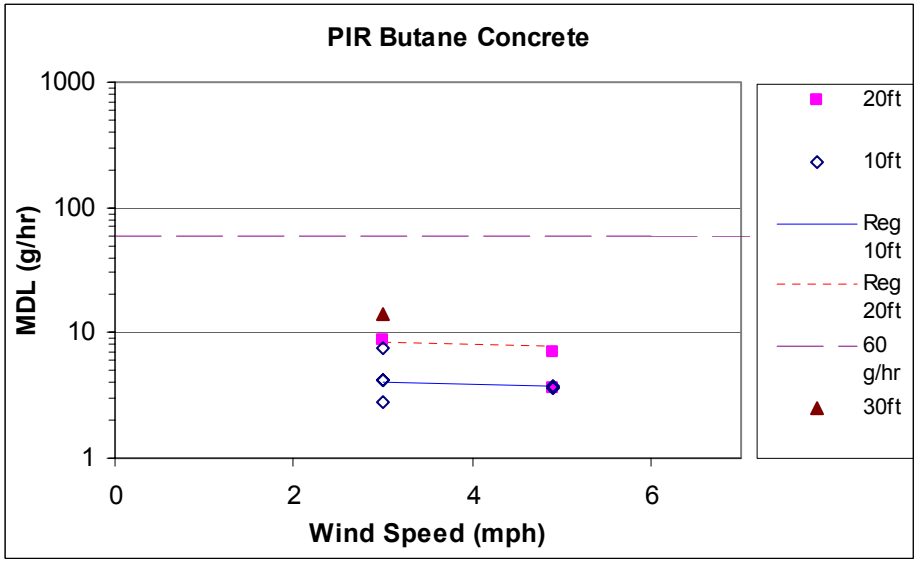
PIR Butane Concrete
MDL (g/hr)
1000
100
10
1
0
2
4
6
Wind Speed (mph)
20ft
10ft
Reg 10ft
Reg 20ft
60 g/hr
30ft

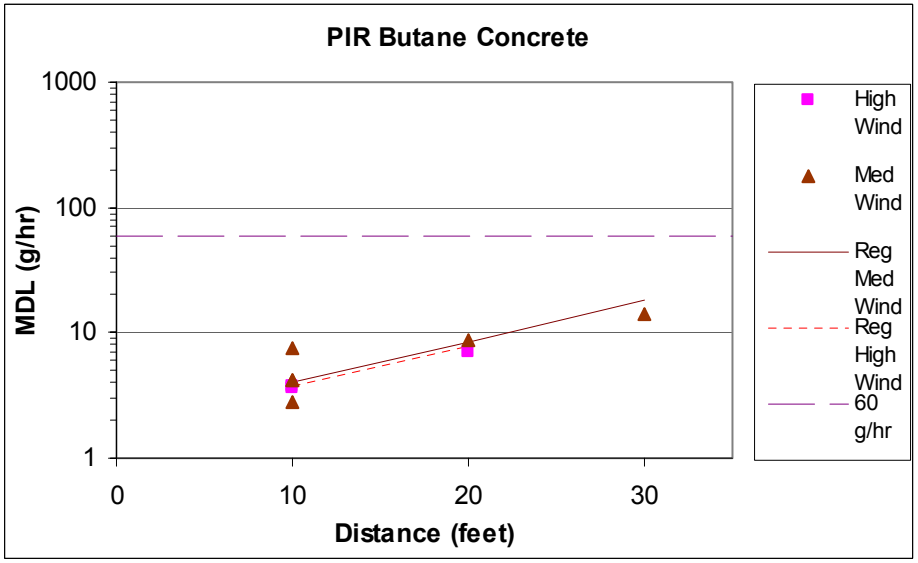
PIR Butane Concrete
MDL (g/hr)
1000
100
10
1
0
10
20
30
Distance (feet)
High Wind
Med Wind
Reg Med Wind
Reg High Wind
60 g/hr

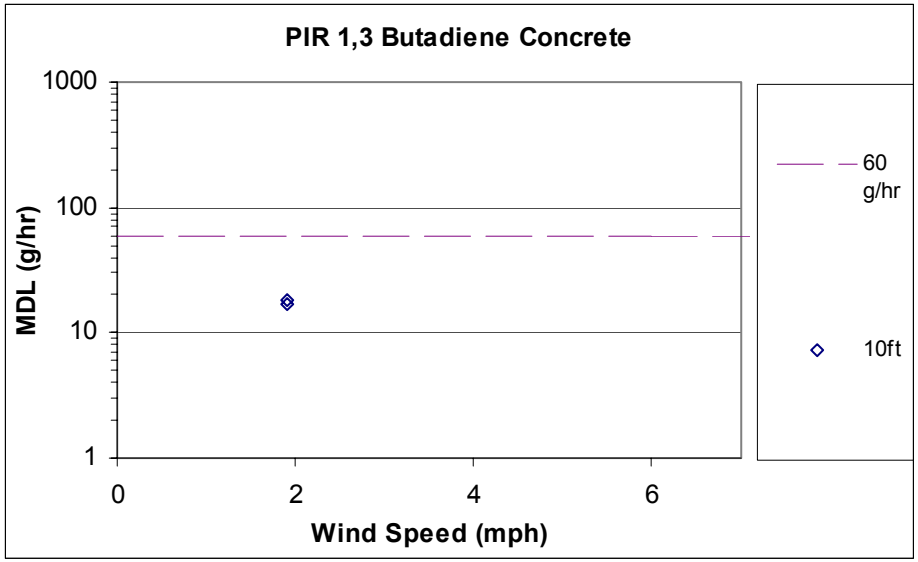
PIR 1,3 Butadiene Concrete
1000
100
10
1
MDL (g/hr)
0
2
4
6
Wind Speed (mph)
60 g/hr
10ft

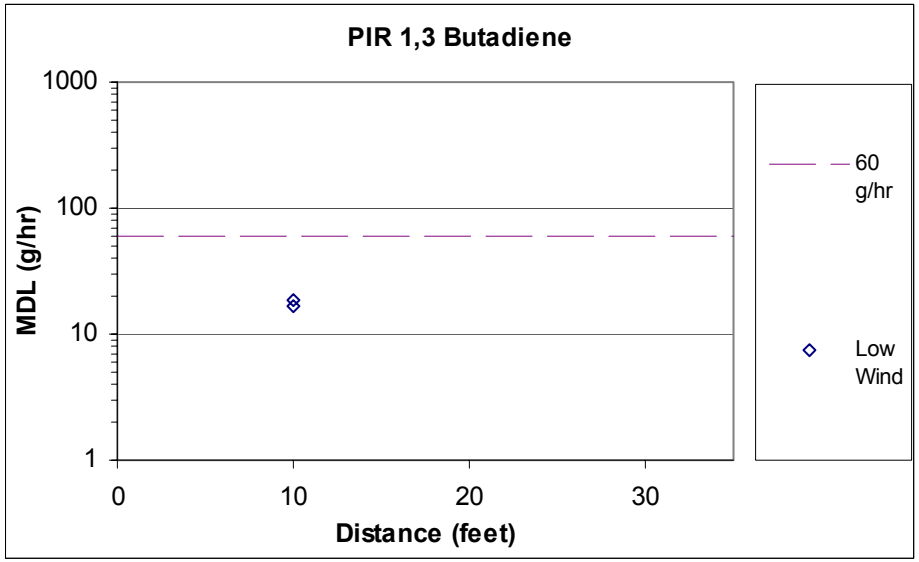
PIR 1,3 Butadiene
1000
100
10
1
MDL (g/hr)
0
10
20
30
Distance (feet)
60 g/hr
Low Wind

APPENDIX H

Evaluation of Emissions Quantification Methods
For Leak Detection and Repair (LDAR) Programs
Using Optical Imaging Techniques

API Discussion Paper – April 2004

DRAFT

Evaluation of Emissions Quantification Methods For Leak Detection and Repair (LDAR) Programs Using Optical Imaging Techniques

API Discussion Paper – April 2004

BACKGROUND

API, in collaboration with the US EPA, is engaged in a mutli-year investigation to identify alternatives to current Leak Detection And Repair (LDAR) requirements at petroleum refineries, with the aim of increasing regulatory flexibility and cost effectiveness, while simultaneously reducing fugitive emissions. Initially, 'conventional wisdom' indicated that a subset of "chronic leakers" could be identified for targeted maintenance to significantly reduce emissions. However, studies conducted by API (API, 1997) have concluded that there was no defined universe of "chronic leakers", though over 90% of the emissions were contributed by less than 1% of the components. These findings were confirmed further by the US EPA and various compliance audits undertaken by the US EPA National Enforcement Investigative Center (NEIC) and the South Coast Air Quality Management District (SCAQMD) in southern California. It was therefore concluded that an LDAR program that focuses on "high leakers" rather than on "chronic leakers" could lead to more effective emission reductions when compared with currently required practices.

This was the nascence of the concept dubbed 'Smart LDAR'. 'Smart LDAR' is a work-practice framework for efficiently locating and repairing the relatively small number of leaky valves, pumps, connectors, etc., within the large population of process components at petroleum refineries. Allowing quicker repairs of leaking components may lead to improved environmental performance while allowing flexibility in implementing regulatory requirements. Efforts focused for the past several years on the development and demonstration of innovative technologies - primarily remote optical imaging techniques - for the rapid detection of leaking components while providing real-time imaging data allowing operators to locate components that are leaking above a set threshold in accordance with regulatory requirements.

The current work practice (CWP) produces monitoring (screening) data using Method 21, and these data can be used both for identifying leaks above a mandated threshold and as a surrogate to mass emission rates when using the appropriate correlation equations. In contrast, optical screening techniques are being developed and dubbed currently as 'Smart LDAR'. These optical techniques have the potential of correctly identifying leakers 100% of the time, but are not yet amenable to provide mass emissions rates directly. Therefore, if, and when, these new 'Smart LDAR' work practices are to be adopted as "equivalent", or alternative work practices (AWP) refineries may no longer have routine access to Method 21 screening data and the corresponding quantification methods currently available.

This summary that follows provides a listing of emission rates quantification methods that are currently available, or could be more fully developed, in order address the issue of alternative quantification methods. Each of the methods will be described briefly and will include a discussion on its applicability, including considerations about its implementation in practice.

ALTERNATIVE QUATIFICATION METHODS

The text below provides a brief discussion of the alternative emissions quantification methods and provides a brief evaluation and outlines considerations on how they might be applied in practice. For each method, some variants (options) are described and discussed briefly in a corresponding "box".

METHOD A: AVERAGE EXPECTED

Three potential variants of the classical average expected quantification method were evaluated; and are summarized in the box below. All three options are based on the procedures outlined for average emission factors, as published in the U.S. EPA Protocol
(U.S. EPA, 1995).

Method A - Options	*Description and discussion*
Option 1: **EPA Average Emission Factors**	Under this option mass emissions are easily computed by using the plant component counts - by equipment type – and multiplying them by the appropriate EPA average emission factors to generate an estimate of total plant emissions. However, this is the least accurate of the methods presented in the EPA 1995 Protocol, since no measurements are taken, and the tabulated emission factors do not necessarily represent individual plants' mass emissions. The average emission factors that are used are typically constant, unless new "control efficiency" factors are applied to them according to local control regime. Typically, this method will not enable the documentation of year-to-year decreases in total plant emissions, with improved leak detection and repair (LDAR) performance, unless new emission factors are derived or the plant reduces its components count.
Option 2: **Plant-Specific Average Emission Factors**	In order to apply this option the plant must have a complete set of screening data for all components. This can be achieved either by using existing screening data or by obtaining a new set and calculating average emission factors by equipment type using the EPA correlation equations. Total plant emissions would then be calculated as in Option 1 (component counts by equipment type are multiplied by the appropriate site-specific average emission factors). This option is more accurate than Option 1 above since the individual plant's mass emission rates distribution is used to derive the average emission factor. However, as in Option 1, total plant emissions will not decrease with improved LDAR performance, since new Method 21 screening data will be required to update the emission factors and document improved LDAR performance.
Option 3: **Lookup Tables Based on Monte Carlo Simulation of Mass Emissions**	This option relies on using Monte Carlo simulations to develop average emission factors which would be displayed in lookup tables (or spreadsheets) for different leakers frequencies (i.e., the steady-state control level achieved for each component type), monitoring frequencies (4, 6, 8 & 12 times per year), and leak definitions (or detection limits). Monte Carlo simulations could be performed using existing SAS software that has been developed by the U.S. EPA (U.S. EPA, 1999) to compare different work practices, and would be based on a large enough number of simulations to provide robust statistical results. The simulation will be based on different CWP scenarios with corresponding assumptions about the monitoring intervals for the AWPs.

In assessing all the options associated with Method A, it is recognized that mass emissions are easily computed, with the differences among the options being the specificity of the average emission factors used. This set of methods is less accurate than others presented in the EPA Protocol, because no new measurements will be typically obtained, and an individual plant's mass emissions distribution may, or may not, be represented by the intrinsic distribution used to derive the average emission factors used. Nonetheless, the Monte Carlo simulation look-up tables will be the most accurate among these options since the average emission factors will account for screening data distributions, monitoring and repair intervals used, and the definition of leak thresholds.

It should be noted that for Option 3 above to attain its potential accuracy a compiled set of current Method 21 screening data that are representative of US refineries would be needed. Such a data set would be used to construct representative screening value distributions for refineries and the currently available correlation curves will be used for quantification of mass emission rates distributions.

METHOD B: LEAK / NO-LEAK

The U.S. EPA 1995 Protocol (U.S. EPA, 1995) provides details on estimating emissions using average Leak/No-Leak emission factors that are merely average emission factors for a certain range of screening values. Commonly, the Leak/No Leak factors in use are based on a Method 21 based 10,000ppm leak definition as the delineation between leaking and non-leaking components.

Method B - Options	*Description and discussion*
Option 1: **EPA Leak/No-Leak Emission Factors**	In order for this method to be applicable for use with Optical Imaging techniques a key assumption to be made is that the optical screening device identifies leakers equivalently to those identified by Method 21 screening for a specified leak definition. In other words, the optical device detects distributions of mass emission rates that are equivalent to those detected using Method 21 definitions. As with Method A - Option 1, mass emissions are easily computed here. Plant component counts for leakers and non-leakers - by equipment type - are multiplied by the appropriate EPA average Leak/No-Leak emission factors to derive an estimate of total plant emissions. This is the second least accurate of the methods presented in the EPA Protocol despite the fact that some actual measurement data are used. Since the specific screening values are not used directly, the Leak/No-Leak averaging factors may not necessarily represent individual plant's mass emissions. Nonetheless, estimates made using this method are somewhat more accurate than those made using the average emission factors described in Method A.
Option 2: **Plant-Specific Leak/No-Leak Factors**	This option is a variant that relies on the availability of a complete set of Method 21 screening data for the plants, either from new on-site monitoring data or from existing data from previous years. As with Option 1, the same key assumption will apply, namely that the optical screening device identifies leakers equivalently to Method 21 screening for a specified leak definition. To apply this method a plant must determine its counts of leakers and non-leakers at the specified leak definition. The plant also needs to derive average emission factors for the leakers and non-leakers separately by using monitoring data for the various equipment types and applying the EPA correlation equations to derive the corresponding mass emission rates. This option is more accurate than Option 1 above, since the plant's mass emissions will be based on the intrinsic distribution of the plant's Method 21 screening data distributions. However, in order to document emissions decrease with improved LDAR

	performance, new monitoring data will be required periodically. This optional approach also lends itself to the development of site-specific Leak/No-Leak emission factors for different leak definitions and the same basic methodology will apply.
Option 3: **Generic Leak/No-Leak Factors for Different Leak Definitions**	In this approach, rather than mere averaging, Monte Carlo simulations may be used to develop generic Leak/No-Leak emission factors, which can be displayed in lookup tables (or spreadsheets). Several scenarios can be anticipated such as different leakers frequencies (i.e., the steady-state control level achieved for each component type), monitoring frequencies (4, 6, 8 & 12 times per year), and leak definitions (or detection limits). These Monte Carlo simulations could be performed by building on the approach developed in collaboration with the U.S. EPA (U.S. EPA, 1999) and would need to be based on a large enough number of simulations (>1,000) to provide robust statistical results. In this case too the simulations of plant mass emission rates distributions will be based on using EPA's correlation equations and applying them to appropriate screening value datasets. The implementation of this method will benefit from the use of current refinery screening value distributions that are representative of refineries across the US.

Under the Leak/No-Leak approach (Method B), Option 3 is potentially the most accurate among all the options, but all of them will depend on documenting the relation between the Method 21 leak thresholds vs. the equivalent mass emission rates for the corresponding optical imaging technique. A key consideration for all of these options will be the proper quantification of mass emissions rates for instrument readings identified as "pegged", where no specific data resolution has so far been attainable.

METHOD C: RANDOM SAMPLE SCREENING

Method C is based on the premise that Method 21 could be used to screen randomly sampled components periodically and the results will be extrapolated by equipment type and service across the unscreened components to calculate plant emissions. The steps to be taken include:

1. Mass emissions will be calculated for the randomly-screened components using the correlation equation,
2. An average emission factor will be calculated for each of the component types,
3. The same factor will be multiplied by the number of unscreened components of the same type, and
4. The two sums will be combined to obtain total emissions per component type.

This approach assumes that there is an equal chance of finding leaking components in any process unit or another physical "area" of a plant; that all leakers occur randomly; and that the leakers' frequency is the same across all equipment types and services.

Method C - Options	*Description and discussion*
Option 1: **Random Sample Screening and Application of EPA Correlation Equations**	In this option component counts and "known" leakers frequencies at a plant would be used in statistical calculations for specified confidence and precision levels to determine the number of random samples to be screened by Method 21. In some cases the sample size required for screening could be quite large, in order to achieve a statistically robust estimate (due to the small proportion of leakers). In this method the estimates will be based on periodically measured data that relies on Method 21 and it will allow documenting decreases in total plant emissions with improved LDAR performance.
Option 2: **Random Sample Screening and Application of Plant-Specific Correlation Equations**	This option is basically the same as that described in Option 1 above, however, site-specific correlation equations developed from plant-specific screening/bagging data pairs could be used – if available - in lieu of the US EPA correlation equations. Emission estimates will be based on correlation equations that relate site-specific screening values to mass emission rates.

This approach will require the development of statistical tables and special guidance for implementing the process of random selection of components and the proper extrapolation to the rest of the components of the same type and service.

Although this approach seems feasible in theory, it will impose a very large implementation burden in practice. It will require maintenance of two sets of instruments, optical imaging along with Method 21, including training of personnel, equipment maintenance and calibrations as well as data management systems. .

METHOD D: PERIODIC SCREENING

This method would rely on using the existing Method 21 technique to periodically screen all the refinery components and use these data to estimate emissions. This approach is similar to the one currently used and it extends the sampling approach of Method C above and applies it to the refinery as a whole, once in a pre-specified periodic interval, without retaining it for routine monitoring.

Method D - Options	*Description and discussion*
Option 1: **Agreed Schedule for Screening**	This option is based on periodic screening of all plant components using the existing Method 21. It could entail using Method 21 in lieu of optical imaging once per year. This approach might have the lowest acceptance hurdle since it relies on well-established methods and provides the needed information in a familiar format.
Option 2: **"Skip Monitoring" Screening**	This Option is similar to the approach of the "skip monitoring" concept, i.e. reducing the frequency of periodic screening with improved LDAR performance. This option could allow for extended intervals between repeated screenings based on demonstrating improved plant performance (i.e., lower % leakers at a given leak threshold).

Both of the options described for Method D will require the determination of reasonable monitoring frequencies in order to avoid duplicative requirements of using Method 21 in addition to optical imaging and thus curtail the efficiency gained from implementing an alternative work practice (AWP). As mentioned for Method C above, it would be further complicated by requiring the availability of two (2) types of monitoring instruments, would entail additional complexity in data management and reporting and might complicate compliance if the two methods are not compatible.

METHOD E: HIGH-LEAKERS SNIFFING

This method incorporates the use of Method 21 in conjunction with a new AWP standard that uses optical imaging. It is based on identifying leakers by optical imaging, followed immediately by screening the leaking component by a portable 'sniffer' and recording the screened concentrations, as required by the reference test procedure (Method 21).

Method E - Options	*Description and discussion*
Option 1: **Screen Leaking Components identified by Optical Imaging**	This option uses well-established methods and techniques and enables the use of existing US EPA correlation equations with Method 21 screening data. In addition, it focuses efforts on high leakers which are the primary contributors to plant emissions. This approach can also be used to develop empirical equations relating Method 21 screening values to Optical Imaging pixels intensities.
Option 2: **'Bagging' Leaking Components identified by Optical Imaging**	This variant of the method is envisioned to use a whole sample capture – or "bagging" method - to quantify mass emission rates for high-leakers identified by optical imaging. This approach could be used to conduct "bagging" on only a few representative components and thus utilize the data to generate a new correlation equation relating optical imaging data directly to mass emission rates. This optional approach will lead to higher accuracy estimates. It could be implemented either by deriving new correlation equations that represent the industry, or by site-specific applications. Using this approach with the higher measurement precision of optical imaging could avoid some of the uncertainty associated with the existing correlation equation approach, which is primarily due to Method 21 variability.

Method E addresses the High Leakers and thus could account for over 90% of the emitted mass. It is based on an inherent assumption that those components not detected by optical imaging will follow similar screening value distributions as those previously derived from Method 21 screening.

This approach, similar to methods C and D might also impose a high implementation burden since it relies on the availability of dual monitoring techniques with appropriate technician training and availability of compatible data management systems.

METHOD F: INSTRUMENT MASS READING

This method would utilize direct reading of digitized signals from the optical image obtained from the leaking component. This image, with proper calibration, can be used to determine mass emission rates directly from an optical imaging system. Since it has the potential to read directly mass emission rates, it could avoid the use of correlation equations to relate concentrations to mass emissions. However, its usefulness will depend on the development of appropriate calibration curves and special routines that could be programmed to quantify emissions of classes of compounds or individual compounds.

It is not clear that this will be available in the near term, as remaining technical challenges will need to be overcome. In particular:

- Instrument sensitivity and threshold detection limits might vary with identity of chemical compound class and species,
- Standardized calibration might become an issue as the instrument's optical sensitivity varies with chemical components in the mixture, and
- Field operations will require highly trained technicians to properly calibrate and tune the instruments.

IMPLEMENTAION CONSIDERATIONS

The previous section provided a listing and some discussion of various alternative techniques that are available to quantify plant emissions. The methods discussed represent techniques that range from using currently available average emission factors to new approaches relying on Monte-Carlo simulations or the use of calibrated optical scanners. Some of the methods considered retain the use of organic vapor analyzers ('sniffers'), as currently used under Method 21, in addition to optical imaging devices.

All the methods described above have some advantages and some disadvantages. Some tend to overestimate plant emissions but are very simple to implement, while others are resource intensive but will provide a much lower emissions estimate. Each plant operator will have to make their own assessment when selecting the approach that best fits their needs. Factors that will need to be considered will depend on data needs and their intended use, including:

- Operational complexity for implementation of the various emissions quantification techniques available,
- Assurance of compliance and verifiability of the monitored and estimated data, and
- Desired level of accuracy for the resulting plant emissions inventory

We have already addressed above the accuracy of the various methods listed along with other considerations that might be key to proper implementation of either one of the six (6) methods listed. So just to reiterate briefly, if we are to maintain Method 21 for screening as a tool for determining emissions (e.g. Methods C, D and E) there might be operational and compliance implications, as well as increased resource burden for implementation. As mentioned previously, plant operators will need to maintain two sets of instruments and technicians that are trained in deploying both optical imaging and the reference Method 21. In addition, periodic checks with Method 21, or side-by-side checks of Method 21 with Optical Imaging could lead to compliance uncertainty by creating confusion in the required repair schedule, due to potential inconsistency between the readings obtained by the two methods when deployed simultaneously.

Therefore, in evaluating the feasibility of implementing alternative quantification methods that are suitable for AWPs, it is important to assess the regulatory compliance and operational aspects that would make the alternative system more attractive to participating refineries.

REFERENCES

API, 1997, *Analysis of Refinery Screening Data,* API Publication 310, American Petroleum Institute, Washington DC, November 1997.

U.S. EPA, 1995: *1995 Protocol for Equipment Leak Emission Estimates;* Office of Air and Radiation, Office of Air Quality Planning and Standards, EPA-453/R-95-017. Research Triangle Park, NC 27711.

U.S. EPA, 1999: *Monte Carlo Simulation Approach for Evaluating Alternative Work Practices for Equipment Leak;* Office of Air and Radiation, Office of Air Quality Planning and Standards, Draft report. Research Triangle Park, NC 27711.

Prepared By:
Dr. Miriam Lev-On
The LEVON Group, LLC

Mr. Hal Taback
The Hal Taback Company

Dr. David Epperson
Consulting Statistician

Prepared For:
The American Petroleum Institute (API)
Contract Number: 2002-100212

API Contact:
Karin Ritter, RASA Department
ritterk@api.org
(202) 682-8472

April 2004